ELEMENT SPECIFIC IMAGING IN COMPUTER ASSISTED TOMOGRAPHY USING A TUBE SOURCE OF X-RAYS AND A LOW RESOLUTION DETECTOR.

A thesis for the degree of
PHILOSOPHIAE DOCTOR

Presented to
DUBLIN CITY UNIVERSITY

By
CHARLES EDWARD MARKHAM B.Sc.(HONS)
THE SCHOOL OF PHYSICAL SCIENCES
DUBLIN CITY UNIVERSITY

Research supervisors
JOSEPH FRYAR B.Sc Ph.D. (DECEASED)
Prof. EUGENE KENNEDY B.Sc. Ph.D. C.Phys F.Inst.P.

August 1993.

DECLARATION

I hereby certify that this material, which I now submit for assessment on the programme of study leading to the award of philosophiae doctor is entirely my own work and has not been taken from the work of others save and to the extent that such work has been cited and acknowledged within the text of my work.

Signed : Charles Markham Date: 13th October 1993

Charles Markham

In memory of Dr. Joseph Fryar, 1947 - 1990.

Requiescat in pace.

CONTENTS

TABLE OF FIGURES

LIST OF TABLES

ELEMENT SPECIFIC IMAGING IN COMPUTER ASSISTED TOMOGRAPHY USING A TUBE SOURCE OF X-RAYS AND LOW RESOLUTION DETECTOR.

CHARLES E. MARKHAM

ABSTRACT

A new technique for element specific imaging in computerised tomography has been developed. The technique allows two or more elements to be imaged independently of the matrix in which they are contained. The technique uses a filtered tube source of x-rays and low energy resolution detector.

Fractional transmittance measurements were recorded at a number of tube potentials along each of the beam paths required for standard CT reconstruction. This data was used to obtain monochromatic information about the absorber. K-edge differential absorptiometry was then used to obtain the equivalent thickness of each element of interest. Using the algebraic reconstruction technique (ART), element specific images were generated. The technique was successfully used to separately image iodine and barium distributed in a water matrix.

In a refinement of the technique, a single channel analyser was used to increase the percentage of counts in the fractional transmittance measurement providing information about the elements of interest. Using this approach, cadmium and indium, elements with a K-edge separation of 1.23keV, were separately imaged. The technique was also tested for matrix independence and linearity using homogeneous samples.

Using computer simulations the optimum operating conditions and characteristics of the technique were examined.

Finally, future developments of the technique are discussed along with a possible application.

TABLE OF IMPORTANT SYMBOLS

α	Photoelectric absorption parameter keV^3.
α'	Photoelectric mass absorption parameter m^2keV^3/kg.
β	Compton scatter absorption parameter.
β'	Compton scatter mass absorption parameter m^2/kg.
$C_a(x,y)$	Concentration of analyte in pixel x,y kg/m^3.
$C(V_t)_i$	Count recorded in channel i, spectrum recorded at V_t.
d	Diameter of region scanned m.
E	X-ray energy keV.
E_K	K-edge absorption energy keV.
E(i)	X-ray energy equivalent to channel i keV.
i	Tube current mA.
I	X-ray intensity.
$I(V_t,E)$	X-ray intensity at energy E produced by a tube operating at a potential V_t.
$K_{\alpha,\beta}$	Characteristic K-lines of an element.
Lag	Energy difference between V_t and discriminator threshold keV.
l	Width of absorber m.
m	Number of projections.
μ	Linear attenuation coefficient m^{-1}.
n	Number of ray-sums in a projection.
N	Number of ray-sums required for a reconstruction.
P(E)	$1/E^{-3}$.
r,ϕ	Polar coordinates.
R(E)	Detector efficiency function.
ρ	Density kg/m^{-3}.
$\sigma(E)$	Detector energy resolution at energy E keV.
S(E)	Klein Nishina function.
t	Equivalent thickness kg/m^2.
t_x	Equivalent thickness of x kg/m^2.
U	Mass attenuation coefficient m^2/kg.
V_t	Tube potential V.
w	Cell width.
w_{ij}	Mean path length of beam j through cell i.
ω	Weight fraction.
x	Absorber thickness m.

Chapter 1

Introduction to Computer Assisted Tomography (CAT) .

Introduction

The thesis describes two new methods of imaging specific elements located in a defined plane intersecting an object. In chapter 1 computer assisted tomography (CAT) is described. This imaging technique is central to the ideas contained in this thesis. This is then followed by a brief history of x-ray imaging. A review of current tomographic imaging techniques identifies some of the limitations of existing techniques and helps define the requirements of the techniques developed. The objectives of the project are described at the end of the chapter.

1.1 OVERVIEW OF CAT.

1.1.1 DESCRIPTION OF CAT

Computer assisted tomography (CAT) provides a method of measuring the spatial distribution of some material property in a defined plane intersecting an object, without interference from structures contained in other planes.

The term CAT was first used to describe the medical imaging system developed by Hounsfield [1]. This produced an image representing the x-ray linear attenuation coefficient in a slice through the head of a patient.

A CAT or CT (computed tomography) image is produced in three stages. These are data collection, reconstruction and display. Data collection involves measuring the attenuation of a collimated x-ray beam at a set of equally spaced positions across the object. This set of measurements is called a projection. Projections are collected at equally spaced angles around the object. If enough data have been collected then a representation of

the attenuation in the plane can be reconstructed into a two dimensional matrix. An extensive discussion of the background to this procedure is provided in the reference texts by Herman and Natterer [2][3]. The matrix is normally displayed as a grey scale or colour coded image. Three dimensional and contour plots are also used. See figure 1.01.

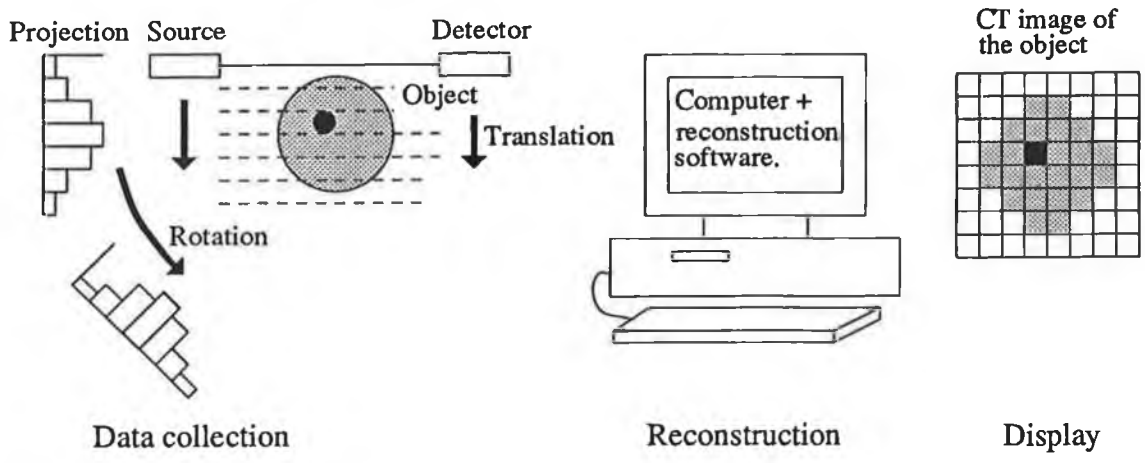

Figure 1.01
CAT image production.

The incorporation of decision-making algorithms into image reconstruction techniques is seen by Veklerov [4] as the next stage in the development of image reconstruction. These algorithms would assist the viewer of the image to identify regions of interest.

CT techniques have also found industrial applications. CT has been used by RARDE to image the construction and distribution of explosive in shells [5]. The research device built by RARDE used a commercial medical scanner modified to include a 420kV x-ray generator. An industrial CT facility has been developed by BAM (Bundesanstalt fur Marterialprufung) which was used to image the scale and rust deposits in pipes [5]. Dickin *et al* review the CT techniques currently being developed for industrial application [6].

Conventional X-ray CT has been used to image items from as large as a complete Trident C4 rocket motor, two metres in diameter, with an image resolution of 1024 x 1024 pixels to items as small as a mouse [7]. A portable CT machine has even been developed to image the annual rings

of a living tree [8].

Microtomography based on CCD array detectors and synchrotron light sources are being developed for material analysis. Using this approach Nusshardt *et al* [9] imaged a Al_2O_3 fibre reinforced aluminium material with a pixel resolution of 23μm. The use of CT techniques removes the need for the surface preparation required with other microscopic techniques such as scanning electron microscopy. The ultimate resolution of microtomography technique based on synchrotron radiation is about 1μm. The limit in resolution is set by the photon flux available from such highly collimated sources [10]. Using a tube source of x-rays and microtomography technique Elliot and Dover [11] produced CT images of the structure of bone. The image they produced had a resolution of 15μm but took nearly twenty hours to record.

1.1.2 HISTORY OF X-RAY IMAGING.

Wilhelm Conrad Roentgen discovered x-rays in 1895. The discovery was made while he was carrying out experiments on cathode rays. A discharge tube driven by a large Ruhmkorff coil was covered with black card. The x-rays were detected with a fluorescent screen made from paper washed with barium-platinocyanide solution. The apparatus allowed Roentgen to produce shadow graph images of various objects [12]. The technique found almost immediate application in non-destructive testing in both medical and industrial applications. In 1901 Roentgen received the first Nobel prize for physics for his work with x-rays.

Roentgen's x-ray tube produced x-rays by accelerating electrons towards a metal anode. The electrons were produced by positive gas ions hitting the cathode. The output of the tube depended on the gas pressure in the tube. The tube, however, only operated over a narrow range of pressures. In 1913 the limitations associated with the Roentgen tube were solved by W.D. Coolidge [13]. The Coolidge tube used an electrically heated filament at the cathode to produce electrons. The electrons could be

focused to give a small spot size on the target. The tube operated at high vacuum. The intensity of the x-rays was adjusted by the filament temperature. The penetrating power of the x-rays was adjusted with the tube potential. The design of the modern x-ray tube is essentially the same as that of the Coolidge tube.

In a conventional radiograph the image produced is a shadow of all the structures contained between the x-ray source and the film [14]. Structures of interest can be hidden behind more attenuating structures. The first attempt to produce an image of a specific plane through the body was made by Bocage in 1921 [15]. The x-ray source and film were made to pivot about the patient. Structures in the pivotal plane remained in focus, other structures were smeared over the image. This technique is called classical tomography. See figure 1.02.

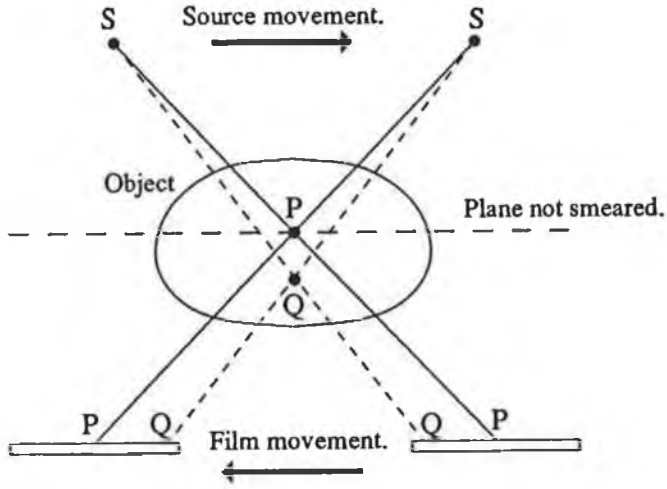

Figure 1.02
Classical tomography.

In 1956 Bracewell [16] developed a technique for imaging the microwave emission from the surface of the sun. The antennae then available only allowed him to measure the total intensity of radiation along a strip passing across the sun. The concept of reconstructing an image from strip-sums or ray-sums is central to the technique of computerised tomography.

In 1961 Oldendorf [17] used a I^{131} source of gamma rays and detector placed either side of a turn table to image a test object. The image was reconstructed by backprojection. This produced the first tomographic image where the radiation only passed through the defined plane

of interest.

In 1963 Cormack [18] imaged phantoms using an x-ray source. An accurate reconstruction technique was used to produce images. The demonstration showed that transmission tomography was practical.

In 1972 EMI Ltd. introduced the first medical CT scanner. It was developed by G.N. Hounsfield [1]. The machine was capable of producing 80 x 80 pixel images of the human head; it had an immediate impact on the medical imaging of the time. The clinical results of the work were reported by Ambrose [19]. Although the image produced by such machines had a much lower spatial resolution than x-ray film, the ability to identify small changes in x-ray attenuation allowed it to differentiate between different types of soft tissue. The machine could be used to locate both tumours and regions of haemorrhage in the brain. Hounsfield and Cormack received the 1979 Nobel prize for medicine for their work on computerised tomography.

Since the initial design of the CT scanner, spatial resolution has improved. Medical images up to 512 x 512 pixels are now possible. Some commercial machines allow this data to be displayed in a 1024 x 1024 grid [20]. Whole body scanners are currently capable of imaging any part of the body, not just the head. There have been four generations of CT scanner [21]. These are shown in figure 1.03.

First generation scanners collected data by scanning a single beam across the object. The source/detector gantry was then rotated and the procedure repeated until all projections had been collected. The technique was very slow.

Second generation scanners used a fan-beam x-ray source and a number of detectors. The fan beam was made wide enough to cover the patient. The source and detector needed to be moved to collect a full projection. The third generation scanners contained enough detectors to collect a full projection without any movement.

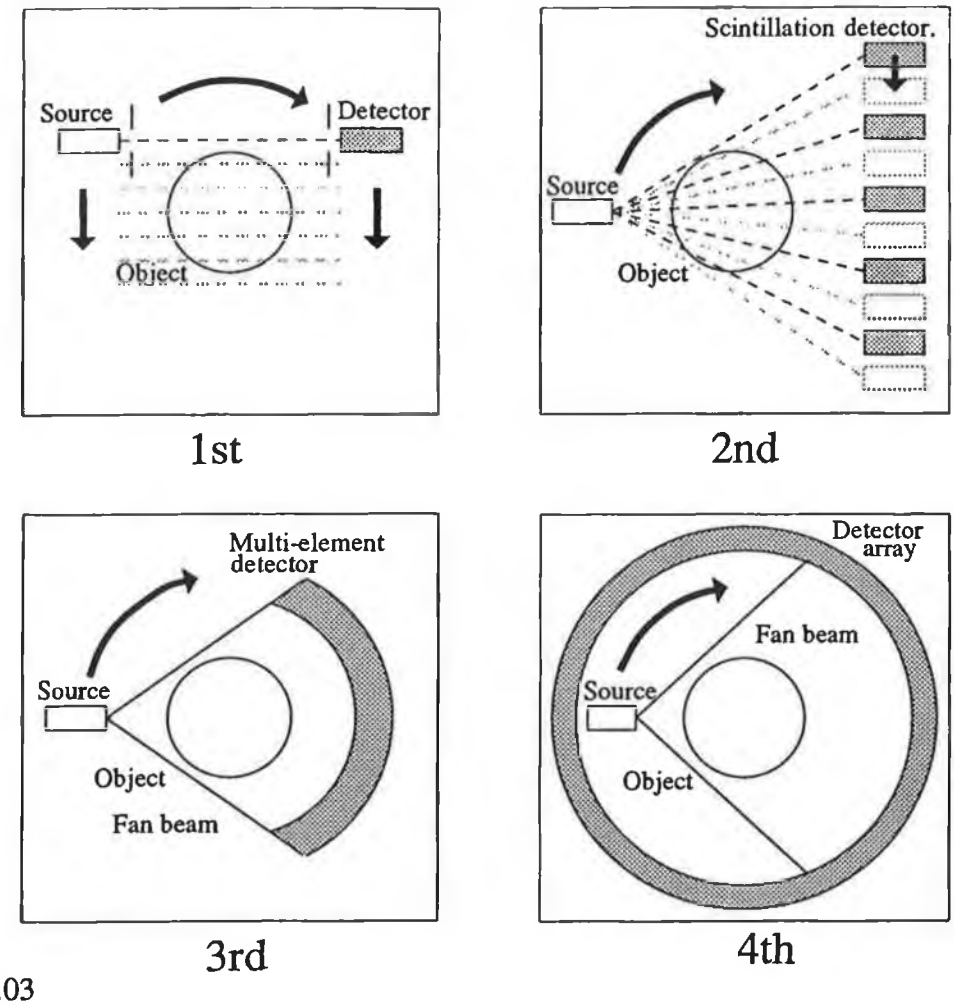

Figure 1.03
Schematic diagrams of the four generations of CAT scanner.

In fourth generation scanners the detectors are located in a ring about the patient. The x-ray source then moves around the patient. The fastest CT scanning technique is CVCT (Cardiovascular CT). In CVCT [22] the x-ray source is made to move by deflecting an electron beam incident on a semicircular target placed around the patient. This technique collects data very quickly and has allowed a beating heart to be imaged.

Recently Spiral CT has been developed to image an entire organ [23][24] without the need to image a number of planes separately. This is achieved by moving the patient through the scan plane as projection data is being collected. Reconstruction allows planes intersecting the helix traversed by the x-ray source during the scan to be imaged.

1.2 REVIEW OF EXISTING TECHNIQUES FOR IMAGING CONTRAST AGENTS.

1.2.1. OVERVIEW OF IMAGING TECHNIQUES

Since the introduction of CT there has been a large development in methods of imaging a single plane within an object. The following sections describe some of these techniques. Most of the techniques discussed are capable of imaging a specific element or contrast agent. The contrast agent may be used to locate a particular structure or process contained in the object. The limitations and ideas contained in these techniques lead to the technique developed in the rest of the thesis. Figure 1.04 shows the relationship between the different techniques.

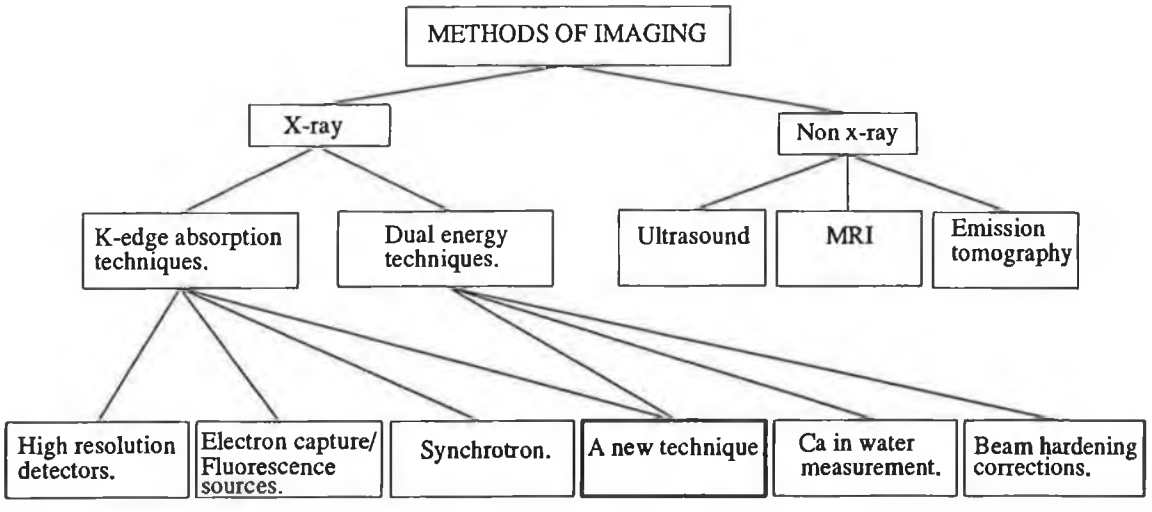

Figure 1.04
Overview of existing imaging techniques.

1.2.2 NON-XRAY TECHNIQUES OF IMAGING

Overview

The imaging methods described in this section do not contribute directly to the technique developed. However they demonstrate that there are many different material properties that can be imaged. The techniques described highlight some of the advantages and disadvantages of using x-ray imaging techniques.

Magnetic Resonance Imaging MRI

MRI imaging is a recent technique capable of imaging the distribution of hydrogen in the body. The patient is placed in a strong magnetic field (≅1T). The field is uniform across the plane to be imaged but the field reduces from the patient's head to toe. The field causes the protons to align with the field; this results in a longitudinal magnetisation. A small RF field disturbance is then produced at right angles to the body. The pulse causes the protons in the plane of interest to precess in phase and reduces the longitudinal magnetisation. After the RF pulse a horizontal field gradient is turned on across the body. A short duration vertical field gradient is also applied. The precessing protons re-emit RF at a frequency proportional to the field intensity [25][26]. The horizontal location of the re-emitted signal is obtained from the frequency of the re-emitted signal. The vertical location is determined by the phase of the signal. The amplitude of the signal at a given frequency is a measure of the proton density. Information required to produce an image is produced by taking the Fourier transform of the received signal. Information weighted towards longitudinal magnetisation recovery time or the time taken for the protons to lose phase may be obtained by using different pulse sequences [21]. The risk associated with imaging techniques that use ionising radiation are removed when MRI is used. MRI can be used to differentiate tissues that prove difficult to differentiate with conventional CT. Other nuclei can also be imaged using MRI. The nuclei must have an uneven number of protons and neutrons. ^{13}C, ^{19}F, ^{23}Na and ^{31}P can be imaged using MRI [21]. Specific clinical applications of these isotopes are described by Bligh et al [27]. A MRI image can take several minutes to be produced. The machine needs to be located where the field produced by the superconducting magnet will not interfere with other equipment and *vice versa*.

Emission computed tomography (ECT)

ECT scanners image the distribution of a radiopharmaceutical injected into the patient. There are two types of ECT: these are positron emission computerised tomography (PET) and single photon emission computed tomography (SPECT). To reduce patient dose, both techniques use isotopes with short half lives.

SPECT images the distribution of any gamma ray isotope injected into the body. The most commonly used isotope is technetium-99m [21]. This is used since it can be produced on site with a technetium generator. A collimated detector is used to measure the gamma ray intensity along each of the beam paths required to produce an image. Most systems use an array of collimated detectors to collect projection data simultaneously. The collimation makes the technique inefficient, since most of the photons emitted in the plane of interest are not detected. Data collection times are of the order of several minutes. Image resolution ranges from 10mm to 20mm [28]. These limitations make the study of certain physiological processes as difficult. Some gamma cameras provide SPECT imaging.

In PET the radioisotope contained in the radio -pharmaceutical is a short half-life positron emitter. The positrons produced by the source travel a short distance before they combine with an electron. The e^+ and e^- annihilation produces two 511keV gamma rays travelling in opposite directions. These can be detected in coincidence by a ring of detectors placed around the patient. The total count recorded by pairs of coincident detectors is used to produce the projection data for image reconstruction. The technique was developed by Phelps [29]. Some PET scanners use the gamma ray flight times to aid the location of the gamma ray source. The attenuation of the gamma rays by the body is corrected for by moving a point source of gamma rays around the patient. The PET scanner has been used to image brain chemistry and brain metabolism [34]. Many different pharmaceuticals have been labeled allowing the physiology of many organs to be studied. Since the detectors are placed around the patient

the PET scanner has a higher efficiency than SPECT. This would allow smaller doses to be administered or faster data collection times. It is, however, a very expensive technique. Each scanner needs to be located near a cyclotron and a pharmaceutical laboratory where short lived positron emitting isotopes can be produced.

Both forms of ECT require the inclusion of a radioactive tracer into the object being examined. Due to the risk of contamination, the use of unsealed radioactive sources requires care. The resolution of images produced by ECT are lower than that available with CT. Typical spatial resolution of a CT scanner is 1mm [20]. See figure 1.05 for a comparison of SPECT and PET.

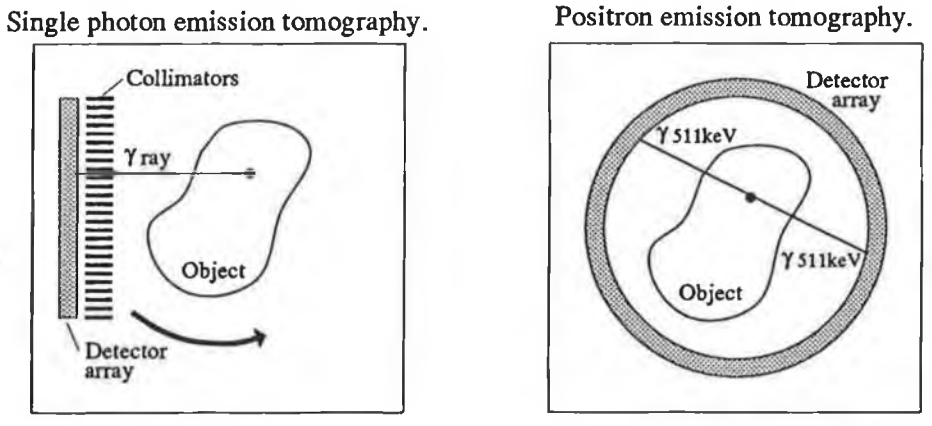

Figure 1.05
Schematic of SPECT and PET.

A technique of measuring element concentration by x-ray fluorescence was described by Morita et al [30]. A collimated x-ray beam was passed through the object. A collimated detector at an angle to the beam was used to measure the fluorescence at the point of intersection of the collimator paths. Pulse height analysis could separate the fluorescence counts associated with the elements of interest. The technique of image reconstruction based on this idea has been investigated by Hogan *et al* [31]. The technique requires a conventional absorption image to be made of the object before the fluorescence image can be reconstructed. X-ray fluorescence has been used clinically by Green *et al* to measure lead levels in the tibia [32]. This technique could measure lead concentration with precisions down to $\pm 5\mu g$ of lead per gram of bone mineral.

Ultrasound

Ultrasound images are produced by transmitting a pulse of ultrasound into the body. To reduce diffraction effects the wavelength of the ultrasound is chosen to be short in relation to the diameter of the transducer. The ultrasound propagates from the transducer as a parallel beam away from the transducer face. The signals reflected from different structures contained within the body are received by the same transducer. The time interval between transmitted and received signals is used to locate the structure. Images can be produced from the data collected by moving the transducer horizontally across the patient or by sweeping the beam through an arc at one fixed location [33].

Instead of moving a single transducer a linear array of transducers can be used to direct the ultrasound through the body. This is achieved by introducing a delay between the pulse sent to each transducer [34].

Ultrasound techniques can be used to image flow rate using the Doppler shift of the reflected signal [35]. (The multi-element imaging technique developed in this thesis may provide another method of imaging flow rate, this is discussed in appendix A). Contrast agents for ultrasonic imaging have been produced [36]. The high reflectivity of the contrast agent is produced by very small bubbles suspended in a liquid.

High intensity ultrasound can cause heating effects in biological material. However at the intensities used for imaging the technique poses no risk to the patient [37].

Neutron CT

A method of producing element specific CT images using a neutron source and detector was described by Overley [38]. The neutrons were produced using a pulsed deuteron accelerator (5MeV, 1nS, 0.5MHz). The deuterons strike a beryllium target where neutrons are produced.

$$^{9}_{4}Be + ^{2}_{1}D \longrightarrow ^{10}_{5}B + ^{1}_{0}n$$

The neutrons were detected with a liquid scintillation

detector. A time to amplitude converter synchronized with the neutron source was used to produce neutron flight time spectra for each beam path through the object. The relative contribution of each element to the spectra was determined. From this information element specific images were produced of a phantom containing a number of elements. The elements contained in the phantom were known.

X-ray and neutron attenuation as a function of atomic number are very different. Neutron radiography can produce images of organic compounds in thick metal cases; this would not be possible with x-rays. A review of neutron radiography by A. Spowart highlights these differences [39]. Clinical applications of neutron CT are restricted by the large radiation dose associated with the technique. The quality factor for neutrons is between 2.3 and 10 [40]. However boron neutron capture therapy (BNCT) is being investigated for clinical application. In this technique boron containing compounds are localized in cells that are to be destroyed. The high cross section for the boron neutron interaction increases the dose to cells containing boron [41].

1.2.3 ELEMENT SPECIFIC X-RAY IMAGING TECHNIQUES

Overview

Most elements contain a jump in their absorption spectrum called the K-edge. The position of the K-edge is different for each element. The origin and nature of this jump is discussed in section 2.1.2. Measurements made of the attenuation of x-rays at energies either side of this edge allow the amount of the element along the beam path to be determined. The measurement is independent of other elements contained in the object. By using these measurements instead of conventional projection data an image of element concentration can be reconstructed [42]. The quantitative imaging of elements has been investigated by McCarthy [43] and Fenelon [44]. A study of the imaging of different contrast agents was made by O'Hare [45]. A number of different methods of measuring x-ray attenuation either side of the K-edge have been developed.

Synchrotron X-ray source

The suitability of synchrotron radiation for CT imaging was first discussed by Grodzins [46]. A synchrotron produces x-ray radiation by accelerating electrons around a ring. Bremsstrahlung radiation is emitted by the electrons as they change direction [47]. The radiation is emitted in the plane of the electron orbit and is suitable for a fan beam CT geometry. The NSLS (National synchrotron light source, Brookhaven CA.) synchrotron fitted with a beam wiggler can be used to produce 30-90keV x-rays [48][49]. A monochromator is used to select the x-ray energy required. Element specific images may be produced by subtracting CT images produced with x-ray energies just above and below the K-edge of the element of interest. Using this technique an image of molybdenum distribution in a test object was produced by Suzuki [50]. An excised pig heart containing iodine contrast agent was imaged by Thomson [51]. Due to the synchrotron's large size the object needs to be rotated in the beam. This would reduce the clinical applications. The high cost and limited access to such machines reduces further the number of applications. At present there are about sixty synchrotron sources worldwide [52]. The clinical applications of synchrotron CT are being investigated by Dilmanian at the National Synchrotron Light Source in Brookhaven CA [53][54][55].

Radioactive/Fluorescence sources

Oldendorf developed an iodine specific method of measuring iodine equivalent thickness along a beam path [56]. In this technique x-rays were produced by exciting the $K\alpha_2$ and $K\alpha_1$ lines in lanthanum using an x-ray tube. These lines lie either side of the K-edge of iodine. The source was collimated and passed through a test object. The detector consisted of an inclined sheet of paper coated with sodium iodide. The $K\alpha_2$ x-rays (below the K-edge) passed through the iodine paper filter and were detected with a scintillation counter. The $K\alpha_1$ (above the K-edge) x-rays were photoelectrically absorbed by the filter, the

absorbed radiation was re-emitted as 28kV fluorescent radiation. This radiation was detected by a second scintillation counter. With this apparatus the differential absorption either side of the the K-edge could be measured and used to find the equivalent thickness of iodine in the beam path. The system has the advantage that pulse height discrimination is not required. However, the technique is specific to iodine only. High photon fluxes are difficult to obtain by x-ray fluorescence.

McCarthy and Fryar [42] imaged palladium using a Cd_{109} electron capture source of x-rays. The K_{α} and K_{β} lines of silver produced by the source lie either side of the K-edge of palladium. By measuring the attenuation of the K_{α} and K_{β} x-rays the amount of palladium along the beam path could be determined. The technique required a high energy resolution detector system to separate the K_{α} and K_{β} lines. There may not be an electron capture source available for an element of interest. The technique lacks versatility since only one element can be imaged.

McCarthy and Fryar [42] imaged caesium using fluorescent radiation from barium excited by an Am_{241} source. This also required a high energy resolution detector.

X-ray tube and high energy resolution detector

A method of imaging many elements simultaneously was developed by McCarthy and Fryar [57]. A filtered tube source of x-rays was used to produce a continuous x-ray spectrum. A high energy resolution detector system was used to measure the differential absorption across each K-edge of interest. CT techniques were used to reconstruct separate images of palladium, cadmium and silver distributed in a test object. This method is able to image many elements close together in the periodic table. No information concerning the composition of the body is required to make the measurements. However, the technique requires a high resolution detector and associated counting electronics.

1.2.4. IMAGING TECHNIQUES THAT USE POLYCHROMATIC ABSORPTION INFORMATION

Overview

The x-ray techniques described in section 1.2.3 require elaborate apparatus to extract the monochromatic information required to make attenuation measurements either side of the K-edge. When the composition of the object is restricted to a few components, it is possible to determine the contribution of each component by using absorption measurements made using a polychromatic source and a resolutionless detector system. These techniques are discussed in this section.

Dual energy scanning

The dual energy method of imaging involves switching the x-ray tube in a standard CT machine between two potentials. This changes the shape of the output spectrum of the tube. The human body is considered a two component mixture of calcium and water. Water and calcium have absorption curves that are shaped differently. Fractional transmittance (x-ray intensity transmitted / x-ray intensity incident) measurements are recorded at both tube potentials. The use of two measurements of fractional transmittance made at different tube potentials allows the relative contribution of calcium and water to be calculated using simultaneous equations. This technique was used by Kalender *et al* and subsequently Van Riet *et al* to produce images of bone mineral content [58][59][60]. The evaluation of the calcium content of bone currently being used to investigate osteoporosis. A review of the techniques available to measure bone mineral density has been made by Lang *et al* [61]. In practice a simpler technique is used for bone densitometry. This is done by comparing the CT numbers produced by imaging reference cells containing known concentrations of K_2HPO_3 and the image of the bone [62]. The errors associated with the dual energy technique were recently investigated by Gingold and Hasegawa [63].

A technique similar to dual-energy scanning was

described by Glantsching and Holliday. They used the technique to image germanium dopant contained in an optical fibre preform before it was collapsed [64].

An exact treatment of the dual-energy method in CT was made by Christ [65]. In this paper it was demonstrated that the dual-energy method could produce images of effective atomic number and electron density of the object.

Iodine imaging techniques

Hounsfield's original paper on CT [1] describes a simplified dual energy method of imaging iodine contrast agents. This was achieved by subtracting images recorded at 100kV and 140kV tube potential. This procedure will highlight regions containing high atomic number elements.

A method of imaging iodine using polychromatic source spectra was proposed by Riederer and Mistretta [66]. In this technique the body was assumed to be composed of three components. These were tissue, bone and iodine. The absorption for each component was described by a polynomial with four terms. The constants in the polynomials were obtained from measured transmissions of known bone, tissue and iodine combinations. The tube voltage was switched between three values. The measured transmissions at the three tube potentials could be used to generate three equations. These could then be solved for the relative values of tissue, bone and iodine thicknesses. A simulated reconstruction was achieved. All these techniques require absorption information characterising each component in the object being imaged.

1.2.5 BEAM HARDENING CORRECTIONS

Polychromatic x-ray beams are used in conventional CT machines. The low energy photons produced by the source are preferentially absorbed by the body. The reconstruction algorithms used assume the beam was monochromatic. This leads to artifacts in the image. The effect is called beam hardening. Beam hardening can be reduced by extracting monochromatic absorption information

from a number of polychromatic measurements. On commercial machines this is achieved by filtering the X-ray source and by mathematical correction of the fractional transmittance measurements [34].

Macovski and Alverez [67] described a dual energy technique that could be used to separate the Compton and photoelectric contributions to the absorption. This technique was based on the basic underlying physical processes involved in x-ray absorption. Instead of changing the tube potential they suggest using two different filters to change the spectral shape of the source. The use of a discriminator in conjunction with an energy dispersive detector is also suggested as a means of generating two populations of photons. Two constants describing the photoelectric and Compton scatter contributions to the absorption could be obtained from the transmission measurements. Different tissues could then be identified by the two constants. The two constants could also be used to infer absorption information at one specific x-ray energy and reduce the effect of beam hardening. This assumes that the body contains only low atomic number elements ($Z<20$). The method was tested by simulation.

1.3 AIMS OF THE PROJECT

The overall objective of the project was to develop an element specific imaging technique with the following properties.

1/ The technique must be able to image specific elements without knowledge of the composition of the object scanned. The only way of quantifying the thickness of a single element along a beam path, independently of other elements, was to measure the jump in absorption across a suitable absorption edge.

2/ The technique should be able to image a number of elements simultaneously and without modification to the apparatus. The techniques that use fluorescence sources and electron capture can only image one specific element. An x-ray tube produces x-rays over a range of energies that would allow a number of elements to be imaged.

3/ The system should use low resolution detector systems. The element specific techniques that use energy dispersive detector systems are suitable for first generation scanners. The use of low energy resolution detector arrays allows fast counting or analogue circuitry to be used. The cost and complexity of such detector arrays would be far less than an equivalent array with high energy resolution.

Chapter two describes in detail techniques that were developed to achieve the objectives stated above. The techniques bring together many of the concepts behind the dual-energy technique, beam hardening corrections and K-edge imaging already described in this chapter.

References

[1] Hounsfield, G.N.
"Computerized transverse axial (tomography): Part 1 Description of system"
Br. Jour. Radiology, Vol. 46, pp 1016-1022, 1973.

[2] Herman, G.T.
"Image reconstruction from projections : The fundamentals of computerized tomography"
Academic press, 1980.

[3] Natterer, F.
"The mathematics of computerised tomography"
John Wiley & Sons, 1986.

[4] Veklerov, E.
"On decision making in tomography: Extending computerization beyond image reconstruction"
IEEE Eng. in Med & Biol., pp 56-61, March 1993.

[5] Reimers, P. and Gilboy, W.B. and Goebbels, J.
"Recent developments in the industrial application of computerized tomography with ionizing radiation"
NDT International, Vol. 17, No. 4, pp 197-207, 1984.

[6] Dickin, F.J.
"Tomographic imaging of industrial process equipment: techniques and applications"
IEEE Proc.-G, Vol. 139, No. 4, pp 72-81, 1992.

[7] Burnstein, P. et al.
"The largest and smallest x-ray computed tomography systems"
Nucl. Inst. & Meth., Vol. 221, pp 207-212, 1984.

[8] Onoe, M.
"Computed tomography for measuring the annual rings of a live tree"
Nucl. Inst. & Meth., Vol. 221, pp 213-220, 1984.

[9] Nusshardt, R. et al
"Microtomography: A tool for nondestructive study of materials"
Synchrotron Radiation News, Vol. 4, No. 3, pp 21-23 1991.

[10] Spanne, P. and Rivers, M.L.
"Computerized microtomography using synchrotron radiation from the NSLS"
Nucl. Inst. & Meth., Vol. B24/25, pp 1063-1067, 1987.

[11] Elliott, J.C. and Dover, S.D.
"X-ray microscopy using computerized axial tomography"
Jour. of Microscopy, Vol. 138, Pt. 3, pp 329-331, 1985.

[12] Roentgen, W.K.
"On a new form of radiation"
The Electrician Jan 24 1896, pp 415-417.

[13] Coolidge, W.D.
"A powerful Roentgen ray tube with pure electron discharge"
The Physical Review Vol. 2,No. 6, pp 409-430, 1913.

[14] Gifford, D.
"A handbook for radiologists and radiographers"
Wiley & Sons, 1984.

[15] Bocage, E.M.
Patent No. 536,464 Paris, France.
(Quoted in Brooks and Di Chiro "Principles of Computer assisted Tomography in radiographic and radioisotopic imaging" Phys. Med. Biol. Vol. 21, No. 5, pp 689-732 1976).

[16] Bracewell, R.N.
"Strip integration in radio astronomy"
Aust. Jour. Phys., Vol. 9, No. 2, pp 198-217, 1956.
(Quoted in Brooks and Di Chiro "Principles of Computer assisted Tomography in radiographic and radioisotopic imaging" Phys. Med. Biol. Vol. 21, No. 5, pp 689-732 1976).

[17] Oldendorf, W.H.
"Isolated flying-spot detection of radiodensity discontinuities; displaying the internal structural pattern of a complex object"
IRE Trans. Bio-Med. Elect., BME-8, pp 68-72, 1961.
(Quoted in Brooks and Di Chiro "Principles of Computer assisted Tomography in radiographic and radioisotopic imaging" Phys. Med. Biol. Vol. 21, No. 5 pp 689-732 1976).

[18] Cormack, A.M.
"Representation of a function by its line integrals, with some radiological applications"
J. Appl. Phys., Vol. 34, pp 2722-2727, 1963.

[19] Ambrose, J.
"Computerized transverse axial scanning (tomography): Part2. Clinical application"
Br. Jour. Radiology, Vol. 46, pp 1023-1047, 1973.

[20] Shimadzu SCT-3000T, Technical reference manual.

[21] Webb, S.
"The physics of medical imaging"
Adam Hilger, 1988.

[22] Boyd, P.D. and Lipton M.J.
"Cardiac computed tomography"
Proc. of the IEEE, Vol. 71, No. 3, pp 298-307, 1983.

[23] Soucek, M. et al.
"Spiral-CT:A new volume scanning technique"
Rontenpraxis, pp 1-21, 1990.

[24] Kalender, W.A. et al.
"Spiral Voulmetric CT with Single-Breath-Hold Technique, Continuous Transport, and Continuous, Scanner rotation"
Thoracic Radiology, pp 181-183, 1990.

[25] Schild, H.H.
"MRI made easy (...well almost)"
Schering AG Berlin, ISBN 3-921817-41-2, 1990.

[26] Chen, C.N. and Hoult, D.I.
"Biomedical magnetic resonance technology"
Adam Hilger, 1989.

[27] Bligh, A. and Sadler, P.
"Labels and contrast agents in biomedical magnetic resonance spectroscopy and imaging"
IPSM report No. 60, pp 71-82, 1987.

[28] Knoll, G.F.
"Single photon emission computed tomography"
Proc. of the IEEE, Vol. 71, No. 3, pp 320-329, 1983.

[29] Phelps, M.E. et al
"Application of annihilation coincidence detection to transaxial reconstruction tomography"
Jour of Nucl. Med., Vol. 16, No. 3, pp 211-225, 1974.

[30] Morita, Y.
"Simultaneous quantitation of seven elements by an x-ray fluorescence system for the microsphere method"
IEEE Trans. on Nucl. Sci., Vol. 36, No. 1, pp 978-982, 1989.

[31] Hogan, J.A. and Gonsalves, R.A. and Krieger S.A.
"Fluorescent Computer Tomography: A Model for Correction of X-ray Absorption"
IEEE Trans. Nucl. Sci., Vol. 38, No. 6, pp 1721-1727 1991.

[32] Green, S.
"An enhanced sensitivity K-shell fluorescence technique for tibial lead determination"
Phys . Med. Biol., Vol.38, pp 389-396, 1993.

[33] Macovski, A.
"Medical imaging systems"
Prentice-Hall, New Jersey, pp 173-224, 1983.

[34] Krestel, E.
"Imaging systems for medical diagnostics"
Siemens, 1990.

[35] Evans, D.
"Doppler Ultrasound signals from blood flow"
Physics in Medical Ultrasound,
IPSM, report No. 47, pp 119-126, 1986.

[36] Schlief, R.
"First steps in ultrasound contrast media"
Contrast media from the past to the future : symposium Berlin, 27th March, 1987. Schering. Ed. by R. Felix. pp 179-187.

[37] Hussey, M.
"Diagnostic ultrasound, an introduction to the interactions between ultrasound and biological tissue"
Blackie, 1975.

[38] Overley, J.C.
"Element-sensitive computed tomography with fast neutrons"
Nucl. Inst. & Meth., Vol. 24/25, pp 1058-1062, 1987.

[39] Spowart, A.R.
"Neutron Radiography"
Jour. of Phys. E: Sci Inst., Vol 5, pp 497-510, 1972.

[40] Martin, A. and Harbinson, S.
"An introduction to radiation protection"
Chapman and Hall, 1982.

[41] Orn-Anong et al.
"Quantitative neutron capture radiography for boron in biological samples"
Phys. Med. Biol., Vol. 38, pp 1089-1097, 1992

[42] Fryar, J. and McCarthy, K. and Fenelon A.
"Differential x-ray absorptiometry applied to computerised x-ray tomography"
Nucl. Inst. and Meth., Vol. A259, pp 557-565, 1987.

[43] McCarthy K.J.
"A study of the imaging of atomic elements by computerised axial tomography"
Ph.D. Thesis, Dublin City University, 1989.

[44] Fenelon, A.G.R.
"A X-ray scanning machine for imaging atomic elements"
M.Sc. Thesis, Dublin City University, 1988.'

[45] O'Hare, N.J.
"A study of the imaging of contrast agents for use in computerised tomography"
Ph.D. Thesis, Dublin City University, 1991.

[46] Grodzins, L.
"Optimum energies for x-ray transmission tomography of small samples"
Nucl. Inst. & Meth. , Vol. 206, pp 541-545, 1982.

[47] Read, F.H.
"Electromagnetic radiation"
John Wiley & Sons., 1980.

[48] Svanberg, S.
"Atomic and molecular spectroscopy"
Springer verlag, pp 95-99, 1991.

[49] Personal communication.

[50] Susuki, Y. et al.
"X-ray Computerised Tomography using monochromated synchrotron radiation"
Japanese Jour. App. Phys., Vol. 27, No. 3,
pp L461-L464, 1988.

[51] Thomson, A.C. et al.
"Computed tomography using synchrotron radiation"
Nucl. Inst. Meth., pp 319-323, 1984.

[52] Winick, H. and Williams, G.P.
"Overview of synchrotron radiation sources world-wide"
Synchrotron Radiation News, Vol. 4, No. 5, 1991.

[53] Dilmanian, F.A. et al
"Monochromatic computed tomography of the human brain using synchrotron X-rays: technical feasibility"
Nuc. Inst. Meth., Vol. A319, No.1-3,pp 305-310, 1992

[54] Zeman, H.D. and Dilmanian, F.A. et al.
"An x-ray monochromator for dual-energy computerized tomography using synchrotron radiation"
Nuc. Inst. Meth., Vol. B56-57, pp 1218-1222, 1991.

[55] Dilmanian, F.A. et al
"Computed tomography with monochromatic X -rays from the National Synchrotron Light Source"
Nuc. Inst. Meth., Vol. B56-57, pp 1208-1213, 1991.

[56] Oldendorf, W.H. et al.
"An inherently stable system for measuring tissue iodine using its K-absorption edge"
American Jour. Roentgenology., Vol. 120, No. 3,
pp 583-588, 1974.

[57] Fryar, J. and McCarthy, K. and Fenelon A.
"Multielement imaging in computerised x-ray computerised tomography"
Nucl. Inst. and Meth., Vol. A259, pp 557-565, 1987.

[58] Kalender, W.A. et al.
"Evaluation of a prototype dual-energy computed tomography apparatus. I. Phantom studies"
Med. Phys., Vol. 13, No. 3, 1986.

[59] Kalender, W.A. et al.
"Evaluation of a prototype dual-energy computed tomography apparatus. II. Determination of vertebral bone mineral content"
Med. Phys., Vol. 13, No. 3, 1986.

[60] Van Riet, B. et al.
"Basic methods in quantitative CT"
JBR-BTR, Vol. 69, pp 423-430, 1986.

[61] Lang, P. et al.
"Osteoporosis, current techniques and recent developments in quantitative bone mineral densitometry"
Radiol. Clin. of North America, Vol. 29, No. 1, pp 49-76, 1992.

[62] Karantanas, A.H. et al.
"Quantitative computed tomography for bone mineral measurement: technical aspects, dosimetry, normal data and clinical applications"
Brit. Jour. Rad., Vol. 64, pp 298-304, 1991.

[63] Gingold, E. and Hasegawa, B.
"Systematic bias in basis material decomposition applied to quantitative dual-energy x-ray imaging"
Med. Phys.,Vol. 19, No. 1, pp 25-32, 1992.

[64] Glantschnig, W.J. and Holliday, A.
"Mass fraction profiling based on x-ray tomography in application to characterizing porous silica boules"
App. Optics, Vol. 26, No. 6, pp 982-989, 1987.

[65] Christ G.
"Exact treatment of the dual-energy method in CT using polyenergetic x-ray spectra"
Phys. Med. Biol., Vol. 9, No. 12, pp 1501-1510, 1984.

[66] Riederer, S.J. and Mistretta, C.A.
"Selective iodine imaging using K-edge energies in computerized x-ray tomography"
Med. Phys., Vol. 4, No. 6, pp 474-481, 1977.

[67] Macovski, A. and Alvarez, R.E. et al.
"Energy dependent reconstruction in x-ray computerised tomography"
Comput. Biol. Med., Vol. 6, pp 325-336, 1976.

Chapter 2.

Theoretical background.

Introduction

The basic experimental configuration used for the techniques developed in this work consisted of an x-ray source, absorber and detector. See figure 2.01

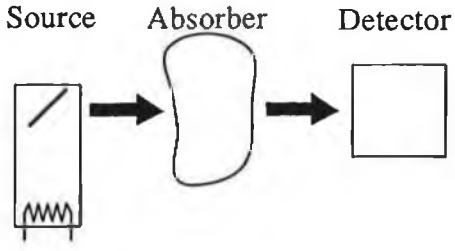

Figure 2.01
Basic experimental configuration.

In this chapter the physical processes involved in the generation of x-rays by an x-ray tube is described. A method of describing the absorber in terms of a few simple parameters is then developed. The operation and response of a number of relevant detectors is also discussed. These concepts are then brought together to produce two techniques for evaluating the absorption parameters. The first is called the total count method; the second, a refinement of the first, is called the tracking discriminator technique. Using the absorption parameters, a method of quantifying the amount of one element contained in the absorber along any x-ray beam path is then described.

Finally, using a standard CT reconstruction algorithm the technique is extended to a method of producing element specific images.

2.1 EXAMINATION OF THE PHYSICAL PROCESSES INVOLVED

2.1.1 X-RAY TUBE OUTPUT AS A FUNCTION OF TUBE POTENTIAL

The construction of a typical modern x-ray tube is shown in figure 2.02. The tube consists of an evacuated glass vessel. A heated filament is used to produce electrons by thermionic emission. The electrons are accelerated through a potential difference V_t and then strike the target. The target is normally made of a high melting point material such as tungsten or molybdenum and is usually water cooled. The x-rays produced at the target are allowed exit the tube via a beryllium window. The entire system is shielded to prevent the operator being exposed to x-rays. Stationary anode tubes operate with power dissipations up to approximately 5kW [1].

The construction of a high output x-ray tube is different. The anode consists of a beveled disc of rhenium-tungsten-molybdenum alloy mounted on a molybdenum or graphite base. The disk is rotated to reduce the mean power dissipation on the target surface. The base is a heat sink that must be allowed to cool after period of operation [1]. Rating charts are provided with a tube to enable the calculation of allowed dissipation for a given period of time [2][3]. Typically in pulsed mode such tubes can operate at 15kW [4].

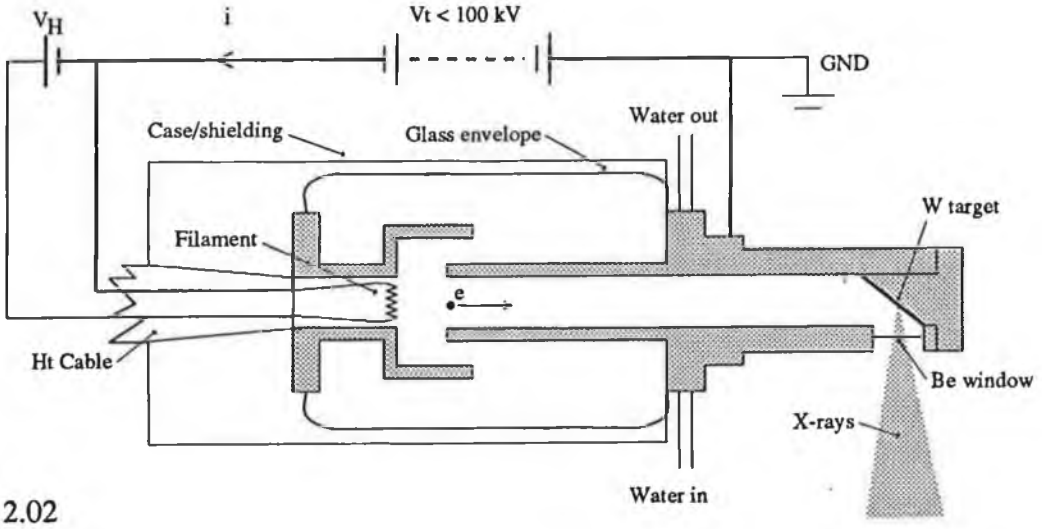

Figure 2.02
X-ray tube of the type used.

The output spectrum of the x-ray tube consists of a continuous spectrum on which is superimposed a series of lines. See figure 2.03.

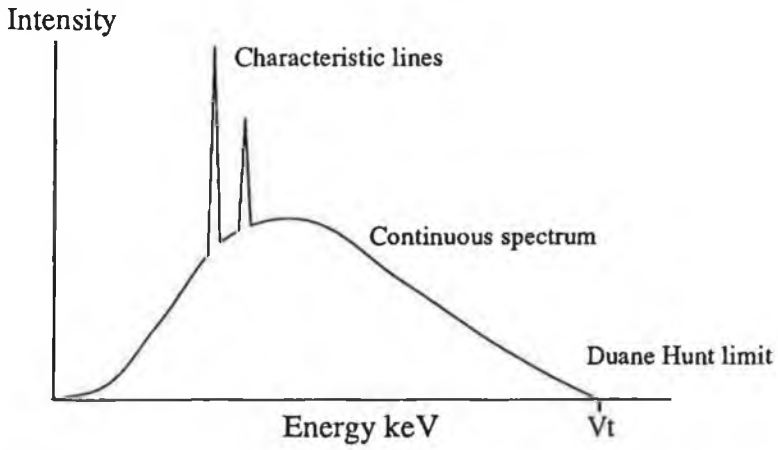

Figure 2.03
Features of the spectral output of an x-ray tube.

The continuous spectrum is produced by inelastic Rutherford scattering of the accelerated electrons as they pass near the target atoms [5]. They give up their kinetic energy as x-ray photons. About 0.5 - 1% of electrons interact with the target in this way [6]. The maximum energy of an x-ray photon produced will be equivalent to the energy of the electrons incident on the target. Thus

$$E = e\ V_t \qquad (2.01)$$

where e is the charge on the electron, V_t is the tube potential and E is the maximum x-ray energy produced. This upper limit to the continuum is called the Duane-Hunt law [6]. X-ray energy is normally measured in eV or keV. A popular function used to describe the continuous x-ray spectrum is Kramer's equation [7].

$$I_\lambda\ d\lambda = k\ i\ Z \left(\frac{1}{\lambda} - \frac{1}{\lambda_{min}} \right) \frac{1}{\lambda^2}\ d\lambda \qquad (2.02)$$

where λ is the x-ray wavelength, λ_{min} is the shortest wavelength produced, i is the tube current, k is a tube activity constant and Z the atomic number of the target. This equation is produced by considering the interaction of the electron with successive layers of the target.

Since

$$\lambda = \frac{h\ c}{e\ E} \qquad (2.03) \qquad d\lambda = -\frac{h\ c}{e\ E^2}\ dE \qquad (2.04)$$

Kramer's equation, when rewritten in terms of energy, becomes

$$I_E \, dE = k' \, Z \, i \, (V_t - E) \, dE \qquad (2.05)$$

This shows that, at any x-ray energy, the intensity of continuum radiation is proportional to the tube current. This is because the number of electrons striking the target is determined by the tube current. The intensity of x-rays with energies below the Duane Hunt limit increases with increasing tube potential. As such, Kramer's equation produces many of the response features of an x-ray tube. However, many effects, such as reabsorption of x-rays produced in the deeper layers of the target, the ripple present on the supply to most x-ray tubes and the absorption caused by the beryllium window, are not accounted for. A comparison of the spectral output of tubes operating with different types of power supply was recently carried out by Matsumoto *et al* [8].

The lines in the spectrum are produced when the accelerated electrons interact with the inner electrons of the target atoms. The target atom then de-excites with the emission of a photon characteristic of the shell from which the electron was expelled. K and L lines of the target material may be present in the x-ray tube spectrum. See figure 2.04. The main lines produced by a tungsten tube operating over 70kV are $K_{\alpha 1}$ = 59.32keV, $K_{\alpha 2}$ = 57.98keV and $K_{\beta 1}$ = 67.24keV [9].

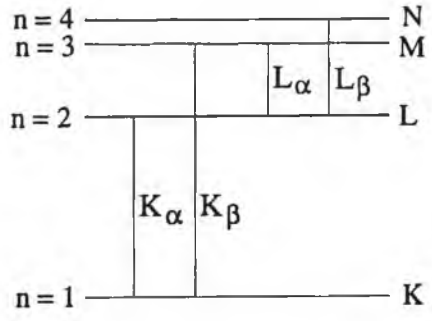

Figure 2.04
Electron energy levels in the target atom.

The wavelength of the characteristic lines can be predicted roughly by the Bohr formula as long as the shielding of the nucleus by inner orbits is taken into account [10].

$$\frac{1}{\lambda} = R\ (Z - S)^2 \left(\frac{1}{n_2^2} - \frac{1}{n_1^2} \right) \qquad (2.06)$$

where n_2 and n_1 are the principal quantum numbers of the shells through which the electron is de-exciting, R is the Rydberg constant, S is a factor which corrects for the screening of the atomic charge by inner electrons. S = 1 for the K_α line.

The limitations of Kramer's equation, and other functions like it, coupled with the presence of characteristic lines means that the only reliable way of accurately describing the output of an x-ray tube is to record the x-ray spectrum at a number of different tube voltages and use software to interpolate the response of interest.

2.1.2. X-RAY ABSORPTION PROCESSES

The attenuation of a monochromatic collinear x-ray beam by an absorber may be described by Beer's law [6].

$$I = I_0 \exp -\mu x \qquad (2.07)$$

where I_0 is the incident x-ray intensity, I the transmitted intensity and x is the thickness of the absorber. μ is the linear attenuation coefficient which is a measure of the absorption per unit thickness.

Two new terms need to be introduced which will simplify the following work [6]. Re-writing 2.07 gives

$$I = I_0 \exp -\left(\frac{\mu}{\rho}\right)(\rho x) = I_0 \exp - U\ t \qquad (2.08)$$

where ρ is the density of the absorber.

The term μ/ρ is referred to as the mass attenuation coefficient U. The mass attenuation coefficient is the absorption per unit mass per unit area (m^2/kg); it is an atomic property of each element independent of its state or physical aggregation. The term ρx is referred to as the equivalent thickness or area concentration t.

$$t = \rho x \quad kg/m^2 \qquad (2.09)$$

There are three absorption processes which will attenuate a collinear x-ray beam. These are

1. Pair production U_{Pair}
2. Photoelectric absorption U_{Photo}
3. Scatter $U_{Scatter}$

The total absorption of a material will be the result of the sum of these absorption processes, i.e.

$$U_{Absorber} = U_{Pair} + U_{Photo} + U_{Scatter} \qquad (2.10)$$

Each of these processes will be considered separately. They will then be brought together to produce a model that can describe any x-ray absorber.

Pair production occurs when a photon with sufficient energy passes close to an atomic nucleus. This results in the conversion of the photon to an e^+ and e^-. Since the rest mass energy of the electron is 0.511 MeV, the threshold photon energy for pair production is 2 x 0.511 MeV = 1.022 MeV [11]. This energy exceeds the maximum energy of the x-rays used in the experiment by an order of magnitude and so does not contribute to the absorption.

$$U_{Pair} = 0 \qquad E < 1.022\text{MeV} \qquad (2.11)$$

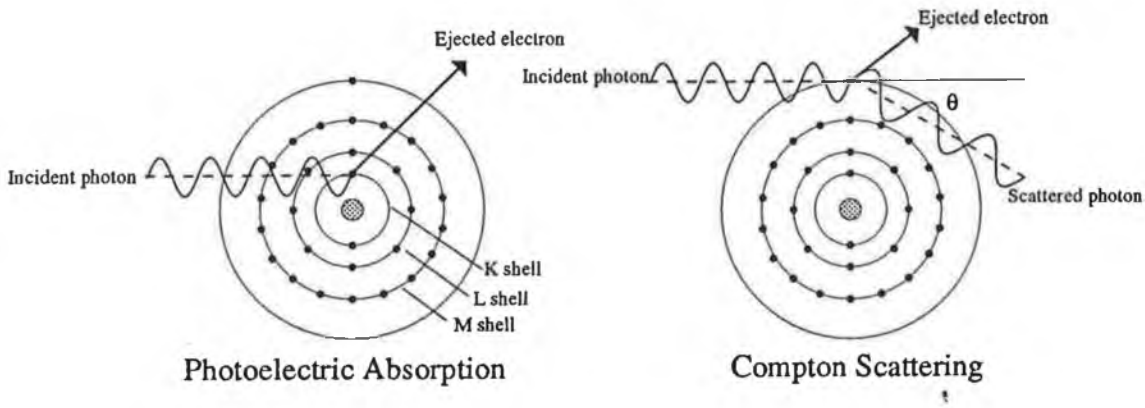

Figure 2.05
Photoelectric absorption and Compton scatter.

Photoelectric absorption is due to the ejection of atomic electrons from an atom. See figure 2.05. It is a significant absorption process for the x-ray energies used. There exists a minimum photon energy that will expel an electron from an atomic level. Therefore, the absorption

is due to the sum of absorptions for each level with which the photon can interact. There is a marked increase in x-ray absorption as the binding energy of a level is exceeded by the x-ray due to the inclusion of the absorption of a new level. This jump in absorption is referred to as an edge [6][11]. The principal edges are produced by the K and L levels within the atom. Equation 2.06 and 2.03 could be used to show how the position of these edges vary with atomic number. The K-edge energy for each element is different; it is this property of x-ray absorbers that allows element specific imaging to be achieved. Table 2.01 lists the K-edge energies for some elements relevant to this project.

At. No.	Element	K-edge keV.	At. No.	Element	K-edge keV.	At. No.	Element	K-edge keV.	At. No.	Element	K-edge keV.
42	Mo	20.002	53	I	33.168	64	Gd	50.207	75	Re	71.670
43	Tc	21.048	54	Xe	34.551	65	Tb	51.965	76	Os	73.869
44	Ru	22.123	55	Cs	35.966	66	Dy	53.761	77	Ir	76.111
45	Rh	23.229	56	Ba	37.414	67	Ho	55.593	78	Pt	78.400
46	Pd	24.365	57	La	38.894	68	Er	57.464	79	Au	80.729
47	Ag	25.531	58	Ce	40.410	69	Tm	59.374	80	Hg	83.109
48	Cd	26.727	59	Pr	41.958	70	Yb	61.322	81	Tl	85.532
49	In	27.953	60	Nd	43.538	71	Lu	63.311	82	Pb	88.008
50	Sn	29.211	61	Pm	45.152	72	Hf	65.345	83	Bi	90.540
51	Sb	30.499	62	Sm	46.801	73	Ta	67.405	84	Po	93.113
52	Te	31.817	63	Eu	48.486	74	W	69.517	85	At	95.730

Table 2.01
Table of K-edge energies.

Between the absorption edges, the absorption may be described by the Bragg Pierce Law [6].

$$U_{Photo} = k' Z^4 \lambda^3 \qquad (2.12)$$

where Z is the atomic number of the absorber, and λ the x-ray wavelength. k' is constant between edges. Since

$$E = \frac{hc}{\lambda} \qquad (2.13)$$

$$U_{Photo} = \frac{k Z^4}{E^3} \qquad (2.14)$$

where the constants h,c and k' are absorbed into a new constant k. For a compound, the total photoelectric absorption will be

$$U_{Photo} = \frac{k_1 Z_1^4}{E^3} + \frac{k_1 Z_2^4}{E^3} + ... = \frac{\alpha'}{E^3} = \alpha' \; P(E) \qquad (2.15)$$

where α' is a constant for the compound and

$$P(E) = 1/E^3 \qquad (2.16)$$

Scatter may be subdivided into elastic or Rayleigh scattering and inelastic or Compton scattering. Compton scattering is due to the interaction of the outer electrons of the atom with the x-ray photon. See figure 2.05. This results in the recoil of the electron and a reduction in the x-ray energy. Since the x-ray is deviated from the collinear beam, it is effectively lost. The change in wavelength of the x-ray photon is given by [12]

$$\Delta\lambda = \frac{h}{m_e c} [1 - \cos \theta] \qquad (2.17)$$

and written in terms of energy becomes

$$E' = \frac{E}{1 + \frac{E}{m_e c^2} [1 - \cos \theta]} \qquad (2.18)$$

where E' is the scattered x-ray energy, E the incident x-ray energy and θ the photon scattering angle.

The scattered electron will have an energy given by

$$E_{electron} = E - E' \qquad (2.19)$$

The relative proportion of Compton scatter increases with increasing x-ray energy or reducing atomic number. The Klein-Nishina formula may be used to describe the cross section for Compton scatter and so infer the absorption [13].

$$S(x) = \frac{1+x}{x^2} \left[\frac{2(1+x)}{1 + 2x} - \frac{1}{x} \ln(1+2x) \right] +$$

$$+ \frac{1}{2x} \ln(1 + 2x) - \frac{(1 + 3x)}{(1 + 2x)^2} \qquad (2.20)$$

where

$$x = \frac{E}{510.975keV} \qquad (2.21)$$

$$U_{Scatter} = \beta' \, S(E) \qquad (2.22)$$

The total absorption of any absorber may be described in terms of the Compton and photoelectric absorption only. Substituting 2.11, 2.15, and 2.22 in 2.10 gives

$$U_{absorber} = \alpha' \, P(E) + \beta' \, S(E) \qquad (2.23)$$

If the absorber has an equivalent thickness t then applying Beer's law,

$$U_{absorber} \, t = \ln\left(\frac{I(E)_0}{I(E)}\right) = \alpha \, P(E) + \beta \, S(E) \qquad (2.24)$$

where $\alpha = \alpha' t$ (2.25)

and $\beta = \beta' t$. (2.26)

Between edges the absorber may be described using 2.24.

To describe an absorber over an energy range containing a number of edges requires a different value of α for each interval. β remains constant. Thus to describe an absorber containing two K edges would require three values of α and a single value of β.

A graph of the photoelectric, P(E), and scattering, S(E), functions is shown in figure 2.06.

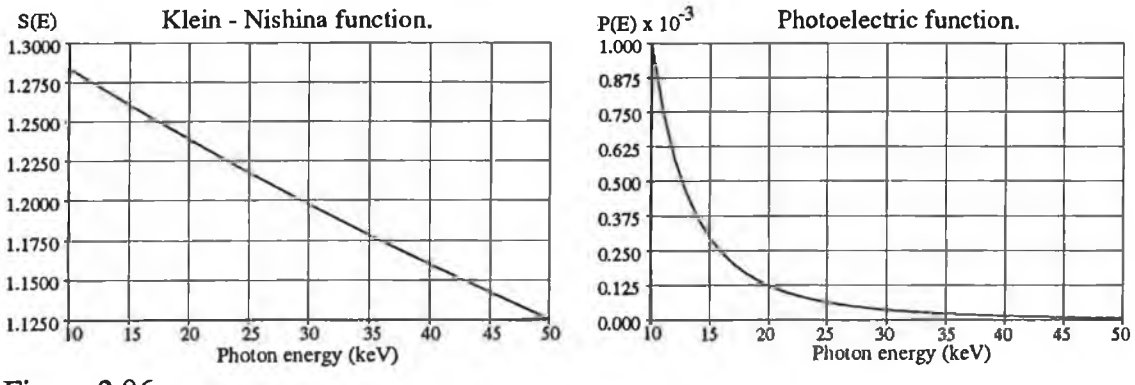

Figure 2.06
Graphs of photoelectric absorption and scatter absorption functions.[1]

There are a number of processes which cause a broadening of the K-edge. These include the elevation of a K electron to the Fermi level in a metal, fine structure due to neighbouring atoms, valence state and short range order and lattice and temperature effects [6]. Typically the edge can have a width of up to 200 eV. A detailed

account of the origin of the K-edge broadening is given by Koningsberger and Prins [14].

2.1.3 DESCRIPTION OF DETECTOR'S RESPONSE

For work on this project three detectors were available. These were the lithium drifted silicon detector, the scintillation detector and the gas proportional detector.

The Si(Li) detector is a pn junction device with a large depletion region. It is formed by diffusing and drifting lithium, an n type dopant, into a block of p type silicon crystal. Gold ohmic contacts are deposited on the front and back of the device [15]. Since lithium will rediffuse, the detector needs to be maintained at a low temperature. The low temperature also reduces detector and preamplifier noise. Cooling is achieved using a copper spine in a flask of liquid nitrogen. The device is contained in an evacuated chamber which prevents condensation forming. A thin beryllium window allows x-rays to enter the chamber with minimum attenuation. See figure 2.07.

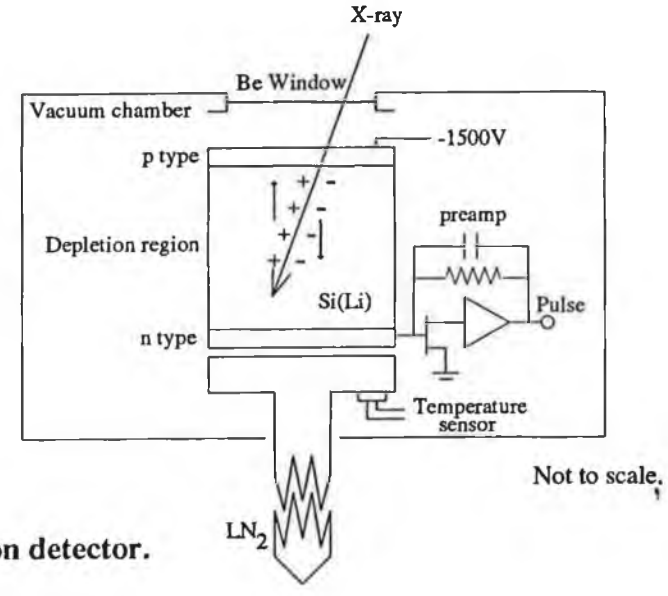

Figure 2.07
Lithium drifted silicon detector.

An x-ray incident on the detector may be absorbed photoelectrically by a silicon atom. The photoelectron produced then generates electron-hole pairs until it has expended all its kinetic energy. To produce each electron hole pair requires 3.8eV [15]. The electron-hole pairs are swept across the depletion region by the electric field

provided by the reverse-bias potential. The number of electron-hole pairs produced is proportional to the x-ray energy. With suitable amplification the charge collected, and so the pulse height, will be directly proportional to the incident x-ray energy. The beryllium window reduces efficiency at low energies. High energy efficiency is reduced due to the reduction in the likelihood of an interaction. Figure 2.08. shows the efficiency curve for different thickness Si(Li) detectors, with different thickness beryllium windows [16].

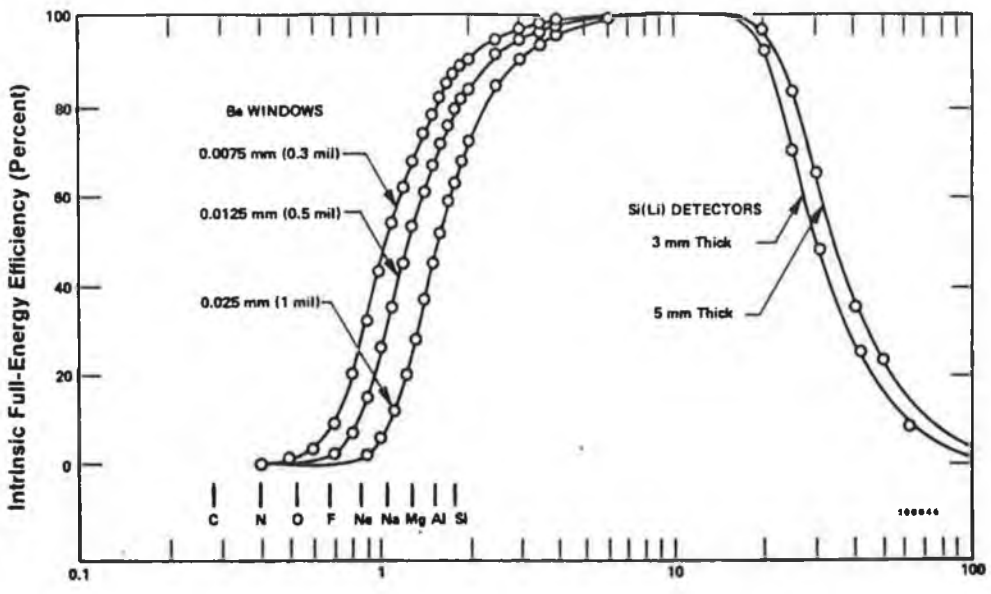

Figure 2.08
Si(Li) detector efficiency as a function of x-ray energy for different beryllium window thicknesses.

The scintillation detector consists of two components; the scintillator and the photomultiplier tube. See figure 2.09.

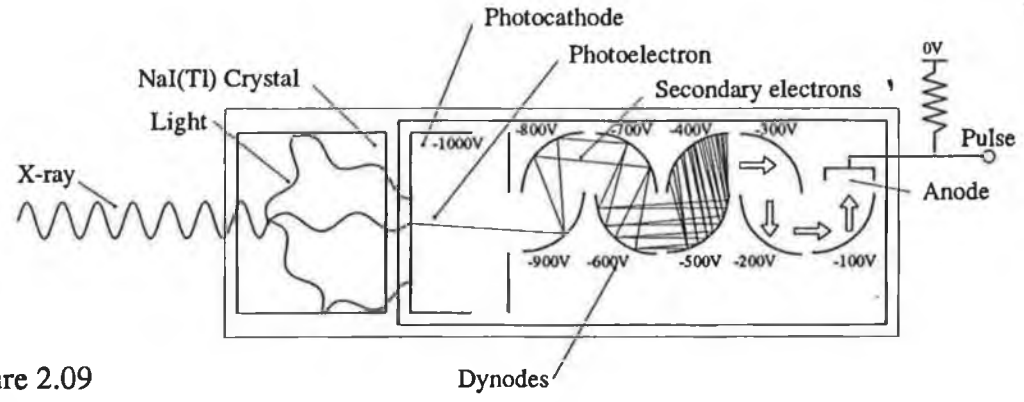

Figure 2.09
Scintillation detector.

Scintillators are materials which produce light when ionizing radiation passes through them. Although there are many different types of scintillator, they may be divided into three main groups. These are inorganic, organic and gaseous.

Typical of the inorganic scintillator is the thallium activated sodium iodide crystal NaI(Tl). The detector used in this project contained this scintillator. The incident x-ray may eject a photoelectron from an atom in the phosphor. The photoelectron loses its kinetic energy by exciting electrons to the conduction band in the crystal. The holes and electrons produced excite the activator atom (thallium). When the activator de-excites it emits radiation detectable by a photomultiplier tube. The number of photons produced by the scintillator is proportional to the energy of the incident x-ray. However the x-ray may also be photoelectrically absorbed by the K or L shell of the phosphor atom. The phosphor atom then de-excites with the emission of a K or L photon. It is probable that this photon may not be reabsorbed. The photoelectron will then produce a number of photons equivalent to the energy of the x-ray less the K or L photon energy. With a monochromatic source this produces a second peak in the spectrum called the escape peak [6].

The incident x-ray may also be Compton scattered by the scintillator. The scattered electron can have an energy up to a limit set by equation 2.19 when the photon is scattered through 180°. This leads to a continuum in the pulse height spectrum; the high energy limit of this continuum is called the Compton edge.

Since detector efficiency depends on the scintillator's absorption, the K-edge of the iodine in the phosphor could introduce a jump in efficiency in a region where the device is being operated. This is overcome by making the scintillator thick enough to absorb nearly all radiation incident on it. The scintillation or flash of light produced by the scintillator is then detected by a photomultiplier tube. Efficient coupling of the light produced to the detector is required. This is achieved by

coating the scintillator with a reflective surface and using index matching fluid to couple it to the photomultiplier tube window.

The light ejects photoelectrons from the photocathode of the photomultiplier tube. These electrons are accelerated toward the first dynode. They eject a number of secondary electrons from this dynode. These in turn accelerate to the next dynode and so on. A large number of electrons are collected at the anode, producing a pulse proportional to the intensity of the flash of light. Scintillation detectors have low energy resolution, with a pulse height spectrum that may be complicated by escape-peaks and Compton scatter.

Detectors that use a photodiode use CsI(Tl) scintillators. This material has a slightly higher absorption coefficient per unit size than NaI(Tl) and emits light at a wavelength suitable for detection with a photodiode [17].

The gas proportional detector consists of a cylindrical metal cavity along the centre of which runs a thin wire. The cavity is filled with a mixture of 90% argon and 10% methane (other gases may be used as well). A thin window allows the x-rays to enter the detector region unattenuated. See figure 2.10.

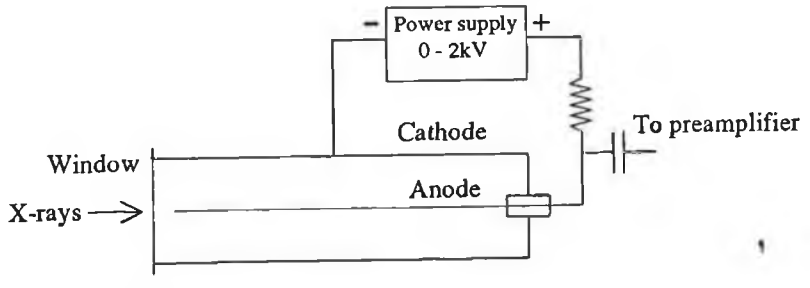

Figure 2.10
Gas proportional detector.

The x-ray may eject a photoelectron from the gas atom. The photoelectron then loses its energy by ionizing gas atoms with which it interacts. The electrons produced are accelerated by the anode cathode potential and can cause

secondary ionization. This is called gas amplification. The total collected charge is proportional to the x-ray energy. This type of detector has better resolution than the scintillation detector. A comparison of the relative resolution of the three detectors is shown in figure 2.11.

The difference in energy resolution between the three basic types of detector was studied by Finch and Delaney [18]. The scintillation detector produces an electrical pulse in a three stage process. This is x-ray absorption and the emission of UV photons from the scintillator, then the production of electrons at the photocathode and finally dynode amplification in the photomultiplier. The proportional counter is a two stage process. The first is the production of ion pairs by the photoelectron, the second stage gas amplification. The semiconductor detector detectors produces a pulse directly related to the number of electron hole pairs produced. It is by considering each stage required to produce the electrical pulse that the resolution of the detector can be evaluated. This is treated in detail by Finch and Delaney [18].

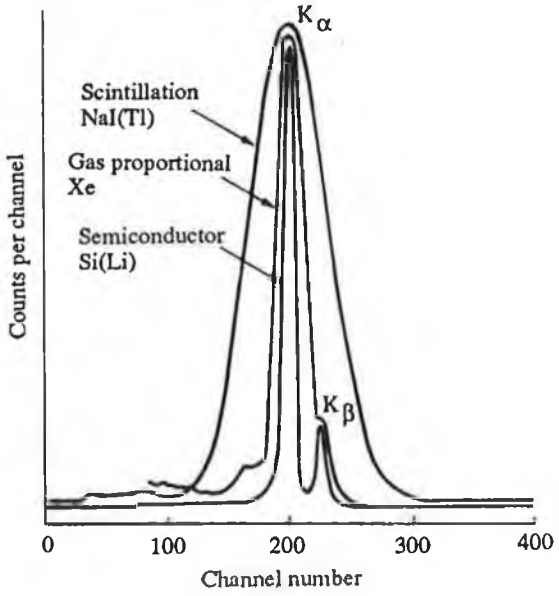

Figure 2.11
Comparison of the resolution of three detectors [15].
(Fe fluorescence K_α= 6.40 keV, K_β= 7.06 keV).

2.2 DIFFERENTIAL ABSORPTIOMETRY

In this section a method of measuring analyte equivalent thickness is developed. The method of differential absorptiometry was first described by Glocker and Frohnmeyer [19] and was subsequently used by McCarthy and Fryar for element specific imaging [20][21].

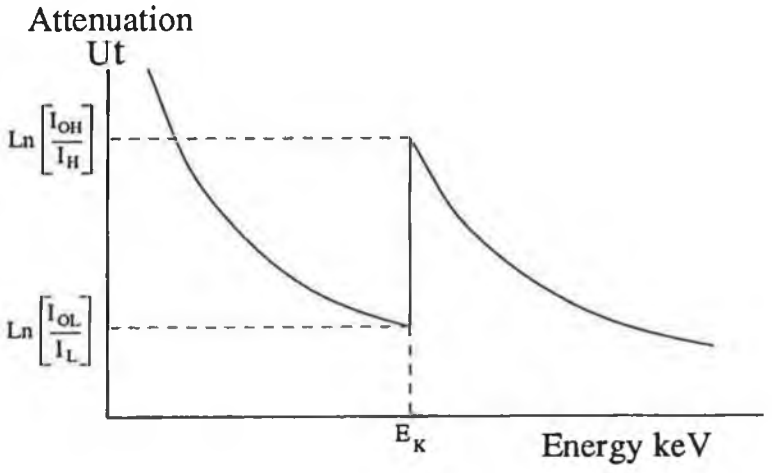

Figure 2.12
Absorption spectrum for an absorber containing one analyte.

Figure 2.12 shows the absorption curve for a typical absorber. The absorption edge identified by E_K is produced by the K-edge absorption jump of the element of interest. This element will be referred to as the analyte; relevant variables are subscripted a. All other absorbers in the body are referred to collectively as the matrix; relevant variables are subscripted m. The aim of this section is to derive an expression for the equivalent thickness of analyte without the need to know information about the matrix.

Mass attenuation coefficients may be combined in proportion to the weight fraction ω of each constituent element in the compound or mixture to give the mass attenuation coefficient of that mixture. So, in general, 2.27 applies.

$$U = U_1\omega_1 + U_2\omega_2 + \ldots = \sum_{i=1}^{\text{no elements}} U_i\,\omega_i \quad m^2/kg \qquad (2.27)$$

Reducing the constituents to analyte and matrix gives.

$$U = U_a\,\omega_a + U_m\,\omega_m \qquad (2.28)$$

Consider two collimated monochromatic beams incident on an absorber.

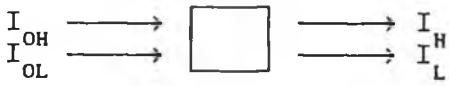

where I_{OH} and I_{OL} are the incident x-ray intensities at two different x-ray energies.

Applying Beer's law 2.08 to each beam gives the transmitted intensities I_L and I_H.

$$I_H = I_{OH}\, e^{-U_H t} \qquad (2.29)$$

$$I_L = I_{OL}\, e^{-U_L t} \qquad (2.30)$$

U_L is the mass attenuation coefficient measured on the low side of the K-edge. U_H is the mass attenuation coefficient measured on the high side of the K-edge.

Applying 2.28 for an analyte matrix combination gives

$$U_H = U_{Ha}\, \omega_a + U_{Hm}\, \omega_m \qquad (2.31)$$

$$U_L = U_{La}\, \omega_a + U_{Lm}\, \omega_m \qquad (2.32)$$

Combining 2.29 with 2.31 and 2.30 with 2.32 and taking the ratio of the resulting equations gives

$$\frac{I_L}{I_H} = \frac{I_{OL}\, e^{-[\,\omega_a U_{La} + \omega_m U_{Lm}\,]\, t}}{I_{OH}\, e^{-[\,\omega_a U_{Ha} + \omega_m U_{Hm}\,]\, t}} \qquad (2.33)$$

Since $\omega_a t = t_a$, the equivalent thickness of analyte and $\omega_m t = t_m$ the equivalent thickness of matrix, equation 2.33 can be rewritten in terms of analyte and matrix equivalent thickness to give

$$\frac{I_L}{I_H} = \frac{I_{OL}}{I_{OH}}\, e^{\underbrace{-[U_{La} - U_{Ha}]t_a}_{A \neq 0}}\, e^{\underbrace{-[U_{Lm} - U_{Hm}]t_m}_{B = 0}} \qquad (2.34)$$

To remove the need for information concerning the matrix, term B must go to zero. This is achieved when the x-ray beam energies E_L and E_H are chosen to be just either side of the analyte K-edge. Equation 2.34 may then be solved for the analyte equivalent thickness in terms

independent of the matrix.

$$t_a = \frac{Ln\left(\frac{I_L}{I_{OL}}\right) - Ln\left(\frac{I_H}{I_{OH}}\right)}{U_{Ha} - U_{La}} \qquad (2.35)$$

The absorption jump across the K-edge of the analyte is given by

$$\Delta U_a = U_{Ha} - U_{La} \qquad (2.36)$$

Substituting in 2.35 gives

$$t_a = \frac{Ln\left(\frac{I_{OH}}{I_H}\right) - Ln\left(\frac{I_{OL}}{I_L}\right)}{\Delta U_a} \qquad (2.37)$$

By measuring the fractional transmittance of a monochromatic beam at energies either side of the K-edge, the equivalent thickness of the analyte can be determined. Values of ΔU_a are obtainable from tables of absorption data for the elements [22].

2.3 TOTAL COUNT TECHNIQUE FOR MEASURING THE ABSORPTION PARAMETERS

Introduction

In this section the total count method of finding the absorption constants required to characterise an absorber is described. The explanation is limited to an absorber containing two analytes. Using these constants the absorption response of the absorber can be evaluated. It may, in theory, be possible to extend the method to three or more elements but for simplicity and some practical limitations two analytes are assumed.

The two analyte restriction means that technically you do need to know about the matrix, that is that there are no unknown edges within the band of x-ray energies used. If there was an element producing an edge not of interest but present in the band of energies used, then the technique requires it to be considered as another analyte. This is unlikely to be a problem since the analytes may be chosen

to have K-edge energies well away from K-edges found in the matrix. The technique does not require information describing the absorption of the matrix.

2.3.1 THEORY OF MEASURING THE ABSORPTION PARAMETERS

Consider a polychromatic x-ray beam produced by an x-ray tube incident on the sample. The photon flux incident on the sample is given by

$$T_0 = k \int_0^{V_t} I(V_t,E)dE \qquad (2.38)$$

where k is the tube activity constant and V_t the tube voltage. $I(V_t,E)$ is the relative intensity of x-rays produced at energy E by an x-ray tube operating at V_t.

The sample containing the two analytes of interest will have an absorption spectrum of the form shown in figure 2.13.

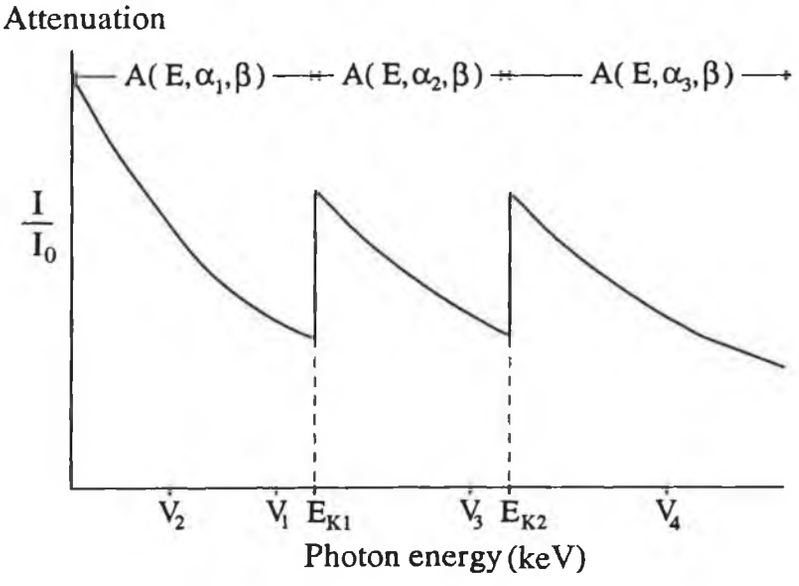

Figure 2.13
Attenuation of monochromatic radiation as a function of energy for a typical absorber containing two analytes.

The transmitted intensity is given by

$$T_T = k\left[\int_0^{E_{K1}} I(V_t,E)A(\alpha_1,\beta,E)dE + \int_{E_{K1}}^{E_{K2}} I(V_t,E)\ A(\alpha_2,\beta,E)\ dE + \int_{E_{K2}}^{\infty} I(V_t,E)\ A(\alpha_3,\beta,E)\ dE\right] \qquad (2.39)$$

where $A(\alpha,\beta,E)$ is the fractional transmittance of a

monochromatic x-ray beam of energy E. Using 2.24 gives

$$A(\alpha,\beta,E) = \exp - (\alpha P(E) + \beta S(E)) \qquad (2.40)$$

When $V_t \leq E_{K1}$

When the x-ray tube is operated at a potential such that no x-rays are produced with energies greater than the first K-edge equation 2.39 simplifies to the first term. ($I(V_t,E) = 0$ for all $E > V_t$). In this case, taking the ratio of equations 2.38 and 2.39 removes the need to know the tube activity constant and gives

$$\frac{T_T}{T_0} = \frac{\int_0^{V_t} I(V_t,E)\, A(\alpha_1,\beta,E)}{\int_0^{V_t} I(V_t,E)\, dE} = F_t \ (V_t \leq E_{K1}) \qquad (2.41)$$

where F_t is the fractional transmittance i.e. total count transmitted divided by total incident count. A detector system without energy resolution can be used to measure the fractional transmittance. Rewriting equation 2.41 and defining the function $\mathbb{F}(F_t,V_t,\alpha_1,\beta)$ gives

$$\frac{\int_0^{V_t} I(V_t,E)\, A(\alpha_1,\beta,E)}{\int_0^{V_t} I(V_t,E)\, dE} \frac{1}{F_t} - 1 = \mathbb{F}(F_t,V_t,\alpha_1,\beta) = 0 \qquad (2.42)$$

Operating the tube at two voltages V_1 and V_2 below the first K-edge and measuring the resulting fractional transmittances F_1 and F_2 generates two equations.

$$\mathbb{F}(F_1,V_1,\alpha_1,\beta) = 0 \qquad (2.43)$$

$$\mathbb{F}(F_2,V_2,\alpha_1,\beta) = 0 \qquad (2.44)$$

Equations 2.43 and 2.44 may be solved simultaneously for α_1 and β. The technique used is outlined in section 2.6.

When $E_{K1} < V_t < E_{K2}$

The tube voltage may be raised to a potential V_3 so that x-rays are produced above the first K-edge but below

the second. The fractional transmittance F_3 is recorded at this voltage. The first two terms of equation 2.39 must be included to describe the fractional transmittance. Following the same argument as that used to obtain 2.42 the following expression is obtained.

$$\frac{\int_0^{E_{K1}} I(V_t,E)\ A(\alpha_1,\beta,E)\ dE + \int_{E_{K1}}^{V_t} I(V_t,E)\ A(\alpha_2,\beta,E)\ dE}{\int_0^{V_t} I(V_t,E)\ dE} \frac{1}{F_t} - 1 = 0 \qquad (2.45)$$

$$\text{i.e} \qquad \mathbb{F}(F_3,V_3,\alpha_1,\alpha_2,\beta) = 0 \qquad (2.46)$$

Since α_1,β have already been obtained, equation 2.46 may be solved directly for α_2.

When $V_t > E_{K2}$

Increasing the tube voltage so that x-rays are produced with energies greater than the second K-edge results in a fourth equation produced in the same manner as 2.46.

$$\mathbb{F}(F_4,V_4,\alpha_1,\alpha_2,\alpha_3,\beta) = 0 \qquad (2.47)$$

Since α_1,α_2 and β have already been found, equation 2.47 may be solved directly for α_3.

Using $\alpha_1,\alpha_2,\alpha_3$ and β the absorption response of the absorber can be evaluated at any energy.

2.4 THE TRACKING DISCRIMINATOR METHOD FOR MEASURING ABSORPTION PARAMETERS

2.4.1. JUSTIFICATION FOR THE TRACKING DISCRIMINATOR TECHNIQUE.

With the total count technique the percentage of the total count that provides new information about the absorber decreases as the tube potential increases. It is only photons with energies above the previous maximum energy produced by the tube that provide new information about the absorber. This is shown in figure 2.14.

The x-rays in the region between V_2 and V_3 provide information about α_2, the x-rays below V_2 constitute noise and are accounted for using α_1. A reduction in the number of low energy x-rays detected with energies below V_2 increases the signal available to measure α_2. Filtering the source reduced the percentage of these low energy x-rays and improved the performance of the total count method.

A further improvement can be achieved by using the low level discriminator of a single channel analyser to prevent pulses originating from low energy x-rays from reaching the counter. The discriminator threshold is set to track a fixed distance behind the maximum x-ray energy being produced by the tube; this energy difference is called the lag. If a detector with an output proportional to the x-ray energy is used, the addition of the discriminator will increase the percentage of the total count containing information about the x-rays from the high energy end of x-ray the spectrum produced by the tube.

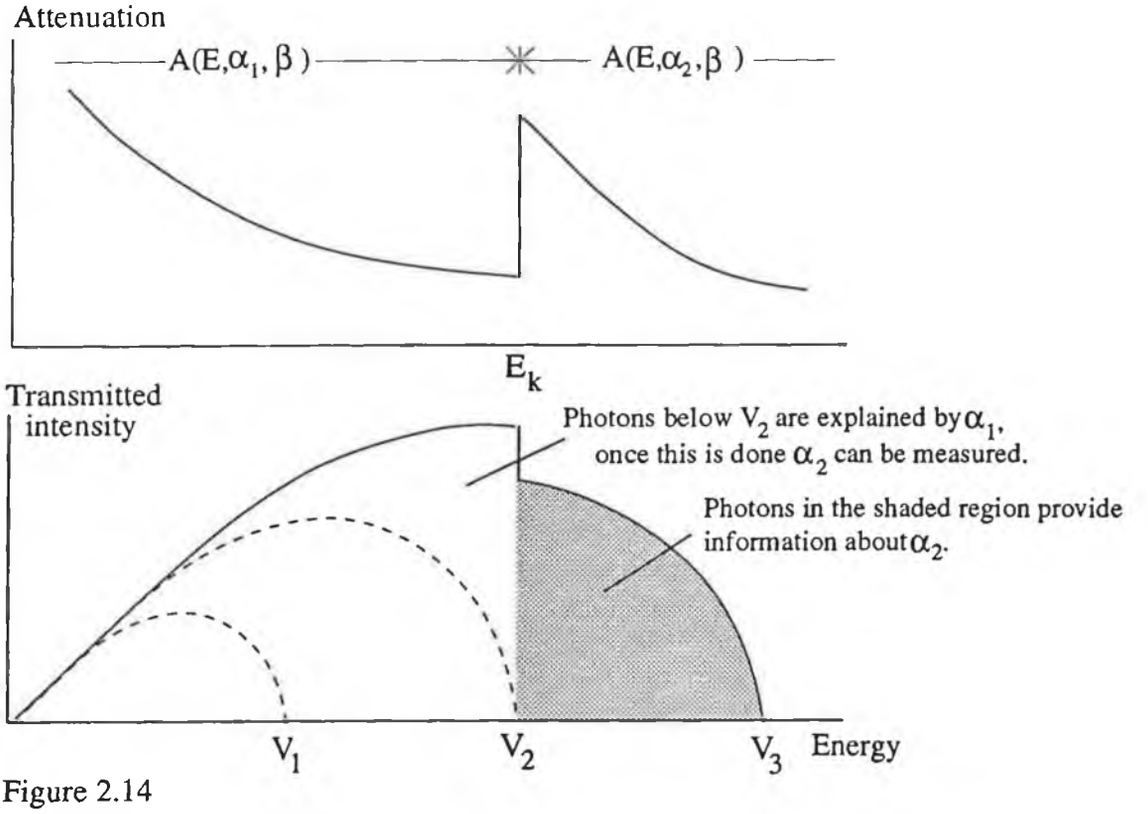

Figure 2.14

Demonstration of the improvement in signal produced by removing low energy photons. α_1 has been measured using spectra at V_1 and V_2, the spectrum at V_3 is being used to measure α_2.

The detectors that could be used with the technique do not have high energy resolution; this was a requirement in the original aims of the project. The incident x-ray spectra on the detector and the pulse height distributions produced by the detector are different. However, by careful analysis of the processes involved in the detector and counting chain, it is still possible to evaluate the absorption parameters from fractional transmittances recorded with a counter placed after the single channel analyser. The methods developed to evaluate the absorption parameters are discussed in the remainder of section 2.4. The improvements associated with this approach are demonstrated by computer simulation and experiment, this is described in chapters 5 and 6.

2.4.2. THEORY OF MEASURING THE ABSORPTION PARAMETERS USING THE TRACKING DISCRIMINATOR METHOD

The basic configuration of the tracking discriminator technique is shown in figure 2.15. The low level discriminator placed between the detector and counter has a threshold set to exclude pulses with heights less than the highest x-ray energy produced at V_t less a lag value that is set externally. As with the total count technique, the discussion is limited to describing an absorber containing two analytes.

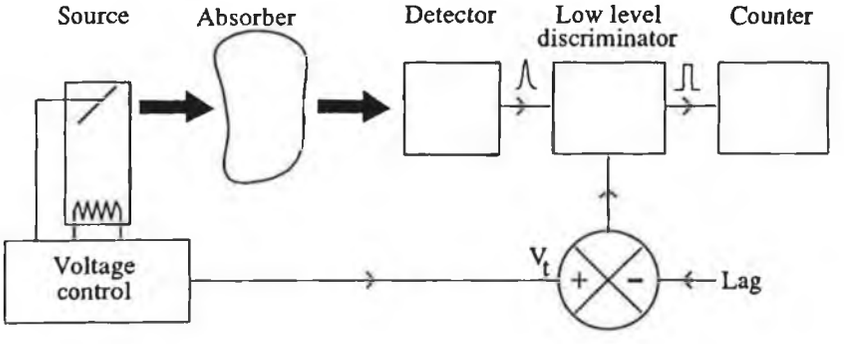

Figure 2.15
Schematic diagram of the experimental configuration used with the tracking discriminator technique.

The intensity detected by the counter when no absorber is placed between source and detector is given by

$$I_o = k \int_{V_t - \text{Lag}}^{\infty} \int_{0}^{V_t} I(V_t,E)\, D(E,Y)\, dE\, dY \qquad (2.48)$$

where E is the x-ray energy and $I(V_t,E)$ is the intensity of X-rays at energy E produced by a tube operating at V_t. Y is the channel energy in the pulse height distribution. The function D(E,Y) gives the contribution of a count at energy E to the channel of energy Y in the pulse height distribution.

The function D(E,Y) can be split into two functions describing the resolution and the efficiency of the detector separately.

$$D(E,Y) = R(E)\, H(E,Y,\sigma(E)) \qquad (2.49)$$

where R(E) is the absolute efficiency of the detector to x-rays of energy E and $H(E,Y,\sigma(E))$ is the intensity of x-rays detected at channel energy E produced by a source of energy Y, by a detector with energy resolution $\sigma(E)$. The resolution of the detector varies as a function of energy hence $\sigma(E)$.

The function used to describe the detector resolution has a Gaussian shape [17].

$$H(E,Y,\sigma(E)) = \frac{1}{\sqrt{2\Pi}\,\sigma(E)} \exp\left[- \frac{(E - Y)^2}{2\sigma(E)^2} \right] \qquad (2.50)$$

The values used for detector resolution $\sigma(E)$ and the detector efficiency are given in section 5.1.5.

The sequence of events that generate the equation for I_o are summarised in figure 2.16.

(a) Graph of x-ray intensity as a function of energy for a tube at potential V_t.

(b) Graph showing intensity observed at channel energy Y from an x-ray source of energy E.

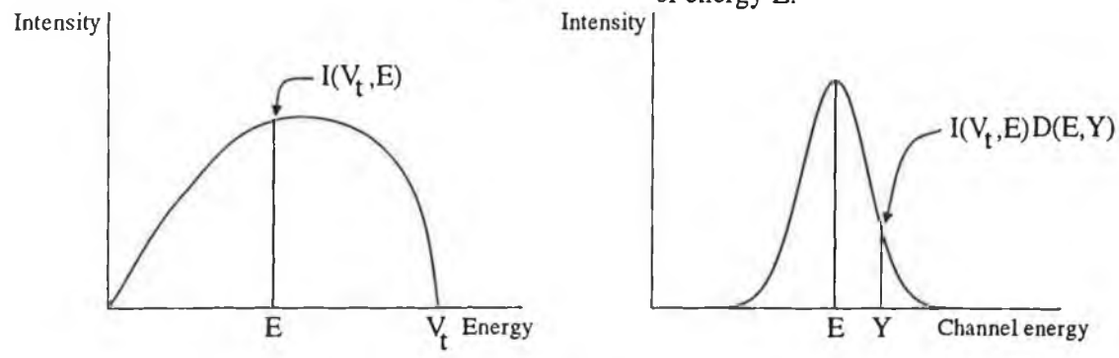

(c) Pulse height distribution produced by a detector illuminated by an x-ray tube at potential V_t.

(d) Count detected after a low level discriminator removes counts below V_t-Lag.

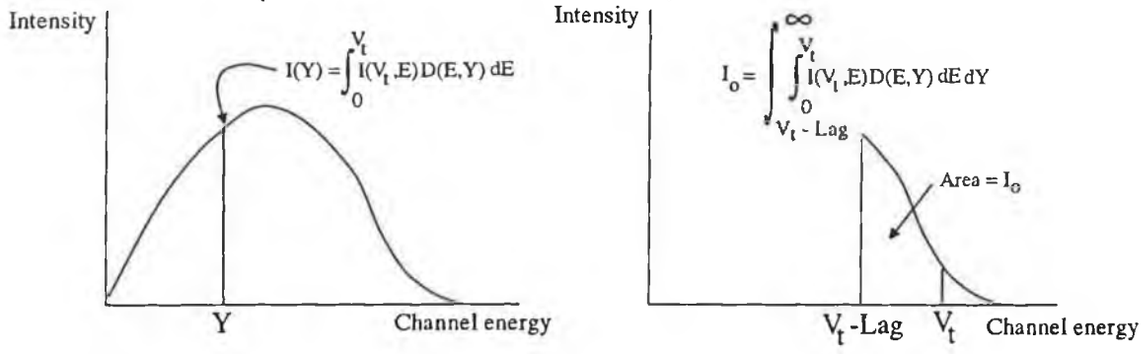

Figure 2.16
Graphic representation of the tracking discriminator technique.

The transmitted spectrum is given by

$$I_T = k \int_{V_t - Lag}^{\infty} \int_0^{V_t} I(V_t,E)\ A(\alpha(E),\beta,E))\ D(E,Y)\ dE\ dY \qquad (2.51)$$

where $A(\alpha(E),\beta,E)$ is the absorption at energy E described by the photoelectric and scatter absorption coefficients α and β. In the total count technique the integral could be written as a sum of smaller integrals describing the region between each edge. This was possible since the total count detected did not depend on the detector resolution. The effect of detector efficiency was accounted for by modifying the reference spectra function $I(V_t,E)$. This is not the case in the tracking discriminator technique, the detector resolution affects the count recorded. The α's need to be written as a function of energy. The α's still have discrete values that explain the photoelectric absorption between edges as before.

$$\alpha(E) = \alpha_1 \quad E < E_{K1} \tag{2.52}$$

$$\alpha(E) = \alpha_2 \quad E_{K1} < E < E_{K2} \tag{2.53}$$

$$\alpha(E) = \alpha_3 \quad E_{K2} < E < E_{K3} \tag{2.54}$$

Taking the ratio of equations 2.48 and 2.51 removes the tube activity constant and moving terms to the LHS gives

$$\frac{\int_{V_t - Lag}^{\infty} \int_{0}^{V_t} I(V_t,E)\, A(\alpha(E),\beta,E))\, D(E,Y)\, dE\, dY}{\int_{V_t - Lag}^{\infty} \int_{0}^{V_t} I(V_t,E)\, D(E,Y)\, dE\, dY} \frac{1}{F_t} - 1 = 0 \tag{2.55}$$

where $F_t = I/I_0$.

When V_t is set such that no x-rays are produced with energies above the first K-edge energy, $\alpha(E)$ is only a function of α_1. Equation 2.55 can be rewritten as

$$\mathbb{F}(F_t, V_t, \alpha_1, \beta) = 0 \tag{2.56}$$

where detector resolution, efficiency and the lag are contained within the function.

As with the total count technique, two fractional transmittance measurements F_1 and F_2 can be recorded at tube potentials V_1 and V_2. This gives two equations that can be solved simultaneously for α_1 and β.

$$\mathbb{F}(F_1, V_1, \alpha_1, \beta) = 0 \tag{2.57}$$

$$\mathbb{F}(F_2, V_2, \alpha_1, \beta) = 0 \tag{2.58}$$

The tube potential can then be increased to produce x-rays with energies above the first K-edge but below the second K-edge. The function $\alpha(E)$ will then use the values of α_1 and α_2. At this tube potential, V_3, the fractional transmittance F_3 can be recorded. Since α_1 and β are evaluated the resulting equation can be solved for α_2:

$$\mathbb{F}(F_3, V_3, \alpha_1, \alpha_2, \beta) = 0 \tag{2.59}$$

As with the total count technique further increases in the tube potential can be used to evaluate α_3 etc. The values of α and β allow the absorber to be described over a range of energies.

2.5 MEASUREMENT OF EQUIVALENT THICKNESS OF EACH ANALYTE GIVEN THE ABSORPTION PARAMETERS

Using equation 2.24, which describes the absorption of x-rays, the fractional transmittance either side of the K-edge of the first analyte is given by

$$\mathrm{Ln}\left(\frac{I_{OL}}{I_L}\right) = U_L\, t = \alpha_1\, P(E_{K1}) + \beta\, S(E_{K1}) \qquad (2.60)$$

$$\mathrm{Ln}\left(\frac{I_{OH}}{I_H}\right) = U_H\, t = \alpha_2\, P(E_{K1}) + \beta\, S(E_{K1}) \qquad (2.61)$$

Substituting 2.60 and 2.61 in 2.37 gives

$$t_{a1} = \frac{\alpha_2\, P(E_{K1}) - \alpha_1\, P(E_{K1})}{\Delta U_{a1}} \qquad (2.62)$$

Similarly the equivalent thickness of the second analyte can be obtained using

$$t_{a2} = \frac{\alpha_3\, P(E_{K2}) - \alpha_2\, P(E_{K2})}{\Delta U_{a2}} \qquad (2.63)$$

2.6 NUMERICAL METHODS USED TO FIND ABSORPTION PARAMETERS

The methods described in this section refer specifically to the total count method. However the approach used in the tracking discriminator technique is similar. The numerical methods used with the tracking discriminator technique are described in more detail in chapter 5 on computer simulations.

Experimental data consisting of four fractional transmittance measurements F_1, F_2, F_3 and F_4 are recorded at four tube potentials V_1, V_2, V_3, and V_4, using a low energy resolution detector system. These measurements would be recorded along each beam path required for image reconstruction.

Using a high resolution detector and multichannel analyser, four reference spectra are recorded at V_1, V_2, V_3, V_4. These spectra consist of a list of photon counts in

each channel. By calibration, using fluorescence lines, channel number may be converted to x-ray energy. The photon flux incident on the sample can be approximated by the sum over all channels (0 - 1023).

$$\int_0^{V_t} I(V_t,E)\, dE = \sum_{i=0}^{1023} C(V_t)_i \qquad (2.64)$$

The transmitted flux may be approximated by

$$\int_0^{V_t} I(V_t,E)\, A(\alpha_1,\beta,E)\, dE = \sum_{i=0}^{1023} C(V_t)_i\, A(\alpha_1,\beta,E(i)) \qquad (2.65)$$

Function E(i) converts channel number i to x-ray energy E. Substituting 2.65 and 2.64 in 2.42 and operating at tube potentials V_1 and V_2 gives

$$\frac{\sum_{i=0}^{1023} C(V_1)_i\, A(\alpha_1,\beta,E(i))}{\sum_{i=0}^{1023} C(V_1)_i} \frac{1}{F_1} - 1 = F(F_1,V_1,\alpha_1,\beta) = 0 \quad (2.66)$$

$$\frac{\sum_{i=0}^{1023} C(V_2)_i\, A(\alpha_1,\beta,E(i))}{\sum_{i=0}^{1023} C(V_2)_i} \frac{1}{F_2} - 1 = F(F_2,V_2,\alpha_1,\beta) = 0 \quad (2.67)$$

Solving 2.66 and 2.67 for α_1 and β was achieved using the technique shown in figure 2.17.

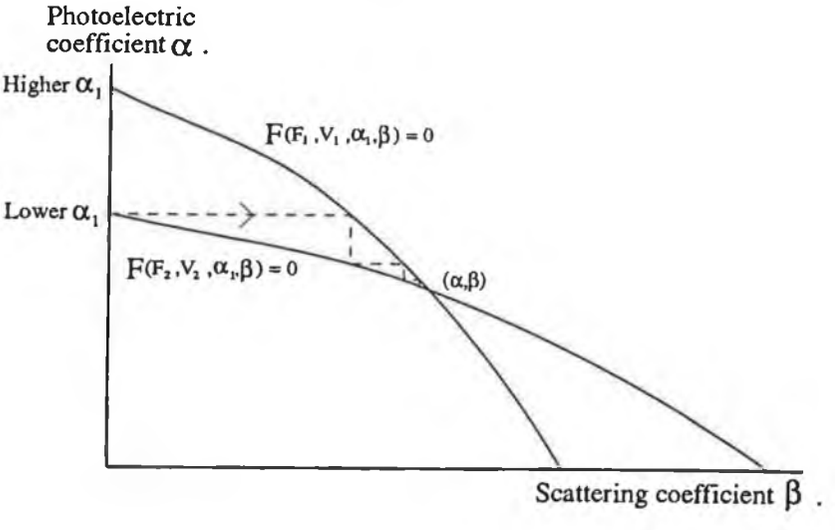

Figure 2.17
Method used to solve simultaneous equations.

With β set to zero equations 2.66 and 2.67 are each solved for α_1 using the bisection method. The lower value of α_1 produced by the two equations is then used in the equation which produced the higher value. This equation is then solved for β. The new value for β is then used in the equation which produced the lower value of α_1 initially to find a new value for α_1. This process converges on a value of α_1 and β which simultaneously satisfy equations 2.66 and 2.67. This procedure is repeated until the difference between successive steps is below the desired error. The technique is similar to fixed point iteration.

The discrete form of 2.46 becomes

$$\frac{\sum_{i=0}^{i(E_{K1})} C(V_3)_i \, A(\alpha_1,\beta,E(i)) + \sum_{i=i(E_{K1})}^{1023} C(V_3)_i \, A(\alpha_2,\beta,E(i))}{\sum_{i=0}^{1023} C(V_3)_i} \frac{1}{F_3} - 1 = 0 \qquad (2.68)$$

where i(E) converts x-ray energy to the nearest corresponding channel number. Since α_1 and β are known 2.68 may be solved, using the bisection method, for α_2. Equation 2.47 may be modified in a similar manner and solved for α_3.

The bisection method is one of the simplest methods of finding the numeric solution to an equation [23]. If a function f(x) is continuous on the interval [a,b] and

$$f(a).f(b) < 0$$

then f(x) changes sign on [a,b], and f(x)=0 has at least one root on the interval. The bisection method works by repeatedly halving the interval, keeping the half on which f(x) changes sign [24]. The algorithm to achieve this is shown in figure 2.15.

The tolerance error Δx associated with the solution x is given by

$$\Delta x = \frac{b - a}{2^n} \qquad (2.69)$$

where n is the number of iterations.

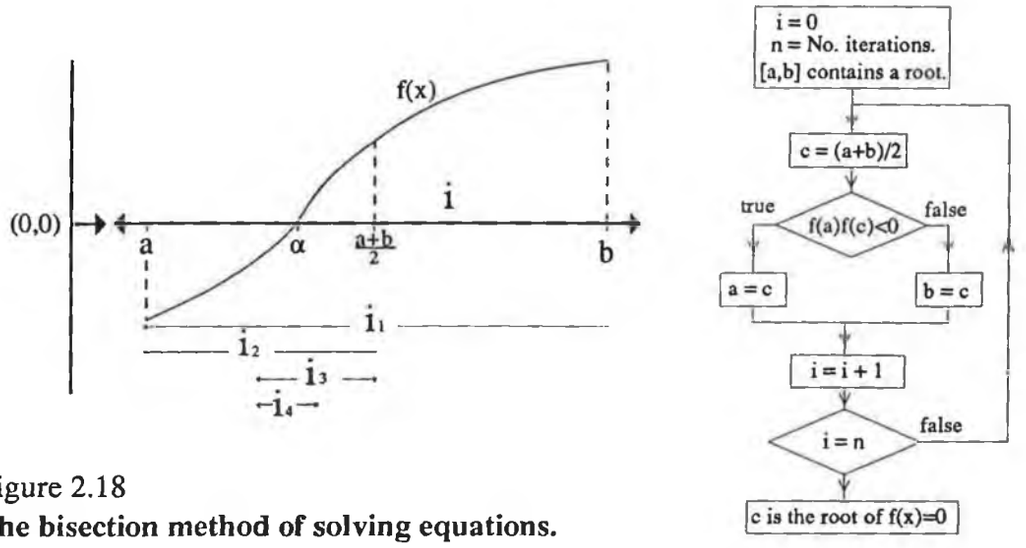

Figure 2.18
The bisection method of solving equations.

2.7 PRODUCTION OF AN IMAGE

2.7.1 DATA COLLECTION

When a beam of unit area passes through a homogeneous absorber of length l, containing concentration C_a of analyte, the amount of analyte encountered is referred to as the equivalent thickness of the analyte, t_a. Thus

$$t_a = C_a \, l \quad kg/m^2 \qquad (2.70)$$

When the absorber is not homogeneous, equation 2.70 becomes:

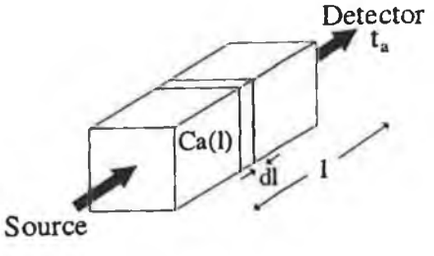

$$t_a = \int_{source}^{detector} C_a \, dl \qquad (2.71)$$

The objective in element specific computerised tomography is to produce an image of element concentration in a plane of interest intersecting the object. Figure 2.19 shows the co-ordinate system used to describe this problem.

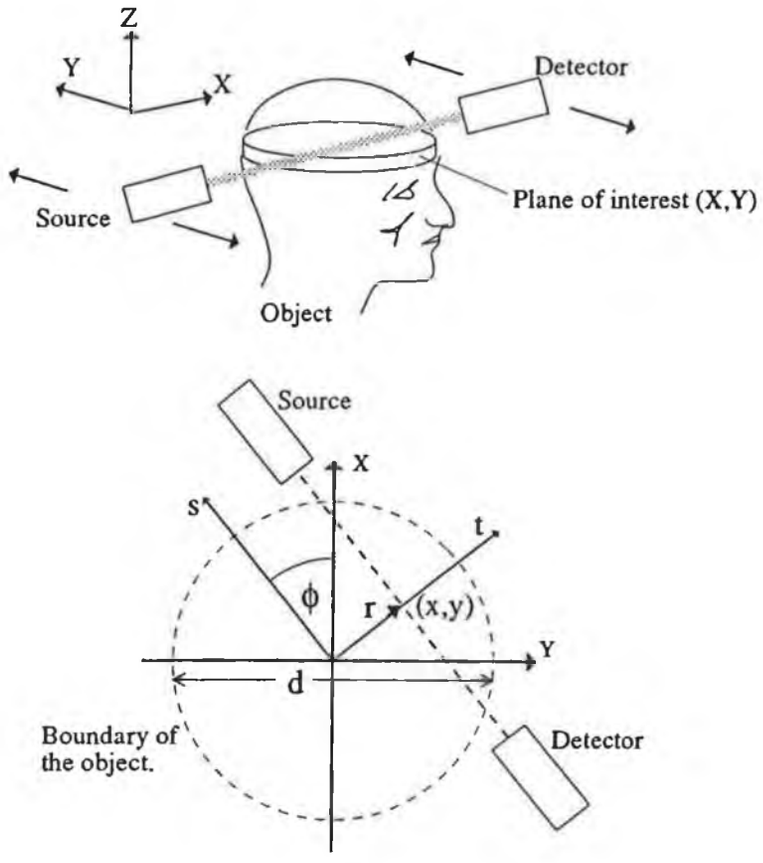

Figure 2.19
The coordinate system used to describe data acquisition in CT.

The xy plane is the plane of interest through the body. The spatial distribution of analyte within this plane is $C_a(x,y)$. The polar coordinates r,ϕ define the ray path between the source and detector. Rewriting equation 2.71 using this coordinate system gives

$$t_a(r,\phi) = \int_{(r,\phi)} C_a(x,y)\, dl \quad \text{Note } x,y = f(r,\phi) \qquad (2.72)$$

The integral in equation 2.72 is called the ray sum. Function $C_a(x,y)$ is continuous; to obtain it using equation 2.72 would require an infinite number of values of $t_a(r,\phi)$. In CT the problem is reduced by limiting $C_a(x,y)$ to a square array of points equally spaced by distance w. The object is also contained within a boundary of diameter d.

Thus there are

$$N = \frac{\pi}{4}\left(\frac{d}{w}\right)^2 \qquad (2.73)$$

values of $C_a(x,y)$.

To solve equation 2.72 for this $C_a(x,y)$ requires at

least N values of $t_a(r,\phi)$. There are a number of different scan geometries that are used to collect $t_a(r,\phi)$. The geometry used in the original CT scanner was used in this project and is called parallel data collection. This is shown in figure 2.20.

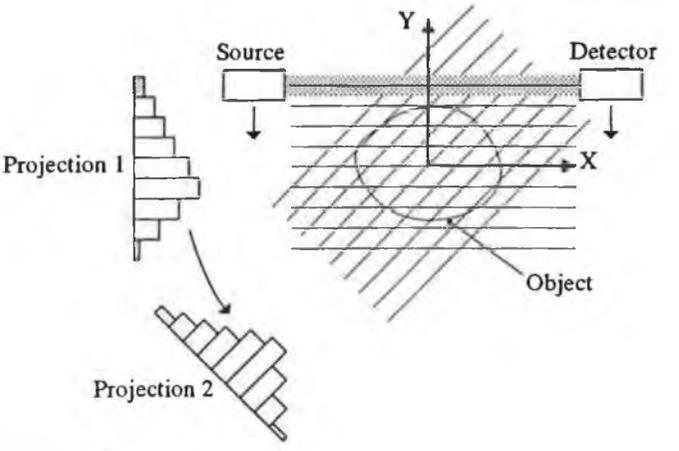

Figure 2.20
Parallel data collection.

r is varied such that the x-ray between source and detector transverses the diameter of the object area in n equally spaced steps. This set of ray sums is called a projection. ϕ is varied so that m equally spaced projections are collected between 0 and 180°. m and n are chosen such that $mn \geq N$. In practice $m = n = d/w$ is used. Thus 1600 values of $t_a(r,\phi)$ will be collected for a 40 by 40 image of $C_a(x,y)$. When extra data is collected in this way the problem is said to be overdetermined; this can reduce image noise. The x-ray beam used to measure $t_a(r,\phi)$ is normally arranged to have a width equal to the grid spacing w so that all regions of the object space are intersected by x-rays. The method of solving equation 2.72 is called reconstruction.

2.7.2 IMAGE RECONSTRUCTION AND DISPLAY

There are many reconstruction techniques used to produce CT images. These are described in detail in the texts by Herman and Natterer [25][26]. These may be divided into two main types, iterative reconstruction and analytic reconstruction.

Analytic reconstruction is based on an exact treatment

of the reconstruction using Fourier techniques. It can be shown [27] that by convolving the projection data with a filter function and then back projecting this information across a reconstruction grid, an image of $C_a(x,y)$ can be produced. This technique is called filtered back projection. It provides one of the fastest reconstruction techniques available and is used on most commercial CT scanners. The algebraic reconstruction technique (ART) is an iterative technique that can be used when projection data is not recorded uniformly over 360 degrees. Recently reconstruction techniques based on neural networks have been developed [28].

The algebraic reconstruction technique (ART) was used in this project to produce images. The image is reconstructed into a grid of n by n cells. These cells represent the area occupied by $C_a(x,y)$. See figure 2.21.

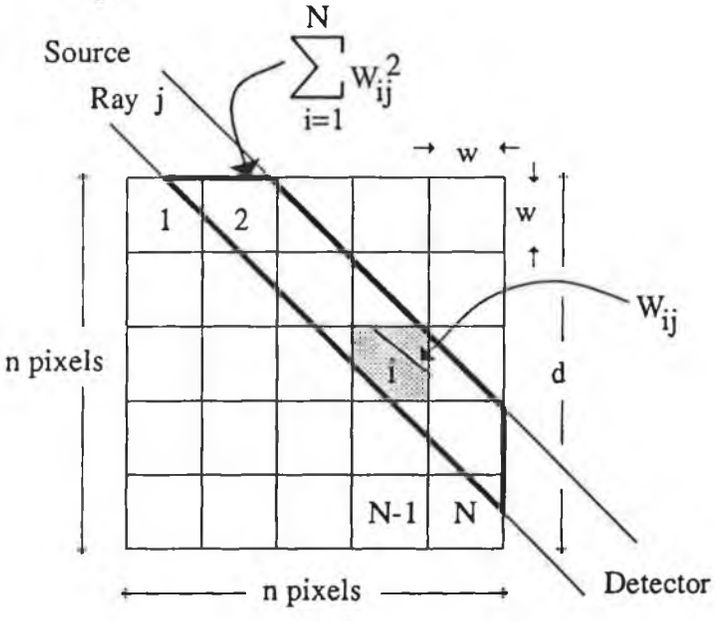

Figure 2.21
Notation used to explain ART.

In terms of the notation used for reconstruction, equation 2.72 may be rewritten as

$$t_{aj} = \sum_{i=1}^{N} W_{ij} C_{ai} \qquad (2.74)$$

where i denotes the cell number, j is the ray-sum. W_{ij} is the contribution cell i makes to the ray-sum j. Thus W_{ij} is the mean path length of beam j through cell i, it may be

approximated by dividing the cell/beam overlap area by the cell width. The ART algorithm starts by filling all cells in the reconstruction grid with an intermediate value of C_{ai}.

The following procedure is then carried out.

1/ Calculate t'_{aj} using the values of C_{ai} in the grid.

2/ Evaluate the difference between the measured ray-sum value t_{aj} and that just calculated t'_{aj}.

$$\varepsilon = t_{aj} - t'_{aj} \tag{2.75}$$

3/ Adjust the values of C_{ai} along the beam paths using

$$C_{ai}^{new} = C_{ai}^{old} + R \frac{W_{ij}}{\sum_{i=1}^{N} W_{ij}^2} \varepsilon \tag{2.76}$$

4/ Repeat steps 1, 2 and 3 for all ray-sums, all values of j.

5/ Calculate the standard deviation of the image using

$$\sigma = \frac{1}{N} \sqrt{\sum_{i=1}^{N} (C_{ai} - \overline{C_{ai}})^2} \tag{2.77}$$

6/ Repeat 1 to 5 until the change in the standard deviation between successive iterations is less than 1%.

Using equation 2.76, C_{ai} is adjusted along the beam path j such that the reconstructed value and experimental value of equivalent thickness agree. When this is done the last few ray sums have a greater effect on the image than the first. To overcome this a dampening factor R is introduced to reduce the speed of convergence. It can take a value between 0 and 1; however, R=0.2 is normally used [29]. The sequence of ray-sums used consists of the first ray-sum in each projection at each angle followed by the second, etc.

Three programs were required for image production.

The first "OVERLAP" (Appendix F) creates a look up table of values for W_{ij}. The second program "RECON" (Appendix F) produces a file containing values of $C_a(x,y)$ given a set of values of $t_a(r,\phi)$ using the ART algorithm and a table of values of W_{ij}. The third program "TESTDISP" was used to display the values of $C_a(x,y)$ as a colour coded image [30].

2.8 SUMMARY

The physical processes involved in the production, absorption and detection of x-rays were described. Two methods of obtaining absorption information at specific energies using a tube source of x-rays and low resolution detector system were described. These were the total count method and the tracking discriminator technique. The absorption information was used to evaluate analyte equivalent thickness in the path of the beam. The basic numerical methods required to implement the techniques on a computer were described. It was shown that ART could be used to reconstruct element specific images from measurements of analyte equivalent thickness. The techniques can be summarised by figure 2.22.

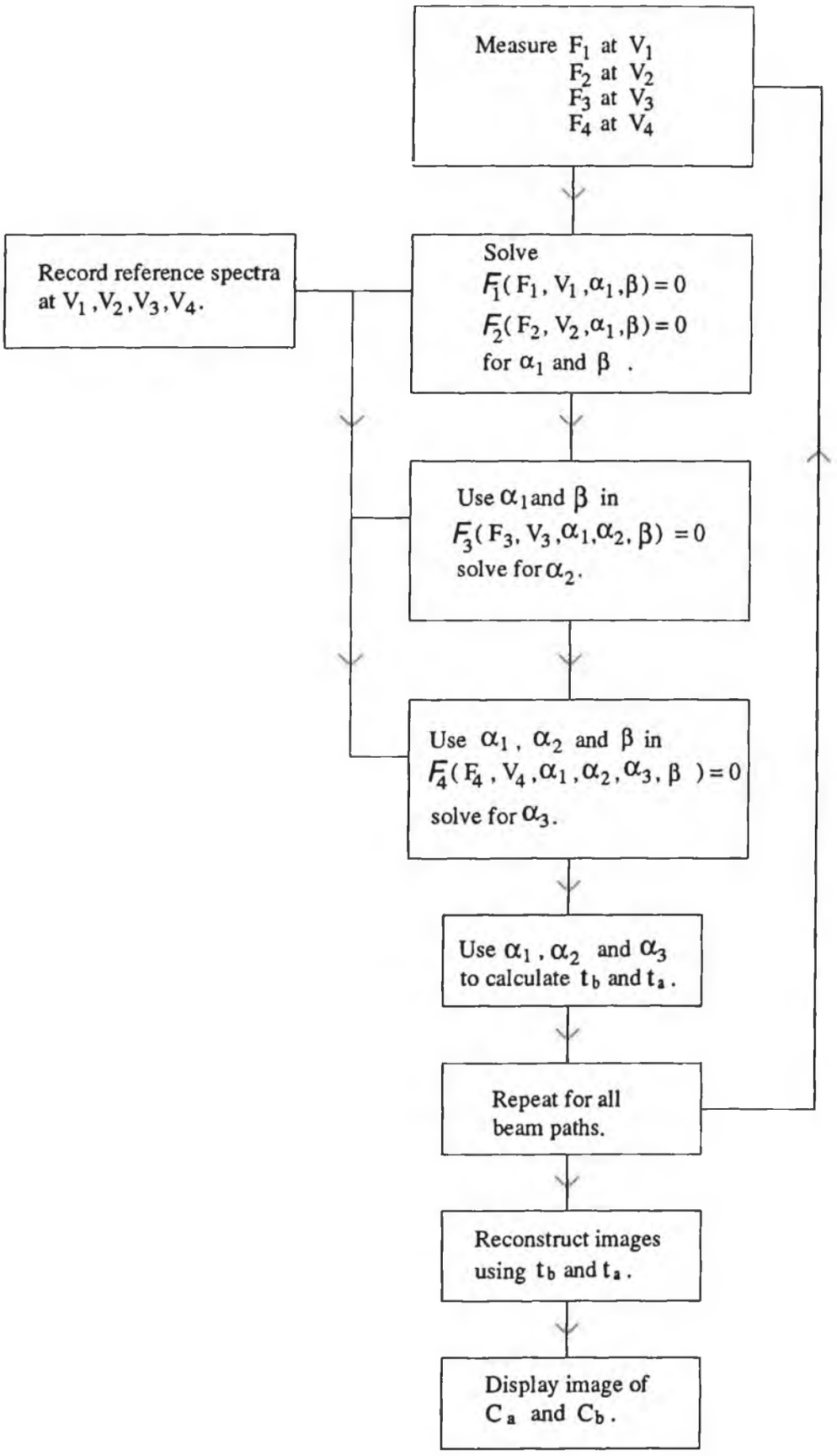

Figure 2.22

Summary of the stages involved in producing an image using the total count or tracking discriminator techniques.

References

[1] Krestel, E.
"Imaging systems for medical diagnostics"
Siemens, 1990.

[2] Gifford, D.
"A handbook for radiologists and radiographers"
Wiley & Sons, 1984.

[3] Ammann, E.
"X-ray Tubes and Generators for Interventional Radiology"
IPSM Report No.61, Physics in diagnostic radiology 1990.

[4] "ROTANX Single tank X-ray generator for computerized tomography"
Siemens data sheet SIC980.

[5] Read, F.H.
"Electromagnetic radiation"
John Wiley & Sons., 1980.

[6] Bertin, E.P.
"Principles and practice of x-ray spectrometric analysis"
Plenum Press, New york, 1975.

[7] Heinrich, K.F.J.
"Electron beam x-ray microanalysis"
Van Nostrand Reinhold Company, 1981.

[8] Matsumoto et al.
"Effects of voltage ripple and current mode on diagnostic x-ray spectra and exposures"
Med. Phys. Vol. 18, No. 5, pp 921-927, 1991.

[9] Bearden, J.A.
"X-ray Wavelengths and X-ray Atomic Energy Levels"
National standards reference data series 14, U.S. Government printing office, 1967.

[10] Elwell, D. and Pointon, A.J.
"Physics for Engineers and Scientists"
Ellis Horwood, 1978.

[11] Read, F.H.
"Electromagnetic radiation"
John Wiley & Sons., 1980.

[12] Marion, J.B. and Hornyak, W.F.
"Physics for science and engineering"
Saunders College Publishing, 1982.

[13] Macovski, A. et al.
"Energy dependent reconstruction in x-ray computerized tomography."
Comput. Biol. Med.,Vol. 6,pp 325-336, 1976.

[14] Koningsberger, D.C. and Prins, R.
"X-ray absorption, Principles, applications, techniques of EXAFS, SEXAFS and XANES"
John Wiley & Sons, 1988.

[15] Tsoulfanidis, N.
"Measurement and detection of radiation"
Mc Graw-Hill Book Company, 1983.

[16] EG & G Ortec
93/94 Nuclear instruments catalogue.
pp 9-7, 1994.

[17] Knoll, G.F.
"Radiation detection and measurement"
John Wiley & Sons., pp 176, 1989.

[18] Delaney, C. and Finch, E.
"Radiation detectors, Physical principles and applications"
Oxford university press, 1993.

[19] Glocker,R. and Frohnmeyer, W.
"Roentgen-Spectroscopic Determination of the quantity of an element in mixtures"
Ann. Phys., Vol 76, pp 369-395, 1925.
Quoted in ,Bertin, E.P. ,"Principles and practice of x-ray spectrometric analysis Plenum Press, New York, 1921.

[20] Fryar, J. and Mc Carthy, K.J. and Fenelon, A.
"Differential x-ray absorptiometry applied to computerised x-ray tomography"
Nucl. Inst. and Meth., Vol. A259, pp 557-565, 1987.

[21] Fryar, J. and Mc Carthy, K.J. and Fenelon, A.
"Multielement imaging in computerised x-ray tomography."
Nucl. Inst. and Meth., Vol. A271, pp 671-677, 1988.

[22] Hubble, J.H.
"Mass Attenuation and Energy Absorption Coefficients from 1keV to 20MeV"
Int. J. Appl. Radiat. Isot.,Vol. 33, pp 1269-1290, 1982.

[23] Press et al.
"Numerical recipes in C, The art of scientific computing"
Cambridge University Press, 1988.

[24] Hartley, P.J. and Wynn-Evans, A.
"A structured introduction to numerical methods."
Stanley Thorns (Publishers) Ltd., 1979.

[25] Herman, G.T.
"Image reconstruction from projections : The fundamentals of computerised tomography"
Academic press, 1980.

[26] Natterer, F.
"The mathematics of computerized tomography"
John Wiley & Sons, 1986.

[27] Brooks, R.A. and Di Chiro, G.
"Principles of computer assisted tomography (CAT) in radiographic and radioisotopic imaging."
Phys. Med. Biol., Vol. 21,No. 5, pp 689-73, 1976.

[28] Srinivasan, V. and Han, Y.K. and Ong, S.H.
"Image reconstruction by a Hopfield neural Network"
Imgage and vision computing, Vol 11, No 5,
pp 278-282, 1993.

[29] Mc Carthy, K.
"A study of the imaging of atomic elements by computerised axial tomography."
Ph.D. Thesis, Dublin City University, 1989.

[30] O'Hare, N.
"A study of the imaging of contrast agents for use in computerised axial tomography."
Ph.D. Thesis, Dublin City University, 1991.

Chapter 3
Experimental apparatus.

Introduction

In this the design and construction of the apparatus used is discussed. The experiments described in this section were all carried out to verify the performance of the apparatus and to check the basic assumptions on which the technique was based. The chapter is divided into two sections, the x-ray detection methods employed and the x-ray source itself.

3.1 DESIGN AND COMMISSIONING OF THE COUNTING SYSTEMS USED

Introduction

A lithium drifted silicon detector, scintillation detector and gas proportional detector were available. In this section the pulse counting systems developed around these detectors are described. These systems will be referred to in subsequent experimental chapters. The characteristics of the detectors were also examined.

3.1.1 DESCRIPTION OF THE COUNTING SYSTEM USED TO RECORD SPECTRA

The x-ray spectroscopic counting system developed for all experiments was configured as shown in figure 3.01. The system was built into a Nuclear Instrumentation Modules rack (NIM-bin). An ORTEC 459 HT supply was used to bias the lithium drifted silicon Si(Li) detector (ORTEC SLP-06180). This HT supply contained a remote shutdown facility which turned off the HT supply if the detector was not sufficiently cool. The detector was biased to -1500V. The HT supply had to be slowly ramped up to full potential,

and for this reason a circuit on the power supply to the NIM-bin was included to prevent accidental repowering of the detector at full potential. An ORTEC 475 spectroscopic amplifier was used to power the preamplifier contained in the detector and to amplify and shape the pulses leaving the detector. These pulses were then displayed on an oscilloscope to check that the maximum pulse height was not exceeded and that the pole zero was set correctly. The amplifier was configured to work with a 0.5μs pulse duration. The pulses were then applied to the ORTEC 7100 configured as a multichannel analyser. In the mode used the height of each pulse between 10.24V and 0.20V (the low level discriminator setting) was measured and assigned to one of 1024 channels according to its amplitude. Every time a pulse was recorded, the count in the corresponding channel was increased by one. After the MCA had run for sufficient time, a histogram of pulse height vs frequency of occurrence was produced.

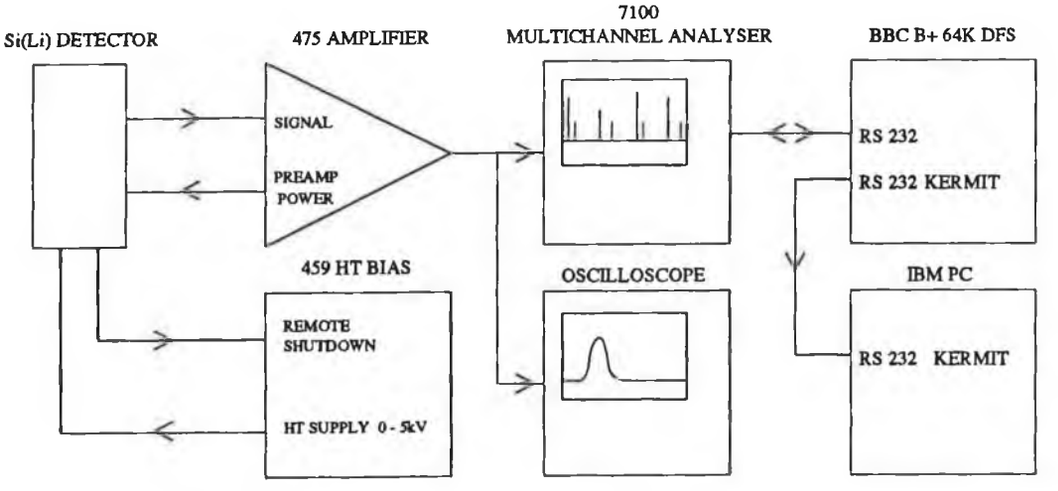

Figure 3.01
High energy resolution counting system.

The MCA used had a bidirectional RS-232 interface. Control codes from a computer or external terminal could be used to control the device instead of using the key pad on the front of the device. The MCA could also download count/channel data and machine settings via this link. A BBC B+ DFS(64k) running program "SPECTRA" was used to setup and record pulse height spectra. (Appendix F contains a listing). The recorded information was saved as a single

disk file which included the date, experiment description, real time, live time and the count in each of the 1024 channels.

Each set of spectra was recorded along with a calibration spectrum. To calibrate the system an Amersham AMC.2084 variable energy x-ray source was used. This contained a 10mCi Am241 source which was used to excite x-ray fluorescence in one of a number of targets moved in its way. The source was provided with documentation identifying the energy of the fluorescence lines [1]. A single spectrum containing Rb, Mo, Ag, Ba and Tb fluorescence lines was recorded and saved as a file.

Both the experimental spectra and calibration spectrum were sent to the IBM-PC using "KERMIT", a file transfer program that is available for most computers. The data was then converted to ASCII format using "BBC-DAT.EXE" [2].

A program written for the IBM to analyse spectra, "DISPLAY", was used to find the channel number corresponding to the peak of each of the ten fluorescence lines. The method of least squares was then used to fit a line to this data. The slope and intercept of the line was used to correlate channel number with x-ray energy.

Once calibrated, the detector efficiency could be removed from the pulse height spectrum using program "DETECT.EXE" (Appendix F). The efficiency data used was in the form of a graph provided with the detector. Since the Si(Li) detector had a high energy resolution, the calibrated pulse height spectrum corrected for detector efficiency and the x-ray spectrum incident on the detector was sufficiently similar for most work. The spread introduced in the spectrum by the detector resolution could be deconvolved out of the spectrum. Deconvolution programs were written (Appendix D) but were not used on spectra recorded with the Si(Li) detector. Unless great care is taken, deconvolution can move lines or even split them artificially. The continuous spectra describing the x-ray source would not be changed greatly by deconvolution. For presentation in this thesis the analysed data was produced using "GRAPHBOX" and "DRAW" running on an ARCHIMEDES 440.

3.1.2 RECORDING OF Si(Li) DETECTOR'S RESPONSE

Using the procedure outlined in section 3.1.1. a spectrum containing the fluorescence lines of Rb, Mo, Ag, Ba and Tb was produced using the variable energy x-ray source. This is shown in figure 3.02 . The data tabulated with this graph [1][3] was used to calibrate the spectrum. The calibration data has been graphed in figure 3.03. The correlation coefficient measured using linear regression of the data (CC = 0.999976) demonstrates the excellent linearity of the counting system.

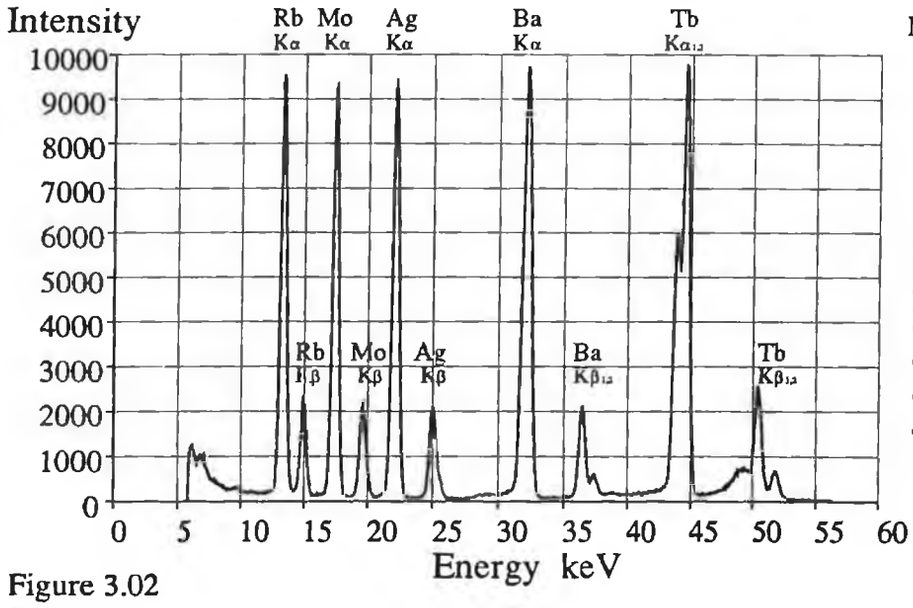

Mean peak energy
Rb Kα= 13.37 keV
Rb Kβ= 14.97
Mo Kα= 17.44
Mo Kβ= 19.63
Ag Kα= 22.10
Ag Kβ= 24.99
Ba Kα=32.06
Ba Kβ= 36.55
Tb $K\alpha_1$= 43.74
Tb $K\alpha_2$= 44.82
Tb $K\beta_1$= 50.32
Tb $K\beta_2$= 51.72

Figure 3.02
Calibration spectrum produced using the variable energy x-ray source and high resolution counting system.

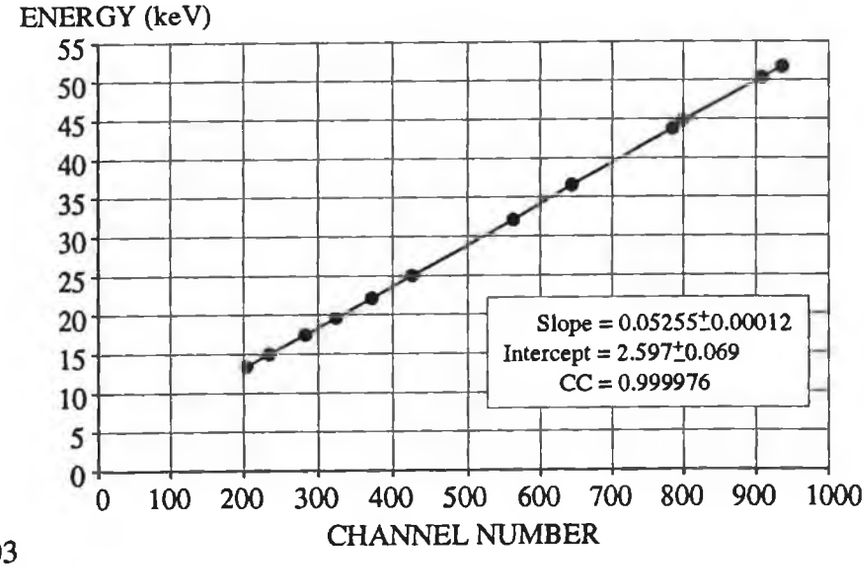

Figure 3.03
Graph of x-ray energy vs MCA channel number. [Si(Li) detector.]

The FWHM (full width half maximum) energy was measured for the narrowest fluorescence lines that did not show interference from other lines. These were the Tb $K_{\beta 1}$ (735eV) , Ba $K_{\beta 1}$ (580eV) and Rb K_{α}(520eV). The percent energy resolution for each of these line was calculated. The system was shown to have a percent energy resolution not greater than 4% over the energy range used (15kV-50kV).

A check on the curve describing detector efficiency was carried out by fixing the adjustable x-ray source above the Si(Li) detector. Over periods of 300 seconds spectra were recorded for each target in the adjustable source. Using "DISPLAY.EXE" the count contained in each fluorescence line was recorded. The count was then corrected using the efficiency function contained in program "DETECT.EXE" the data for which was obtained from figure 2.08. The measured total count was then converted to a relative photon yield. This yield was compared with the yields quoted for the source [1]. See table 3.01.

Source	Line.	Mean energy. keV	Count	Detector efficency. %/100	Corrected count.	Total count.	Measured yield.	Amersham yield (Expected)
Tb	Kα Kβ	44.23 50.65	352,712 73,806	0.292 0.260	1,207,918 283,869	1,491,787	1.000	1.000
Ba	Kα Kβ	32.06 36.55	460,905 93,865	0.578 0.429	797,413 218,799	1,016,212	0.681	0.612
Ag	Kα Kβ	22.10 24.99	476,926 113,706	0.904 0.840	527,573 135,364	662,937	0.444	0.505
Mo	Kα Kβ	17.44 19.63	312,054 76,969	0.965 0.952	323,372 80,849	404,221	0.271	0.319
Rb	Kα Kβ	13.37 14.97	134,020 30,864	0.986 0.980	135,923 31,494	167,417	0.112	0.116
Cu	Kα Kβ	8.04 8.91	26,765 5,810	1.000 1.000	26,765 5,810	32,575	0.022	0.033

Table 3.01
Check on Si(Li) detector efficiency curve.

This only provides a rough check on the detector efficiency function. However it does demonstrate the importance of correcting for detector efficiency when counts are being compared in different parts of the same spectrum.

3.1.3 RECORDING OF THE SCINTILLATION DETECTOR'S RESPONSE

The scintillation detector formed part of the original equipment supplied with the x-ray source; little information remained available on the detector. The main objective of this set of experiments was to establish the characteristics of the detector.

The scintillator was removed from the detector and was placed in the path of a collimated x-ray beam. The x-ray spectrum transmitted through the sample was recorded using the counting system described in section 3.1.1. The incident spectrum was recorded by removing the scintillator from the beam and counting for the same period of time. The ratio of the transmitted and incident count in corresponding channels was then calculated. The transmission spectrum produced is shown in figure 3.04.

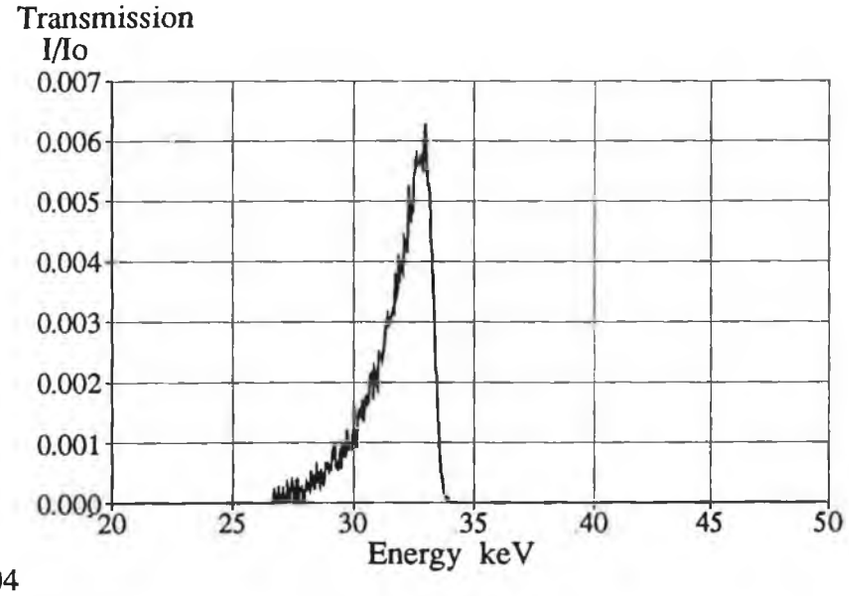

Figure 3.04
Graph of transmittance vs energy for the scintillator used.
(55kV filtered x-ray tube source.)

The position of the fall in transmission was consistent with the K-edge of iodine (E_k Iodine = 33.168keV). The transmission spectrum is also a measure of the relative efficiency of the scintillator. Even where the transmission is a maximum, just below the K-edge, the efficiency of the detector is very high as 99.4% of all incident x-ray photons are absorbed. At other energies where the transmission is less the detector is virtually

100% efficient.

The scintillation detector was reassembled and installed in a counting system schematically the same as that shown in figure 3.01. The method outlined in section 3.1.1 was used to record pulse height spectra of the detector's output. The photomultiplier tube was biased to 620V. Four pulse height spectra were produced using the Tb, Ba, Ag and Mo fluorescence lines of the adjustable source. These are shown in figure 3.05.

Energy calibration was achieved by identifying the channel number corresponding to the main peak in each spectrum. The width of each peak was measured by counting the channels between the maximum and the channel where the intensity fell to 0.607 of the maximum value on the left hand side of the peak; this gave an approximate value for the standard deviation in terms of channel numbers. Different high energy resolution fluorescence spectra were produced such that the K_α and K_β peaks roughly coincided in terms of channel with the low resolution spectra. These spectra were accurately calibrated and convolved with a Gaussian function with the appropriate standard deviation. The energies where the peak occurs in these convolved spectra were then used to calibrate the original pulse height spectra.

The main peak in the Tb spectrum was at 44.9keV. The K_α energy for iodine is 28.6keV [3]. The second peak is most probably an escape peak since 44.9-28.6 = 16.3keV. The measured peak value was 15.8keV. Compton scatter would produce a Compton edge at 7.5keV (equation 2.18 ϕ=180°) thus this process was not significant at the energies used.

The existence of the escape peak means that some of the x-rays with energies above the K-edge of iodine can produce low energy counts. Using the total count technique this was not a problem, since it only requires the total number of counts to be recorded: energy discrimination is not required. It would need to be considered in the tracking discriminator technique.

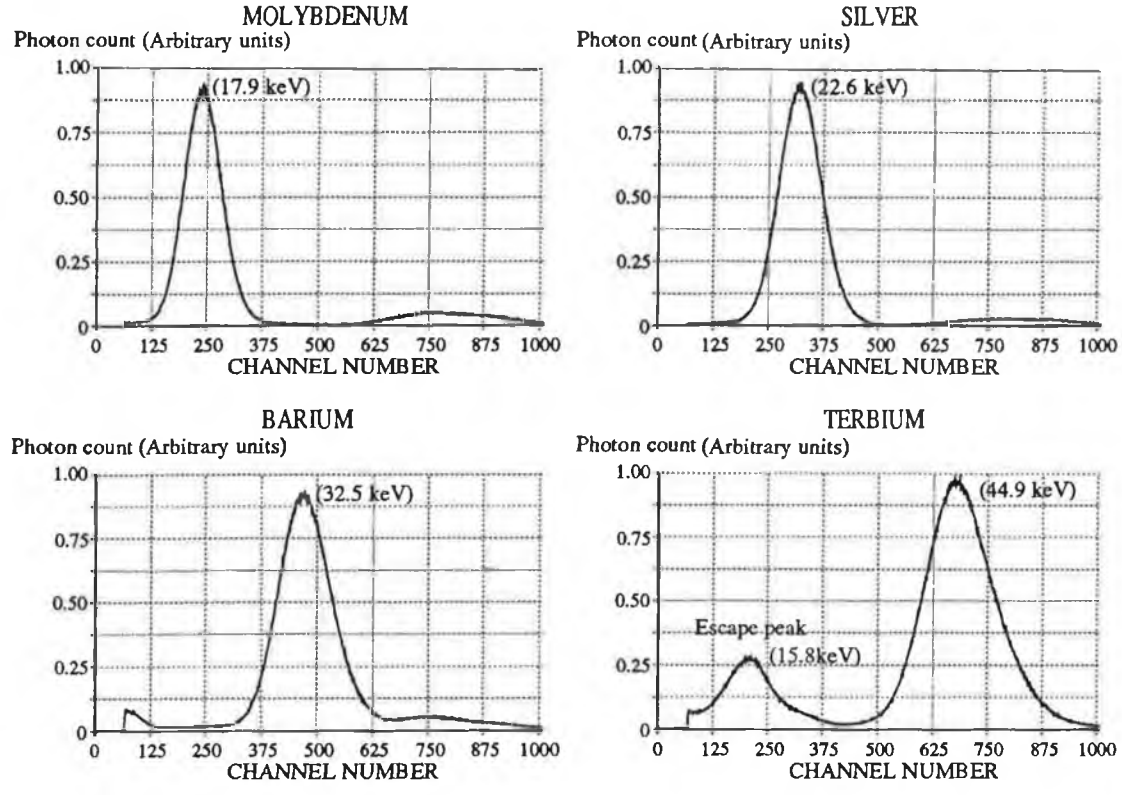

Figure 3.05
Fluorescence spectra of various elements recorded with a scintillation detector.

In summary, the scintillation detector contained an iodine based scintillator, most probably NaI(Tl). Change in efficiency was of the order of 0.6% across the energy range used. The percent energy resolution was of the order of 25% .

Iodine was one of the analytes used in subsequent experiments. The slight change in detector efficiency may have needed compensating for if the total count technique produced non-zero equivalent thickness values for absorbers containing no iodine.

3.1.4 RECORDING THE PROPORTIONAL DETECTORS RESPONSE

A gas flow proportional counter was obtained from the equipment supplied with the x-ray source. The body of the detector consisted of a machined block of aluminium containing a 3cm long, 2cm wide cylindrical cavity. A 0.04mm thick tungsten wire mounted on Teflon discs passed through the centre of this cavity. An opening on one side of the cavity supported a 6μm thick Mylar window. This was

coated with aluminium to keep the electric field uniform in the cavity. Since the cavity was pressurised, the window was supported by a collimator consisting of closely spaced metal foils. A cylinder containing P10 gas (10% CH_4, 90% Ar) was used to supply the detector. Gas pressure in the cavity was set at 0.7kp/cm^2. The flow rate through the detector was initially set to 3 litres/hr, for long duration experiments the flow rate was reduced to 2 litres/hr. Bias potential was set at 1600 volts. Early work with the detector demonstrated the poor quality of the integral amplifier. This was replaced by an externally mounted Ortec 142PC preamplifier. A gas density stabiliser supplied with the counter was used to maintain constant gas density inside the detector cavity. The configuration of the proportional counter system is shown in figure 3.06.

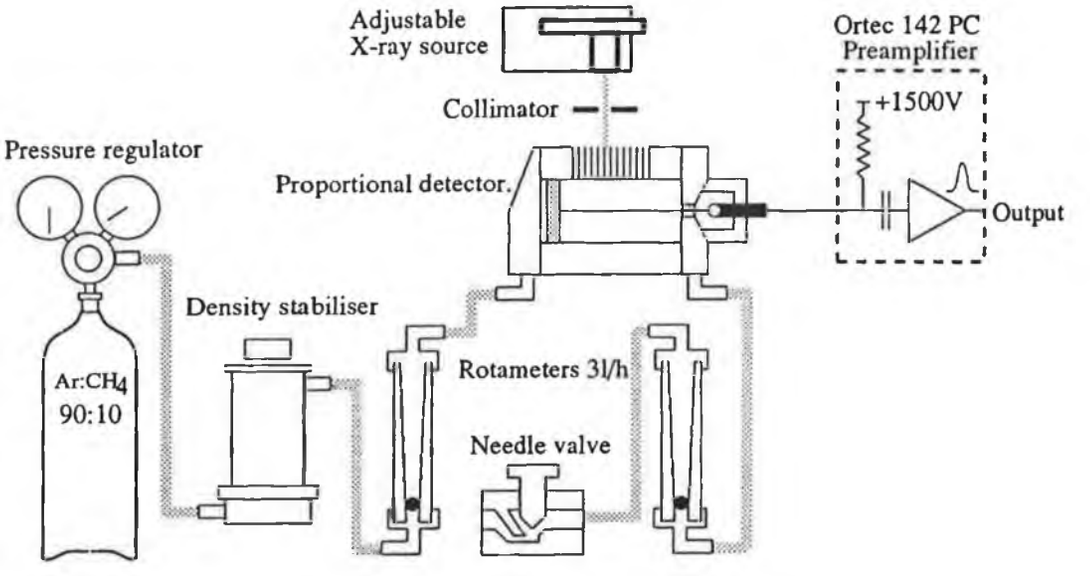

Figure 3.06
Experimental configuration used with the proportional detector.

To study energy resolution, the x-ray source was placed on top of the detector. Pulse height distributions from the detector were recorded using the multichannel analyser, for each of the target materials available in the source. Each pulse height spectrum produced contained a single broad peak. This peak contained counts originating from the K_α and K_β lines of the source. The channel corresponding to the maximum of the peak in each spectrum was identified. To find the energy of this peak a program

was written to convolve the detector response with a high energy resolution spectrum of the fluorescence lines. The program used previously measured values of the relative intensities of the K_α and K_β lines. The energy of the maximum in this convolved spectrum could then be used to calibrate the proportional counter spectra. The FWHM of the peak produced by the proportional detector was then measured in terms of energy for each of the spectra. Software was then used to find the standard deviation of a Gaussian describing the resolution that will produce a peak with a FWHM the same as that measured when convolved with the appropriate K_α and K_β lines. The results are shown in table 3.02.

Energy (keV)	Resolution (keV)
8.2	1.65
13.6	1.66
17.7	2.04
22.4	2.16
32.3	2.22
44.4	2.90

Table 3.02
Measured values for the energy resolution of the proportional detector.

A straight line was fitted to this data, giving

$$\sigma = 0.0267\ E\ (keV) + 1.439 \qquad (3.01)$$

The statistical limit of the energy resolution of a proportional counter varies inversely with the square root of the energy deposited by the incident radiation [4], using this function did not provide a better fit to the data. Variations of the E field in the detector coupled with effects in the preamplifier, degrade the resolution and so complicate this function.

The efficiency of the proportional counter varies as a function of energy; this was studied as follows. The adjustable x-ray source was fitted with a collimator. The beam produced was incident on the scintillation detector. This detector was nearly 100% efficient over the energy range studied (10 - 50 keV). The activity of the source was measured for each of the target materials available.

This was done by measuring the total count in a period of 1200 seconds. The source was then placed on the proportional counter and the procedure repeated. The efficiency of the counter was then calculated by rationing the scintillation and proportional detector counts for corresponding target materials. Although the fluorescence source contains at least two lines, the energy recorded is that of the convolved peak used to find the detector resolution. The results are shown in table 3.03.

Energy (keV)	Efficiency $x10^{-3}$
8.2	6.32
13.6	4.65
17.7	3.93
22.4	2.22
32.3	0.81
44.4	0.22

Table 3.03
Measured values for the efficiency of the proportional detector.

These data were used in the computer simulations (section 5.1.5.) and subsequent work on the tracking discriminator method (chapter 6).

3.1.5 DESCRIPTION OF HIGHER SPEED COUNTING SYSTEM

Using the total count technique to measure element concentration requires no energy resolution in the detector/pulse counting system. To measure total count with the multichannel analyser system is inefficient since the count in each channel has to be downloaded and then summed over all channels. The multichannel analyser pulse counting system was unable to process count rates higher than 10,000 counts per second without incurring significant dead times (>10%).

The SR7 Scalar Ratemeter (Nuclear Enterprises) based system was designed to overcome some of these limitations providing a high maximum count rate (at least 100,000 c/s) with faster readout times. See figure 3.07.

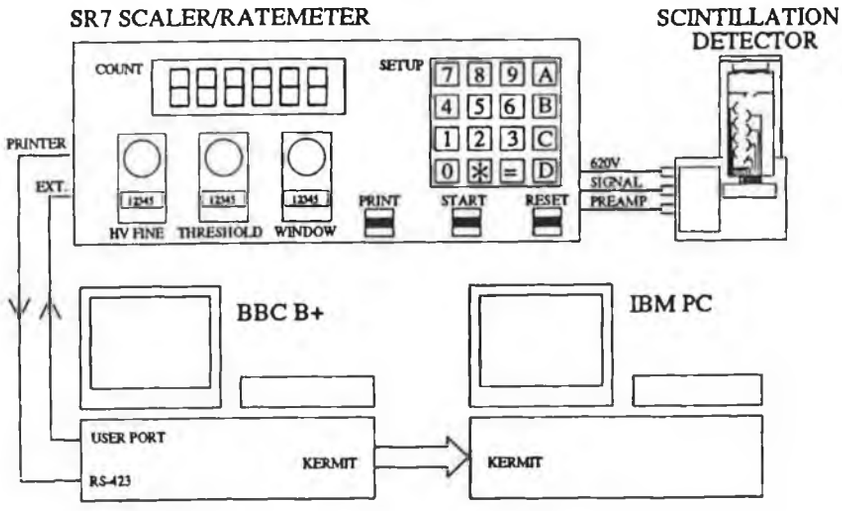

Figure 3.07
Higher speed counting system used with scintillation detector.

The SR7 was modified to provide the -12V required by the scintillation detector preamplifier. The 620V required by the photomultiplier tube of the detector was produced by the SR7. The output pulses of the detector preamplifier were connected to the SR7 amplifier input. The SR7 was configured to count all pulses above the amplifier/detector noise.

The SR7 may be configured to count over a fixed period of time and then print out the resulting count. Computer control of the SR7 was achieved by modifying the SR7 so that the start and reset switches could be controlled from the BBC user port (and the SR7 front panel). The printer output of the SR7 was connected to the RS-423 interface of the BBC. The count could be extracted from the printout data. The software to control and read information from the SR7 forms part of program "Carousel" (Appendix F).

3.2 DESIGN AND COMMISSIONING OF THE X-RAY SOURCE

3.2.1 DESCRIPTION OF THE X-RAY MACHINE

The x-ray machine consisted of three steel cabinets bolted together to form a single entity. These cabinets originally formed part of a Philips PW1270 automatic simultaneous spectrometer. The original machine was considerably modified to make it suitable for the research carried out in this project. The first cabinet contained the low voltage control circuitry. The second contained the HT tank. The third contained the x-ray tube, scan table and detector system. See figure 3.08.

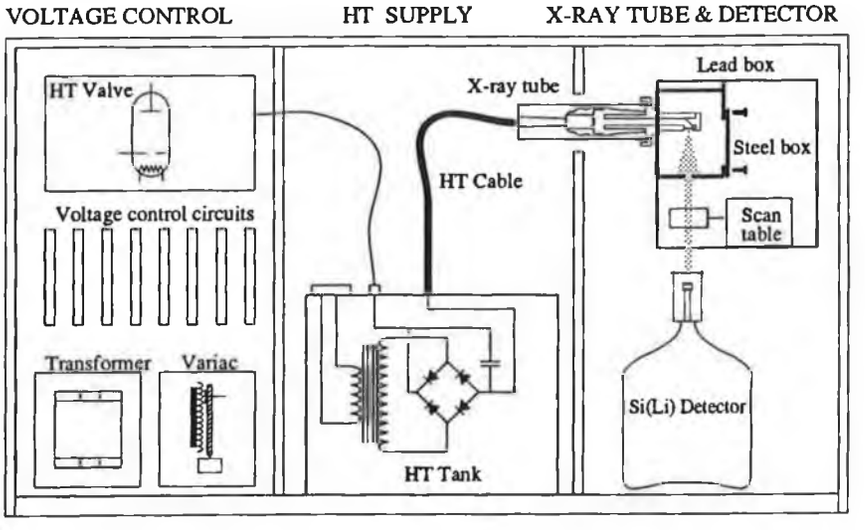

Figure 3.08
The x-ray machine.

The machine generated the 20-60kV DC from the mains AC supply as follows. See figure 3.09. Single phase 220/240 V A.C. was connected to the input of the variable auto-transformer (Variac). The Variac output was under the control of a servo motor. The output of the Variac drove the primary of the step-up transformer contained in the HT tank. A bridge rectifier rectified the secondary voltage. The HT was smoothed using a capacitor. The HT tank output was carried to the tube by a single HT lead (chassis ground). A potential divider across the output produced a low potential "measured value" proportional to the HT output. A control loop drove the servo motor to keep set and measured values the same. A high speed voltage control circuit was used to remove some of the output ripple and

remove the quantization error due to the windings on the variac. This was achieved by varying the grid bias voltage on the HT valve.

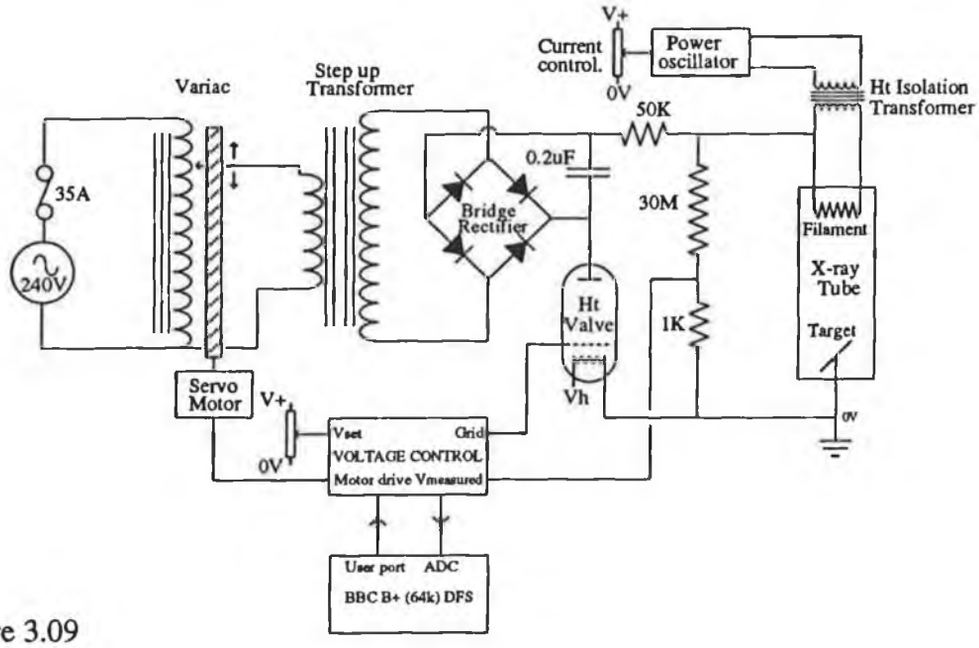

Figure 3.09
Overview of x-ray tube power supply.

In a number of the experiments it was necessary to record the tube potential. This was achieved by installing a differential amplifier to measure the potential across the panel meter displaying tube potential on the machine. A differential amplifier was used so that chassis ground/mains earth could be used as signal zero volts. The amplifier was powered by its own power supply. The unit was fitted inside the cabinet, its output was brought to the front of the main panel by two 4mm sockets. V_{out} = 50mV per kV . A lab amplifier was constructed so that output voltage could be scaled to make it suitable for the analogue to digital converter (ADC) used. An inverter in the lab amplifier meant that the output could also be used to control an ORTEC 551 SCA discriminator level.

On the original machine it was not possible to continuously vary the tube potential. The machine was modified such that the original switched resistor network, used to define the set value, could be switched out of circuit and replaced with a potentiometer allowing continuous control of the tube voltage. A toggle switch on the front panel provided this function.

The tube voltage could be controlled by a computer in two ways. With the first, a stepper motor driven by the computer was used to set the potentiometer to the desired value using the ADC for feedback. Alternatively, an external control box could be connected to the machine. This disabled the potentiometer installed on the machine. Any one of the four potentiometers provided on the control box could then be switched into circuit. This could be achieved manually with a selector switch or externally using two data lines of the BBC user port. Circuit diagrams for the laboratory amplifier, the differential amplifier and the voltage control box are contained in appendix E.

3.2.2 CONSIDERATION OF THE SHIELDING REQUIREMENTS

The shielding calculations to verify the safety of the x-ray machine are contained in appendix C. From these calculations it is shown that the estimated additional maximum possible dose ($2x10^{-6}$ mG/h) obtainable from the machine by an operator standing by it, is lower than the average background radiation level ($3x10^{-4}$ mG/h) [5]. The machine was verified for safety by the Nuclear Energy Board.

The calculated dose is exceedingly small. One chest x-ray can deliver a dose as low as 0.1mSv [5]. The ICRP (International Commission on Radiological Protection) recommended that the average effective dose equivalent for a member of the public should not exceed 1mSv/year additional to the natural background [6].

3.2.3 RECORDING OF TUBE OUTPUT SPECTRUM

To design filters for the x-ray source it was necessary to record the x-ray tube output spectrum.

The Si(Li) detector was placed under the exit hole of the lead box of the x-ray machine. One millimetre collimators were placed over the exit hole of the steel box and the lead box. A lead cap containing a 0.2mm hole was placed over the detector. This attenuated the beam without changing its spectrum. Serious pulse pile up would occur

within the detector system without this extra attenuation.

The x-ray machine was set to operate at 30kV and a spectrum was recorded using the procedure outlined in section 3.1.1. This is shown in figure 3.10.

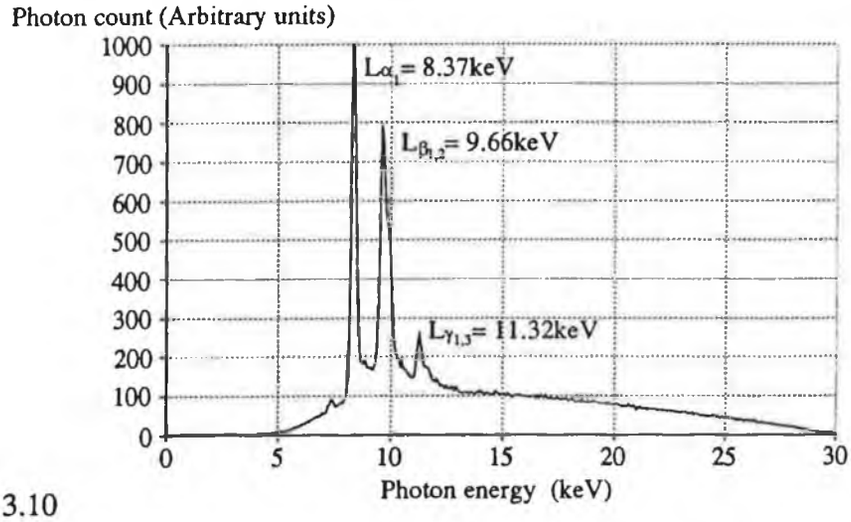

Figure 3.10
Unfiltered x-ray spectrum, recorded with a tube potential of 30kV.

Figure 3.10 shows the characteristic output spectrum of an x-ray tube consisting of a continuous spectrum on which is superimposed a number of fluorescence lines.

3.2.4 IDENTIFICATION OF THE FLUORESCENCE LINES

It was desirable to identify the lines in the tube source spectrum. Identification of the lines proved the identity of the target of the tube. Lines could also be produced by fluorescence of the materials used in the construction of the tube and collimation system. These lines produced little information for the total count technique and were ultimately filtered out of the spectrum. Using the adjustable x-ray source in conjunction with the Si(Li) detector a fluorescence spectrometer was configured as shown in figure 3.11.

The terbium target of the adjustable x-ray source was used to produce ≃ 50keV x-rays. (Tb K_α = 44.23. keV, K_β = 50.65 keV [1]). These x-rays were used to excite fluorescence in the material of interest. The detector was collimated so it could only see this secondary fluorescence.

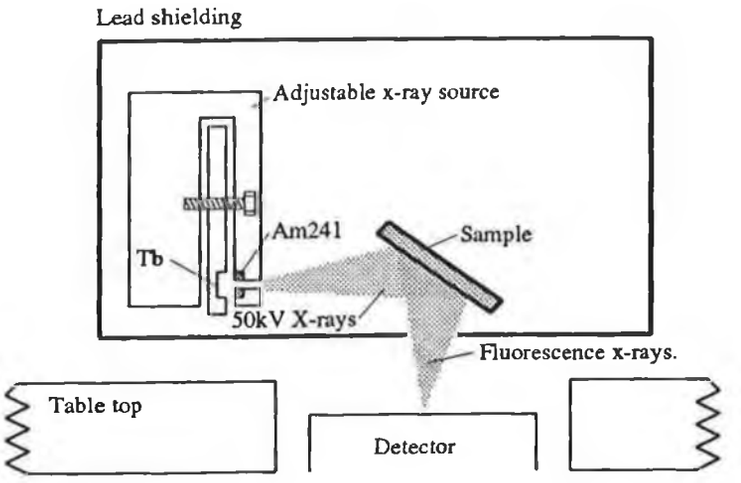

Figure 3.11
X-ray fluorescence spectrometer used to help identify target fluorescence lines.

Spectra were recorded for samples of lead, copper, iron and tungsten. A sample of pure tungsten was not available, so epoxy resin loaded with powdered tungsten sulphate was used. The parts of the apparatus the beam was incident on are made out of these four elements. The corresponding fluorescence spectrum for each element is shown in figure 3.12.

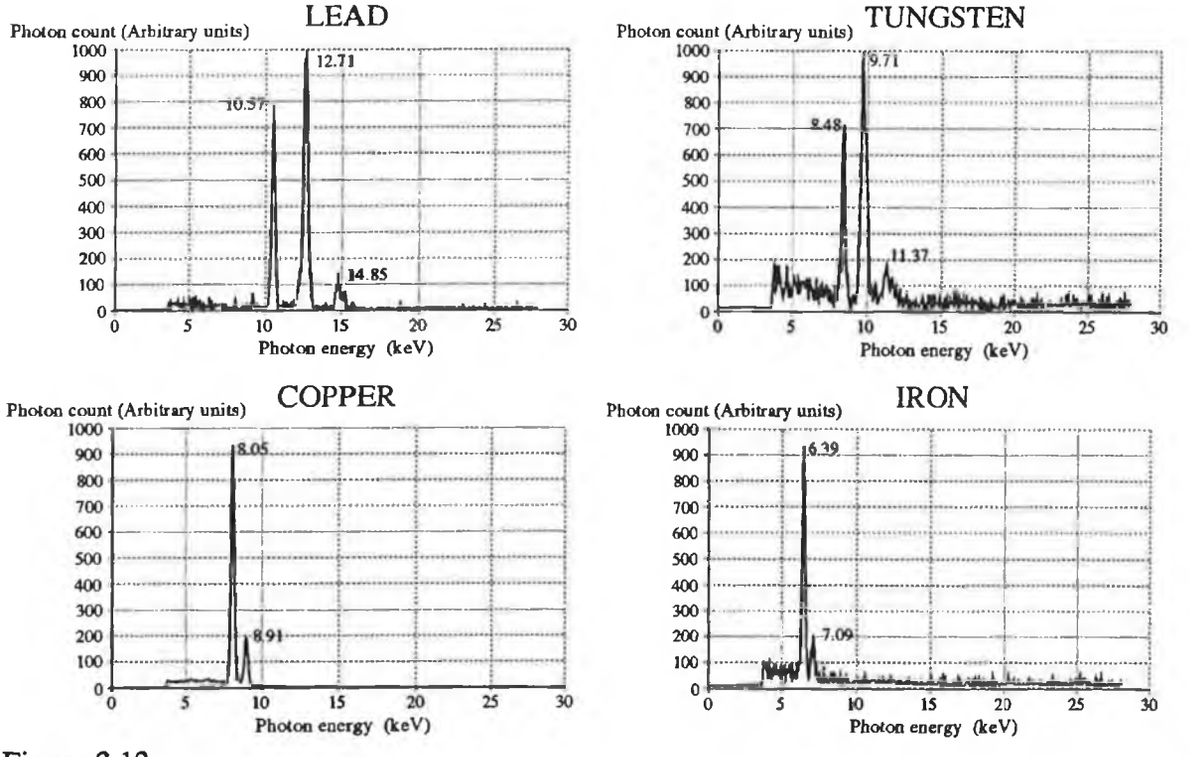

Figure 3.12
Fluorescence spectra of the main component elements of the source.
(Measured energy of fluorescence peaks are in keV)

Comparison of these spectra with the tube source spectra showed that the lines were due to fluorescence of the tungsten target of the x-ray tube and so could not be removed by a change of collimator or apparatus geometry.

Since the lines were known to be of tungsten they could be identified using tables [3]. Table 3.04 correlates the different notations [3][7].

Siegbahn designation	Level designation	Electron transition.	Energy keV	Apx. yield. ($L\alpha_1$=100%)
$L\alpha_1$	$L_{III}M_V$	$2^2P_{\frac{3}{2}} \longrightarrow 3^2D_{\frac{5}{2}}$	8.396	100
$L\beta_1$	$L_{II}M_{IV}$	$2^2P_{\frac{1}{2}} \longrightarrow 3^2D_{\frac{3}{2}}$	9.672	50
$L\beta_2$	$L_{III}N_V$	$2^2P_{\frac{3}{2}} \longrightarrow 4^2D_{\frac{5}{2}}$	9.959	20
$L\gamma_1$	$L_{II}N_{IV}$	$2^2P_{\frac{1}{2}} \longrightarrow 4^2D_{\frac{5}{2}}$	11.284	10
$L\beta_3$	$L_I M_{III}$	$2^2S_{\frac{1}{2}} \longrightarrow 3^2P_{\frac{3}{2}}$	9.819	6
$L\gamma_3$	$L_I N_{III}$	$2^2P_{\frac{1}{2}} \longrightarrow 4^2D_{\frac{3}{2}}$	11.675	2

Table 3.04
Fluorescence lines of tungsten.

3.2.5 DESIGN OF A FILTER FOR THE SOURCE

The techniques outlined to date for measuring analyte equivalent thickness using fractional transmittances may work using the output spectrum of a standard x-ray tube. However, filtering the source greatly improves its suitability for the technique. A good filter would have the following properties:

(i) Since x-ray tubes have a limited output power, a filter with a response of the correct shape but, at the same time, strongly attenuating, would result in long counting times and inefficiency in the system. For this reason the filter should not be strongly attenuating in the region where counts are required.

(ii) The filter should strongly attenuate all low energy counts which provide little spectral information and increase detector dead times.

(iii) The filter should preferentially allow counts in the front end of the x-ray spectrum.

(iv) The technique developed for the current problem works from the first K-edge and above in the absorber. Such a filter should prevent low energy K-edge jumps of elements contained in the matrix but not of interest from being "visible".

Due to the various requirements stated above it was difficult to define what the ideal filter response should be. Even if this filter response was known it would be difficult to achieve in practice with the elements available. With the above ideas in mind the following procedure was used to produce an adequate filter.

To design a suitable x-ray filter the "Hubble" program was written (See Appendix G). This contained a database of 9 tube source spectra recorded in 5kV steps between 20kV and 60kV (obtained using the technique outlined in 3.1.2), absorption data obtained from tables [8] for many elements, water and some compounds, and the detector response for the Si(Li) detector. Using this program it was possible to combine source, absorber and detector responses and produce a prediction of the filter response and resulting spectra. Using the program a filter containing copper, bromine and water had a response suitable for the system. The predicted response for this filter is shown in figure 3.13.

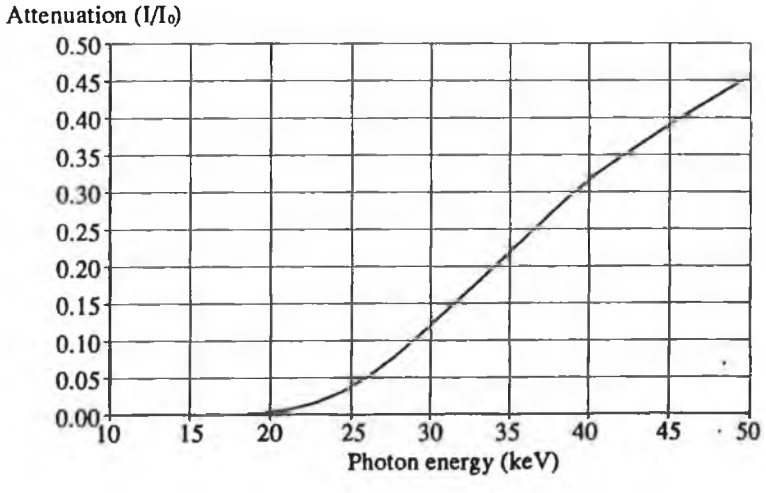

Figure 3.13
Filter response designed using progam "Hubble"
(0.6 kg/m^2 Bromine, 0.3 kg/m^2 Copper, 20kg/m^2 Water)

This filter was realised by dissolving potassium bromide and cupric chloride in distilled water. The resulting solution was contained in a sample cell accurately constructed so that the physical thickness of solution the beam passed through was 2cm. The concentration of the solutes in the solution were calculated as follows.

Cell thickness = 2cm (So that t_{H_2O} = 20 kg/m^2)

K = 39.1 AMU	Cu = 63.55 AMU
Br = 79.9 AMU	Cl = 35.45 AMU
KBr = 119.0 AMU	$CuCl_2.2H_2O$ = 170.45 AMU

1g Br = 119/79.9g KBr

t_{Br} = 0.6 kg/m^2

C_{Br} = 0.6 kg/m^2 / 0.02m

$$C_{KBr} = \frac{0.6}{0.02} \times \frac{119}{79.9} \text{ kg/m}^3$$

= 44.68 kg/m^3

= 4.468 g/100cc

1g Cu = 170.45/63.55g $CuCl_2.2H_2O$

t_{Cu} = 0.3 kg/m^2

C_{Cu} = 0.3 kg/m^2/ 0.02 m

$$C_{CuCl_2} = \frac{0.3}{0.02} \times \frac{170.45}{63.55} \text{ kg/m}^3$$

= 40.23 kg/m^3

= 4.023 g/100cc

3.2.6 RECORDING OF TUBE OUTPUT AT DIFFERENT POTENTIALS

The filter was installed in the x-ray machine over the exit hole in the steel box. Using the procedure described in section 3.2.3. the tube source spectrum was recorded for a fixed live time at different tube voltages. Program "SPECTRA" was modified so that the tube voltage was under software control. Spectra were recorded automatically for tube voltages decrements of 700V in the interval 42kV to 27kV. The resulting spectra are shown if figure 3.14.

This new data was included in the "Hubble" database and used to assist with the configuration of subsequent experiments.

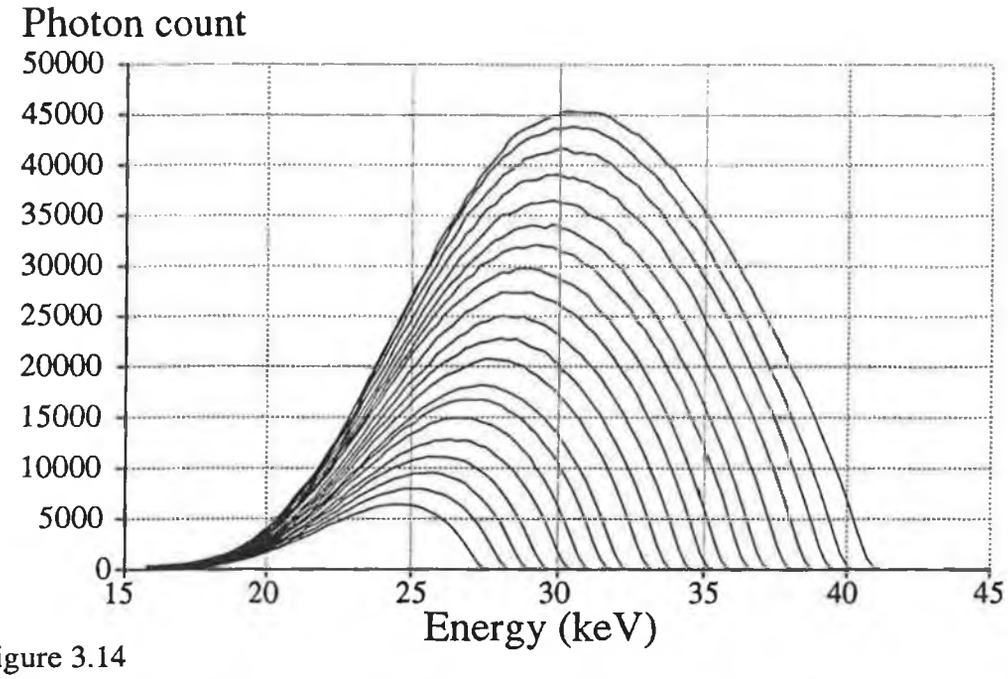

Figure 3.14
Filtered x-ray spectra recorded between 27kV and 42kV in 700V steps.

3.3 SUMMARY

A high resolution spectroscopic pulse counting system based on a Si(Li) detector and MCA was designed and commissioned. The system has high energy resolution, and excellent linearity. The pulse height spectra produced by the system required correcting for detector efficiency.

A gas proportional detector system was developed that was compatible with MCA based spectroscopic counting system.

A low resolution counting system based on a scintillation detector was designed to provide a fast counting system with fast readout times. The system recorded only the total incident count on the detector.

The x-ray source was modified so that the tube potential could be computer controlled. A filter was designed to make the shape of the output spectrum more suitable for the techniques developed.

References

[1] "Instrument calibration sources"
Amersham International plc, catalogue.

[2] McCabe, S. & Giessel, A.
Software "BBC_DAT". Dublin City University.

[3] Bearden, J.A.
"X-ray Wavelengths and X-ray Atomic Energy Levels"
National standards reference data series 14, U.S. Government printing Office, 1967.

[4] Knoll, G.F.
"Radiation detection and measurement"
John Wiley & Sons., pp 178, 1989.

[5] Reville, W.J.
"Radioactivity"
ENFO briefing sheet 7, 17 Andrews Street Dublin 2, 1990.

[6] Martin, A. and Harbinson, S.A.
"An introduction to radiation protection"
Chapman and Hall, 1990.

[7] Bertin, E.P.
"Principles and practices of X-ray spectrometric analysis"
Plenum press, New york, 1975.

[8] Hubble, J.H.
Mass attenuation and Energy Absorption coefficients from 1keV to 20MeV"
Int. J. Appl. Radiat. Isot.,Vol. 33, pp 1269-1290, 1982.

Chapter 4

Experimental results : Verification of the Total Count Technique

Introduction

A set of experiments was carried out to check the total count technique of measuring analyte equivalent thickness. Each aspect required of the technique was checked independently before an attempt was made to produce an image. Production of an image required all these aspects to work together simultaneously; if there was a flaw in any one part of the technique it would have been difficult to identify it using CT images alone. It also requires a great deal more data and computer time to produce an image which at the early stages of verification produces little additional information about the technique than a single measurement of equivalent thickness. The key requirements of the total count method of measuring analyte equivalent thickness are that the technique is linear, independent of the matrix, can measure two elements simultaneously and will work with a detector with little or no energy resolution.

4.1 MEASUREMENT OF ELEMENT CONCENTRATION IN A HOMOGENEOUS SAMPLE

Introduction

The experiments described in this section tested the linearity and matrix independence of the total count technique. The simultaneous measurement of two elements contained in the same beam path was also investigated.

The Si(Li) detector was used throughout this set of experiments so that the results obtained using the total

count technique could be compared with those obtained using differential absorptiometry. Using the Si(Li) detector for recording both the fractional transmittances and reference spectra removed the need to include the effect of detector efficiency.

4.1.1 DEMONSTRATION OF LINEARITY

The equivalent thickness of an analyte distributed homogeneously in an absorber of known thickness was measured. The concentration of analyte was adjusted over a range of values so that a comparison between the measured and set values of analyte equivalent thickness could be compared. Iodine was the analyte chosen for initial experiments. The K-edge of iodine (E_K = 33.168 keV) is located within the range of x-ray energies available from the x-ray machine (20-60keV).

Iodine based pharmaceuticals are already used as contrast agents in medical imaging. The doses administered to the patients are sufficient to be unpleasant for the patient (e.g. 70ml iopromide delivered at rate 17ml/s containing 300mg/ml iodine has been used for peripheral angiography [1]). Techniques that might suggest how the dose of contrast agent delivered can be reduced may be of benefit.

Tube potential V_2 was chosen so that the highest x-ray energy produced was just below the K-edge of iodine. The other two tube potentials were then chosen using the simulation program "Hubble", see appendix G. The lower tube potential V_1 was chosen so that spectra produced at V_1 and V_2 were different enough to allow α_1 and β to be determined. If V_1 was very low then the count rate would be too low to be practical. The tube potential V_3 above the K-edge was chosen so that a significant percentage of the x-rays detected had energies above the iodine K-edge. The tube potentials used were V_1 = 27kV, V_2 = 32kV and V_3 = 38.5kV. Eight samples were investigated with iodine equivalent thicknesses in the range 0.35 kg/m^2 to 0 kg/m^2. See figure 4.01.

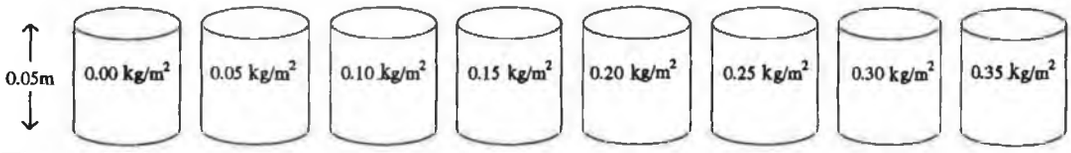

Figure 4.01
Sample cells used for linearity experiment.
Equivalent thickness of iodine shown in each cell.

Eight sample cells were constructed from PVC pipe cut and ground to a length of 50mm. Clear plastic discs were glued on the end of the tube. A plastic collar on the tube supported the cell so that the beam path through the cell was 50mm. The cells could be filled through ports glued in the side of the tube using a 100ml glass syringe. See figure 4.02.

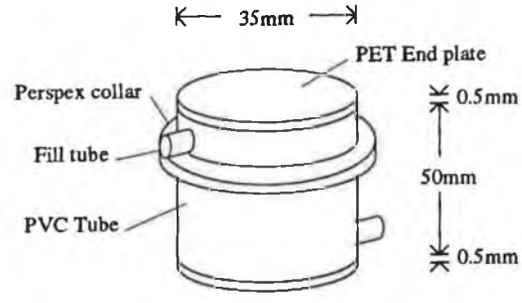

Figure 4.02
Construction of a typical sample cell.

A stock solution containing 2500kg/m^3 iodine was prepared by dissolving potassium iodide in distilled water.

K = 39.1 AMU
I = 126.9 AMU
KI = 166.0 AMU

$$2500 \text{ kg/m}^3 \times \frac{166.0}{126.9} = 32.70 \text{ g/litre KI}$$

A 40ml sample of stock solution contained 1g of iodine. Samples of stock solution were diluted to provide the solutions required to fill the sample cells. Dilutions were calculated using equation 4.01.

$$\text{Vol} = \frac{M\ l}{t_a} \qquad (4.01)$$

where M was the mass of analyte (0.001kg), l was the sample length (0.05m), t_a was the analyte equivalent thickness and Vol the dilution volume. See table 4.01

Equivalent thickness of iodine. kg/m^2	Dilution volume. 40cc of stock soln. made up to X cc.
0.35	143
0.30	167
0.25	200
0.20	250
0.15	333
0.10	500
0.05	1000
0.00	N/A

Table 4.01
Dilutions used for linearity experiment.

A sample carousel was constructed which could position accurately any one of sixteen sample cells in the beam path between source and detector. The cell was selected by a 4 bit number sent from the BBC user port. (See appendix E and F for details). The eight sample cells were placed in the carousel in alternate positions, the other locations being left empty. See figure 4.03

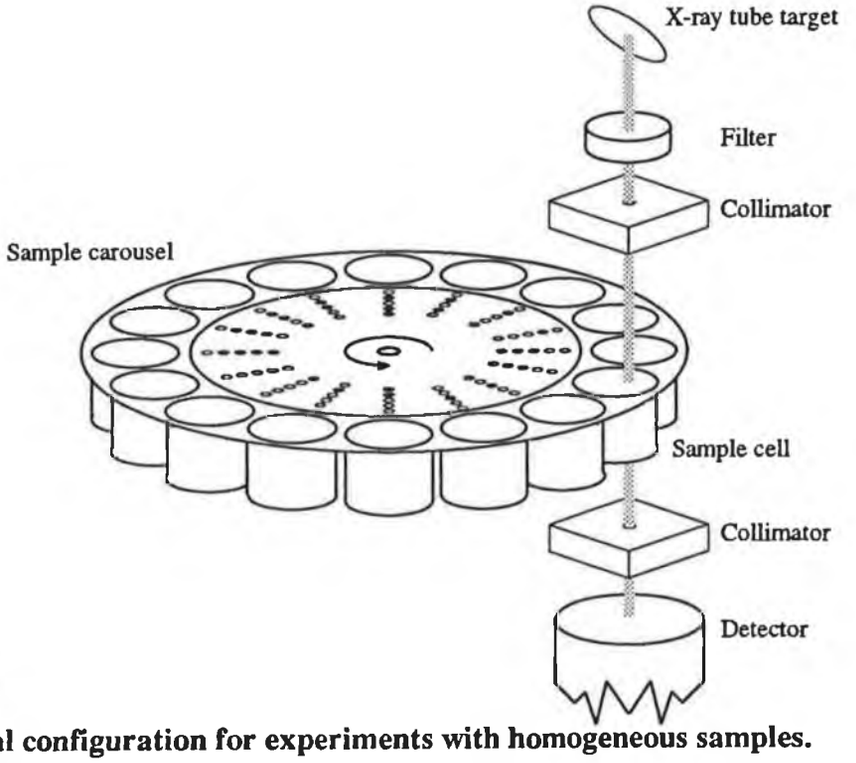

Figure 4.03
Experimental configuration for experiments with homogeneous samples.

The program "Carousel", running on a BBC B+ 64K, was

used to control the x-ray machine, multichannel analyser and sample carousel (see appendix F). Under this software control, spectra were recorded for each of the sixteen carousel positions. Taken in pairs these spectra represented the spectrum incident on the sample and the spectrum transmitted through the sample. The procedure was repeated for the three tube potentials V_1, V_2 and V_3. Detector live time for each spectrum was 2000 seconds. The forty eight spectra were downloaded from the BBC B+ 64K to an IBM PC. The adjustable x-ray source was used to calibrate the spectra.

Using the total count technique, program "Linear/Matrix" (Appendix F) evaluated the equivalent thickness of iodine in each sample. The procedure used was detailed in section 2.3. The total count in the transmitted spectra was obtained by summing over all multichannel analyser channels. This was then divided by the total count in the reference spectrum to obtain the fractional transmittance.

Software was written to measure the equivalent thickness of iodine using differential absorptiometry. The software produced a new spectrum file containing the logarithm of the ratio of incident and transmitted counts for each channel location. This was used on spectra recorded at the highest tube potential. Using the spectrum display program, values of $\ln(I/I_0)$ were recorded at two energies just below the K-edge. A line projected through these points to the K-edge was used to find $\ln(I/I_0)$ at the low side of the K-edge. Using a similar technique, a value of $\ln(I/I_0)$ on the high side of the K-edge was obtained. Using equation 2.37 the iodine equivalent thickness was calculated. The results of this and the total count technique are shown in table 4.02.

Both techniques produced results in agreement with the set values. A graph of set value against measured value for the total count technique is shown in figure 4.04

Equivalent thickness of iodine.		
Set value. kg/m^2	Differential absorptiometry. kg/m^2	Total count technique. kg/m^2
0.35	0.354	0.333
0.30	0.322	0.294
0.25	0.228	0.251
0.20	0.216	0.165
0.15	0.157	0.123
0.10	0.096	0.107
0.05	0.035	0.043
0.00	0.025	0.001

Table 4.02

Table of measured values of analyte equivalent thickness obtained using differential absorptiometry and the total count technique. Used to test the linearity of the total count technique.

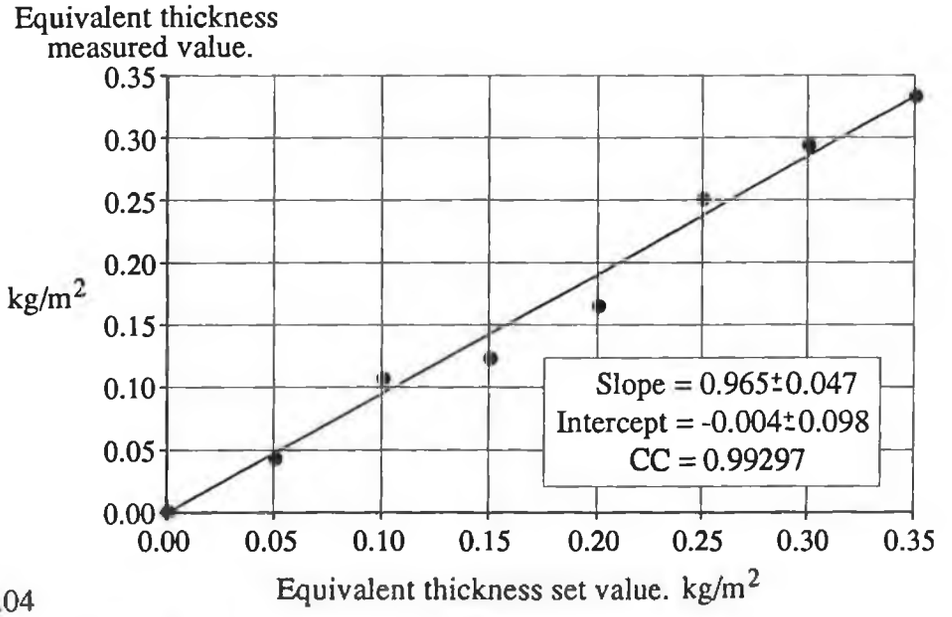

Figure 4.04

Graph of set value of iodine equivalent thickness vs measured value. Demonstrating the linearity of the total count technique.

Using the method of least squares, the slope, intercept, error in slope, error in intercept and correlation coefficient were calculated for this data. The slope was equal to one within error. The intercept was zero within error. The measured values of analyte equivalent thickness obtained by the total count technique were shown to be in agreement with the values obtained using differential absorptiometry and those set by dilution of the stock solution.

4.1.2 DEMONSTRATION OF MATRIX INDEPENDENCE

A set of sample cells of varying length were constructed. These were each filled with a concentration of analyte such that the equivalent thickness of analyte was the same in each cell. The effect of the matrix on the total count technique could be examined by comparing the measured values of analyte equivalent thickness with the value expected.

Six sample cells were constructed varying in length between 1cm and 6cm. See figure 4.05.

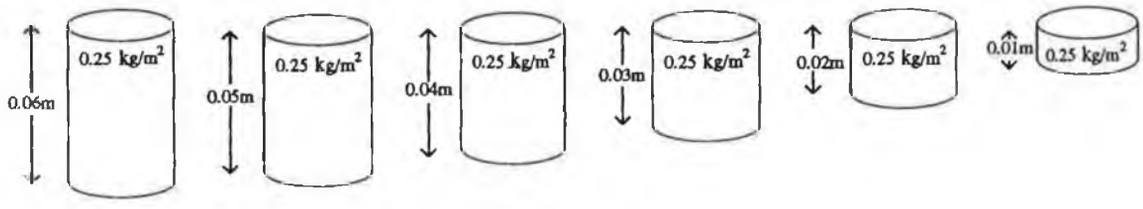

Figure 4.05
Sample cells used to show matrix independence. Equivalent thickness of iodine shown in each cell.

The sample cells were filled with dilutions of the stock solution such that each produced an iodine equivalent thickness of 0.25kg/m^2. The sample cells were placed in the sample carousel. The procedure outlined in section 4.1.1 was used to measure the iodine equivalent thickness using differential absorptiometry and the total count technique. The results are shown in table 4.03.

	Equivalent thickness of iodine.		
Sample thickness mm	Set value. kg/m^2	Differential absorptiometry. kg/m^2	Total count technique. kg/m^2
60	0.25	0.277	0.231
50	0.25	0.225	0.208
40	0.25	0.268	0.238
30	0.25	0.242	0.194
20	0.25	0.238	0.238
10	0.25	0.218	0.208
		$\bar{x} = 0.245$ $\sigma = 0.002$	$\bar{x} = 0.220$ $\sigma = 0.017$

Table 4.03
Table of measured values of analyte equivalent thickness obtained using differential absorptiometry and the total count technique. Used to demonstrate matrix independence of the total count technique

The total count method shows a larger variance in the

measured value of iodine equivalent thickness than differential absorptiometry. However, there was no significant trend in the measured value of iodine equivalent thickness as a function of sample thickness. This indicated that, over the range examined, the total count technique was independent of the matrix.

4.1.3 MEASUREMENT OF TWO ELEMENTS SIMULTANEOUSLY

The equivalent thickness of two elements was measured simultaneously using the total count technique and differential absorptiometry.

Barium and iodine were chosen as analytes. The K-edge of barium is at 37.41keV. This is 4.25keV above the K-edge of iodine. V_1 and V_2 were chosen as before V_3 was set at 37kV and V_4 set at 43.5kV.

Two sample cells were placed one above the other. One cell was filled with potassium iodide solution such that the equivalent thickness of iodine was 0.25kg/m^2. The second cell was filled with barium chloride solution such that the equivalent thickness of barium was 0.50kg/m^2. Barium has a smaller K-edge jump than iodine so the concentration was increased above that of iodine.(ΔU_{Ba} = 2.53 m^2/kg, ΔU_I = 3.00m^2/kg). High concentrations of iodine could reduce the counts above the iodine K-edge to such an extent that it may be difficult to detect barium.

The spectrum incident on the sample cells and transmitted through the pair of cells was recorded at each of the four tube potentials. Using software almost identical to program "Linear/Matrix", the values of the equivalent thickness of each analyte were calculated. The results are shown in table 4.04.

	Equivalent thickness of iodine.		
	Set value. kg/m^2	Differential absorptiometry. kg/m^2	Total count technique. kg/m^2
Iodine	0.25	0.23	0.23
Barium	0.50	0.50	0.40

Table 4.04
Results of two analyte experiment.

These results showed that it was possible to measure

two analytes simultaneously using the total count technique. It also demonstrated that V_4 should be set higher to increase the counts above the second K-edge and so improve the measured value of barium equivalent thickness.

4.2 MEASUREMENT OF EQUIVALENT THICKNESS USING A LOW RESOLUTION DETECTOR WITH THE TOTAL COUNT TECHNIQUE

The experiments described in section 4.1 used a Si(Li) detector/multichannel analyser counting system, to record all count information. This allowed a comparison to be made between the results obtained using differential absorptiometry and the total count technique. It also eliminated the need to correct the reference spectra for detector efficiency.

The linearity experiment described in section 4.1.1 was repeated to demonstrate that the total count technique would still operate using a low resolution detector. The experiment was made different by using a NaI(Tl) scintillation detector to measure fractional transmittances at V_1, V_2 and V_3. Reference spectra were recorded using the Si(Li) detector. The spectra were corrected for detector efficiency using program "Detect" (see appendix F).

The results of this experiment are shown in table 4.05

Equivalent thickness of iodine.	
Set value. kg/m^2	Total count technique. kg/m^2
0.35	0.339
0.30	0.282
0.25	0.228
0.20	0.191
0.15	0.153
0.10	0.102
0.05	0.069
0.00	0.019

Table 4.05
Linearity experiment using low resolution detector

A graph of set value against measured value of iodine equivalent thickness was plotted. See figure 4.06.

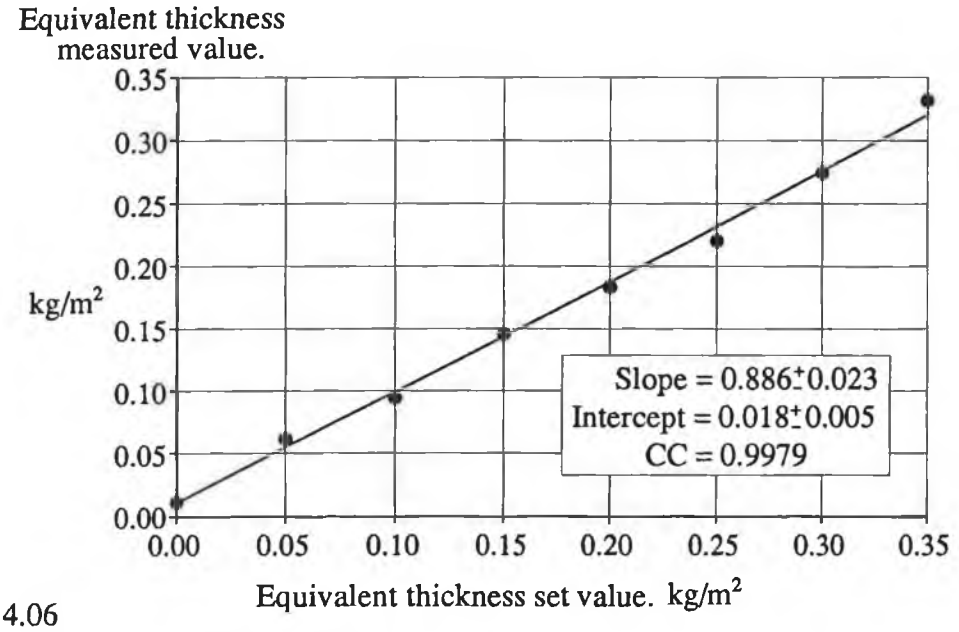

Figure 4.06
Graph of set value of iodine equivalent thickness vs measured value. Experimental data collected using a low resolution detector.

The slope, intercept, error in slope and error in intercept were calculated. The measured value of the slope was slightly below the expected value of one. This may be due to the reference spectra not being corrected for Si(Li) detector efficiency with sufficient accuracy. The result showed that it was possible to measure analyte equivalent thickness using fractional transmittance recorded with a low resolution detector.

4.3. IMAGE PRODUCTION

Introduction

In this section the experimental work that produced element specific and conventional computerised tomographic images of an object is described. Two elements were distributed in different regions of a specially constructed object. A comparison of the images produced by the two techniques was made.

4.3.1. APPARATUS FOR IMAGE PRODUCTION

The experimental configuration that was used to produce images is shown in figure 4.07.

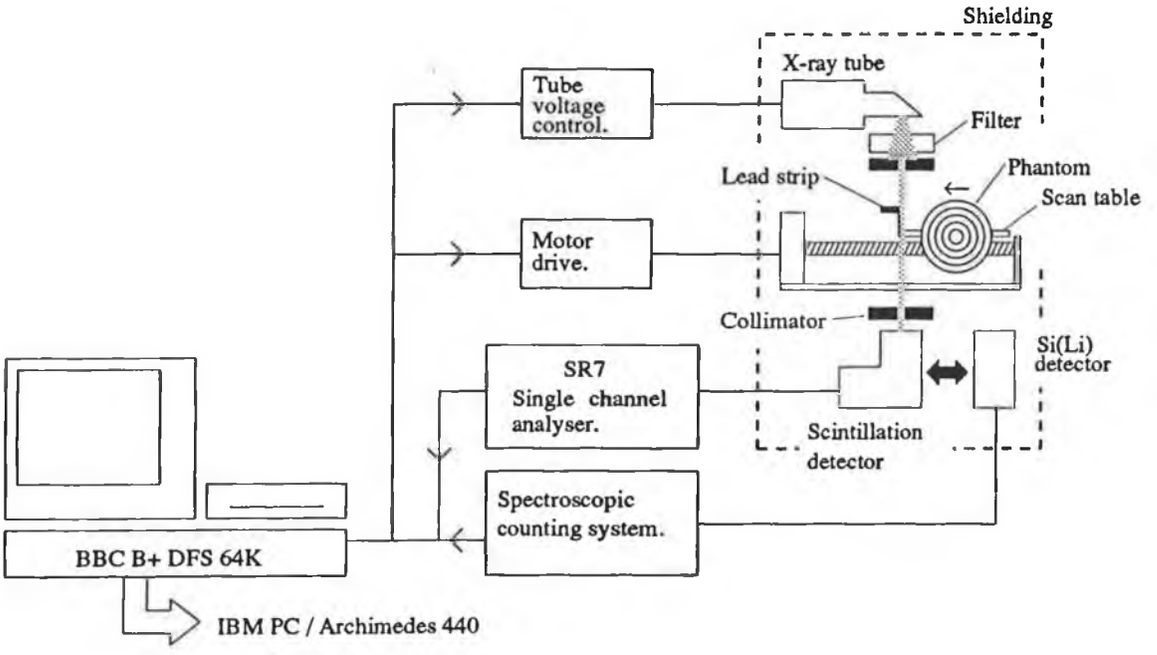

Figure 4.07
Data collection system used to produce images.

The filtered x-ray tube source described in section 3.2.5 was used. The source was collimated using a pair of lead plates containing 2mm diameter round holes. Square holes would have been more suitable but were too difficult to fabricate. A control box attached to the x-ray machine allowed the tube potential to be set to one of four preset values under software control.

The object being studied was mounted on a scan table. The scan table was mounted on a screw driven by a stepper motor. This was used to move the table in a horizontal plane. A second motor on the table was used to rotate the object. The object was attached to a plate mounted on the motor's drive shaft. Both motors were under software control. The system allowed parallel data to be collected for reconstruction.

The low resolution counting system described in section 3.1.5 was used to collect total count data and so allow the evaluation of fractional transmittances. The Si(Li) based counting system was required to record the

reference spectra at the four tube potentials.

4.3.2 DESIGN OF THE PHANTOM

The object examined contained a number of cavities which could be filled with different fluids. In CT such objects, termed phantoms, are used to imitate the attenuation of the human body for test procedures.

To produce a 40x40 pixel image of a phantom would require 1600 measurements of equivalent thickness. For an object containing two analytes 6400 measurements of fractional transmittance would be needed. The minimum integration time on the counting system is about 100 seconds. To collect the data for one image would require 6.4×10^5 seconds or 7.4 days. (This is not a fundamental limitation of the technique. The speed could be greatly increased by using an array of detectors to measure fractional transmittance. A brighter source and faster counting system could also be used.)

Conversion of the four measurements of fractional transmittance to two values of equivalent thickness takes about 20 minutes on an IBM PC 25MHz 80386+80387. The algorithm could be made to converge faster by reducing the precision of the calculation. The bisection method could be replaced by faster algorithms such as the secant method [2].

The large data collection times would have been difficult to work with. The chance of shutdown on the x-ray machine, or crash of the data collection software over a period of eight days was quite likely. The image resolution could have been reduced to allow data collection in an acceptable time (i.e. 10x10 Image). In this experiment a different approach was taken, the reduction in the amount of data that needed to be collected was achieved by making the phantom circularly symmetric. When properly centred, all the projections of this type of phantom are identical. A single projection contains the information required to reconstruct an image. If one projection is used repeatedly during reconstruction, noisy points in the projection can cause rings to appear. When many

projections are recorded and used, then the noise appears distributed over the entire image. For this reason the noise, when a single projection is used, needs to be less than that when all projections are available.

If required, noise can be added to a single noise-free projection to produce a set of projections. This would be best done by adding Poisson noise to suitably scaled count information before it is used to calculate the equivalent thickness values.

The phantom consisted of five concentric rings of 0.2mm thick polystyrene. The ends were sealed with rings of 4mm thick perspex. The five cavities produced could be filled with different solutions through ports mounted in the perspex rings. See figure 4.08.

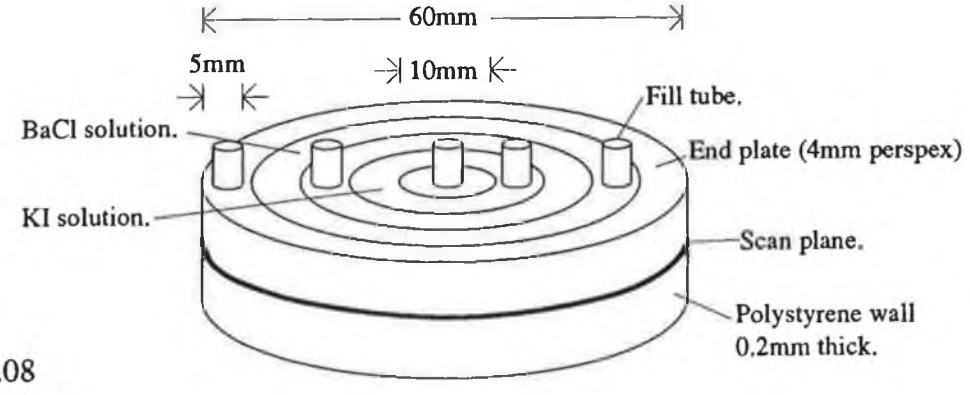

Figure 4.08
The phantom.

The phantom was used to produce two sets of images. The two analytes used were barium and iodine. The location of the analytes for the two runs of the experiment are shown in figure 4.09.

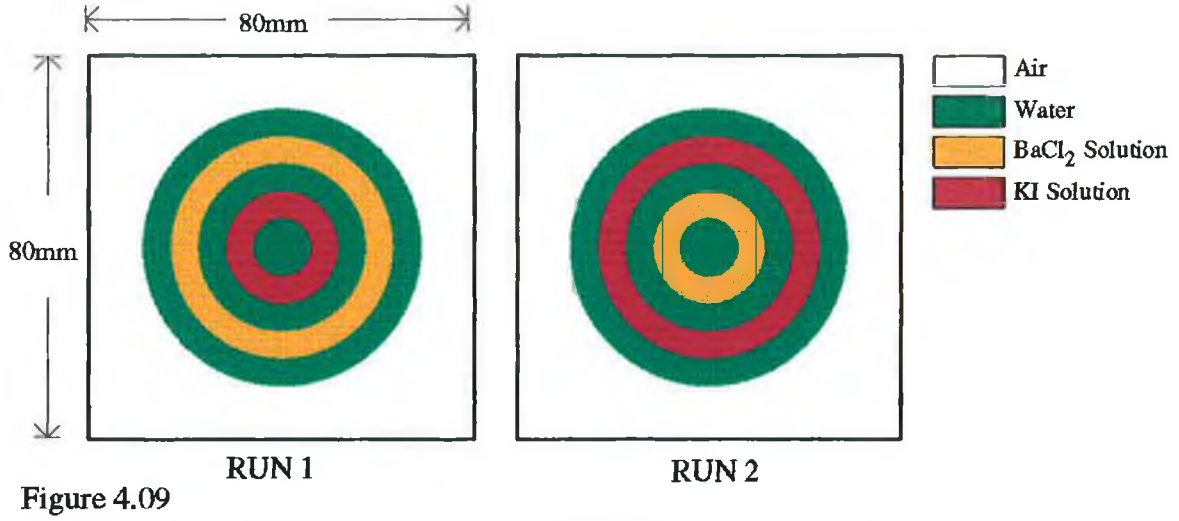

Figure 4.09
Location of air, water and analyte solutions in the region scanned.

The iodine concentration was set at 12.5kg/m^3 and the barium concentration was set at 25kg/m^3.

4.3.3 IMAGING THE PHANTOM

The diameter of the phantom was 60mm. The image size was 40x40 pixels. The pixel width was set at 2mm. The area represented by the image was 80mm x 80mm. The phantom was mounted rigidly on the scan table, a lead strip was mounted 10mm to the side of the phantom. The beam path through the system was checked by placing a 60W quartz halogen bulb in front of the window of the x-ray tube. The position of the spot of light on the phantom could be used to identify the section being taken through the phantom.

The tube potentials V_2 and V_3 were set by placing a sample cell containing both analytes in the path between source and detector. The spectroscopic counting system was then used to locate the K-edge of each analyte. The tube potential was then adjusted until the maximum x-ray energy produced by the tube coincided with the appropriate K-edge. The tube potentials used were V_1 = 27.3kV , V_2 = 32.7kV , V_3 = 37.2 kV and V_4 = 47.4kV.

The low resolution detector system was then installed in the beam path. Software was used to display the count rate incident on the detector; it also allowed the scan table to be moved. The scan table was adjusted until the beam just passed the side of the lead strip. This was the location of the first point in the projection. See figure 4.07.

The data collection program "Image" (Appendix F) was then loaded. This recorded the count incident on the detector for a period of 400 seconds. The phantom was then moved 2mm. The procedure was repeated for the 40 positions required to produce a projection. At the end of the projection the phantom was wound back to the start position. The tube potential was then changed and the procedure repeated. The total count incident on the detector at each location in the projection at each tube potential was recorded on disk. Data collection took about

twenty hours. The data was sent via KERMIT to an IBM-PC.

After the scan was completed, reference spectra were recorded at V_1, V_2, V_3 and V_4. A calibration spectrum containing known fluorescence lines was also recorded.

The count incident on the sample was evaluated by taking the average value of the first three and last three counts in each projection. The beam did not pass through the phantom at these points. The count data was then converted to a set of fractional transmittances. The total count technique program, "IMSCAN", (Appendix F) was then used to convert the fractional transmittance measurements to values of barium and iodine equivalent thickness. The values of equivalent thickness formed the projection data for the reconstruction algorithm. The projections were replicated forty times to generate files compatible with the reconstruction program. An arbitrary amount of noise was added to the replicated data.

Images of barium and iodine were reconstructed using the algebraic reconstruction technique. The program used was "ART-Recon" [3]. This software used filtered back projection to produce the initial iteration values of Ca(x,y); this allowed the ART technique to converge faster. Convergence took between five and eight iterations. The convergence criterion used was that the difference between the standard deviations in the images produced by successive iterations was less than 1.5% of the value of the standard deviation. The image files were displayed on an Archimedes 440 running program "Testdisp" [3]. A screen save facility on the Archimedes was used to bring the images produced into "DRAW" by Acorn. A hard copy of the image was then produced on a HP colour ink jet printer.

A conventional computerised tomography image of the phantom was produced by taking the log of the fractional transmittances for the data recorded at the highest tube potential. This projection data was then processed in the same way as the projections of analyte equivalent thickness to produce an image. The image produced represents the linear attenuation coefficient of the absorber.

4.3.4. EVALUATION OF THE IMAGES

Figure 4.10 shows the images produced using conventional CT for both phantom configurations.

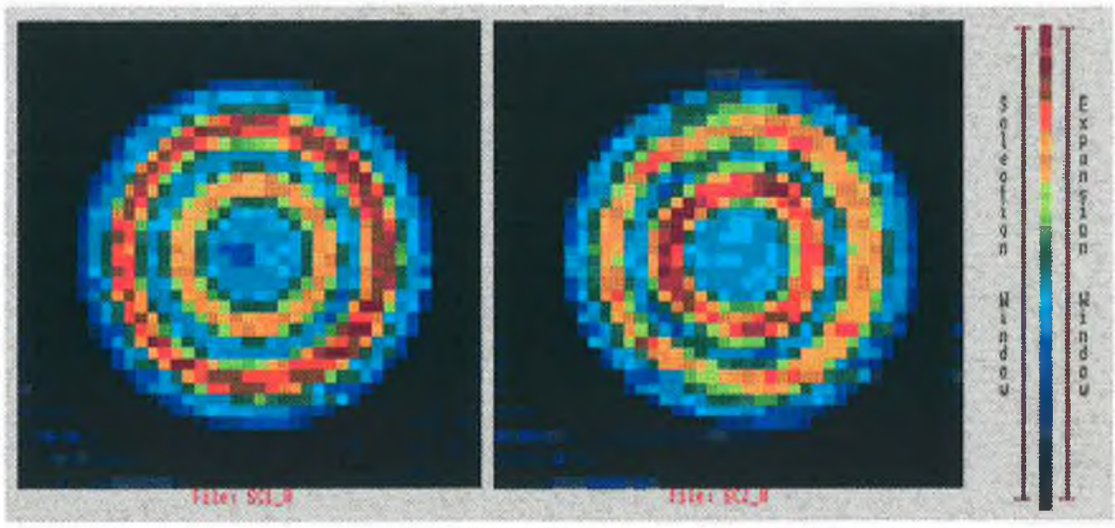

Figure 4.10
Conventional CT images of the phantom.

The colour scale on the right hand side of the image represents a linear range of pixel values between minimum and maximum set values. On the sides of this scale are two lines, the length and position of which may be adjusted. Colours bracketed by the left hand side line are displayed, all other colours become black. The right hand side line represents the maximum and minimum set values relative to the maximum and minimum values contained in the image. All images displayed show both these lines at their full extent. This means that no attempt to extract a region of interest has been made, all images show the full range of the image data. The regions representing air appear black in the image. The blue areas are water. The location of the iodine and barium solutions can be identified by the extra attenuation they introduce, these regions contain red/orange pixels. From the images it would be impossible to say which region contained iodine and which contained barium.

The images shown in figure 4.11 were produced using the total count technique.

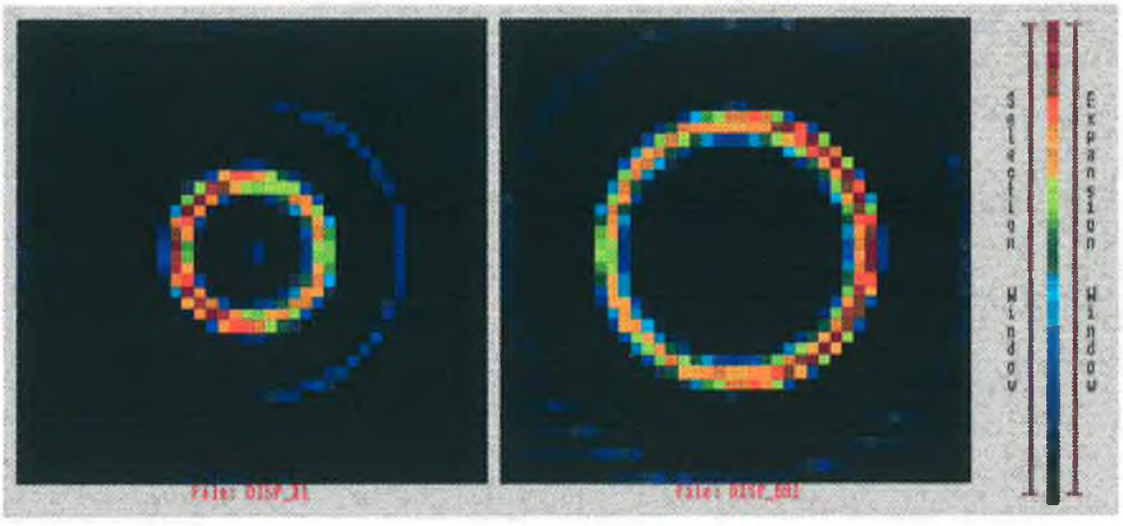

IODINE BARIUM

Figure 4.11
Barium and iodine images produced for RUN 1.

The iodine image coincides accurately with the cavity filled with iodine solution. The image is matrix independent since no change in signal is visible across the air/water boundary or in the region containing barium. The barium image correctly locates the barium, producing an image independent of the matrix. The ring artifact consisting of a set of dark blue pixels to the right of the iodine image was caused by a bad point in the iodine projection at step thirty two, see figure 4.12.

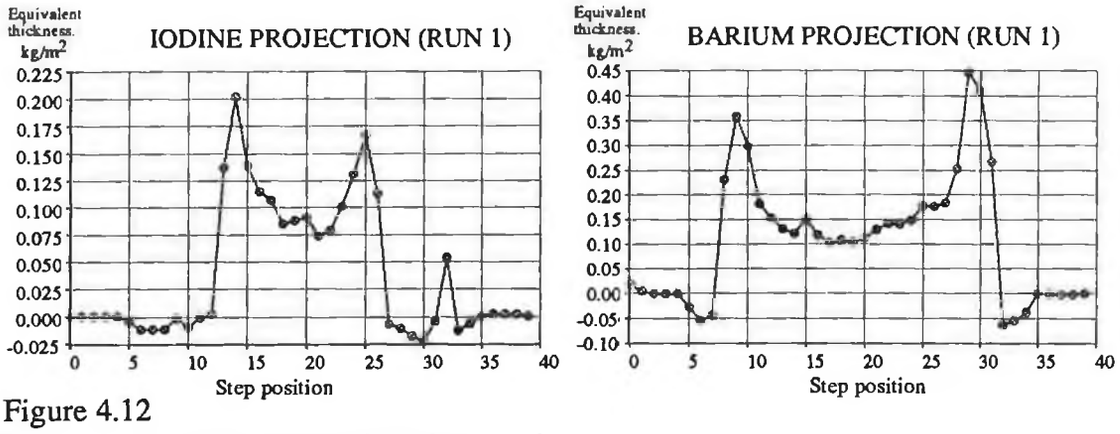

Figure 4.12
Iodine and barium projections for run 1.

The reconstructed pixel values for the barium image ranged from 0 to 22kg/m^3 and for the iodine image 0 to 13kg/m^3.

The location of the iodine and barium solutions was interchanged and the experiment repeated. The images produced are shown in figure 4.13.

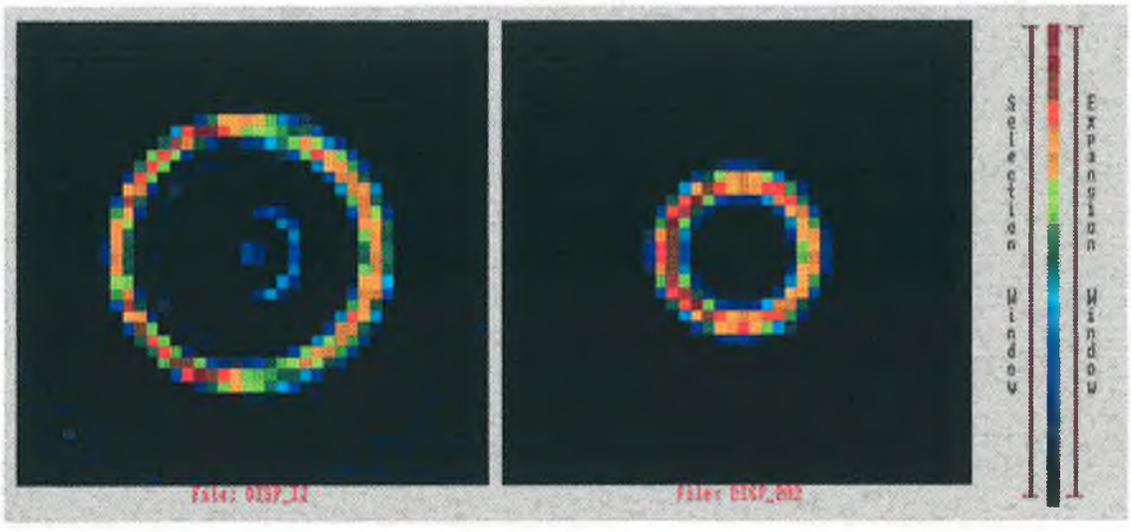

IODINE BARIUM

Figure 4.13
Barium and iodine images produced for RUN 2.

The images demonstrated that the location of the analyte did not have an effect on the technique. The location of the barium and iodine were correctly identified.

As a summary of the technique, table 4.06 records the calculation of the equivalent thickness of barium and iodine along one ray path for the first run of the experiment.

Experimental data.	
Incident count. Mean of paths 1,2,3,38,39,40.	Transmitted count.
687,075	17,146
917,287	53,162
2,393,438	187,276
9,533,482	950,122
+ reference spectra at V_1, V_2, V_3, V_4.	

⇨

Intermediate values.	
Fractional transmittance.	Absorption constants.
0.024955	$\sqrt[3]{\alpha_1}$ = 32.0327 keV
0.057956	$\sqrt[3]{\alpha_2}$ = 36.4994 keV
0.078246	$\sqrt[3]{\alpha_3}$ = 40.2620 keV
0.099662	β = 1.0070

⇨

Result.
t_{iodine} = 0.13712 kg/m^2
t_{barium} = 0.13044 kg/m^2

Table 4.06
Calculation of iodine and barium equivalent thickness for RUN 1 step position 14.

4.4. SUMMARY OF THE TOTAL COUNT TECHNIQUE

The set of experiments described in this chapter demonstrated that the method of measuring analyte equivalent thickness using the total count technique functioned well enough to provide the data required for image reconstruction. It was shown that a quantitative measurement of analyte equivalent thickness could be made, independent of the matrix in which it was contained. This was achievable using a counting system with no energy resolution. Two analytes were successfully imaged in a phantom using the total count technique. Reconstruction data was collected with only a low resolution detector and counter. For the spatial resolution desired, a full set of reconstruction data could not be collected in a reasonable time with the apparatus available. A circularly symmetric phantom allowed an image to be produced with a single projection. A check on the technique was made by interchanging the location of the analytes.

References

[1] Cramer, B.M. and Schlegel, E.
"Relationship between pain in arteriography and the osmolality of the contrast medium."
Contrast media from the past to the future :symposium Berlin, 27th March, 1987. Schering. Ed. by R. Felix.
pp 53 - 61

[2] Hartley, P.J. and Wynn-Evans, A.
"A structured introduction to numerical mathematics"
Stanley Thorns (Publishers) Ltd., 1979.

[3] O'Hare, N.
"A study of the imaging of contrast agents for use in computerised axial tomography."
Ph.D. Thesis, Dublin City University, 1991.

Chapter 5
Computer simulations.

Introduction

The total count technique was developed without the need for computer simulation. The lag discriminator approach described in section 2.4 greatly increased the complexity of the problem and it was found necessary to write a simulation program to check the operation of the code used to extract equivalent thickness values from experimental data. Once the simulation was developed it was further used to find the optimum operating conditions for experimental work and the effects of disturbances such as interference from other analytes and statistical noise on the technique itself.

The simulation was restricted to studying measurements of equivalent thickness. This was done for a number of reasons:

(i) Equivalent thickness measurements form the projection data for reconstructions of analyte concentration. The evaluation of minimum visible analyte concentration can depend on subjective analysis of images and is difficult to study.

(ii) The correlation between error in projection data and error in the final image depends on a great many extra factors such as resolution, size of the region of interest, the reconstruction algorithm used etc.

(iii) Generating large amounts of simulated data, reconstructing an image and repeating the procedure to evaluate the variance in the resulting concentration would require excessive computing time. Others have studied the correlation between projection noise and image noise [1] [2] and [3].

function was used to generate the experimental data which was then passed to the crunch() function to reproduce equivalent thickness values. By comparing the equivalent thickness values before and after this sequence the model was used to see how the experimental system responds to disturbances.

It was straightforward to modify the program so that it could analyse real experimental data. This was achieved by using the load() function followed by the crunch() function.

A working model allowed the program required to analyse experimental data to be fully debugged before it was used. It also allowed the optimisation of the experimental configuration, and assisted in the choice of analytes suited to the technique.

5.1.2. VISUAL VERIFICATION AND SELF CONSISTENCY TEST OF THE COMPUTER MODEL

Two arrays were generated consisting of 1024 real numbers. These would ultimately contain the incident and transmitted pulse height distributions associated with operating at a specific tube potential. A high energy resolution spectrum at the first tube potential of interest was loaded into both arrays. This spectrum was obtained using a Si(Li) detector corrected for detector efficiency. See figure 5.01(a). The spectrum in one array was then multiplied by the response of the absorber. At this stage the arrays contained the incident and transmitted spectra at V_1, figure 5.01(a) and 5.01(b). The spectra were then modified by the detector efficiency and convolved with the detector response to give the pulse height distributions shown in figure 5.01(c) and 5.01(d). This was repeated for V_2 to V_4.

To allow the effect of noise to be studied, each of the incident spectra was rescaled so that the total count contained in each spectrum was fixed to some preset value, in this example 500,000. Each of the transmitted spectra was then adjusted by the same scaling factor.

If required, Poisson noise was then added to both

incident and transmitted spectra, figures 5.01(g) and 5.01(h) were obtained.

At any stage IDL could be used to view graphically all the stages used in the simulation. Figure 5.01 was taken directly from IDL.

Once the final pulse height spectrum was produced the channel corresponding to V_1-lag was evaluated and the counts above this channel totalled. The ratio of the count in the incident and transmitted spectra gave the fractional transmittance that was passed to the crunch() function. This was done for V_1 to V_4.

Figure 5.01 shows the sequence of events involved in modelling a two analyte absorber. The four lines in each graph represent the four tube potentials. As such it represents a visual verification that the program was operating.

The non-graphic output from the program is shown in table 5.01.

Model()

Input	Intermediate values	Output
50.0 kg/m^2 Water	$\sqrt[3]{\alpha_1}$ = 29.8577 keV	F_1 = 0.0798846
0.1 kg/m^2 Iodine	$\sqrt[3]{\alpha_2}$ = 33.9108 keV	F_2 = 0.1431174
0.1 kg/m^2 Barium	$\sqrt[3]{\alpha_3}$ = 37.3842 keV	F_3 = 0.1553852
	β = 0.8328431	F_4 = 0.1594518

Crunch()

Input	Intermediate values	Output
F_1 = 0.0798846	$\sqrt[3]{\alpha_1}$ = 29.7019 keV	0.105 kg/m^2 Barium
F_2 = 0.1431174	$\sqrt[3]{\alpha_2}$ = 33.9518 keV	0.093 kg/m^2 Iodine
F_3 = 0.1553852	$\sqrt[3]{\alpha_3}$ = 37.1864 keV	
F_4 = 0.1594518	β = 0.8400923	

Table 5.01
Table of values calculated during the model() - crunch() cycle of simulation.

Setting the total count to 500,000 meant that the amount of noise added to the spectra was insufficient to affect adversely the resulting measurement of equivalent thickness.

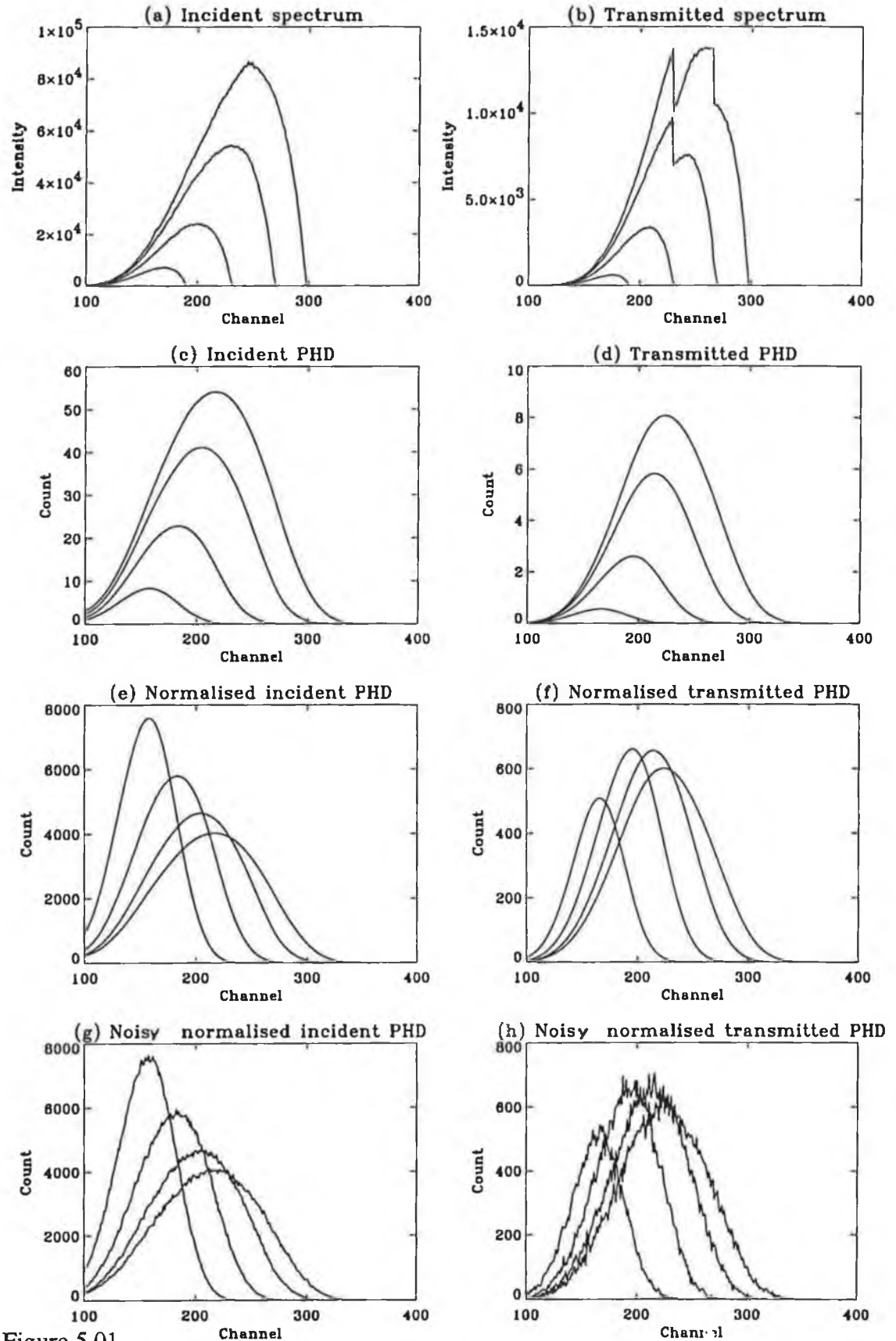

Figure 5.01

Visual verification of the simulation method used to investigate the tracking discriminator method. The analytes used were 0.1kg/m^2 iodine and 0.1kg/m^2 barium. The matrix was 50kg/m^2 water.

5.1.3. POISSON NOISE

The noise associated with a given count is governed by Poisson statistics. Equation 5.01 describes the Poisson distribution

$$P(v,Q) = \frac{e^{-Q}\, Q^{v}}{v!} \qquad (5.01)$$

where P(v,Q) is the probability of a count of v being detected when the most likely or mean count is Q. The standard deviation of the Poisson distribution is $\sqrt{Q}$ [4].

For very low values of Q this distribution is asymmetric, however as Q increases the distribution tends towards a Gaussian distribution. For Q>30 the difference is minimal [4]. See figure 5.02

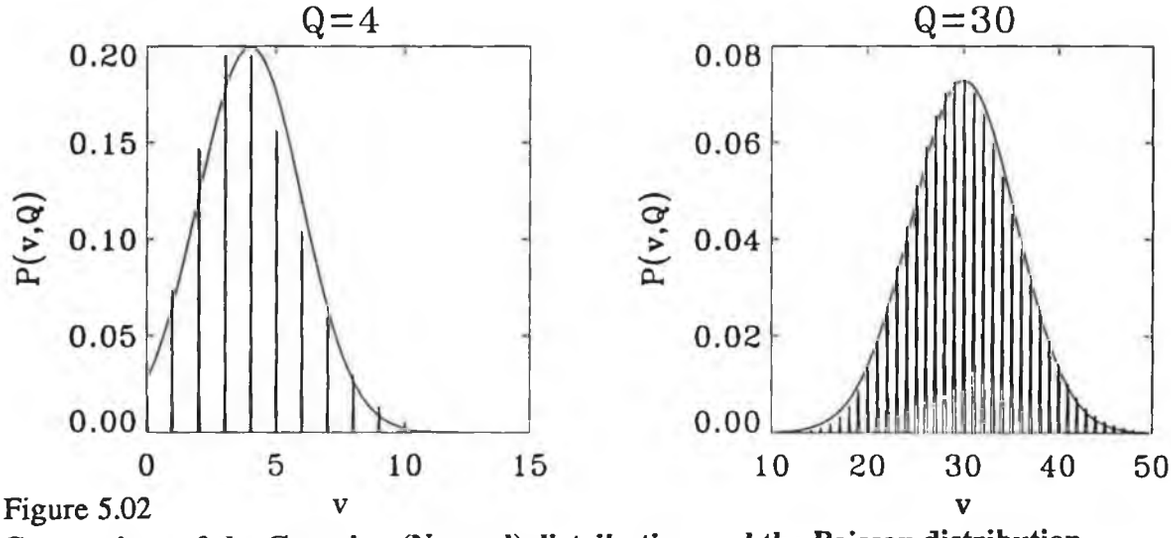

Figure 5.02

Comparison of the Gaussian (Normal) distribution and the Poisson distribution at two different values of mean count (Q).

The Gaussian distribution is computationally more favorable for a computer model since it does not require the evaluation of large factorials. It is the Gaussian distribution that was used to add noise to count data.

$$P(v,Q) = \frac{1}{\sqrt{2\pi Q}} \exp\left(-\frac{(V-Q)^2}{2Q^2}\right) \qquad (5.02)$$

Figure 5.02 demonstrates graphically that for Q>30 the Poisson and Gaussian distributions are similar. The Gaussian distribution is a continuous function while the

Poisson distribution has discrete values.

To add noise to a count Q, the standard deviation was evaluated $\sqrt{Q}$. A random number between 0 and 1 was generated with an equal probability distribution by the computer. The Gaussian distribution was then integrated using the trapezoidal rule from $Q-3\sqrt{Q}$ until the integral exceeded the value of the random number. The value of Q when the random number was exceeded is the count with noise added. See figure 5.03.

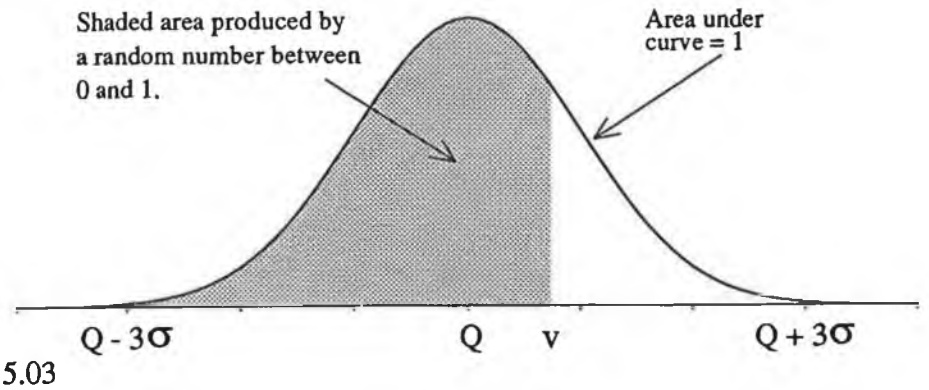

Figure 5.03
Gaussian distribution used to add noise to a count.

To check the operation of the routine a histogram was produced using 200,000 evaluations of the noise on the count of 1000. This is shown in figure 5.04.

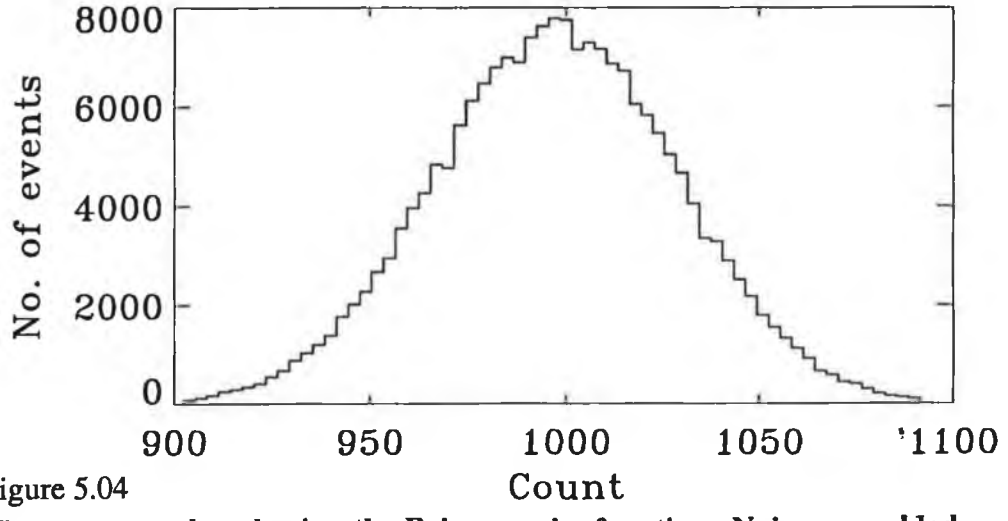

Figure 5.04
Histogram produced using the Poisson noise function. Noise was added to a count of 1000, 200,000 times to produce the graph.

It is very important that the mean over a large number of counts and the true count is the same. Noise is added to each channel which means that over the 1024 channels in a spectrum systematic errors can build. The table 5.02

shows the mean and standard deviation for 2000 values of the noise added to the value of set count.

Set count	$\sqrt{\text{Set count}}$	Mean	Standard deviation
1,000,000	1000.0	1,000,530	1130.64
100,000	316.2	100,054	309.40
10,000	100.0	10,006	99.63
1,000	31.6	1,004	30.84
100	10.0	99.7	9.76
10	3.2	10.0	3.14
1	1.0	0.98	0.98
0	0	0	0

Table 5.02
Verification of the Poisson noise function.

5.1.4. ABSORBER DESCRIPTION

Each element of the absorber was described in terms of a set of photoelectric constants α'_1, α'_2 and a scattering constant β'. The data used to evaluate the constants was obtained from tables produced by the NBS [5]. These tables provide a list of mass attenuation coefficient U as a function energy E. The values listed were separated by 10keV, the following procedure was used to evaluate the attenuation at any energy.

Between edges

$$U = \alpha' P(E) + \beta' S(E) \qquad (5.03)$$

where U is the mass attenuation coefficient. The evaluation of S(E) and P(E) was described in the theory section 2.1.2.

Rewriting equation 5.03 gives

$$\frac{U}{S(E)} = \alpha' \frac{P(E)}{S(E)} + \beta' \qquad (5.04)$$

A graph of U/S(E) vs P(E)/S(E) was plotted. The slope, α', and intercept, β', of the straight line produced was evaluated using the method of least squares. Different values are obtained if you divide 5.03 through by P(E) such that α' is the intercept and β' the slope. In general α' varied under 5%, β' varied under 30%. It was an average of the values that was used in the computer model. The

evaluation was made using four points either side of the absorption edge spanning approximately 30kV. For analytes the absorption edge jump was evaluated using

$$\Delta U = \alpha_2' P(E_k) - \alpha_1' P(E_k) \qquad (5.05)$$

where E_k is the K-edge energy.

The results are tabulated below.

Material	K-edge (keV)	α_1' m^2keV^3/kg	α_2' m^2keV^3/kg	$\beta' m^2/kg$	$\Delta U\, m^2/kg$
Water	-----	491.26	-----	0.01602	-----
Cadmium	26.727	11802.00	95431	0.28625	4.380
Indium*	27.953	12471.00	99969	0.30400	4.006
Tin	29.211	13130.00	104478	0.31400	3.665
Iodine	33.168	15925.20	125370	0.22500	2.999
Barium	37.414	18049.21	151477	0.24059	2.530

Table 5.03
Constants used to describe absorber and matrix in the computer simulations.

The mass attenuation coefficient of an absorber at a specific energy can be evaluated using equation 5.06 and the data in the table above. The attenuation due to a number of components is given by

$$I = I_0 \exp -(U_1 t_1 + U_2 t_2 + .. + U_x t_x) \qquad (5.06)$$

where t_x is the equivalent thickness of component x.

5.1.5. DETECTOR CHARACTERISATION

The intrinsic efficiency $\xi(E)$ of a detector to x-rays of energy E is defined as

$$\xi(E) = \frac{\text{pulses recorded}}{\text{number of incident quanta}} \qquad (5.07)$$

A photon detected is a photon absorbed by the detector. Thus

$$\text{Attenuation} = 1 - \xi(E) \qquad (5.08)$$

The experimental data describing the efficiency of the detector as a function of energy was used to model the

detector response. The following procedure was used to evaluate efficiency values between known values.

Using the absorption theory described in the section 2.1.2.

$$\xi(E) = 1 - e^{-[\,\alpha P(E) + \beta S(E)\,]} \qquad (5.09)$$

The constant α and β were evaluated by solving a pair of simultaneous equations generated by evaluating 5.09 at the two energies E_1 and E_2 for which the efficiency was known. E_1 and E_2 are the experimental data points either side of E the energy of interest.

$$\alpha = \frac{S(E_1)X_2 - S(E_2)X_1}{P(E_2)S(E_1) - P(E_1)S(E_2)} \qquad (5.10)$$

$$\beta = \frac{P(E_1)X_2 - P(E_2)X_1}{P(E_1)S(E_2) - P(E_2)S(E_1)} \qquad (5.11)$$

where

$$X_1 = -\ln(1 - \xi(E_1)) \qquad (5.12)$$

and

$$X_2 = -\ln(1 - \xi(E_2)) \qquad (5.13)$$

The approach produced a reasonable fit at higher energies. In reality a straight line or simple spline would have produced a similar result. Figure 5.05 shows the modelled detector efficiency function.

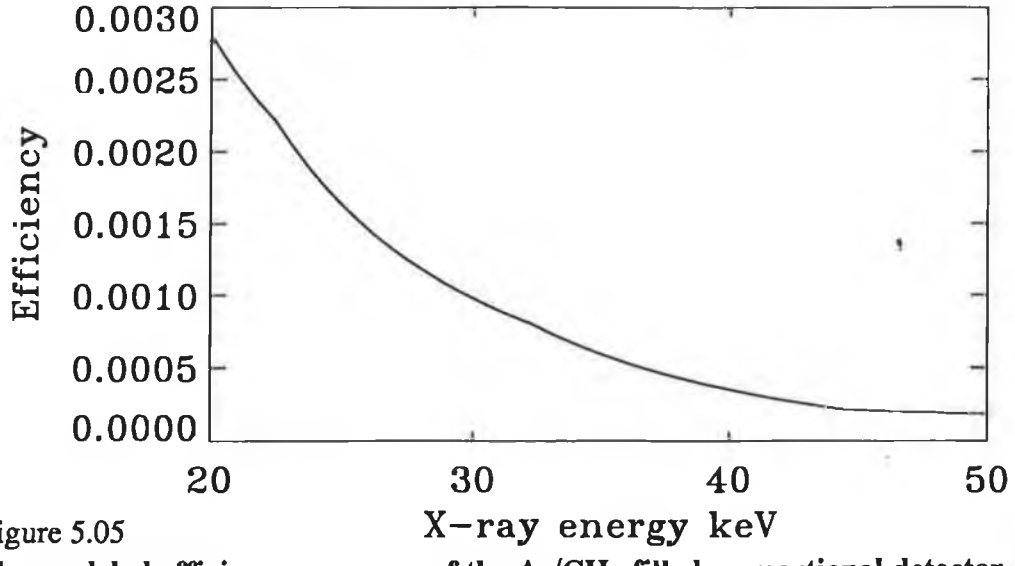

Figure 5.05
The modeled efficiency response of the Ar/CH_4 filled proportional detector.

Experiment demonstrated that the energy resolution of the gas proportional detector varied linearly. The standard deviation describing the detector resolution was given by

$$\sigma(E) = 0.0267\ E\ (keV) + 1.4399 \qquad (5.14)$$

A Gaussian curve was used to describe the line spread function of the proportional detector system [6].

The effects of escape peaks did not appear in the pulse height spectra produced by the proportional detector. The size of the escape peak decreases as the incident x-ray energy increases away from the K-edge energy of the detector gas [7]. The K-edge for argon is 2.956keV, the x-ray energies used were greater than 20keV. If other detectors such as a krypton or xenon filled proportional detector or a scintillation detector were used then the effect of escape peaks may need to be included.

5.2 APPLICATION OF THE COMPUTER MODEL

Overview

Once the computer model was commissioned, it could be used to simulate many experimental configurations. In this section the computer simulations that were carried out to study the performance of the tracking discriminator technique are described. The simulations were also used to investigate the optimum operating conditions for the technique. The computer model could also be used to investigate experimental configurations not available.

5.2.1. INVESTIGATION OF THE OPTIMUM DISCRIMINATOR SETTING

The discriminator could be set at a given energy from the maximum x-ray energy being produced by the x-ray tube. The energy between the maximum x-ray energy and the discriminator threshold is called the lag. When lag is very small (or even negative) the percentage of counts containing information about the front end of the spectrum and so the absorption edge is high. However the count rate

would be very low since most counts would be excluded by the discriminator. When lag is very large (total count technique) then the number of counts providing information about the new α as compared to those that are being explained by previous values of α is low. This means that very few of the extra new counts are proving new information. Between these two extremes lies a region where the system will be most sensitive.

It should be noted that computationally the total count technique is just the lagging discriminator technique in the limit when the lag is large.

The aim of this simulation was to demonstrate that there exists an optimum lag for the experimental system and as such the lagging discriminator is an improvement to the total count technique. It was also shown that the tracking discriminator method might allow an unfiltered source to function. A filtered source is always favourable. All experimental work was carried out with a filtered source.

Three iodine equivalent thicknesses 0.30kg/m^2, 0.20kg/m^2 and 0.10 kg/m^2 in a matrix of 50 kg/m^2 were investigated. The tube potential were fixed at 27.4kV, 33.1kV and 37.6kV. The pulse height spectra were normalized to a total incident count of 600,000 before noise was added.

The model() function was then used to produce fractional transmittance measurements for the four tube potentials for a lag value of 30keV. The crunch() function then calculated the iodine concentration. The procedure was repeated twenty times. The mean and standard deviation in the iodine concentration was recorded. The error in the iodine measurement was taken to be the standard deviation in the value divided by the mean value. The procedure was repeated for lag values of 20, 10, 6, 4, 2, 0, -2, -4 keV.

The result of the simulation using unfiltered reference spectra is shown in figure 5.06. For small and negative values of lag, the noise in the measured values is very high. A minimum is reached for a lag of about 3keV. Above this lag the error in the measure analyte

concentration increases. The slight drop in the measured error at 30keV is due to counts below channel 0 being excluded by the software. The counts above channel 0 are normalized using the total count set for the incident spectrum. It is not of physical significance and only occurs when the model is used to examine large lags on an unfiltered source.

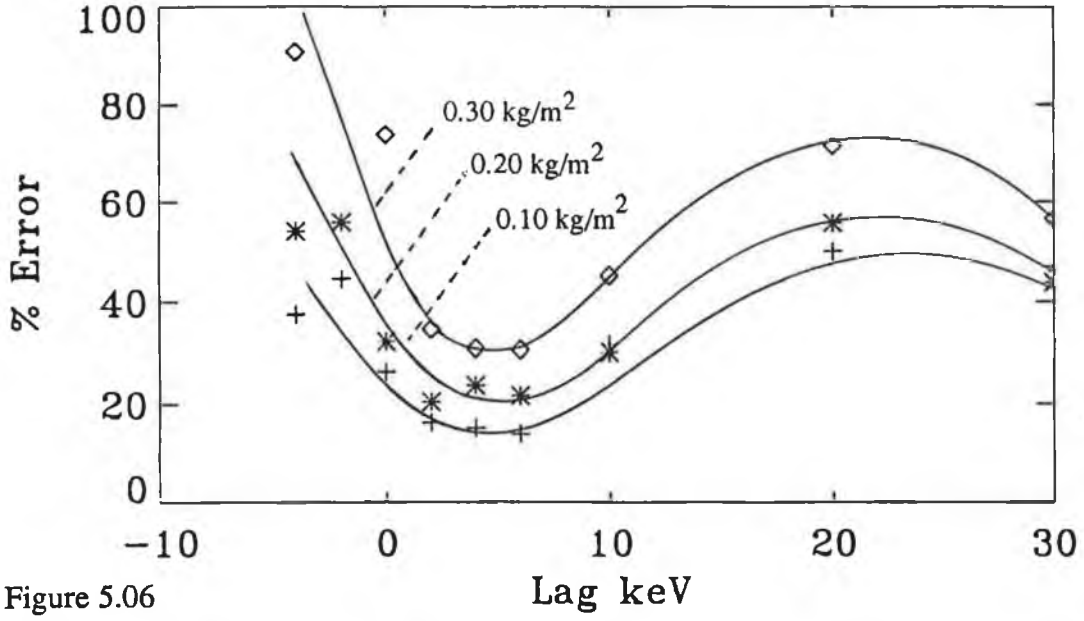

Figure 5.06

Graph showing how the error in the measured iodine equivalent thickness varies with discriminator lag. The reference spectra used were unfiltered.

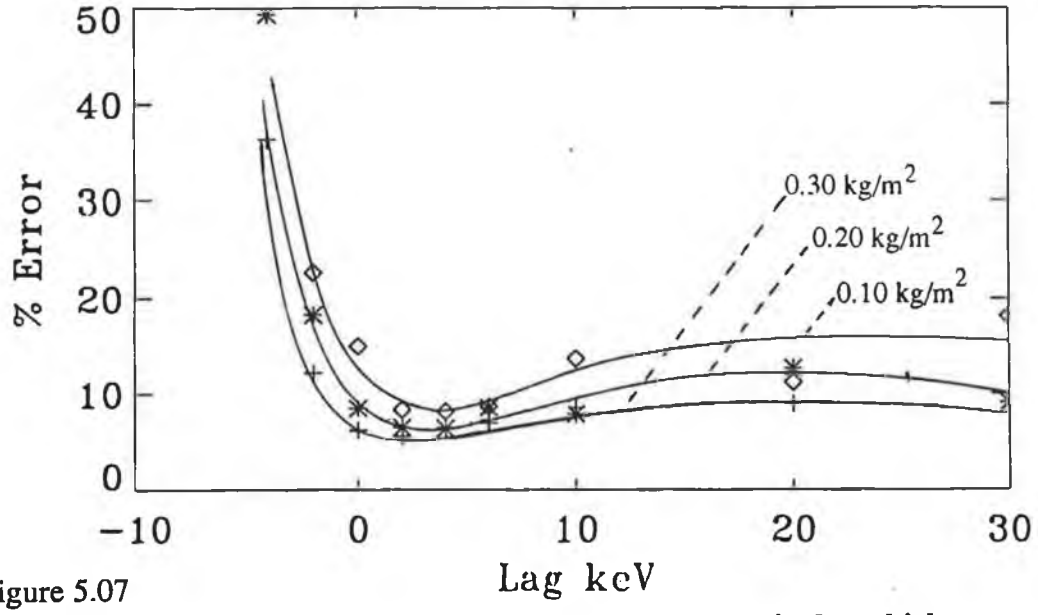

Figure 5.07

Graph showing how the error in the measured iodine equivalent thickness varies with discriminator lag. The reference spectra used were filtered.

When repeated using reference spectra that were filtered, the result shown in figure 5.07 is obtained. Again an optimum lag occurs at about 3keV. However as lag increases, the error in measured value only gradually increases.

Both 5.06 and 5.07 show an improvement in sensitivity for a lag value in the range 2 to 5 keV. For data produced using the filtered spectrum large lag values still allow satisfactory measurements of equivalent thickness to be made. It was the filtering of the spectrum in the total count technique that allowed it to work satisfactorily. However, it should be noted that the error in the iodine measurement for the filtered spectrum is always less than that for the unfiltered for the same lag value.

The conclusion was that future experiments should be run with filtered spectra and a lag of about 3keV for maximum sensitivity.

It should be noted that 3keV may not necessarily be the most favourable value for resolving elements close to each other, it is the optimum for detecting iodine for the tube potentials chosen. The above simulation only studied one element.

5.2.2. INTERFERENCE BETWEEN ANALYTES

As the concentration of an analyte increases, the number of counts providing information about the other analytes decreases. In this simulation the equivalent thickness of one analyte was held constant, the error in the measurement of this analyte was then monitored as the equivalent thickness of another analyte was varied. Figure 5.08 shows the error in measurement of a $0.10 kg/m^2$ sample of barium as the equivalent thickness of iodine was varied between 0 and $1 kg/m^2$. The lag was set to 3keV and total incident count was normalised to 650,000. The K-edge of iodine is below that of barium. When the disturbing analyte is not present there is an error in measurement due to statistical noise. As the concentration of iodine increases the error in the barium measurement increases.

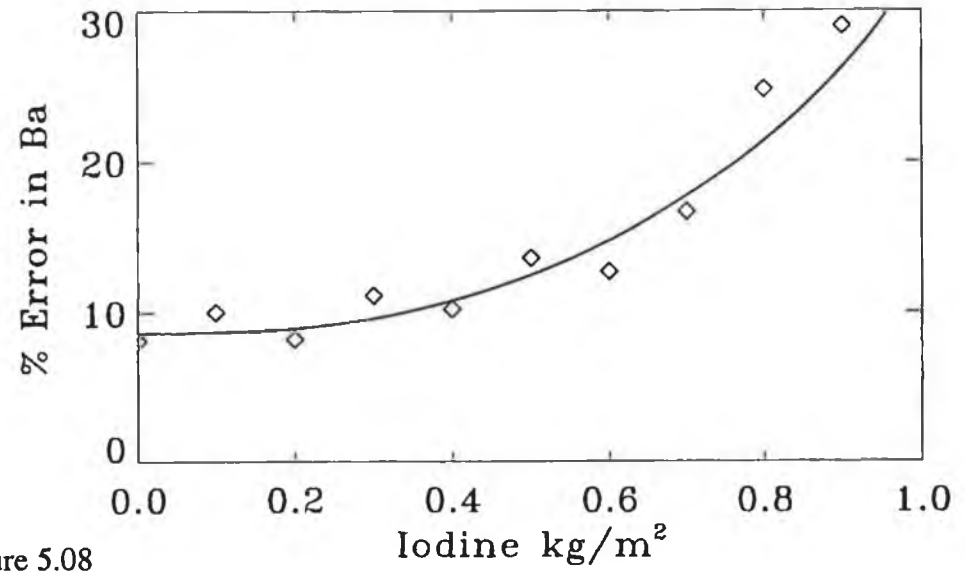

Figure 5.08

Demonstration of how analytes with K-edges below the analyte of interest can increase the error in the measurement.

Figure 5.09 shows how the error in the measurement of iodine equivalent thickness varies as the barium equivalent thickness was varied. In this case the effect on the measurement was far less.

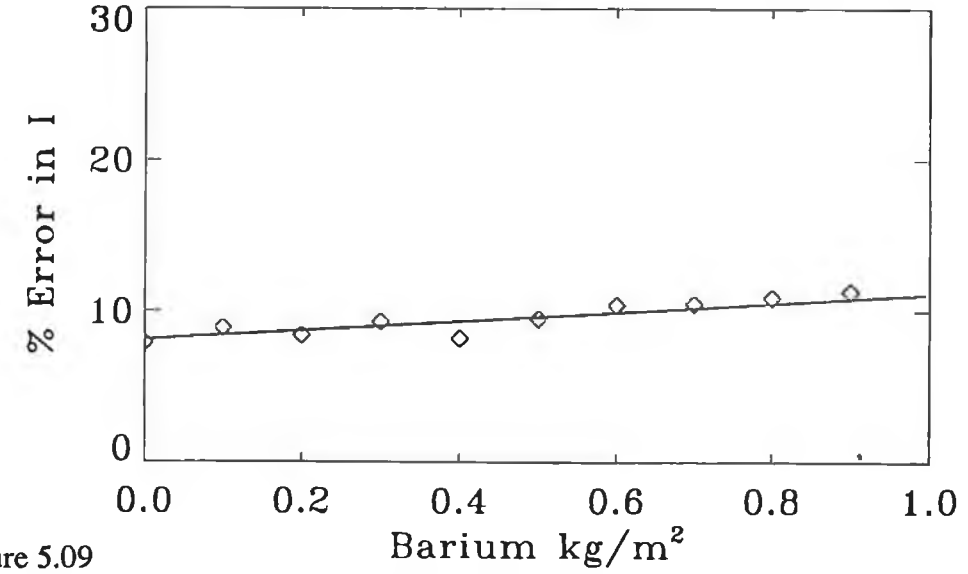

Figure 5.09

Demonstration that analytes with K-edges above the analyte of interest do not interfere with measurement of the analyte.

The difference between figures 5.08 and 5.09 is for

two reasons. The first is that the barium measurement (higher K-edge energy) requires an accurate measurement of absorption parameters below it. Thus the error in the iodine measurement will affect the measurement of the barium. The reverse is not true, it is not necessary measure the barium concentration to make a measurement of the iodine concentration. The second reason is that the absorption on the high side of an edge is higher than on the low side. Large concentration of a low K-edge energy analyte will reduce the counts available to make measurements of analytes at higher energies.

5.2.3. ERROR IN EQUIVALENT THICKNESS MEASUREMENT AS A FUNCTION OF TOTAL COUNT

As the count increases in the pulse height spectra the degree of noise decreases. The reduction in noise allows more accurate measurement of analyte equivalent thickness. It should also reduce the minimum detectable equivalent thickness.

For very low values of analyte equivalent thickness the attenuation is almost entirely due to the matrix. For this reason the variation of measured analyte equivalent thickness in a model where the analyte concentration was set to zero was investigated.

Figure 5.10 shows the variation in measured iodine equivalent thickness as a function of total incident count. The error was produced by repeating twenty simulations and evaluating the standard deviation in the result.

The error tends to level above a count of 10^7 due to the precision defined in the program for convergence of the simultaneous equations. Precision could be increased at a cost to computation time. A noise free model() - crunch() returns a variation of $0.001 kg/m^2$ between set and measured iodine concentrations. This error represents the systematic error in the computation in the model().

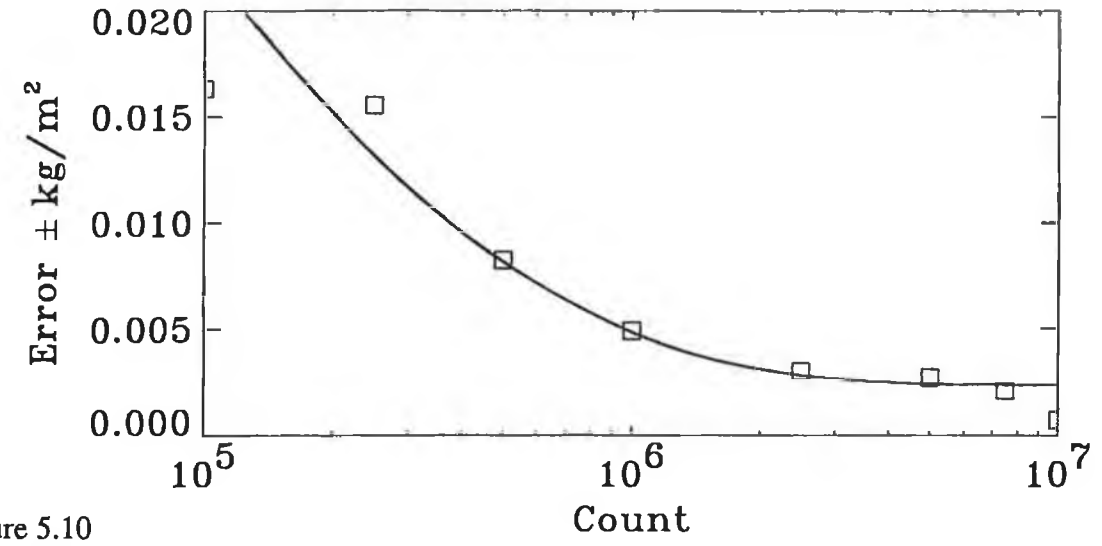

Figure 5.10

Error in the measurement of iodine equivalent thickness as a function of the total count available. Matrix = 30kg/m^2 water, Lag = 3keV.

5.2.4. INVESTIGATION OF THREE ELEMENT IMAGING

A potential benefit of the tracking discriminator method as opposed to the total count technique was that it should be able to image elements next to each other in the periodic table. There is roughly a 1 keV jump between the edge for unit increase in atomic number. If three elements next to each other can be measured using the technique then in theory the technique could be extended to more. In practice all this technique would then require is the K-edge energy of each element in the periodic table and the corresponding absorption jump for the technique to be able to image all elements within the energy range of the X-ray tube. Although the approach would not be very sensitive it does in principle suggest a method that is virtually matrix independent.

To investigate the feasibility of this idea, three elements, cadmium, indium and tin were modelled. The equivalent thickness of each element was set to either 0.1kg/m^2 or to 0kg/m^2. The elements were contained in a matrix of 30kg/m^2 of water. The results are tabulated in Table 5.04. The total count in the spectra was limited to 1,000,000. The discriminator lag was set to 2.25 keV.

	Set values kg/m^2		
Run	Cadmium	Indium	Tin
1	0.1	0.1	0.1
2	0.1	0.1	0
3	0.1	0	0.1
4	0	0.1	0.1
5	0	0	0.1
6	0	0.1	0
7	0.1	0	0
8	0	0	0

	Measured values kg/m^2		
Run	Cadmium	Indium	Tin
1	0.10± 0.01	0.11± 0.03	0.10± 0.03
2	0.10± 0.01	0.11± 0.03	0.00± 0.02
3	0.11± 0.01	0.00± 0.02	0.10± 0.02
4	0.00± 0.01	0.11± 0.02	0.10± 0.02
5	0.00± 0.00	0.00± 0.01	0.10± 0.01
6	0.00± 0.01	0.10± 0.02	0.00± 0.02
7	0.11± 0.01	0.00± 0.02	0.00± 0.01
8	0.00± 0.01	0.00± 0.01	0.00± 0.01

Table 5.04

Measuring analyte concentration for three elements next to each other in the periodic table. Lag = 2.5keV, Matrix = 30kg/m^2 water.

This simulation demonstrated that it may be possible to image a number of elements next to each other in the periodic table.

However, the results demonstrated that even small amounts of statistical noise affected the resulting measurements. It was found in practice that a detector with better energy resolution or at least more stable gain would be required to achieve these results experimentally.

To demonstrate the improved selectivity the tracking discriminator technique provides over the total count technique, the simulation was repeated for a lag value of 20keV. A large lag value simulates the total count technique. The standard deviation in the tin measurement for run 1 was 0.14kg/m^2. Thus with this lag it was no longer possible to evaluate the equivalent thickness of tin from a single set of modelled data.

References

[1] Chesler, D.A. and Riederer, S.J. and Norbert, J.P.
"Noise due to photon counting statistics in computed X-ray tomography"
Journal of computer assisted tomography,
Vol. 1, No. 1, pp 64-74, 1977.

[2] Seitz, P. and Mulle, A. and Ruegsegger, P.
"The influence of photon counting statistics on picture noise an reproducibility in quantitative computed tomography"
IEEE Trans.Nucl.Sci., Vol. NS-32, No. 1, pp 1162-1168, 1985.

[3] O'Hare N.J.
"A study of the imaging of contrast agents for use in computerised tomography"
PhD Thesis, pp 76-78, Dublin City University, 1991.

[4] Barford, N.C.
"Experimental measurements: Precision, error and truth"
Addison-Wesely, pp 91-98, 1967.

[5] Hubble, J.H.
"Mass attenuation and Energy Absorption coefficients from 1keV to 20MeV."
Int. J. Appl. Radiat. Isot.,Vol. 33, pp 1269-1290, 1982.

[6] Knoll, G.F.
"Radiation detection and measurement"
John Wiley & Sons., pp 176 ,1989.

[7] Bertin, E.P.
"Principles and Practice of X-Ray Spectrometric" Analysis"
Plenum Press, pp 348-349, 1979.

Chapter 6

Experimental results : Tracking discriminator method

Introduction

In chapter 4 the experimental verification of the total count technique was described. In chapter 5 a number of computer simulations demonstrated that the tracking discriminator method should provide an improvement both in sensitivity and energy resolution over the total count technique. The improved energy resolution achieved by the tracking discriminator technique suggested the possibility of separating elements adjacent to each other in periodic table.

In this chapter, results are presented that show that the tracking discriminator method can be used to image elements next to each other in the periodic table.

6.1 TECHNIQUE VERIFICATION USING HOMOGENEOUS SAMPLES

Introduction

The tracking discriminator technique was checked in a similar manner to the total count technique. To verify the quantitative nature of the technique, a test on the linearity of the technique was made. The matrix independence was then tested. The ability to separate closely spaced elements was also investigated. These tests were made on carefully prepared homogeneous samples.

It was only after the technique had been tested in this manner that data to produce an image was collected.

6.1.1. DEMONSTRATION OF LINEARITY

The data collection system

The experimental configuration used for data acquisition is shown in figure 6.01.

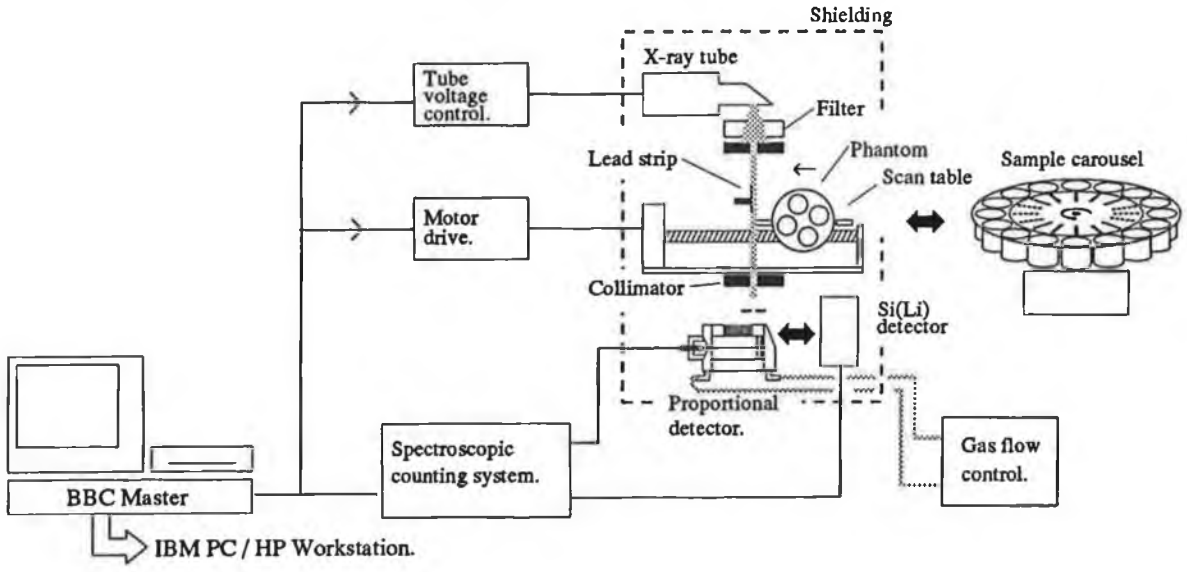

Figure 6.01
Experimental configuration used to verify the tracking discriminator technique.

The X-ray tube was filtered using the filter described in section 3.2.5. The tube voltage control was modified so that the X-ray tube could be set to any of 5 preset tube potentials by the computer. For this experiment the computer could be used to position any one of sixteen sample positions in the path of the X-ray beam using the sample carousel. The counting chain described in section 3.1.4 was used with the proportional counter. The pulses from either the Si(Li) detector or the proportional counter could be connected to the multichannel analyser.

In theory a single channel analyser could have been used to make the measurements of fractional transmittance. In this case the low level discriminator threshold would be set by measurement of the tube potential to which had been subtracted a voltage equivalent to the desired lag. The apparatus to do this was available. See appendix B. However, it was favourable to record all counts with the MCA and set the lag value in software afterwards. This allowed the lag to be chosen after the experimental data

was collected.

Reduction of detector drift

Early attempts at the linearity experiment failed. This was traced to drift in the gain of the proportional counter. The fractional transmittance was obtained by taking the ratio of the incident and transmitted count above a certain channel in the spectra recorded by the MCA. Since the incident and transmitted count spectra were recorded at different times, the value of the fractional transmittance obtained by taking the ratio of counts in similar regions of the two spectra would be incorrect.

A number of actions were taken to reduce this problem. The anode wire in the proportional detector slowly collects carbon deposits causing the detector's gain to continuously reduce. All that could be done was to clean the wire. The gas density stabiliser was originally mounted in a separate cabinet to the proportional detectors. The temperature in the two cabinets may not necessarily have been the same at all times. This was cured by mounting the stabiliser in close proximity to detector. The high voltage power supply to the detector was probably the most important component for keeping the gain stable over the time periods required. The gain of a proportional counter varies exponentially with bias potential [1]. The power supply and counting electronics were effectively left on at all times to settle. The Canberra HVPS 3100-01 was found to cause less drift problems than the Ortec 556. Even after these precautions the drift was enough to cause a single calibration followed by 8 measurements lasting 24 hours, to fail.

Two further steps were taken to reduce the problems of drift. The first was to split the multichannel analyser's memory into two groups. Pulses were recorded in channels 0-512 for x-rays transmitted through the sample. Channels 513 to 1023 were used to record pulses incident on the sample. The sample carousel or scan table was then made to move the sample in and out of the beam repeatedly during a single measurement of fractional transmittance. The MCA

was synchronized with the sample movement system so that counts were recorded in the correct memory group.

The second improvement was to provide a method of continuous recalibration. Two approaches were possible. The first was to move the adjustable fluorescence source in front of the detector after each measurement and calibrate using a number of lines. This would have been difficult to automate and would extend the data acquisition time. The second approach was to deconvolve the detector response from the incident spectrum and use the channel associated with the front end to calibrate. Calibration was achieved by least squares fitting the front end channel with the tube potential for V_1 to V_4.

Sample cells

Eight sample cells 5cm thick were filled with potassium iodide solution such that the equivalent thickness of iodine in the cells was 0, 0.05, 0.10, 0.15, 0.20, 0.25, 0.30, and 0.35 kg/m^2. The procedure used was the same as that described in section 4.1.1. The sample cells were placed in the odd numbered positions, the even positions being left empty to allow incident spectra to be recorded.

Experimental procedure

The following procedure was used to measure the iodine equivalent thickness in the eight sample cells using the tracking discriminator approach.

The Si(Li) detector and spectroscopic counting system was calibrated using the adjustable x-ray source. The Si(Li) detector was then positioned in the beam path and the energy corresponding to the highest x-ray energy detected was noted for seven tube potentials set nominally between 25kV and 55kV. Using this data, the voltage control system was calibrated.

A sample cell containing iodine was then placed in the beam path. A transmission spectrum was recorded at a tube potential of 40kV. The channel corresponding to the K-edge

was noted. V_2 was set by adjusting the voltage control until the maximum x-ray energy produced by the tube coincided with iodine K-edge. V_3 was set close to the K-edge energy of barium. V_4 was set as high as possible without causing dead times to exceed 5%. V_1 was set 5kV below V_2.

Tube potentials were preset to V_1 = 28.45kV , V_2 = 33.43kV, V_3 = 37.94kV, V_4 = 41.26kV. Reference spectra were recorded using the Si(Li) detector at these four tube potentials.

The Si(Li) detector was then removed from the beam path and replaced by the proportional counter. A program similar to "CAROUSEL", (see appendix F) was then run, it carried out the sequence below.

Set tube potential to V_1. Move carousel position 0 into the X-ray beam path, record pulses in the low memory group channel 0-511 for 300 seconds. Move carousel position 1 into the beam path and record pulses in memory group 512-1023 for a further 300 seconds. This procedure was repeated four times. The total integration time for the incident and transmitted pulse height spectra was 2400 seconds. These spectra were then saved to a disk file on the BBC. The procedure was then repeated for tube potentials V_2, V_3 and V_4. The entire procedure was then repeated for carousel pairs 2 and 3 to 14 and 15.

The data collected was initially transferred to the IBM PC. Each of the 32 incident pulse height spectra recorded were deconvolved with the detector response. The front end channel of each of the resulting spectra was noted. For each sample the front end channel was then plotted against the set tube potential and the resulting slope and intercept used to calibrate the pulse height spectrum.

The data collected from the apparatus was then transferred to the workstation using Ethernet. A program similar to "SIMULATION" in appendix F was used to extract the iodine equivalent thickness. Fractional transmittances were evaluated by taking the ratio of counts contained in

channels above the deconvolved front end energy less the lag energy.

Results

The results of this experiment are shown in figure 6.02. The slope of set value of iodine equivalent thickness against measured value was slightly high. This could indicate that the stock solution used to prepare the iodine samples was slightly high. When differential absorptiometry was used on the sample the slope was found to be 1.136 and the intercept 0.0008.

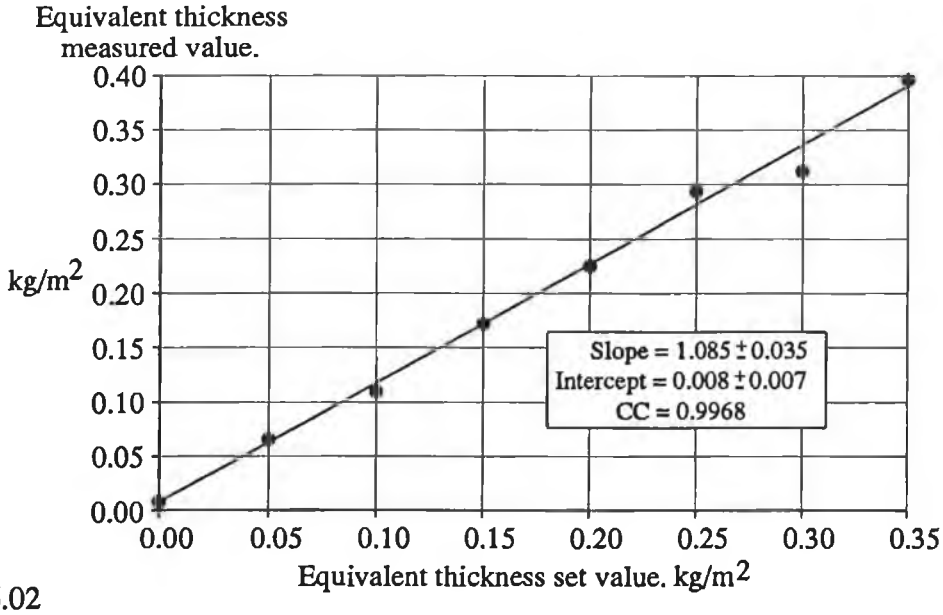

Figure 6.02

Graph of set value of iodine equivalent thickness vs measured value. Demonstrating the linearity of the total count technique.

6.1.2. DEMONSTRATION OF MATRIX INDEPENDENCE

The ability of the tracking discriminator to make quantitative measurements of analyte equivalent thickness independent of the matrix in which the analyte was contained was verified. The approach used was similar to that described in section 4.1.2. Six sample cells varying in thickness from 1cm to 6cm were filled with potassium iodide solution such that the equivalent thickness of iodine through each was 0.25kg/m^2. These were placed in the sample carousel. The procedure outlined in 6.1.1. was then carried out to measure the analyte equivalent

thickness using the tracking discriminator method. The lag was set to 3kV. The results of this experiment are shown in table 6.01

	Equivalent thickness of iodine.	
Sample thickness. mm	Set value. kg/m^2	Tracking discriminator technique. kg/m^2
60	0.25	0.276
50	0.25	0.275
40	0.25	0.264
30	0.25	0.263
20	0.25	0.263
10	0.25	0.215
		Mean = 0.259 SD = 0.021

Table 6.01
Table of measured values of analyte equivalent thickness obtained using the tracking discriminator technique. Used to demonstrate matrix independence of the technique.

The results demonstrate that the technique is quantitative, when the attenuation due to the matrix is varying. The fractional transmittances varied by a factor of roughly two over the range examined.

6.1.3. SELF GENERATED REFERENCE SPECTRA

In all previous work reference spectra were obtained using the Si(Li) detector. Similar spectra can be obtained from the incident pulse height spectrum, by deconvolving the detector's response. This approach has the advantage that it would allow equivalent thickness measurements to be made without any use of the Si(Li) detector.

Using the experimental data obtained for the linearity experiment, each of the incident pulse height spectra had the detector's response function removed. The eight resulting spectra produced at each tube potential were then averaged. Before averaging, the front end channels for a specific voltage were shifted to a common position; this was to overcome the problems of drift. Figure 6.03 makes a comparison between the two sets of reference spectra.

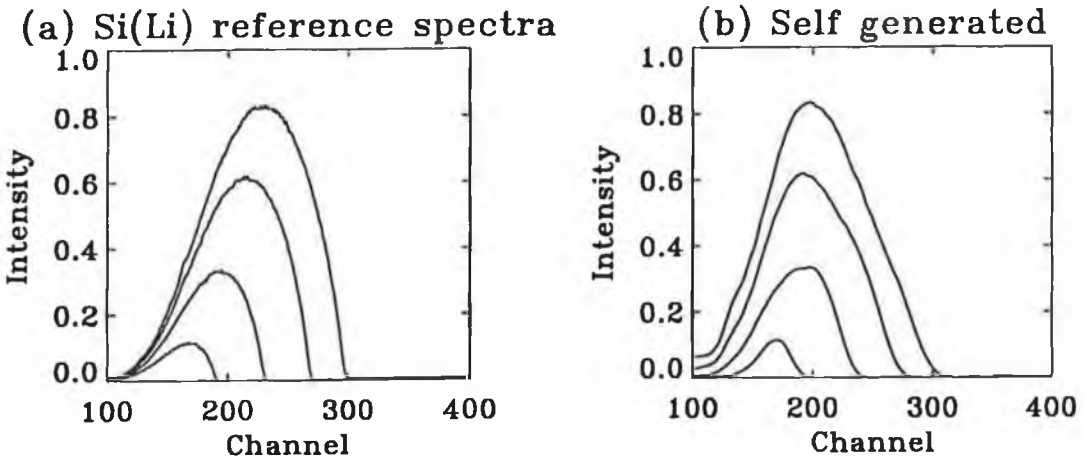

Figure 6.03
Reference spectra generated using the Si(Li) detector and the proportional detector recorded at four tube potentials.

The deconvolution routine used assumed a fixed Gaussian width of approximately 3keV for the detector resolution and flat efficiency response. A more precise deconvolution may have produced spectra that were closer to the correct spectra.

These spectra were then used with the same software that was used for the linearity experiment. The result of this experiment is shown in figure 6.04.

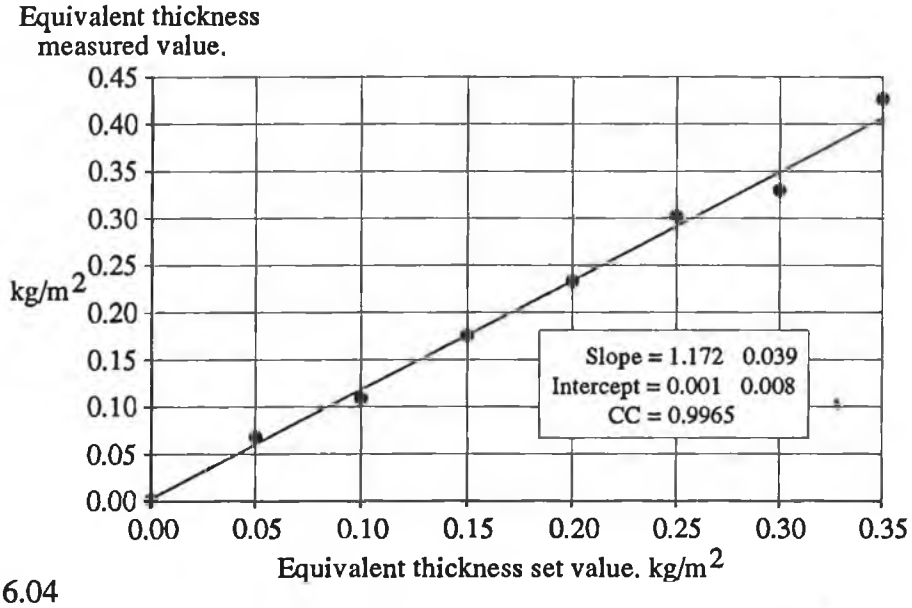

Figure 6.04
Graph of set value of iodine equivalent thickness vs measured value. Demonstrating that self generated reference spectra may be used instead of using the Si(Li) detector system.

The result is a technique that works nearly as well as the technique that uses the Si(Li) detector for reference spectra.

6.1.4. MEASUREMENT OF THREE ELEMENTS

It was shown in the computer simulation section that it should just be possible to image three, and so in theory more, elements next to each other in the periodic table. An attempt was made to carry out this experiment using the elements cadmium, indium and tin. Although not totally successful it suggested possible improvements that could be made to the technique. It also indicated that, with the apparatus available, an experimental demonstration of imaging using the tracking discriminator should be restricted to two analytes. It is for these reasons that it is included.

Eight sample cells were constructed with a thickness of 3cm. Stock solutions of cadmium chloride, barium chloride and tin chloride were prepared. The same anion was used to avoid the solutions reacting. To keep the tin chloride in solution it was acidified with hydrochloric acid and stored in the presence of metallic tin [2]. 1cm of each stock solution produced an equivalent thickness of analyte of $0.1kg/m^2$. The sample cells were filled as shown in table 6.02(a). All sample cells contained $30kg/m^2$ of water. The samples were placed in the sample carousel. The equivalent thicknesses were measured using a similar approach to that outlined in section 6.1.1 on linearity. The tube potentials used were V_1 = 24.76kV, V_2 = 26.61kV, V_3 = 27.88kV, V_4 = 29.34kV and V_5 = 32.08kV. Using computer simulations an effective lag was found to be 2.25kV. The results of this experiment are given in table 6.02(b).

The sample containing three elements, run 1, has failed. For samples containing one or two analytes only there is some correlation between set and measured values. The sample containing only water, run 8, demonstrates one of the problems. A statistical error leading to a high value of analyte equivalent thickness of the first analyte

will result in a corresponding low value in the second analyte measurement. A similar effect has occurred in run 1 (i.e. cadmium low leading to indium high).

(a)	Set values kg/m^2		
Run	Cadmium	Indium	Tin
1	0.1	0.1	0.1
2	0	0.1	0.1
3	0.1	0.1	0
4	0.1	0	0.1
5	0.1	0	0
6	0	0.1	0
7	0	0	0.1
8	0	0	0

(b)	Measured values kg/m^2		
Run	Cadmium	Indium	Tin
1	-0.02	0.38	-0.25
2	0.03	0.07	0.17
3	0.14	0.12	-0.05
4	0.12	0.04	0.06
5	0.12	-0.01	-0.02
6	0.00	0.11	0.01
7	0.03	-0.01	0.14
8	0.05	-0.06	0.07

Table 6.02
Set values and measured values of analyte equivalent thickness for sample cells containing three analytes.
Lag = 2.5keV, Matrix = 30kg/m^2 water.

Using the same data the software was modified so that the indium equivalent thickness measurement was not made. This meant that the counts contained in the V_4 spectra could be used to quantify the photoelectric absorption constant on the high side of the cadmium k-edge, the extra counts available reduced the statistical noise. The lag was increased to 2.5kV. The results are shown in table 6.03.

Run	Cadmium kg/m^2	Tin kg/m^2
4	0.11	0.11
5	0.11	-0.01
7	0.02	0.11
8	0.02	0.01

Table 6.03
Recalculation of three element data, excluding sample with indium.

As can be seen from the table the set and measured values are in good agreement.

Out of interest, the program was modified to measure cadmium and indium in samples containing no tin, and indium and tin in samples containing no cadmium. The results are shown in table 6.04.

Run	Cadmium kg/m^2	Indium kg/m^2
3	0.14	0.10
5	0.09	0.01
6	0.01	0.11
8	0.02	0.01

Run	Indium kg/m^2	Tin kg/m^2
2	0.11	0.12
6	0.11	0.02
7	0.03	0.09
8	0.04	-0.02

Table 6.04
Recalculation of three element data.

Both these experiments show reasonable agreement.

The second approach has thus made accurate measurements of all the analytes but it does require extra knowledge of the matrix.

The experiment demonstrated that elements next to each other are resolvable. However the interference of a third element (next to the others) reduced the counting statistics such as to make the technique unreliable. A third element further away in the periodic table would work. It was this experiment that indicated that the final imaging work should be limited to two elements. This is described in section 6.2.; similar conclusions were drawn in the computer simulation of this experiment described in section 5.5.

Another conclusion of this experiment was that there may be a better way of solving the equations for the α's and β. This would include using the extra information that for physical reasons $\alpha_1 \leq \alpha_2 \leq \ldots \leq \alpha_{x-1} \leq \alpha_x$. For this to be feasible then the equations need an extra degree of freedom, for example extra β's. A number of approaches were tried. For example when $\alpha_{low} \geq a_{high}$ (i.e. a negative equivalent thickness occurred) the software would recalculate β such that $\alpha_{low} = a_{high}$. The first values of α would then be recalculated and the procedure repeated. In effect the program would try rigorously to obey the rule that $\alpha_1 \leq \alpha_2 \ldots$ while trying to keep the various β's as close as possible to each other.

The investigation of faster methods of convergence, using extra physical information with regard to reducing sensitivity to statistical noise, could improve the technique and would be an area for further research.

6.2 IMAGE PRODUCTION

Introduction

The image produced to verify the total count technique used the fact that all projections of a circularly symmetric phantom are identical to reduce the amount of projection data that needed to be collected. This approach could have been repeated. However, it was decided to produce element specific images of a complex phantom using a full set of projection data.

Images of the distribution of cadmium and indium distributed in a matrix of water were produced. The results were compared with a conventional CT image of the same resolution.

A number of different methods of displaying the result were also investigated.

6.2.1. CONFIGURATION OF THE APPARATUS USED FOR IMAGE PRODUCTION

A diagram of the phantom used is shown in figure 6.05. Four 1 cm diameter 2mm deep circles were machined in a 3cm diameter 4mm thick disk of perspex. The inner chambers were cut from 1cm diameter hard plastic tubing. These were sealed into the recesses machined into end plates. The outside walls were constructed from sheet polystyrene.

The phantom was designed for imaging two elements; for this it needed four cavities, surrounded by a matrix of water. The indium cavity was filled with a solution of indium chloride containing 10 kg/m^3 of indium. The cadmium cavity was filled with cadmium chloride solution to a concentration of 10 kg/m^3 of cadmium. Another cavity was filled with just water and the last was filled with a mixture containing 10 kg/m^3 indium and 10 kg/m^3 cadmium.

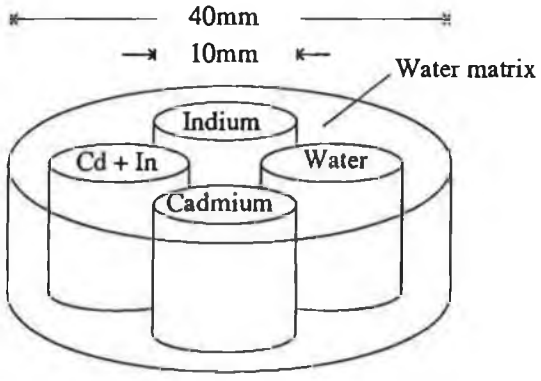

Figure 6.05
Construction of the phantom used to study the tracking discriminator technique.

The phantom to be imaged was 30mm wide. Allowing for some space on the side of the phantom, the region to be scanned was set to be 40mm wide. It was desirable to reduce the amount of reconstruction data that needed to be collected. The only way this could be done was to have a very coarse reconstruction grid. A 10 x 10 reconstruction grid was the limit before the main features of the phantom were lost. To reconstruct into this grid requires 100 measurements of equivalent thickness. To achieve this, ten projections were spaced by 18 degrees, each projection contained ten equivalent thickness measurements. The step size within a projection was set at 4mm. The X-ray beam width was 2mm, which could lead to partial volume effects. Translation was achieved using a stepper motor driving a lead screw. Rotation was achieved manually using a protractor mounted on the side of the phantom.

6.2.2. EXPERIMENTAL PROCEDURE TO PRODUCE ELEMENT SPECIFIC IMAGES

Four reference spectra were recorded by the Si(Li) detector at the tube potentials V_1 = 24.95kV, V_2 = 26.81kV, V_3 = 28.17kV and V_4 = 30.81kV. These voltages were chosen by placing a sample containing indium and cadmium in the beam path. The tube potential was increased until the front end coincided with the K-edge of cadmium. This was used to set V_2. V_1 was set approximately 2kV below this.

V_3 was set at the indium K-edge. V_4 was set about 2.5kV above V_3. The tube current was set to 25mA. This limited system dead time to less than 5%, reducing pulse pile up effects at V_4, while providing total incident counts in excess of 1.5×10^6 at V_1. Since the tube current could not be varied during the scan, this led to longer than necessary integration times for the higher tube potentials.

The phantom was mounted on the scan table. A tungsten light source placed in front of the x-ray tube target was used to locate the beam path. The first step position was located using a mask placed 5 mm to the side of the phantom.

The Si(Li) detector system was replaced by the proportional counter. The data acquisition program then set the tube potential to V_1 and recorded the incident spectrum at step position 0, outside the region containing the phantom, for 155 seconds. The phantom was then moved to the first step position and the transmitted spectrum recorded. This procedure was repeated four times. The two resulting pulse height spectra were saved to a single disk file. This procedure was repeated for each of the four tube potentials. The entire procedure was then repeated as the phantom was moved between position 0 and 2,3,...10. The program terminated after one complete projection was recorded. The forty data files produced by this routine were then transferred to the PC. The procedure was then repeated at ten different evenly spaced scan angles. To obtain the new angle the phantom was manually rotated. The scan angles were chosen in a random order to avoid the risk of systematic errors. Each projection took 22 hours to record, of which 14 hours were count integration time. The incident spectra contained $V_1 = 1.69 \times 10^6$ counts, $V_2 = 5.34 \times 10^6$ counts, $V_3 = 6.99 \times 10^6$ counts and $V_4 = 1.05 \times 10^7$ counts.

The incident spectra were then deconvolved with the detector response and the front end channel as a function of tube voltage noted. These points were used to calibrate the pulse height spectra. All projection data files were then transferred to the workstation. The total count

technique was then used to measure the cadmium and indium equivalent thicknesses. The resulting data was organised into a sequence consistent with the reconstruction software.

The reconstruction technique used for the image based on the total count technique calculated overlap areas by summing the boxes intercepted in a grid 50 times finer than the grid size. For practice two programs were written that ran on either the IBM PC or the Workstation to achieve an additive ART reconstruction using exact overlap areas; appendix F. The overlap areas were calculated by program OVERLAP. This stepped through each ray position at each angle and each projection. For each ray an array containing the pixels intersected and corresponding overlap area was calculated. All the information concerning one ray was written as a single structure to a disk file. This file contained the information about all rays.

Program "RECON" used the ART algorithm described in section 2.7.2. to convert projection data into image data. The use of structures greatly simplified the programming. The approach reduced the program length to about 30 lines of straightforward code. To speed convergence negative image pixel values calculated during reconstruction were set to zero.

Reconstruction into a grid 10x10 produces a very coarse image. Most of the images shown in the following section were produced by reconstruction into a grid of 30x30. The extra projection data was produced by evenly spacing the 10 ray sums within a projection into a projection of 30 ray sums. The ray sums located between the known values were obtained by linear interpolation. Each projection was copied three times. The copied projections were not corrected for the angle change.

Using this approach produces a better looking image. Distances between two points on the image can not be measured any more precisely than in the 10x10 image. Quantitative measurements were taken from the 10x10 image only.

With an image of such low resolution reconstruction into a grid containing 100 hexagons may have been a way of improving the aesthetics of the reconstructed image, without interference to the projection data.

6.2.3. RESULTS

A conventional CT image was produced of the phantom using the pulse height spectra recorded at V_4. See figure 6.06. The projection data used was the natural logarithm of the ratio of the total incident count divided by the total transmitted count. In X-ray absorption CT more of an attempt could be made to make the source monochromatic. The image is probably suffering from some beam hardening effects. The region contained by the phantom is clearly defined inside a ring of blue pixels. The region in the top right hand side of the phantom contained only water, it contains green pixels. The other three regions that contained analyte show an increased attenuation displayed as orange pixels. The phantom was also slightly out of centre, with the axis of rotation, the phantom being displaced sightly to the bottom of the image area.

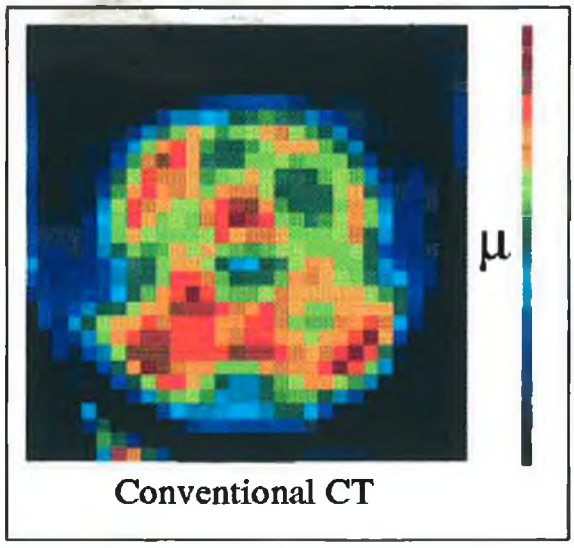

Figure 6.06
Conventional CT image of the phantom produced using V_4 data.

The reconstructed image data shown in table 6.05. were produced from the cadmium and indium equivalent thicknesses measurements.

0.0	0.0	0.0	0.0	0.5	2.4	0.0	0.0	0.0	0.0
0.0	0.0	0.8	0.0	0.0	0.1	0.0	0.0	0.0	0.0
0.0	0.0	0.0	0.0	0.0	0.0	0.0	0.1	0.0	0.0
0.0	0.0	0.0	0.0	0.0	0.0	0.0	0.0	0.1	0.0
3.0	0.0	0.0	0.0	0.0	0.0	0.0	0.0	0.0	0.9
0.2	0.1	0.3	1.9	0.0	0.0	0.0	0.0	2.5	0.0
0.0	0.0	5.0	14.7	2.6	7.3	13.8	4.0	0.0	0.0
1.4	0.0	0.0	7.1	0.0	7.1	16.0	6.0	0.0	0.0
1.2	0.0	0.0	3.2	0.0	0.0	1.9	0.0	0.0	0.0
0.0	0.0	0.0	0.0	0.0	0.0	0.0	0.3	0.1	0.0

Cadmium

0.0	0.0	1.7	0.0	0.0	0.0	0.7	1.2	0.0	0.0
4.2	0.0	0.0	0.0	0.0	0.0	0.6	0.0	0.0	0.0
4.2	0.0	0.0	4.5	0.7	3.6	6.6	0.0	0.0	0.0
0.0	0.0	14.4	19.6	7.3	1.7	0.0	1.5	0.0	0.0
0.0	0.0	6.2	4.4	0.0	0.0	0.0	0.0	3.3	0.0
0.0	0.0	4.8	7.7	0.0	0.0	0.0	0.0	0.0	0.1
0.0	0.0	14.2	20.4	4.8	1.0	0.0	0.0	0.0	0.0
0.0	0.0	18.5	14.2	7.4	0.0	0.0	0.0	0.0	0.1
0.0	0.0	2.0	0.0	0.1	0.0	0.0	0.0	0.0	0.0
0.0	0.9	3.0	0.1	0.1	1.6	0.0	0.0	0.0	0.0

Indium

Table 6.05

Reconstruction data displayed in numeric form.
Values in each pixel show analyte concentration in kg/m^3.

The values in the pixel central to the region containing the analyte are higher than expected. The region around this pixel contain values of analyte equivalent thickness that are lower than expected. The redistribution of concentration is probably an artifact of reconstruction.

The mean of the three highest equivalent thickness values in the projection data for the indium was 0.28 kg/m^2 and for cadmium 0.20 kg/m^2. This occurs for beams that have passed through up to 2cm of analyte solution, or 20 kg/m^2.

The true element specific CT images are shown in figure 6.07. The cadmium image clearly shows the location of cadmium without disturbance from the indium or water matrix. Similarly, the indium image has successfully located the distribution of indium in the phantom.

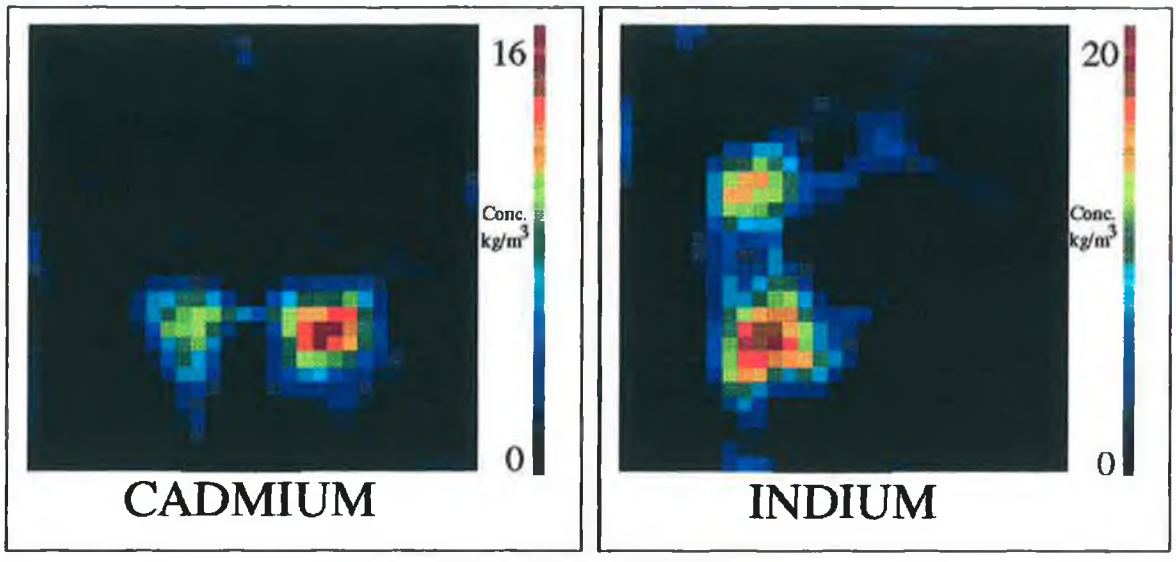

Figure 6.07
Element specific images produced using the tracking discriminator technique.

These images prove experimentally the principle of tracking discriminator technique. The images were produced with a disturbing analyte only one away in the periodic table. This would not have been possible with the total count technique.

6.2.4. ALTERNATIVE DISPLAY TECHNIQUES

There are many ways that a CT image can be displayed. Personal preference means that colour coded images were used in previous sections.

Figure 6.08 shows a number of different ways that reconstruction data can be displayed as an image. The data used is for the cadmium distributed in the water matrix.

The black and white image works well on a computer display where there are a large number of grey levels available. It is also the only image format' that most journals can print. A colour version of the image is shown to the right of the black and white image.

By increasing the amount of projection data, the corners of the pixels in the reconstruction grid can be softened. Finally the 30x30 image can then be spread into a grid 90x90. This is achieved by spacing the 30x30 data evenly in the 90x90 grid and interpolating the pixels

in between.

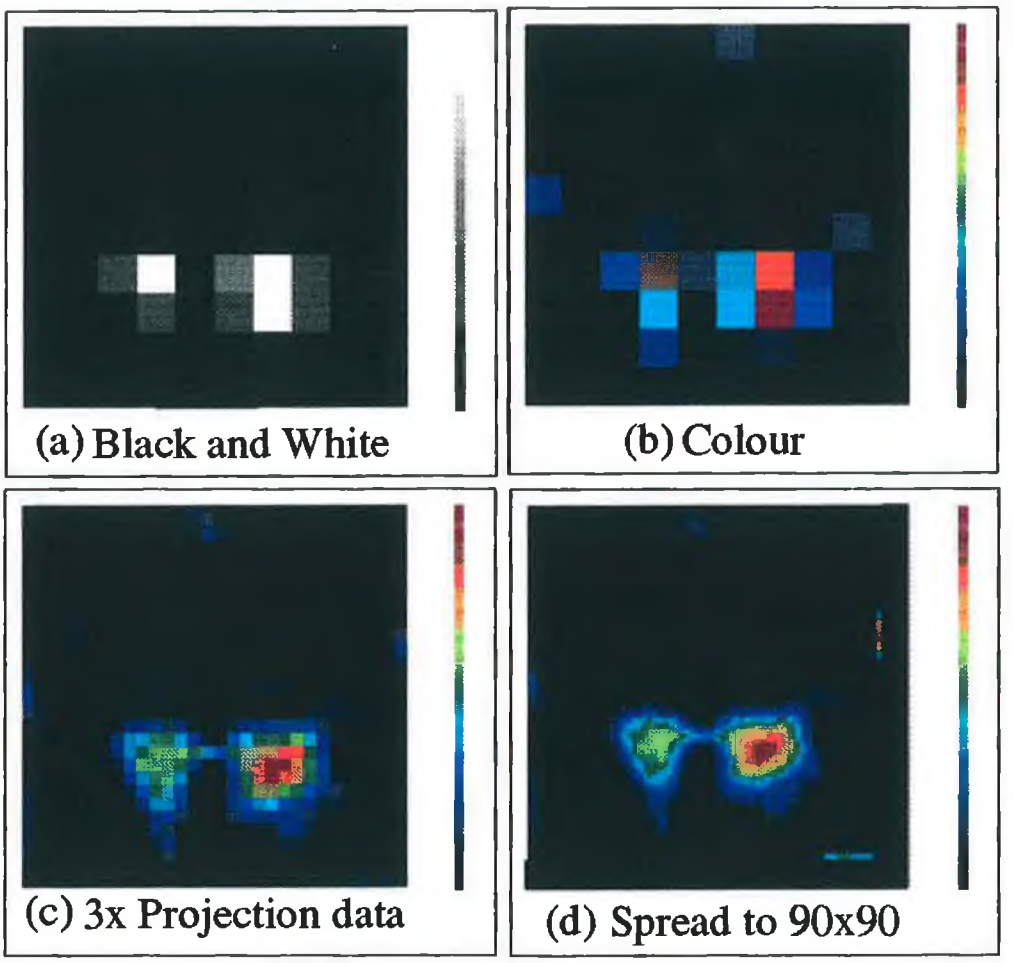

Figure 6.08
Four different ways of displaying the cadmium reconstruction data in an image format.

Any processing of the image after this would require limiting the range of pixel values or using a non-linear intensity scale. This requires some subjective input from the display program user and for this reason was not included.

Using IDL the data can be displayed in contour format. This is shown in figure 6.09.

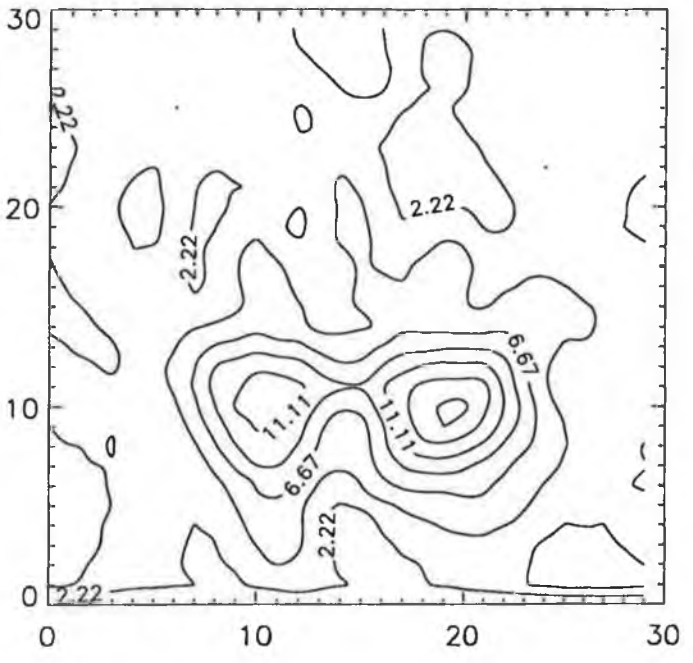

Figure 6.09
Contour plot of the 30x30 cadmium image data. Produced using IDL.

IDL also provides facilities for wire frame and shaded surface plots. These are shown in figure 6.10

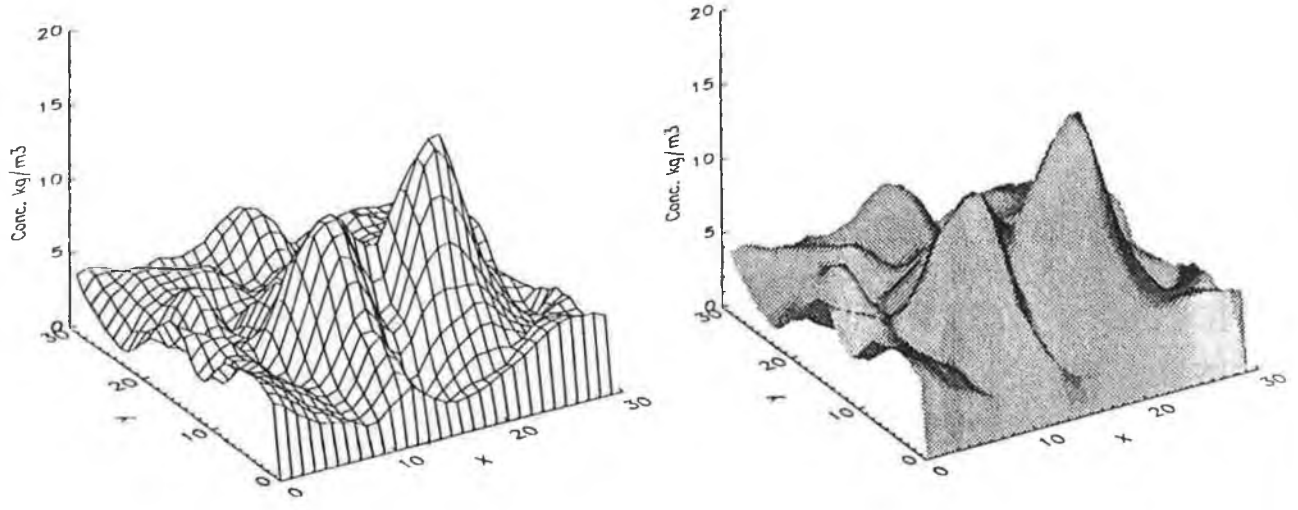

Figure 6.10
Wire frame and shaded surface plots of the cadmium image data. Produced using IDL.

References

[1] Knoll, G.F.
"Radiation detection and measurement"
John Wiley & Sons., pp 172, 1989.

[2] Holmyard, E.J. and Palmer, W.G.
"Higher school inorganic chemistry"
JM Dent, pp 415, 1964.

Chapter 7
Conclusions

7.1 ACHIEVEMENTS

7.1.1 SUMMARY OF THE PROJECT

The research work developed two new techniques for producing element specific images that were within the constraints of the original aims of the project outlined in section 1.3.

The first, called the total count technique, used a tube source of x-rays and a detector system with no energy resolution. This technique could be used with high efficiency but poor energy resolution detectors such as the NaI(Tl) scintillation detector. To record a total count requires no pulse height analysis and so allows the technique to use a simple counting chain [1]. This approach would be straightforward to implement with detector arrays.

To demonstrate the total count technique images of iodine and barium distributed in a specially constructed phantom were produced. A comparison was made between the element specific images and conventional CT images of the same phantom. Measurements made of analyte equivalent thickness in homogeneous absorbers were used to verify the linearity and matrix independence of the total count technique.

The second approach was a development of the total count technique called the tracking discriminator method. This used a single channel analyser to increase the percentage of counts providing information about the analyte of interest. Computer models demonstrated that the tracking discriminator method provided an improvement in selectivity and sensitivity over the total count technique. The improvement was demonstrated experimentally by

producing element specific images of cadmium and indium distributed in a water matrix. These two elements have a K-edge separation of only 1.23keV, demonstrating the improved selectivity. The technique required the energy resolution associated with a proportional detector. This detector is very inefficient with the result that in some applications the dose would be high.

Both approaches used the K-edge absorption jump of the analyte as a measure of analyte equivalent thickness. The absorption of the analytes and matrix was described in terms of the underlying physical processes. Unlike the existing techniques that use polychromatic x-ray sources to image an analyte, this approach allowed analyte equivalent thickness to be determined without detailed knowledge of the absorption response of all the components contained in the object imaged. The only *a priori* information required is a knowledge of the existence of elements within the absorber that have K-edge energies within the range of x-ray energies used. The x-ray energies used in the tracking discriminator method are only those that cause pulses in the region above the highest x-ray energy produced at the lowest tube potential used, less the lag value.

The techniques would be ideally applied to cases where high atomic number contrast agents are introduced into a matrix consisting of lower atomic number elements.

7.1.2 OTHER ACHIEVEMENTS

This section records some of the spin-off achievements of the project, external to the main achievement of producing element specific images with a low resolution detector.

The program "Hubble" was written to simulate the response of any system containing an x-ray source, absorber and detector over the energy range 10 to 100keV (Appendix G). The software produced contained a library of fluorescence and tube source spectra. Absorption data, including the location of K-edge energies for many elements and compounds, were contained in a second library. A third

library contained details about detector responses. The program allowed the absorption information of many elements to be combined and displayed graphically for a range of energies. It also displayed the effect of adding or removing detector and absorber responses from the source spectra.

Using program "Hubble" it was possible to design x-ray filters. The filters were fabricated by dissolving salts of the required elements in water and sealing the solution in a sample cell. This technique allowed a large range of elements to be used as possible filter materials. Normally, metal foils are used to filter x-rays.

Early work on low energy resolution detectors used deconvolution techniques to remove the response of the detector from the pulse height distribution recorded. The deconvolution technique developed used a form of the Algebraic Reconstruction Technique to solve a set of noisy simultaneous equations. The deconvolution method developed was later found to be similar to Gold's ratio method of deconvolution [2]. The algorithm has been recorded in appendix D. The work highlighted the similarity of some reconstruction and deconvolution algorithms.

7.2 FUTURE DEVELOPMENTS

7.2.1 FURTHER DEVELOPMENTS OF THE TECHNIQUES

Improvements could be made to the apparatus that would greatly reduce the data collection and data processing times. Straightforward approaches would include brighter sources, faster counting systems and more powerful computers.

The greatest improvement in data collection time would be achieved by using an array detector. The data collection system would be similar to that used in second generation CT scanners. X-ray sensitive photodiode arrays are already commercially available [3]. Such an array would allow an entire projection of fractional transmittances to be recorded simultaneously. A projection

could then be recorded in the time required to produce a single measurement of equivalent thickness.

It may be possible to use a multiwire array proportional detector or single wire position sensitive proportional counter with the tracking discriminator method. It should be noted that such detectors produce a small signal when used in proportional mode [4].

The only detector gas available was P10 Ar/CH_4 with a resolution of 12.8% at 5.9keV. The use of 0.5% ethylene instead of methane improves energy resolution to 10.1% and Ne/Ar filled detectors have an energy resolution of 9.8% [4].

Recently HgI_2 array detectors have been developed with an energy resolution of 300eV at 6keV [5]. A CdTe array developed by Tsutsui et al. includes amplifier and discriminator circuits. This detector array may be suitable for use with the tracking discriminator technique [6][7].

The low x-ray energies used in this project were set by the limitations of the x-ray source available. This meant that the dose delivered in a clinical application of the technique, imaging the same analytes, would be high. If higher x-ray energies could be produced, then it would be possible to investigate the imaging of elements with higher K-edge energies. This might provide a way of reducing the radiation dose, initially the computer model could be used to test this idea.

There are many small improvements that could be made to the technique. The convergence algorithm is very robust (immune to bad data) however it is slow to converge. Instant improvement could be achieved by using the secant method instead of the bisection method for solving equations . The fact that equivalent thicknesses can not be negative would allow the program to detect bad experimental data and could assist the program to converge on a better solution.

Instead of making a count in a specific period of time, it would be better to measure the time required to

reach a specific count. This would reduce data acquisition time and allow the count statistics to be set in advance of doing the experiment. This facility was not available on the MCA.

Reconstruction into a grid of non-square pixels (e.g. hexagons) for images of low resolution, may provide a subjective improvement in the visibility of features in the image.

7.2.2 POTENTIAL APPLICATIONS

The total count method and tracking discriminator technique may have potential uses in both medical and industrial applications. Both techniques provide a method of making quantitative measurements of element concentration within an object. The methods can be used to quantify the equivalent thickness of analyte along one beam path; in this mode the technique could be used to analyse homogeneous samples. Using tomographic techniques the spatial distribution of an element of interest within an structure can be mapped out.

Spectroscopy

Using the techniques developed it is possible to obtain spectral information about the absorption of a material. At present the technique has sufficient resolution to separately quantify adjacent elements in the periodic table. An alternating current (AC) x-ray tube could be used to continuously vary the tube potential. As the tube potential cycles, the discriminator on the detector tracks a fixed distance behind the highest x-ray energy produced. The pulses recorded by a gas proportional detector would then be gated into different counters as each K-edge energy is exceeded by the highest x-ray energy produced. The resulting data could then be analysed to evaluate the equivalent thickness of each analyte contained in the beam path. The output of such a device would be a spectrum showing equivalent thickness of each element as a function of atomic number.

Flow rate imaging

Jaschke et al. [8] described a method of imaging the distribution of a bolus of contrast agent injected into a pipe as it flowed past the image plane. By synchronizing the injection of the contrast agent with the data collection system, a set of images showing distribution of contrast agent across the pipe as a function of time were produced. This technique is limited, since it is unable to produce an image showing rate of flow in the pipe using a single scan.

The ability to image two elements simultaneously provides a method of overcoming this limitation. In this technique two analytes would be periodically injected into the main flow of the pipe upstream of the image plane. The injection rate of one analyte would increase while the injection rate of the second would decrease. The ratio of concentration of the two analytes injected would vary as a function of time, independent of the dilution caused by the main flow in the pipe. Using multi-element CT imaging techniques the distribution of the two analytes downstream of the point of injection could be determined. If the apparatus is properly synchronized, then it would be possible to correlate the measured ratio of analyte concentrations at a particular pixel location with the time it was injected. From this information an image of flow time could be produced. The work completed to test this idea is outlined in appendix A. The use of two tracers in this way would be new, the subject of flow visualisation has been reviewed recently by Freymuth [9].

Medical applications

The contrast agents that are normally used in medicine are based on only a few elements. An extensive study of the imaging of these contrast agents and other possible elements has been made by O'Hare [10]. Other elements are not desirable due to toxicity or cost. The elements that are commonly used are xenon in lung ventilation studies [11], iodine in blood flow and kidney examinations and barium compounds for imaging the digestive tract [12].

These elements are used to enhance contrast in a region of interest, the total count technique could make quantitative measurements of the distribution of these elements. The dose would be high since the technique requires fractional transmittance measurements which contain photons with energies that do not exceed the K-edge energy of the element of interest.

Some toxic elements localise in specific organs, using K-edge techniques it may be possible to quantify the distribution of these elements. Cadmium for example localizes in the kidney [13] and lead in bone [14].

Once a specific application is defined the computer simulation can then be used to estimate the number of photons required to image the element of interest. The procedure required for evaluating the sensitivity of the technique for a particular procedure would be as follows. The software would require an estimate of the attenuation due to the matrix. In most cases this could be achieved by representing the matrix as an equivalent thickness of water equivalent to the path of greatest attenuation through the plane of interest. Using the simulation software described in section 5.2.3 the total count required to measure the element to the desired precision would then be evaluated. The total count would then be converted to a patient dose using a conversion graph in the British standard data sheets on x-ray shielding [15]. A decision on the practicality of the technique for a specific application would then be based on this dose.

References

[1] Markham, C. and Fryar, J.
"Element specific imaging in computerised tomography using a tube source of x-rays and low energy-resolution detector system"
Nucl. Inst. & Meth., Vol. A324, pp 383-388, 1993.

[2] Jansson, P.A.
"Deconvolution with application to spectroscopy"
Academic press, inc. 1984.

[3] "PCD Linear image sensors S2301-FX series (for x-ray detection)."
Hamamatsu technical data sheet.

[4] Knoll, G.F.
"Radiation detection and measurement"
John Wiley & Sons., pp 160-195, 1989.

[5] Iwanczyk J.S., et al.
"20 Element HgI_2 energy dispersive x-ray detector system"
IEEE Trans. on Nucl. Sci., Vol. 39, No. 5, pp 1275-1279, 1992.

[6] Tsutsui H., et al.
"CdTe Semiconductor X-ray Imaging Sensor and Energy Subtraction Method Using X-ray energy Information"
IEEE Trans. on Nucl. Sci., Vol. 40, No. 1, pp 40-44, 1993.

[7] Tsutsui H., et al.
"CdTe Semiconductor X-ray Imaging Sensor and Energy Subtraction Method Using X-ray energy Information"
IEEE Trans. on Nucl. Sci., Vol. 40, No. 2, pp 95-101, 1993.

[8] Jaschke, W. et al.
"Flow measurements with a high-speed computer tomography scanner."
Med. Physc., Vol. 14, No. 2, pp 238 - 243, 1986.

[9] Freymuth, P.
"Flow visualization in fluid mechanics"
Rev. Sci. Inst., Vol.64, No. 1, 1993.

[10] O'Hare, N.
"A study of the imaging of contrast agents for use in computerised tomography"
Ph.D. Thesis, Dublin City University, 1991.

[11] Bautz, W.B. et al.
"CT Examinations of lung ventilation with stable xenon"
Advances in CT, European Scientific users conference Somatom Plus, March 1990.

[12] Webb, S.
"The physics of medical imaging"
Adam Hilger, 1988.

[13] Tucker, A.
"The toxic metals"
Earth island ltd., 1972.

[14] Green, S.
"An enhanced sensitivity K-shell fluorescence technique for tibial lead determination"
IEEE Trans. Nucl. Sci., Vol.38, No. 6, pp 1721-1727 1991.

[15] British Standard Institution.
"Recommendation for data on shielding from ionizing radiation"
BS 4094: Part 1 : 1966 , pp 48, 1972.

Acknowledgements

The author expresses his deep gratitude to his late supervisor, Dr. Joe Fryar, for his inspiration and help during the early part of this work. Thanks are also give to Professor Eugene Kennedy for his help and guidance in assisting the author to complete this work for presentation.

Thanks are also given to EOLAS for their financial support of the research.

Finally thanks are offered to all the postgraduate students and members of staff at Dublin City University for helpful comments and discussions during this work.

Appendices Page

APPENDIX A : FLOW RATE MEASUREMENT AND IMAGING

The ability to image two elements simultaneously provides a method of imaging the rate of flow in a pipe.

In this technique two analytes would be injected into the main flow upstream of the image plane. The injection rate of one analyte would increase while the injection rate of the second analyte would decrease. By measuring the ratio of the concentration of the two analytes at a point downstream of the point of injection and correlating this with the time when the analyte mixture was injected it is possible to determine the flow time.

The injection profile for each analyte shows the rate at which the analyte is being delivered to the system as a function of time. There are many different profiles that are possible. If the analytes were being delivered by piston pumps driven by a crank, then sinusoidal injection profiles would occur. In this appendix however, only linear injection profiles are considered, one analyte being injected at an increasing rate whilst the other is injected at a decreasing rate. This simplifies both the software required to drive the injection system and the calculation required to extract the flow rate from available data. Figure A.01 shows the proposed injection profiles.

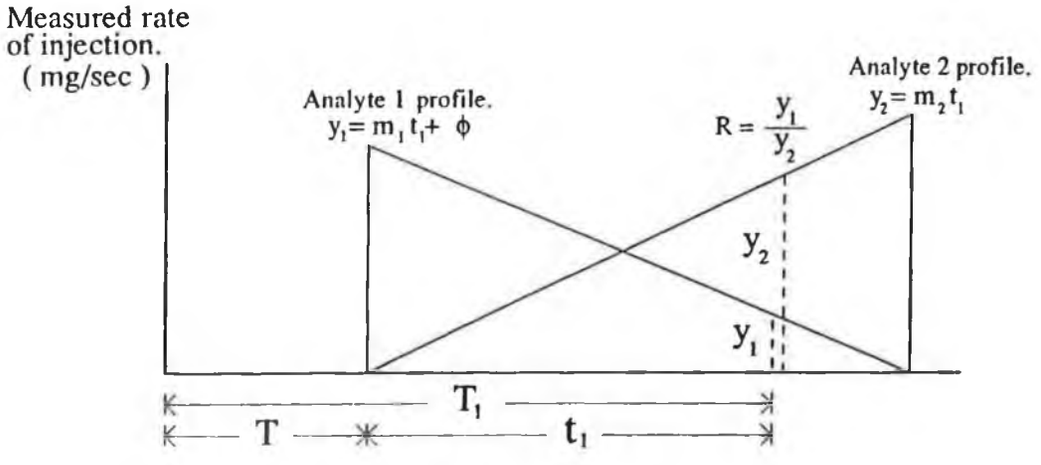

Figure A.01
Linear injection profiles used for flow rate measurement.

After the start of the injection cycle at a time T_1, the ratio of analyte concentration R is measured. This

was injected at a time t_1 after the start of the injection profile. The transit time T is the difference between these two times

$$T = T_1 - t_1 \qquad (A.01)$$

If the analytes have linear injection profiles then the rates of injection y_1 and y_2 at time t_1 are

$$y_1 = m_1 t_1 + \phi \qquad (A.02)$$

$$y_2 = m_2 t_1 \qquad (A.03)$$

where m_1 and m_2 describe the acceleration of the rate of injection (mg/s^2). ϕ is the initial rate of injection for the contrast agent being injected at a decreasing rate. The ratio R is given by

$$R = \frac{y_1}{y_2} = \frac{m_1 t_1 + \phi}{m_2 t_1} \qquad (A.04)$$

Rewriting A.04 gives

$$t_1 = \frac{\phi}{R m_2 - m_1} \qquad (A.05)$$

Substituting A.05 in A.01 gives

$$T = T_1 - \frac{\phi}{R m_2 - m_1} \qquad (A.06)$$

Equation A.06 demonstrates that it is possible to determine flow time T by measuring the ratio of concentrations of the two analytes R. If the distance between the point of injection and the image plane is known then the flow velocity can be determined.

$$\text{Flow velocity} = \frac{T}{L} \qquad (A.07)$$

where L is the distance between the point of injection and the detector system.

In practice two images would be produced showing the distribution of each analyte. The value of R would then be determined by taking the ratio of analyte concentration in corresponding pixel locations. This data would then be used to produce an image of flow time.

Initially the idea was investigated optically. The contrast agents used were red and blue dyes. These were

injected into the central flow of a 12mm diameter glass tube. The delivery system consisted of two 100ml glass syringes each driven by a lead screw and stepper motor. See figure A.02.

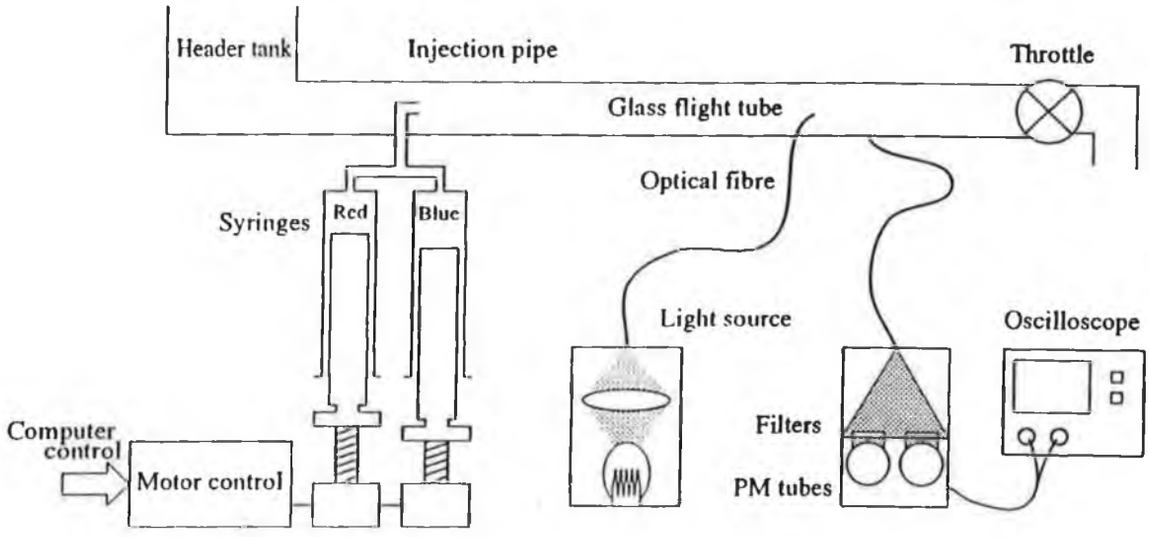

Figure A.02
Experimental configuration for investigating flow rate measurements.

The pulse sequence sent to the stepper motors was produced by an assembly language program running on a BBC. An optical fibre carried light from a white light source to one side of the tube. Another placed the other side carried the light to a box containing two photomultiplier tubes. Interference filters were placed in front of the photomultiplier tubes. The red filter was used to measure the blue dye and the blue filter used to measure the red dye. The red and blue absorption signals were recorded simultaneously on a digital storage scope. Typical traces for linear injection profiles are shown in figure A.03.

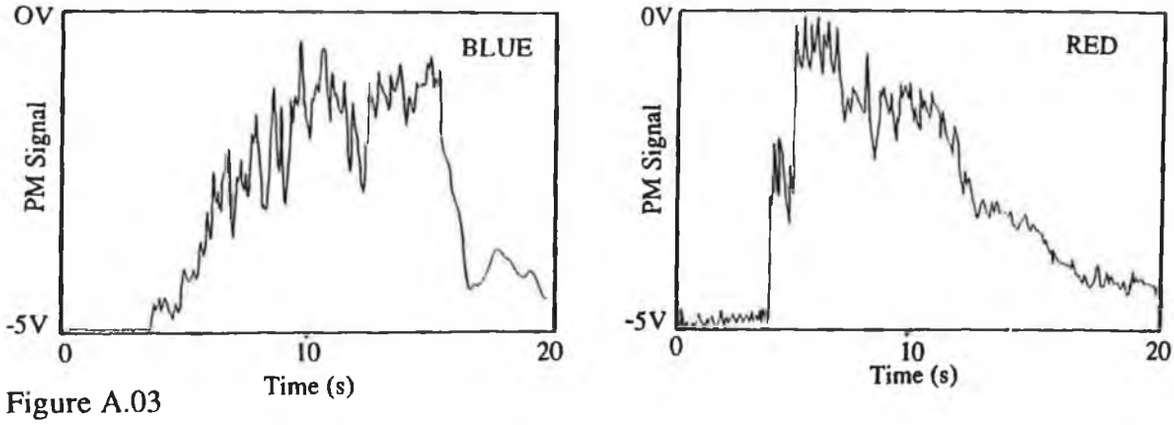

Figure A.03
Oscilloscope traces showing red and blue absorption across the flight tube. Injection - detector distance = 25cm, rate of flow 300cc/min.

The noise in the signals is due to turbulence in the flow. A computer simulation based on laminar flow theory produces the absorber profiles shown in figure A.04.

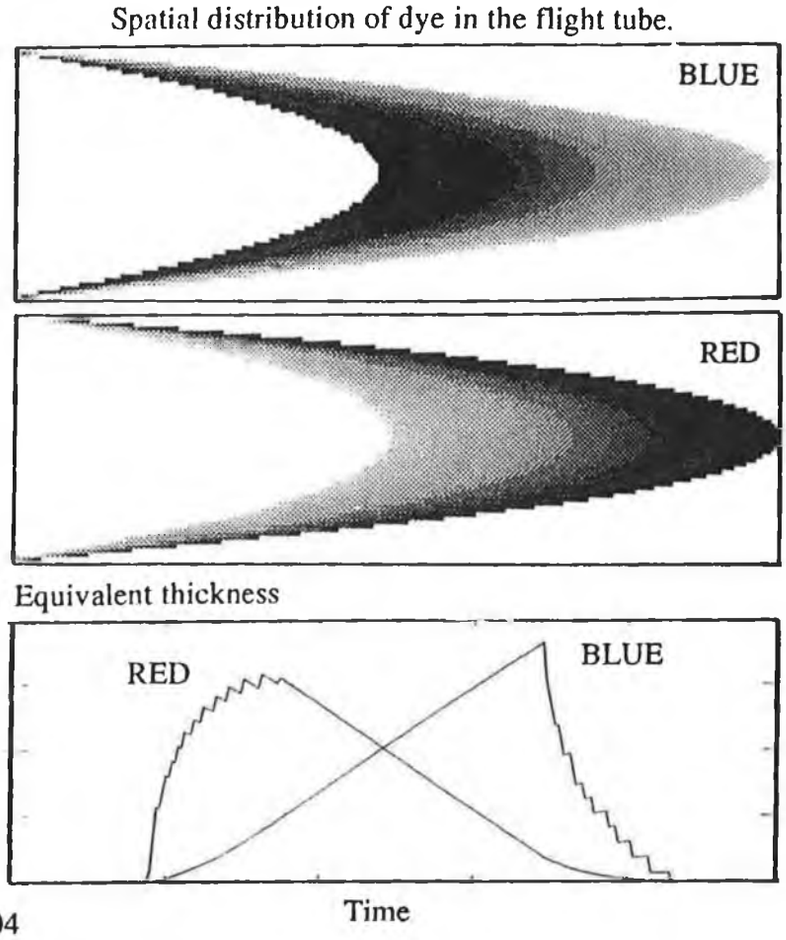

Figure A.04
Modelled absorption traces.

The underlying shape of the modelled profiles are similar to that of the experimental data.

The experiments required to prove the basic principle of the technique need non-turbulent flow conditions. Experimentally this is difficult to achieve, due to the disturbance in the flow caused by the injection of contrast agent.

Finally, the technique described in this appendix used absorption techniques to measure analyte concentration. There are a number of variations on this idea that could be considered. If two different short half life gamma ray emitters were injected into the tube instead of the analytes, the ratio of concentration could be determined using the ratio of counts produced by each emitter. The

counts could be separated using an energy dispersive detector and two single channel analysers.

APPENDIX B : A DIFFERENT EXPERIMENTAL CONFIGURATION FOR THE TRACKING DISCRIMINATOR TECHNIQUE

The experimental verification and production of images using the tracking discriminator technique used a counting system based on a multichannel analyser (MCA). This was described in chapter 6. As a result of this the counting system was slow, allowing a maximum count rate of approximately 10,000 counts per second. As presented the technique required a MCA for each detector used. This would be costly and complex to use with array detectors.

The MCA had the advantage that it allowed the discriminator level to be set in software after the experiment was completed. It also provided a method of calibrating the system and verifying that the apparatus was functioning properly.

Figure B.01 shows a system that was designed that allows faster pulse counting, while still providing a method of calibration.

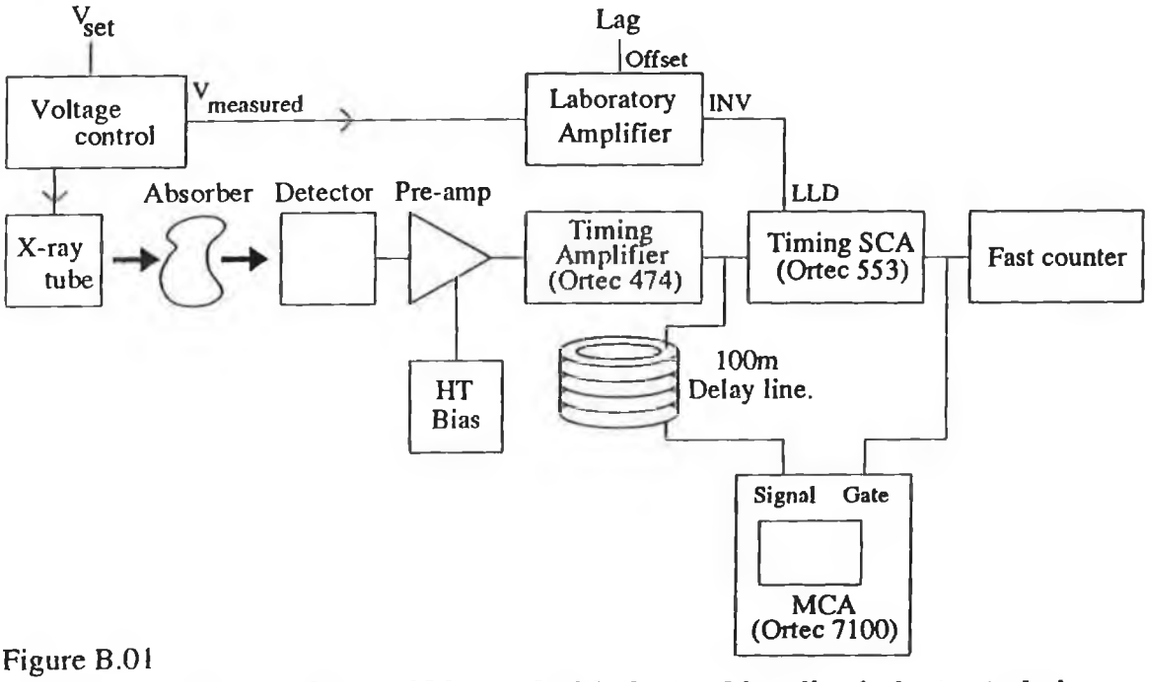

Figure B.01
Fast counting system that could be used with the tracking discriminator technique.

The tube voltage can be set by the voltage control circuit to the values required by the tracking discriminator technique. The control circuit produces a

measured value signal proportional to the accelerating potential. This is scaled by the laboratory amplifier such that the low level discriminator threshold tracks the maximum x-ray energy produced by the tube. The laboratory amplifier contains an offset function that allows the lag value to be added to the discriminator threshold. The detector pulses are amplified by a pre-amplifier and then a timing amplifier. The single channel analyser produces output pulses for input pulses above the externally set low level threshold. The pulses produced by the SCA are counted by a fast counter. Counts recorded by this counter would then be used to calculate fractional transmittances.

A MCA is included in the system to provide a visual indication of the pulse height spectrum reaching the fast counter. This would only be used for setting up the amplifier gain and offset values. A 100 meter length of co-axial cable provides sufficient delay for the gate to close on the MCA before the pulse arrives at the MCA input (Ortec 7100).

APPENDIX C : SHIELDING CALCULATIONS

The X-ray tube could operate over the voltage range 20 to 60 kV with a tube current of 5 to 80 mA. Total dissipation in the tube was limited to 3kW. The tube contained a tungsten target with a 1mm thick beryllium window. The tube was water cooled. The tube was contained in a 10mm thick steel box with a 2mm exit hole. This box was then housed in a 3mm thick lead box containing a 10mm exit hole. This assembly was contained inside a lead lined steel cabinet. See figure C.01. Exposure levels to those operating the machine were calculated as follows. The data used for calculation comes from British standard 4094: Part 1: 1966 and 4094: Part 2: 1971 "Recommendation for data on shielding from ionizing radiation".

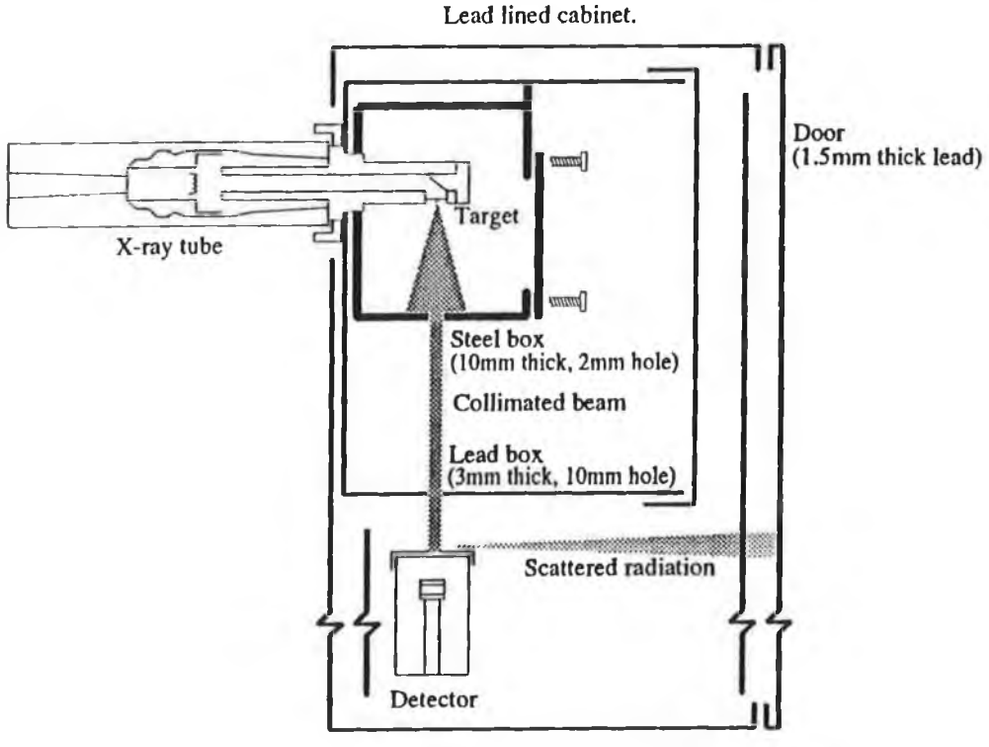

Figure C.01
Configuration of the shielding around the x-ray tube.

The dose rate was calculated in two parts. Firstly, the dose rate receivable from the machine containing no apertures in the lead or steel box was calculated. Secondly, the dose rate from radiation scattered from the x-ray beam in the lower half of the cabinet was considered.

(BS 4094:Part 2: Pg 13) gives the output of a constant

potential tube operated at 60 kV as 10 R/mA.min at 1 metre. The steel plate is 0.18m from the target. The dose rate on the surface of this plate is

$$\frac{1^2}{(0.18)^2} \times 10 \text{ R/mA.min} \times 50 \text{ mA} \times 60 \text{ min/h} \times 0.93 \text{ Rad/R}$$

$$= 8.6 \times 10^5 \text{ Rad/h}$$

$$= 8.6 \times 10^3 \text{ Gy/h}$$

(BS 4094:Part 2: Pg22) by extrapolation of the graph the attenuation of 10mm steel is 10^{-8}.

(BS 4094:Part 2: Pg35) by extrapolation of the graph the attenuation of 3mm lead is 6×10^{-12}.

The dose rate outside of the lead box is

$$8.6 \times 10^3 \text{ Gy/h} \times 10^{-8} \times 6 \times 10^{-12} = 5.2 \times 10^{-16} \text{ Gy/h}$$

The radiation would then have to pass through the 1.5mm thick lead door of the machine. The attenuation of 1.5mm of lead for 60kV radiation is 10^{-7}.

The top of the detector is 0.4m from the source. The radiation produces a spot 4.4mm in diameter on the top of the detector (2mm hole at 0.18m). The area of this spot is 0.15cm^2.

(BS 4094:Part 2: Pg 50) A maximum of 0.05% of the incident radiation is scattered to 1 metre per 100cm^2 irradiated area. The door is 25cm from the detector. The dose rate 0.40m from the source is 1.7×10^3 Gy/h.

The dose rate incident on the door is

$$\frac{0.05\%}{100\%} \times \frac{0.15\text{cm}^2}{100\text{cm}^2} \times 1.7 \times 10^3 \text{Gy/h} \times \frac{(1\text{m})^2}{(0.25\text{m})^2} = 0.02 \text{ Gy/h}$$

(The equation used BS 4094:Part2:Pg49)

The attenuation of 1.5mm lead is 10^{-7}. The scattered radiation transmitted through the door is

$$0.02 \text{ Gy/h} \times 10^{-7} = 2 \times 10^{-9} \text{ Gy/h}.$$

The two dose rates calculated are exceedingly small. It should also be noted that the x-ray machine was never operated over 30mA and the tube voltage for most experiments rarely exceeded 50kV. Some sort of filtering was normally included over the steel exit hole. The beam

through both holes was always collimated with 1mm or 2mm diameter holes drilled through 3mm thick lead. Thus the above calculation can be considered as maximum possible dose rate.

APPENDIX D : DECONVOLUTION ALGORITHM.

The deconvolution algorithm described in this appendix was used to remove the effect of the detector's response on the pulse height spectra recorded with a multichannel analyser. The effect of deconvolution was to produce a spectrum representing the spectrum incident on the detector.

The pulse height distribution recorded by a MCA consists of a set of n counts

$$C_1,\ C_2,\ \ldots\ ,\ C_x,\ \ldots\ C_n$$

at equally spaced energy intervals.

The spectrum incident on the detector was represented by the array

$$A_1,\ A_2,\ \ldots\ ,\ A_x,\ \ldots\ A_n\ .$$

This is equivalent to the pulse height distribution that would have been recorded if a very high resolution detector was used.

The detector response was described by the function g(x,a). This is the relative contribution a count in channel a of array A would make to channel x of array C. For a Gaussian detector response

$$g(x,a) = \frac{1}{\sqrt{2\Pi}\ \sigma} \quad \exp - \frac{(x-a)^2}{2\sigma^2}$$

where σ is the detector resolution expressed as a standard deviation in terms of channel numbers.

Using values of A_1 to A_n and the function g(x,a) the values of C_1 to C_n can be calculated using

$$\begin{aligned}
C_0 &= A_1\ g(0,0) + \ldots + A_x\ g(0,x) + \ldots + A_n\ g(0,n) \\
&\vdots \qquad\quad \vdots \qquad\qquad\quad \vdots \qquad\qquad\quad \vdots \\
C_x &= A_1\ g(x,0) + \ldots + A_x\ g(x,x) + \ldots + A_n\ g(x,n) \\
&\vdots \qquad\quad \vdots \qquad\qquad\quad \vdots \qquad\qquad\quad \vdots \\
C_n &= A_1\ g(n,0) + \ldots + A_x\ g(x,x) + \ldots + A_n\ g(n,n)
\end{aligned}$$

Deconvolution requires solving the above equations for the values of A_1 to A_n given values of C_1 to C_n. The data

in these simultaneous equation is noisy so standard techniques such as Gauss-Jordan reduction may not work. Reconstruction algorithms such as ART (algebraic reconstruction technique) provide a method of solving noisy simultaneous equations.

The method used was based on the multiplicative ART algorithm.

1/ Set all values of A_1 to A_n to some non-zero value (mean of C_1 to C_n).

2/ Generate a set of values of C'_1 to C'_n using g(x,a) and the values of A_1 to A_n.

3/ Adjust each value of A_1 to A_n using

$$A_x^{new} = A_x^{Old} \frac{C_x}{C'_x}$$

4/ Repeat steps 2 and 3 until the technique converges on a set of values of A_1 to A_n.

The values of C_1 to C_n need to be appodized if the start or end of the spectrum ends with a discontinuity. If the data is very noisy then a smoothing function can be used on the values of A_1 to A_n at the end of each iteration to reduce the number of artifacts in the deconvolved spectrum.

Figure D.01 demonstrates this technique. The first graph shows the spectrum before convolution with a Gaussian response. The second curve shows the effect of convolution on the spectrum. The data contained in this spectrum was then used in the deconvolution algorithm. The effect of the deconvolution at a number of stages is shown in the remaining four graphs.

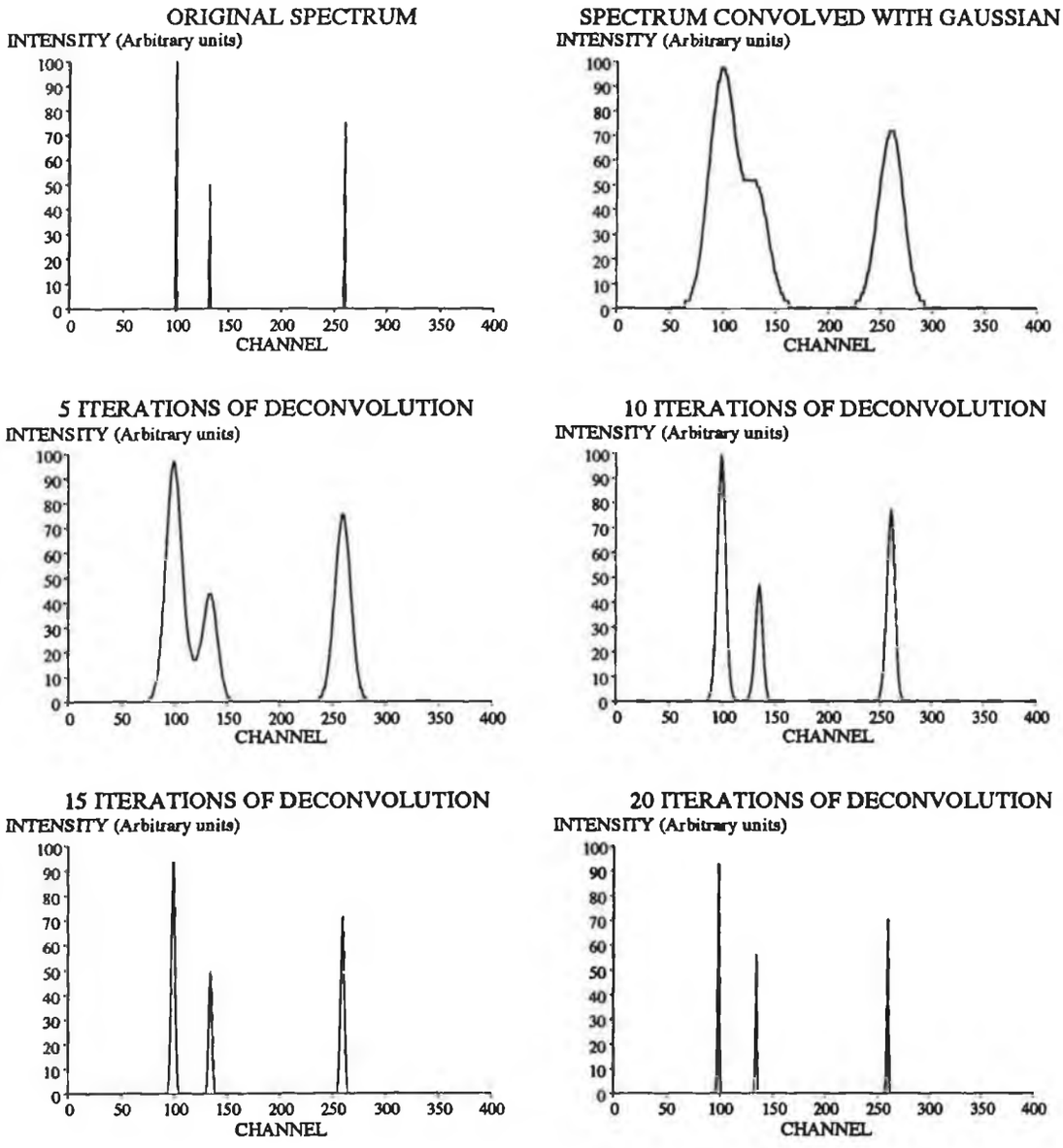

Figure D.01
Demonstration of deconvolution.

APPENDIX E : ELECTRONICS

The differential amplifier shown in figure E.01 was used to measure the tube potential. The circuit was built on a single sided printed circuit board and was housed inside the x-ray machine. The output was brought to a connection at the front of the machine. The circuit was required so that the measured tube potential shared the same ground as equipment external to the machine.

The output of the differential amplifier requires amplifying to make it compatible with the range of potential that the BBC analogue to digital converter requires. The laboratory amplifier shown in figure E.02 was built for this purpose. It also allows the gain to be adjusted accurately and allows an offset to be added to the output potential. This would make it suitable for controlling the discriminator with the tracking discriminator method.

Figure E.03 shows the circuit used to control the sample carousel. When the "start" line is brought low by the BBC the output of the D type flip flop goes high. This turns the motor on the carousel on. The location of the sample cells in the sample carousel is binary coded. When the sample number defined by "bit 0-3" from the BBC equals the number returned by the sensors S1 to S4 and location bit S5 is high the A=B output of the 4 bit comparator goes high. The data (low) is latched to the output of the flip flop and the motor stops. The "found" line goes low when the sample cell is correctly located. A "lock" function was included to prevent electrical noise from restarting the motor.

Figure E.04 shows the circuit used to control the x-ray machine. A two to four line converter was used to define which one of four relays was to be turned on. This could be controlled by a rotary switch or using two lines of the BBC. The relays are used to connect one of four potentiometers to the x-ray machine. The x-ray machine was modified so that external control could only be obtained when the control box was connected.

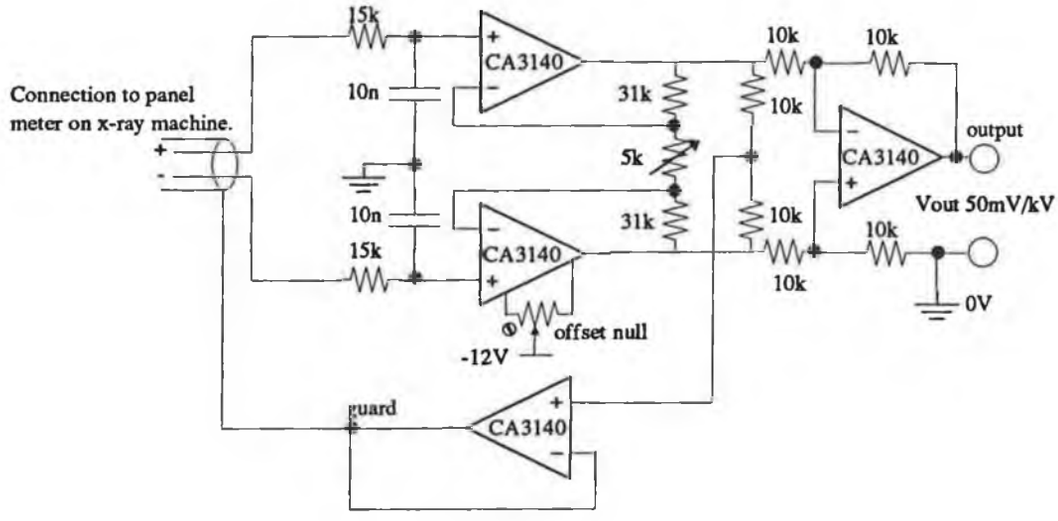

Figure E.01

Differential amplifier used to measure tube potential.

(Supply to op-amps not shown. 12, 0, -12 V)

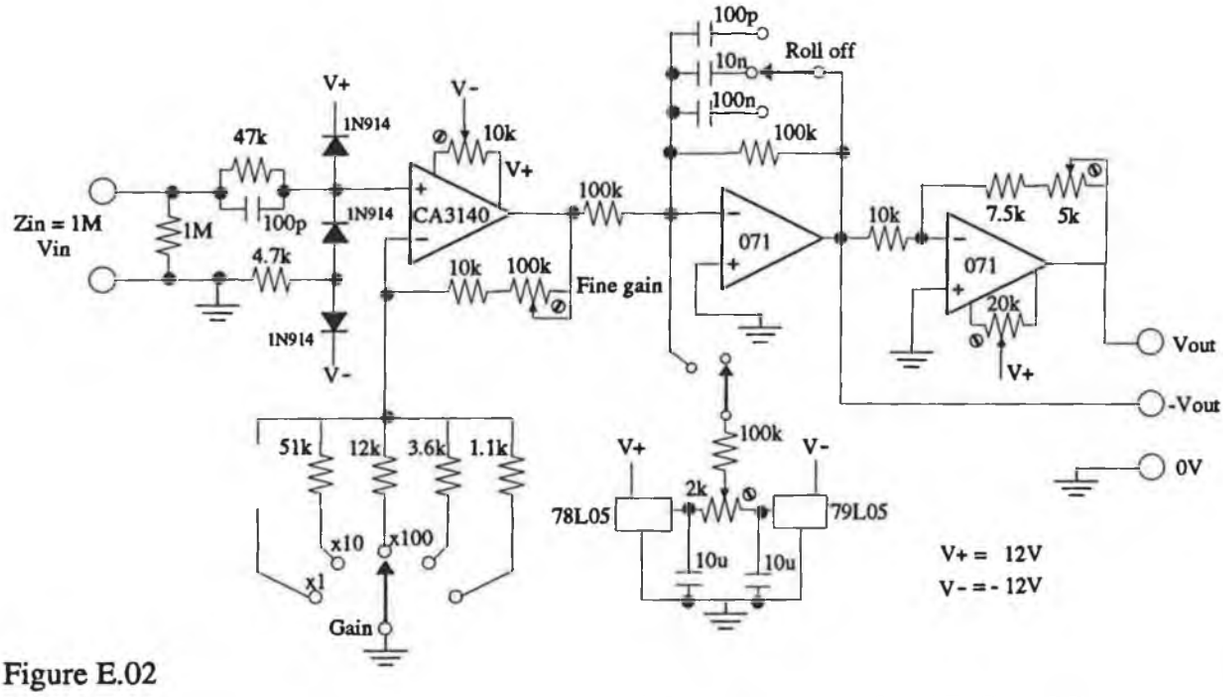

Figure E.02

Laboratory amplifier used to scale tube potential measurement for AD C or SCA.

(Supply to op-amps not shown. 12, 0, -12 V)

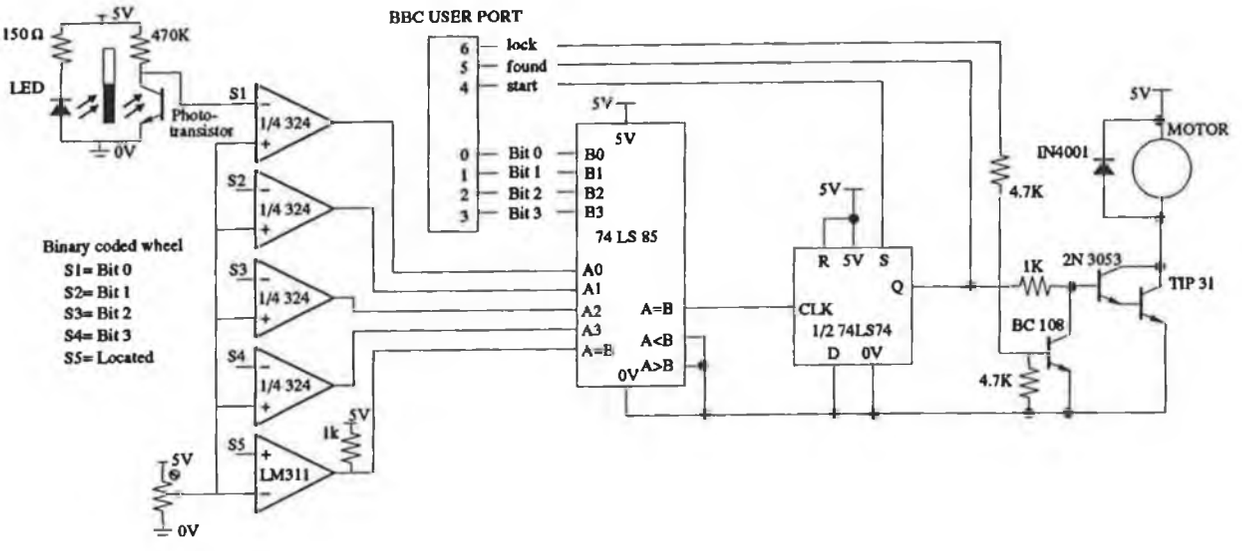

Figure E.03
Circuit to control the sample carousel.

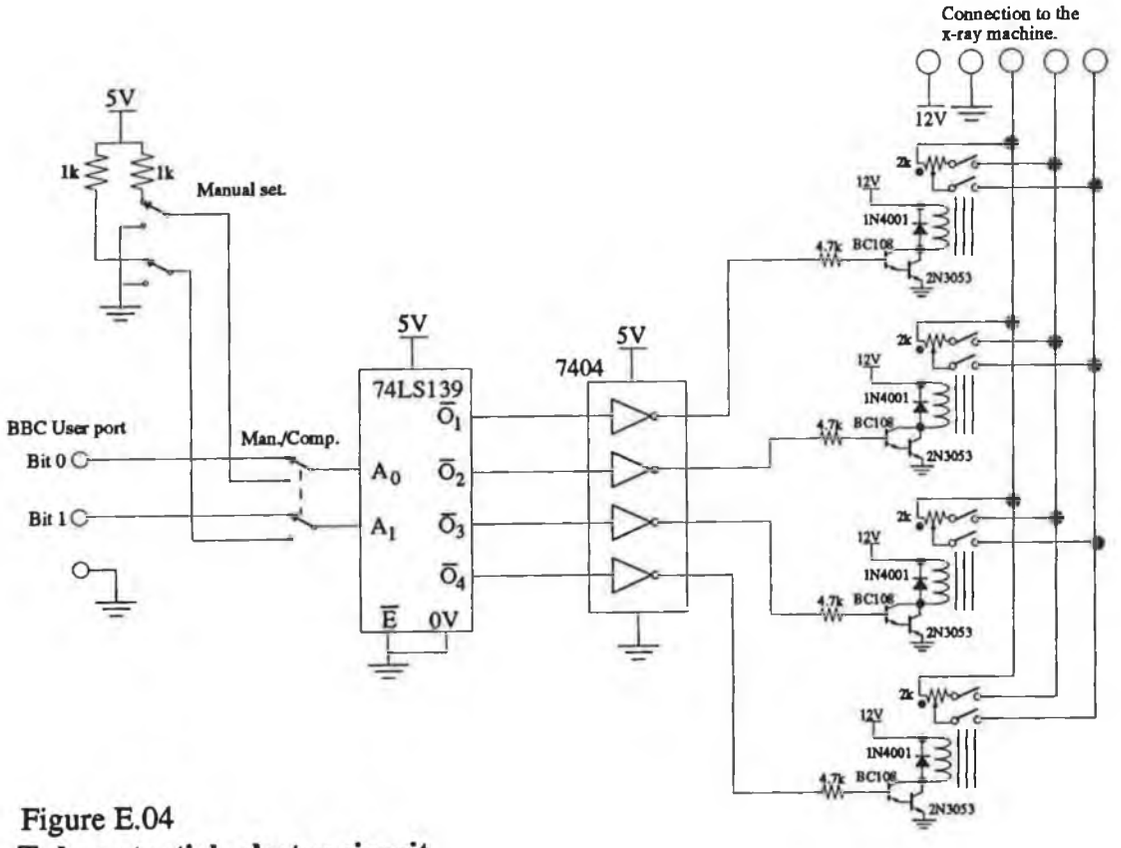

Figure E.04
Tube potential selector circuit.

APPENDIX F : SOFTWARE

PROGRAM NAME : SPECTRA
MACHINE : BBC B+ DFS 64K
SOFTWARE : BBC BASIC
FUNCTION : USED TO RECORD X-RAY SPECTRA.
HARDWARE : ORTEC 7100 MCA.

```
 10 REM "Program to control and collect
        spectra from an ORTEC 7100 MCA."
 20 CLS
 30 DIM NME$(3):DIM DTE$(8):DIM DS$(40)
 40 INPUT "Name of file:" NME$
 50 PRINT:INPUT "Date        :" DTE$
 60 PRINT:INPUT "Description :" DS$
 70 PRINT:INPUT "Duration (S):" DUR$
 80 REM PRINTER CHANNEL = SERIAL OUTPUT
 90 *FX 5,2
100 REM 4800 BAUD TX
110 *FX 8,6
120 REM 4800 BAUD RX
130 *FX 7,6
140 REM COMPILE MACHINE CODE
150 PROCMCODE
160 REM SET PHA
170 O$=CHR$(7)+"CSPN@+NANZ"+DUR$+"NC"
180 REM SET I/O OF MCA
190 O$=O$+"CSIN@XN@1N@UN@DN"
200 REM CLEAR ALL AND START
210 O$=O$+"CO>A"
220 O$=O$+"CRP"
230 PROCOUTPUT
240 REM WAIT FOR SPECTRUM TO BUILD
250 TIME=0:REPEAT:UNTIL(TIME=150*VAL(DUR$))
260 REM REQUEST SPECTRUM
270 O$="CRI"
280 PROCOUTPUT
290 CALL INDAT
300 VDU2:VDU 1,3:VDU3:CLS
310 PRINT "A=SAVE AND DISPLAY"
320 PRINT:PRINT"B=SAVE AND REPEAT"
330 PRINT:PRINT"C=RESTART"
340 PRINT:PRINT"D=QUIT"
350 PRINT:INPUT "A,B,C,D:" D$
360 IF D$="D" THEN END
370 IF D$="C" THEN 10
380 CLS
390 X$="DATA"+NME$
400 XO=OPENOUT X$
410 PRINT #XO,DS$
420 PRINT #XO,DTE$
421 RT$="":LT$=""
422 FOR N=DTA%+5 TO DTA%+13
423 RT$=RT$+CHR$(?(N+13))
424 LT$=LT$+CHR$(?N)
425 NEXT N
430 PRINT #XO,VAL(RT$)
440 PRINT #XO,VAL(LT$)
450 A$=""
460 ADR=DTA%+27:CHK=0
470 FOR Y=1 TO 128
480   A$=""
490   FOR C=1 TO 4
500     A$=A$+CHR$(?ADR)
510     ADR=ADR+1
520   NEXT C
530   PRINT TAB(1,1);"BLOCK:";VAL(A$)/8
540 IF CHK<>VAL(A$) PRINT "BAD DATA"
550 CHK=CHK+8
560   FOR X=1 TO 8
570   A$=""
580     FOR C=1 TO 8
590       A$=A$+CHR$(?ADR)
600       ADR=ADR+1
610     NEXT C
620   PRINT #XO,VAL(A$)
630   NEXT X
640 NEXT Y
650 CLOSE #XO
660 IF D$="A" THEN CHAIN "DISP"
670 IF D$="B" THEN RUN
680 GOTO 10
690 END
700 DEF PROCOUTPUT
710 REM ENABLE PRINTER
720 VDU2
730 FOR N=1 TO LEN(O$)
740  T$=MID$(O$,N,1)
750  FOR Z=1 TO 1000:NEXT Z
760  VDU 1,ASC(T$)
770 NEXT N
780 REM DISABLE PRINTER
790 VDU3
800 ENDPROC
810 DEF PROCMCODE
820 DIM MC% 100
830 DIM DTA% 12000
840 ML%=&80:MH%=&81
850 ?ML%=DTA% MOD 256
860 ?MH%=DTA% DIV 256
870 IOREG=&FE08:DREG=&FE09
880 FOR PASS=0 TO 2 STEP 2
890 P%=MC%
900 [
910 OPT    PASS
920 .INDAT LDA  #3
930        STA  IOREG
940        LDA  #&12
950        STA  IOREG
960 .LOOP  LDA  #1
970        BIT  IOREG
980        BEQ  LOOP
990        LDA  DREG
1000       CMP  #22
1010       BEQ  LOOP
1020       CMP  #23
1030       BEQ  LOOP
1040       CMP  #13
1050       BEQ  LOOP
1060       CMP  #0
1070       BEQ  LOOP
1080       CMP  #10
1090       BEQ  LOOP
1100       CMP  #25
1110       BEQ  LOOP
1120       LDX  #0
1130       STA  (ML%,X)
1140       INC  ML%
1150       BNE  SKP
1160       INC  MH%
1170 .SKP  CMP  #4
1180       BNE  LOOP
1190       RTS
1200 ]
1210 NEXT PASS
1220 CLS
1230 ENDPROC
```

PROGRAM NAME : CAROUSEL
MACHINE : BBC B+ DFS 64K
SOFTWARE : BBC BASIC
HARDWARE : SAMPLE CAROUSEL, 7100 MCA, AND X-RAY MACHINE.

```
  1 REM "Program to contol apparatus for
        linearity and matrix experiments."
 10 ?(&FE62)=223
100 DIM MC% 100
110 DIM DTA% 12000
120 CLOSE#0
130 DUR$="2000"
140 REM
150 CLS
160 DIM DTE$(8):DIM DS$(40):DIM V(3)
170 PRINT:INPUT "Date  <CTRL O> :" DTE$
200 PRINT:  INPUT "SET TO 42 KV "XYZ$:PROCADC
    :V(1)=P1:PRINT P1
203 PRINT:  INPUT "SET TO 33 KV "XYZ$:PROCADC
    :V(2)=P1:PRINT P1
220 PRINT:  INPUT "SET TO 28 KV "XYZ$
    :PROCADC:V(3)=P1:PRINT P1
250 *FX 5,2
260 REM 4800 BAUD TX
270 *FX 8,6
280 REM 4800 BAUD RX
```

```
290 *FX 7,6
300 REM COMPILE MACHINE CODE
310 REM SET PHA
320 O$=CHR$(7)+"CSPN@+NANZ"+DUR$+"NC"
330 REM SET I/O OF MCA
340 O$=O$+"CSIN@XN@1N@UN@DN"
350 VDU2:VDU 1,3:VDU3
360 PRINT:INPUT "PRESS RET TO START" XYZ$
370 PROCOUTPUT
375 SAM=15
380 FOR W=1 TO 3
385 PRINT "SETTING TUBE VOLTAGE ";V(W)
386 PROCSTEP:PROCSTEP:PROCADC:PRINT "*";
387 IF (P1>V(W)) THEN 386
389 PRINT "ADC=";P1;" SET=";V(W)
390 FOR Z=15 TO 0 STEP -1
391 SAM=Z:PROCFIND
400 PRINT "SPECTRUM ";(15-Z)+(16*(W-1))
460 PROCADC
530 O$=CHR$(7)+"C0>A"
540 O$=O$+"CRP"
550 PROCOUTPUT
560 PRINT "RECORDING SPECTRUM"
570 TIME=0
580 REPEAT:UNTIL(TIME=(105*VAL(DUR$))+100)
590 O$="CRI"
600 PROCOUTPUT
610 PRINT "I/O DOWNLOADING"
620 PROCMCODE
630 CALL INDAT
640 VDU2:VDU 1,3:VDU3
650 PRINT "SAVING : ";
660 X$="LIN"+STR$((15-Z)+(16*(W-1)))
670 XO=OPENOUT X$
680 DS$=STR$(W)+"-"+STR$(Z)+"-"+STR$(P1)
690 PRINT #XO,DS$
700 PRINT #XO,DTE$
710 RT$="":LT$=""
720 FOR N=DTA%+5 TO DTA%+13
730 RT$=RT$+CHR$(?(N+13))
740 LT$=LT$+CHR$(?N)
750 NEXT N
760 PRINT #XO,VAL(RT$)
770 PRINT #XO,VAL(LT$)
780 A$=""
790 ADR=DTA%+27:CHK=0
800 FOR Y=1 TO 128
810   A$=""
820   FOR C=1 TO 4
830     A$=A$+CHR$(?ADR)
840     ADR=ADR+1
850   NEXT C
860 IF Y/25=INT(Y/25) PRINT "*";
865 BDAT=0
870 IF CHK<>VAL(A$) BDAT=1:PRINT "BAD DATA"
880 CHK=CHK+8
890   FOR X=1 TO 8
900   A$=""
910     FOR C=1 TO 8
920       A$=A$+CHR$(?ADR)
930       ADR=ADR+1
940     NEXT C
950   PRINT #XO,VAL(A$)
960   NEXT X
970 NEXT Y
975 IF BDAT=1 PRINT #XO,"BAD"
980 CLOSE #XO
990 PRINT:PRINT
1000 NEXT Z
1010 NEXT W
1020 PRINT "FINISHED"
1030 END
1040 DEF PROCOUTPUT
1050 REM ENABLE PRINTER
1060 VDU2
170 FOR N=1 TO LEN(O$)
1080  T$=MID$(O$,N,1)
1090  FOR ZZ=1 TO 1000:NEXT ZZ
1100  VDU 1,ASC(T$)
1110 NEXT N
1120 REM DISABLE PRINTER
1130 VDU3
1140 ENDPROC
```

```
1150 DEF PROCMCODE
1160 ML%=&80:MH%=&81
1170 ?ML%=DTA% MOD 256
1180 ?MH%=DTA% DIV 256
1190 IOREG=&FE08:DREG=&FE09
1200 FOR PASS=0 TO 2 STEP 2
1210 P%=MC%
1220 [
1230 OPT    PASS
1240 .INDAT LDA  #3
1250        STA  IOREG
1260        LDA  #&12
1270        STA  IOREG
1280 .LOOP  LDA  #1
1290        BIT  IOREG
1300        BEQ  LOOP
1310        LDA  DREG
1320        CMP  #22
1330        BEQ  LOOP
1340        CMP  #23
1350        BEQ  LOOP
1360        CMP  #13
1370        BEQ  LOOP
1380        CMP  #0
1390        BEQ  LOOP
1400        CMP  #10
1410        BEQ  LOOP
1420        CMP  #25
1430        BEQ  LOOP
1440        LDX  #0
1450        STA  (ML%,X)
1460        INC  ML%
1470        BNE  SKP
1480        INC  MH%
1490 .SKP   CMP  #4
1500        BNE  LOOP
1510        RTS
1520 ]
1530 NEXT PASS
1540 ENDPROC
1550 DEFPROCADC
1560 P1=0
1570 FOR N=1 TO 800:P1=P1+ADVAL(1):NEXTN
1580 P1=INT(P1/12800)
1590 ENDPROC
1600 DEFPROCSTEP
1630 FOR N=1 TO 30:NEXT N:?(&FE60)=SAM+80+128
1640 FOR N=1 TO 30:NEXT N:?(&FE60)=SAM+80
1650 ENDPROC
1700 DEFPROCFIND
1710 ?(&FE60)=SAM+80:?(&FE60)=SAM+64
     :?(&FE60)=SAM+16
1720 PRINT:PRINT "SAMPLE : ";SAM
1730 FOR N=1 TO 900:NEXT N
1740 IF((?(&FE60) AND 32)=32) THEN 1740
1750 ?(&FE60)=SAM+80
1760 PRINT "LOCK ON":PRINT
1770 ENDPROC
```

PROGRAM NAME : IMAGE

MACHINE : BBC B+ DFS 64K

SOFTWARE : BBC BASIC

HARDWARE : MODIFIED SR7, SAMPLE CAROUSSEL ,X-RAY MACHINE AND SCAN TABLE.

```
   1 REM "Program to collect image data for
         the total count technique."
1000 RST=192:VLT=0:STP=0:DIR=8
1010 *FX7,4
1020 ?(&FE62)=255
1030 ?(&FE60)=RST+VLT+STP+DIR
1040 PROCMCODE
1050 FOR V=0 TO 3
1055 IF (V=3) THEN PRINT "SET TO 20mA THEN
     PRESS <RET>":INPUT " " AA$
1060 VLT=16*V
1065 NME$="SCN"+STR$(V)
1070 Y=OPENOUT NME$
1080 FOR X=1 TO 40
1090 SC=0:FOR Z=1 TO 8:PROCSR7
     :SC=SC+SC1:NEXT Z
1100 PROCNXT
1110 PRINT "VOLT: ";VLT;" POS:";X;" TIME: "
```

```
    ;TIM;" COUNT: ";SC
1115 PRINT #Y,SC
1120 NEXT X
1125 CLOSE #Y
1130 PROCBACK
1140 NEXT V
1150 STOP
1160 DEF PROCSR7
1170 RST=64:?(&FE60)=RST+VLT+STP+DIR
    :FOR N=1 TO 100:NEXT:RST=192
    :?(&FE60)=RST+VLT+STP+DIR
1180 RST=128:?(&FE60)=RST+VLT+STP+DIR
    :FOR N=1 TO 100:NEXT:RST=192:
    ?(&FE60)=RST+VLT+STP+DIR
1190 PROCREAD
1200 FOR N=1 TO 5000:NEXT N
1210 ENDPROC
1220 DEF PROCREAD
1230 *FX21,1
1240 CALL INDAT
1250 A$=""
1260 FOR N=DTA% TO DTA%+NUMCHAR
1270 A$=A$+CHR$(?N)
1280 NEXT N
1290 TIM=VAL(MID$(A$,6,10))
1300 SC1=VAL(MID$(A$,27,7))
1310 ENDPROC
1320 DEF PROCMCODE
1330 NUMCHAR=50
1340 DIM MC% 100
1350 DIM DTA% 130
1360 ML%=&80:MH%=&81
1370 SML%=&82:SMH%=&83
1380 ?SML%=DTA% MOD 256
1390 ?SMH%=DTA% DIV 256
1400 IOREG=&FE08:DREG=&FE09
1410 FOR PASS=0 TO 2 STEP 2
1420 P%=MC%
1430 [
1440 OPT    PASS
1450 .INDAT LDA  #3
1460        STA  IOREG
1470        LDA  #&12
1480        STA  IOREG
1490        LDA   SML%
1500        STA   ML%
1510        LDA   SMH%
1520        STA   MH%
1530        LDY  #NUMCHAR
1540 .LOOP  LDA  #1
1550        BIT  IOREG
1560        BEQ  LOOP
1570        LDA  DREG
1580        LDX  #0
1590        STA  (ML%,X)
1600        INC  ML%
1610        BNE  SKP
1620        INC  MH%
1630 .SKP   DEY
1640        BNE  LOOP
1650        RTS
1660 ]
1670 NEXT PASS
1680 CLS
1690 ENDPROC
1700 DEF PROCSTEP
1710 STP=4:?(&FE60)=RST+VLT+STP+DIR
    :FOR  M=1 TO 50:NEXT M
1720 STP=0:?(&FE60)=RST+VLT+STP+DIR
1730 ENDPROC
1740 DEF PROCNXT
1750 FOR N=1 TO 192
1760 PROCSTEP
1770 NEXT N
1780 ENDPROC
1790 DEF PROCBACK
1800 DIR=0
1810 FOR X=1 TO 40
1820 FOR N=1 TO 192
1830 STP=4:?(&FE60)=RST+VLT+STP+DIR
    :FOR  M=1 TO 40:NEXT M
1840 STP=0:?(&FE60)=RST+VLT+STP+DIR
1850 NEXT N
1860 NEXT X
1870 DIR=8
1880 ENDPROC
```

PROGRAM NAME : DETECT
MACHINE : ANY IBM PC OR CLONE.
SOFTWARE : TURBO C (BORLAND)

```
#include<dir.h>
#include<stdio.h>
#include<stdlib.h>
#include<string.h>
#include<conio.h>
#include<math.h>
#include<dos.h>

double atn(double);

void main(void)
{
  FILE   *fp,*fopen();
  struct ffblk f;

  static double data1[1025];
  static char   title[40];
  static double e,rt,lt;
  int           x;
  char          fil[14],date[12];

  chdir("source");
  printf("Enter name of source file : ");
  scanf(" %s",fil);
  fp=fopen(fil,"r");
  fscanf(fp," %s",title);
  fscanf(fp," %s",date);
  fscanf(fp," %lf",&rt);
  fscanf(fp," %lf",&lt);
  for(x=0;x<=1023;x++)fscanf(fp," %lf"
  ,&data1[x]);
  fclose(fp);
  chdir("..");

  chdir("source");
  printf("Enter name of output file : ");
  scanf(" %s",fil);
  fp=fopen(fil,"w");
  fprintf(fp,"%s\n",title);
  fprintf(fp,"%s\n",date);
  fprintf(fp,"%lf\n",rt);
  fprintf(fp,"%lf\n",lt);
  for(x=0;x<=1023;x++)
  {
   e=(((double)x)*0.048856)+2.390843;
   fprintf(fp,"%6.0lf\n",floor
   (data1[x]/atn(e)));
   printf("%d %lf %lf\n",x,e,atn(e));
  }
  fclose(fp);
  chdir("..");
}

double atn(e)
double e;
{
 double at[11]={100,100,98,95,84,66,46,36,28
                ,26,26};
 double en[11]={0,10,15,20,25,30,35,40,45,50
                ,100};
 double res,el,eh,al,ah;
 int flg,x;

 for(x=0;((x<=10)&&(e>=en[x]));x++);
 ah=at[x]; al=at[x-1];
 eh=en[x]; el=en[x-1];
 res=(((ah-al)/(eh-el))*(e-el))+al;
 return(res/100);
}
```

PROGRAM NAME : LINEAR / MATRIX
MACHINE : IBM PC 80386+80387 20MHz
SOFTWARE : TURBO C (BORLAND)

```
#include<dir.h>
#include<stdio.h>
#include<stdlib.h>
```

```
#include<string.h>
#include<conio.h>
#include<math.h>
#include<dos.h>
#define NOITER 20

double c(double*,double,double,double,
       double);
double ut(int,double,double,double,double);
double s(double);
double p(double);


void main(void)
{
 FILE   *fp,*fopen();
 struct ffblk f;

 static double data1[1025],data2[1025];
 static double xb1,xa1,xa2,xa3,xb,xoa1
              ,xoa2,xoa3,xob,tc1;
 static double xb2,ya1,ya2,ya3,yb,yoa1
              ,yoa2,yoa3,yob,tc2;
 static double eqt,ah,al,bh,bl;

 int    ex,x,n,iter;
 double error,lt,rt,dumy,le,r;
 char   title[40],date[12];
 char   text[5],fil[20];


for(ex=0;ex<=7;ex++)
{
 chdir("source");          /* Read ref. V2 */
 sprintf(text,"%d",17+(ex*2));
 strcpy(fil,"LIN");
 strcat(fil,text);
 strcat(fil,".DAT");
 printf("Opening %s\n",fil);
 fp=fopen(fil,"r");
 fscanf(fp," %s",title);
 fscanf(fp," %s",date);
 fscanf(fp," %lf",&rt);
 fscanf(fp," %lf",&lt);
 for(x=0;x<=1023;x++) {fscanf(fp," %lf"
 ,&data1[x]);}
 fclose(fp);
 sprintf(text,"%d",33+(ex*2));
 strcpy(fil,"LIN");        /* Read ref. V1 */
 strcat(fil,text);
 strcat(fil,".DAT");
 printf("Opening %s\n",fil);
 fp=fopen(fil,"r");
 fscanf(fp," %s",title);
 fscanf(fp," %s",date);
 fscanf(fp," %lf",&rt);
 fscanf(fp," %lf",&lt);
 for(x=0;x<=1023;x++) {fscanf(fp," %lf"
 ,&data2[x]);}
 fclose(fp);

 sprintf(text,"%d",16+(ex*2));
 strcpy(fil,"LIN");      /* Total trans. V2 */
 strcat(fil,text);
 strcat(fil,".DAT");
 printf("Opening %s\n",fil);
 fp=fopen(fil,"r");
 fscanf(fp," %s",title);
 fscanf(fp," %s",date);
 fscanf(fp," %lf",&rt);
 fscanf(fp," %lf",&lt);
 tc1=0;
 for(x=0;x<=1023;x++)
 {
  fscanf(fp," %lf",&dumy);
  tc1+=dumy;
 }
 fclose(fp);

 sprintf(text,"%d",32+(ex*2));
 strcpy(fil,"LIN");      /* Total trans. V1 */
 strcat(fil,text);
 strcat(fil,".DAT");
 printf("Opening %s\n",fil);
 fp=fopen(fil,"r");
 fscanf(fp," %s",title);
 fscanf(fp," %s",date);
 fscanf(fp," %lf",&rt);
 fscanf(fp," %lf",&lt);
 tc2=0;
 for(x=0;x<=1023;x++)
 {
  fscanf(fp," %lf",&dumy);
  tc2+=dumy;
 }
 fclose(fp);
 chdir("..");

 printf("tc1 = %lf   tc2 = %lf\n",tc1,tc2);

 /*****************************/
 /* Find a1 -> F1=0 given b=0 */
 /*****************************/
 xb1=0; al=0; ah=60;
 for(iter=0;iter<=NOITER;iter++)
 {
  xa1=(ah+al)/2.;
  le=c(data1,ah,0,0,xb1)-tc1;
  r =c(data1,xa1,0,0,xb1)-tc1;
  if ((le*r)<0) al=xa1; else ah=xa1;
 }
 printf("\nA1 = %lf\n",xa1);


 /*****************************/
 /* Find a1 -> F2=0 given b=0 */
 /*****************************/
 xb1=0; al=0; ah=60;
 for(iter=0;iter<=NOITER;iter++)
 {
  xa2=(ah+al)/2.;
  le=c(data2,ah,0,0,xb1)-tc2;
  r =c(data2,xa2,0,0,xb1)-tc2;
  if ((le*r)<0) al=xa2; else ah=xa2;
 }
 printf("\nA2 = %lf\n",xa2);

 if(xa1<xa2)
 {
  xoa1=xa1;

  do
  {
   /*****************************/
   /* Find b -> F2=0 given a1=0 */
   /*****************************/
   xob=xb1;
   bh=2; bl=0;
   for(iter=0;iter<=NOITER;iter++)
   {
    xb1=(bh+bl)/2.;
    le=c(data2,xa1,0,0,bh)-tc2;
    r =c(data2,xa1,0,0,xb1)-tc2;
    if ((le*r)<0) bl=xb1; else bh=xb1;
   }
   printf("a1<a2 B1 = %lf ",xb1);

   /*****************************/
   /* Find a1 -> F1=0 given b=0 */
   /*****************************/
   xoa1=xa1;
   al=0; ah=60;
   for(iter=0;iter<=NOITER;iter++)
   {
    xa1=(ah+al)/2.;
    le=c(data1,ah,0,0,xb1)-tc1;
    r =c(data1,xa1,0,0,xb1)-tc1;
    if ((le*r)<0) al=xa1; else ah=xa1;
   }

   error=fabs((xa1-xoa1)/xa1)
         +fabs((xb1-xob)/xb1);
   printf(" A1 = %lf  Error = %lf\n"
   ,xa1,error);

  }while((error>0.00025)&&(xa1<=xoa1));

 }
 else
```

```
 do{
  /*****************************/
  /* Find b -> F1=0 given a2=0 */
  /*****************************/
  xob=xb1;
  bh=2; bl=0;
  for(iter=0;iter<=NOITER;iter++)
  {
   xb1=(bh+bl)/2.;
   le=c(data1,xa2,0,0,bh)-tc1;
   r =c(data1,xa2,0,0,xb1)-tc1;
   if ((le*r)<0) bl=xb1; else bh=xb1;
  }
  printf("a1>a2 B1 = %lf ",xb1);

  /*****************************/
  /* Find a2 -> F1=0 given b=0 */
  /*****************************/
  xoa2=xa2;
  a1=0; ah=60;
  for(iter=0;iter<=NOITER;iter++)
  {
   xa2=(ah+a1)/2.;
   le=c(data2,ah,0,0,xb1)-tc2;
   r =c(data2,xa2,0,0,xb1)-tc2;
   if ((le*r)<0) a1=xa2; else ah=xa2;
  }

  error=fabs((xa2-xoa2)/xa2)
  +fabs((xb1-xob)/xb1);
  printf(" A1 = %lf  Error = %lf\n"
  ,xa2,error);

 }while((error>0.00025)&&(xa2<=xoa2));
 xa1=xa2;

} /* End of IF {} else {} */

printf("Found a1 and b  a1:= %lf  b=%lf\n"
,xa1,xb1);

chdir("source");       /* Read ref. V3 */
sprintf(text,"%d",1+(ex*2));
strcpy(fil,"LIN");
strcat(fil,text);
strcat(fil,".DAT");
printf("Opening %s\n",fil);
fp=fopen(fil,"r");
fscanf(fp," %s",title);
fscanf(fp," %s",date);
fscanf(fp," %lf",&rt);
fscanf(fp," %lf",&lt);
for(x=0;x<=1023;x++) {fscanf(fp," %lf"
,&data1[x]);}
fclose(fp);

sprintf(text,"%d",(ex*2));
strcpy(fil,"LIN");      /* Total trans. V3 */
strcat(fil,text);
strcat(fil,".DAT");
printf("Opening %s\n",fil);
fp=fopen(fil,"r");
fscanf(fp," %s",title);
fscanf(fp," %s",date);
fscanf(fp," %lf",&rt);
fscanf(fp," %lf",&lt);
tc1=0;
for(x=0;x<=1023;x++)
{
 fscanf(fp," %lf",&dumy);
 tc1+=dumy;
}
fclose(fp);
chdir("..");
printf("tc = %lf\n",tc1);

/********************/
/* Find a2 using F3 */
/********************/
a1=0; ah=60;
for(iter=0;iter<=NOITER;iter++)
{
 xa2=(ah+a1)/2.;
 le=c(data1,xa1,ah,0,xb1)-tc1;
 r =c(data1,xa1,xa2,0,xb1)-tc1;
 if ((le*r)<0) a1=xa2; else ah=xa2;
}

eqt=-(((xa1*xa1*xa1)/36488.65492)
    -((xa2*xa2*xa2)/36488.65492))/3.149;

printf("Exp %d a1 a2 b t := %lf %lf %lf %lf
\n",ex,xa1,xa2,xb1,eqt);

/*****************************/
/* Print results for exp. ex  */
/* a1, a2 , b and the iodine  */
/* equivalent thickness.      */
/*****************************/

fp=fopen("PRN","w");
fprintf(fp,"Exp %d a1 a2 b t := %lf %lf %lf
%lf\n",ex,xa1,xa2,xb1,eqt);
fclose(fp);

} /* for(ex..   ){} */

} /* End of program */
```

FUNCTIONS : C FUNCTIONS FOR LINEAR/MATRIX

```
double c(data,a1,a2,a3,b)
double data[],a1,a2,a3,b;
{
 int x;
 double res;
 res=0;

 for(x=220;x<=1000;x++)
 {
  res+=ut(x,a1,a2,a3,b)*data[x];
 }
 return(res);
}

double ut(x,a1,a2,a3,b)
int x;
double a1,a2,a3,b;
{
 double ek1,ek2,e,a;
 double u1,u2,u,res;

 ek1=33.168;   /* Iodine */
 ek2=60.000;   /* Barium */
 e=(0.048899*(double)x)+2.430907;

 if (e<ek1)              a=a1;
 if ((e>=ek1)&&(e<=ek2)) a=a2;
 if (e>ek2)              a=a3;
 u=(a*a*a*p(e))+(b*s(e));

 if   ((e>(ek1-0.32))&&(e<(ek1+0.64)))
 {
  /* K-edge has width */
  u1=(a1*a1*a1*p(ek1-0.32))+(b*s(ek1-0.32));
  u2=(a2*a2*a2*p(ek1+0.64))+(b*s(ek1+0.64));
  u=(((u2-u1)/0.96)*(e-ek1+0.32))+u1;
 }

 if   ((e>(ek2-0.32))&&(e<(ek2+0.65)))
 {
 /* K-edge has width */
  u1=(a2*a2*a2*p(ek2-0.32))+(b*s(ek2-0.32));
  u2=(a3*a3*a3*p(ek2+0.64))+(b*s(ek2+0.64));
  u=(((u2-u1)/0.96)*(e-ek2+0.32))+u1;
 }

 res=exp(-u);
 return(res);
}

double s(e)
double e;
{
 double fx,v,w,x,y,z,a;
 a=e/510.975;
 v=1/a;
 w=a*a;
```

```
x=1+a;
y=1+(2*a);
z=1+(3*a);
fx=((x/w)*(((2*x)/y)-(v*log(y))))
   +((v/2)*log(y))-(z/(y*y));
return(fx);
}

double p(e)
double e;
{
 double res;
 res=1/(e*e*e);
 return(res);
}
```

PROGRAM NAME : IMSCAN

MACHINE : IBM PC 80386+80387 20MHz

SOFTWARE : TURBOC (BORLAND)

```
#include<dir.h>
#include<stdio.h>
#include<stdlib.h>
#include<string.h>
#include<conio.h>
#include<math.h>
#include<dos.h>
#define NOITER 20

double c(double*,double,double,double
       ,double);
double ut(int,double,double,double,double);
double s(double);
double p(double);

void main(void)
{
 FILE   *fp,*fopen();
 struct ffblk f;
 static double data1[1025],data2[1025];
 static double xb1,xa1,xa2,xa3,xoa1,xoa2,xob;
 static double eqt1,eqt2,ah,al,bh,bl;
 int    ex,x,n,iter;
 double error,lt,rt,dumy,le,r,ft1,ft2
       ,ft3,ft4;
 char   title[40],date[12];
 char   text[5],fil[20];

for(ex=1;ex<=40;ex++)
{
 strcpy(fil,"SP2");         /* Read ref. V2 */
 printf("Opening %s\n",fil);
 fp=fopen(fil,"r");
 fscanf(fp," %s",title);
 fscanf(fp," %s",date);
 fscanf(fp," %lf",&rt);
 fscanf(fp," %lf",&lt);
 for(x=0;x<=1023;x++) {fscanf(fp," %lf"
 ,&data2[x]);}
 fclose(fp);

 strcpy(fil,"SP1");         /* Read ref. V1 */
 printf("Opening %s\n",fil);
 fp=fopen(fil,"r");
 fscanf(fp," %s",title);
 fscanf(fp," %s",date);
 fscanf(fp," %lf",&rt);
 fscanf(fp," %lf",&lt);
 for(x=0;x<=1023;x++) {fscanf(fp," %lf"
 ,&data1[x]);}
 fclose(fp);

 /*************************************/
 /* Read in the fractional transmitance */
 /*************************************/
 strcpy(fil,"FRACT.DAT");
 printf("Opening %s\n",fil);
 fp=fopen(fil,"r");
 for(x=1;x<=ex;x++) fscanf(fp,"%lf %lf %lf
 %lf",&ft1,&ft2,&ft3,&ft4);
 fclose(fp);

 printf("FT1 = %lf   FT2 = %lf    FT3  =  %lf
 FT4 = %lf\n",ft1,ft2,ft3,ft4);

 if (ft1>1) ft1=1;  if (ft2>1) ft2=1;
 if (ft3>1) ft3=1;  if (ft4>1) ft4=1;
 ft1=1/ft1;  ft2=1/ft2;
 ft3=1/ft3;  ft4=1/ft4;

 /*****************************/
 /* Working on the A axis     */
 /*****************************/

 /*****************************/
 /* Find a1 -> F1=0 given b=0 */
 /*****************************/
 xb1=0; al=0; ah=120;
 for(iter=0;iter<=NOITER;iter++)
 {
  xa1=(ah+al)/2.;
  le=(ft1*c(data1,ah,ah,ah,xb1))-1;
  r =(ft1*c(data1,xa1,xa1,xa1,xb1))-1;
  if ((le*r)<0) al=xa1; else ah=xa1;
 }
 printf("\nA1 = %lf\n",xa1);

 /*****************************/
 /* Find a1 -> F2=0 given b=0 */
 /*****************************/
 xb1=0; al=0; ah=120;
 for(iter=0;iter<=NOITER;iter++)
 {
  xa2=(ah+al)/2.;
  le=(ft2*c(data2,ah,ah,ah,xb1))-1;
  r =(ft2*c(data2,xa2,xa2,xa2,xb1))-1;
  if ((le*r)<0) al=xa2; else ah=xa2;
 }
 printf("\nA2 = %lf\n",xa2);


 if(xa1<xa2)
 {
  xoa1=xa1;
  do
  {
   /*********************************/
   /*  Find  b  -> F2=0 given a1=0 */
   /*********************************/
   xob=xb1;
   bh=4; bl=0;
   for(iter=0;iter<=NOITER;iter++)
   {
    xb1=(bh+bl)/2.;
    le=(ft2*c(data2,xa1,xa1,xa1,bh))-1;
    r =(ft2*c(data2,xa1,xa1,xa1,xb1))-1;
    if ((le*r)<0) bl=xb1; else bh=xb1;
   }
   printf("a1<a2 B1 = %lf ",xb1);

   /*****************************/
   /* Find a1 -> F1=0 given b=0 */
   /*****************************/
   xoa1=xa1;
   al=0; ah=120;
   for(iter=0;iter<=NOITER;iter++)
   {
    xa1=(ah+al)/2.;
    le=(ft1*c(data1,ah,ah,ah,xb1))-1;
    r =(ft1*c(data1,xa1,xa1,xa1,xb1))-1;
    if ((le*r)<0) al=xa1; else ah=xa1;
   }

   error=fabs((xa1-xoa1)/xa1)
   +fabs((xb1-xob)/xb1);
   printf(" A1 = %lf  Error = %lf\n"
   ,xa1,error);

  }while((error>0.00025)&&(xa1<=xoa1));

 }
 else
 {
  do{
     /*********************************/
     /* Find b  -> F1=0 given a2=0 */
     /*********************************/
     xob=xb1;
     bh=4; bl=0;
     for(iter=0;iter<=NOITER;iter++)
```

```
    {
     xb1=(bh+bl)/2.;
     le=(ft1*c(data1,xa2,xa2,xa2,bh))-1;
     r =(ft1*c(data1,xa2,xa2,xa2,xb1))-1;
     if ((le*r)<0) bl=xb1; else bh=xb1;
    }
    printf("a1>a2 B1 = %lf ",xb1);

    /*********************************/
    /*  Find  a2 -> F1=0 given b=0 */
    /*********************************/
    xoa2=xa2;
    al=0; ah=120;
    for(iter=0;iter<=NOITER;iter++)
    {
     xa2=(ah+al)/2.;
     le=(ft2*c(data2,ah,ah,ah,xb1))-1;
     r =(ft2*c(data2,xa2,xa2,xa2,xb1))-1;
     if ((le*r)<0) al=xa2; else ah=xa2;
    }

    error=fabs((xa2-xoa2)/xa2)
          +fabs((xb1-xob)/xb1);
    printf(" A1 = %lf  Error = %lf\n"
    ,xa2,error);

   }while((error>0.00025)&&(xa2<=xoa2));
   xa1=xa2;
}
printf("Found a1 and b  a1:= %lf  b=%lf\n"
,xa1,xb1);

printf("FR3 = %lf\n",1/ft3);
strcpy(fil,"SP3");        /* Read ref. V3 */
printf("Opening %s\n",fil);
fp=fopen(fil,"r");
fscanf(fp," %s",title);
fscanf(fp," %s",date);
fscanf(fp," %lf",&rt);
fscanf(fp," %lf",&lt);
for(x=0;x<=1023;x++) {fscanf(fp," %lf"
,&data1[x]);}
fclose(fp);

/*********************/
/* Find a2 using F3 */
/*********************/
al=0; ah=120;
for(iter=0;iter<=NOITER;iter++)
{
 xa2=(ah+al)/2.;
 le=(ft3*c(data1,xa1,ah,ah,xb1))-1;
 r =(ft3*c(data1,xa1,xa2,xa2,xb1))-1;
 if ((le*r)<0) al=xa2; else ah=xa2;
}

printf("FR4 = %lf\n",1/ft4);
strcpy(fil,"SP4");     /* Read ref V4 */
printf("Opening %s\n",fil);
fp=fopen(fil,"r");
fscanf(fp," %s",title);
fscanf(fp," %s",date);
fscanf(fp," %lf",&rt);
fscanf(fp," %lf",&lt);
for(x=0;x<=1023;x++) {fscanf(fp," %lf"
,&data1[x]);}
fclose(fp);

/*********************/
/* Find a3 using F4 */
/*********************/
al=0; ah=120;
for(iter=0;iter<=NOITER;iter++)
{
 xa3=(ah+al)/2.;
 le=(ft4*c(data1,xa1,xa2,ah,xb1))-1;
 r =(ft4*c(data1,xa1,xa2,xa3,xb1))-1;
 if ((le*r)<0) al=xa3; else ah=xa3;
}

eqt1=-(((xa1*xa1*xa1)/36488.65492)
     -((xa2*xa2*xa2)/36488.65492))/3.149;

eqt2=-(((xa2*xa2*xa2)/52372.39391)
     -((xa3*xa3*xa3)/52372.39391))/2.436;

 printf("%d a1 a2 a3 b t1 t2 := %lf  %lf  %lf
 %lf %lf\n",ex,xa1,xa2,xa3,xb1,eqt1,eqt2);

 /*************************************/
 /* Print the equivalent thickness of */
 /* Iodine and Barium.                */
 /*************************************/
 fp=fopen("PRN","w");
 fprintf(fp,"%d a1 a2 a3 b t1 t2 :=  %lf  %lf
 %lf %lf %lf %lf\n",ex,xa1,xa2,xa3,xb1
 ,eqt1,eqt2);
 fclose(fp);
} /* for(ex..){} beam path 1..40 */

} /* End of program */
```

FUNCTIONS : C FUNCTIONS FOR IMSCAN

```
double c(data,a1,a2,a3,b)
double data[],a1,a2,a3,b;
{
 int x;
 double res,tot;
 res=0; tot=0;

 for(x=150;x<=1000;x++)
 {
  tot+=data[x];
  res+=ut(x,a1,a2,a3,b)*data[x];
 }
 res/=tot;
 return(res);
}

double ut(x,a1,a2,a3,b)
int x;
double a1,a2,a3,b;
{
 double ek1,ek2,e,a;
 double u1,u2,u,res;

 ek1=33.168;    /* Iodine */
 ek2=37.414;    /* Barium */
 e=(0.045849*(double)x)+2.203933;

 if (e<ek1)               a=a1;
 if ((e>=ek1)&&(e<=ek2)) a=a2;
 if (e>ek2)               a=a3;
 u=(a*a*a*p(e))+(b*s(e));

 if   ((e>(ek1-0.32))&&(e<(ek1+0.64)))
 {
  /* K-edge has width */
  u1=(a1*a1*a1*p(ek1-0.32))+(b*s(ek1-0.32));
  u2=(a2*a2*a2*p(ek1+0.64))+(b*s(ek1+0.64));
  u=(((u2-u1)/0.96)*(e-ek1+0.32))+u1;
 }

 if   ((e>(ek2-0.32))&&(e<(ek2+0.65)))
 {
 /* K-edge has width */
  u1=(a2*a2*a2*p(ek2-0.32))+(b*s(ek2-0.32));
  u2=(a3*a3*a3*p(ek2+0.64))+(b*s(ek2+0.64));
  u=(((u2-u1)/0.96)*(e-ek2+0.32))+u1;
 }
 res=exp(-u);
 return(res);
}

double s(e)
double e;
{
 double fx,v,w,x,y,z,a;
 a=e/510.975;
 v=1/a;
 w=a*a;
 x=1+a;
 y=1+(2*a);
 z=1+(3*a);
 fx=((x/w)*(((2*x)/y)-(v*log(y))))
    +((v/2)*log(y))-(z/(y*y));
 return(fx);
}
```

```
double p(e)
double e;
{
 double res;
 res=1/(e*e*e);
 return(res);
}
```

PROGRAM NAME : TD_IMAGE
MACHINE : BBC B+ DFS 64K
SOFTWARE : BBC BASIC
HARDWARE : SCAN TABLE., 7100 MCA, AND X-RAY MACHINE.

```
 100 ?(&FE62)=255
 110 ?(&FE63)=255
 120 *DRIVE 0
 130 DIM MC% 100
 140 DIM DTA% 12000
 150 CLOSE#0
 160 REM 1/4 OF THE INTEGRATION TIME
 170 DUR$="155"
 180 REM
 190 CLS
 200 DIM NME$(8):DIM DTE$(8):DIM DS$(40)
 210 PRINT:INPUT "Date   :" DTE$
 220 PRINT:INPUT "Prefix :" NME$
 230 *FX 5,2
 240 REM 4800 BAUD TX
 250 *FX 8,6
 260 REM 4800 BAUD RX
 270 *FX 7,6
 280 REM COMPILE MACHINE CODE
 290 REM SET PHA
 300 O$=CHR$(7)
 310 REM SET DISPLAY
 320 O$=O$+"DH1D@OH2C"
 330 REM SET I/O OF MCA
 340 O$=O$+"CSIN@XN@1N@UN@DN"
 350 VDU2:VDU 1,3:VDU3
 360 PROCOUTPUT
 370 OLDLOC=0:LOC=0
 380 PROCFIND
 390 FOR Z=0 TO 9
 400 IF (Z>=5) THEN *DRIVE 2
 420 FOR W=1 TO 4
 430 PRINT "SETTING TUBE VOLTAGE ";W
 440 ?(&FE61)=(W-1):PROCADC
 450 ENVELOPE 2,1,2,-2,2,10,20,10,1,0,0,-1,100
     ,100
 460 SOUND 1,2,100,100
 470 PROCADC
 480 PRINT "ADC    ";P1
 490 PRINT "SAMPLE ";Z
 500 O$=CHR$(7)+"CO>H1"
 510 O$=O$+"CO>H2"
 520 PROCOUTPUT
 530 FOR G=1 TO 4
 540 O$=CHR$(7)+"CSPN@+NH1NZ"+DUR$+"NCRP"
 550 LOC=Z
 560 PROCFIND
 570 PROCOUTPUT
 580 PRINT "RECORDING H1"
 590 TIME=0
 600 REPEAT:UNTIL(TIME>(105*VAL(DUR$))+100)
 610 PRINT "RECORDING H2"
 620 O$=CHR$(7)+"CSPN@+NH2NZ"+DUR$+"NCRP"
 630 LOC=9
 640 PROCFIND
 650 PROCOUTPUT
 660 TIME=0
 670 REPEAT:UNTIL(TIME>(105*VAL(DUR$))+100)
 680 NEXT G
 690 O$="CRI"
 700 PROCOUTPUT
 710 PRINT "I/O DOWNLOADING"
 720 PROCMCODE
 730 CALL INDAT
 740 VDU2:VDU 1,3:VDU3
 750 PRINT "SAVING : ";
 760 X$=NME$+STR$(W+(Z*4))
 770 XO=OPENOUT X$
 780 DS$=STR$(W)+"-"+STR$(Z)+"-"+STR$(P1)
 790 PRINT #XO,DS$
 800 PRINT #XO,DTE$
 810 RT$="":LT$=""
 820 FOR N=DTA%+5 TO DTA%+13
 830 RT$=RT$+CHR$(?(N+13))
 840 LT$=LT$+CHR$(?N)
 850 NEXT N
 860 PRINT #XO,VAL(RT$)
 870 PRINT #XO,VAL(LT$)
 880 A$=""
 890 ADR=DTA%+27:CHK=0
 900 FOR Y=1 TO 128
 910   A$=""
 920   FOR C=1 TO 4
 930    A$=A$+CHR$(?ADR)
 940    ADR=ADR+1
 950   NEXT C
 960 IF Y/25=INT(Y/25) PRINT "*";
 970 BDAT=0
 980 IF CHK<>VAL(A$) BDAT=1:PRINT "BAD DATA"
 990 CHK=CHK+8
1000   FOR X=1 TO 8
1010   A$=""
1020    FOR C=1 TO 8
1030     A$=A$+CHR$(?ADR)
1040     ADR=ADR+1
1050    NEXT C
1060   PRINT #XO,VAL(A$)
1070   NEXT X
1080 NEXT Y
1090 IF BDAT=1 PRINT #XO,"BAD"
1100 CLOSE #XO
1110 PRINT:PRINT
1120 NEXT W
1130 NEXT Z
1140 PRINT "FINISHED"
1150 *DRIVE 0
1160 END
1170 DEF PROCOUTPUT
1180 REM ENABLE PRINTER
1190 VDU2
1200 FOR N=1 TO LEN(O$)
1210  T$=MID$(O$,N,1)
1220  FOR ZZ=1 TO 1000:NEXT ZZ
1230  VDU 1,ASC(T$)
1240 NEXT N
1250 REM DISABLE PRINTER
1260 VDU3
1270 ENDPROC
1280 DEF PROCMCODE
1290 ML%=&80:MH%=&81
1300 ?ML%=DTA% MOD 256
1310 ?MH%=DTA% DIV 256
1320 IOREG=&FE08:DREG=&FE09
1330 FOR PASS=0 TO 2 STEP 2
1340 P%=MC%
1350 [
1360 OPT    PASS
1370 .INDAT LDA  #3
1380        STA  IOREG
1390        LDA  #&12
1400        STA  IOREG
1410 .LOOP  LDA  #1
1420        BIT  IOREG
1430        BEQ  LOOP
1440        LDA  DREG
1450        CMP  #22
1460        BEQ  LOOP
1470        CMP  #23
1480        BEQ  LOOP
1490        CMP  #13
1500        BEQ  LOOP
1510        CMP  #0
1520        BEQ  LOOP
1530        CMP  #10
1540        BEQ  LOOP
1550        CMP  #25
1560        BEQ  LOOP
1570        LDX  #0
1580        STA  (ML%,X)
1590        INC  ML%
1600        BNE  SKP
1610        INC  MH%
1620 .SKP   CMP  #4
```

```
1630        BNE  LOOP
1640        RTS
1650 ]
1660 NEXT PASS
1670 ENDPROC
1680 DEFPROCADC
1690 P1=0
1700 FOR N=1 TO 800:P1=P1+ADVAL(1):NEXTN
1710 P1=INT(P1/12800)
1720 ENDPROC
1730 DEFPROCSTEP
1740 FOR N=1 TO 30:NEXT N:?(&FE60)=SAM+80+128
1750 FOR N=1 TO 30:NEXT N:?(&FE60)=SAM+80
1760 ENDPROC
1770 DEFPROCFIND
1780 SIZE=381
1790 NUM=250
1800 IF (LOC<OLDLOC) NUM=254
1810 FOR ZZ=0 TO SIZE*ABS(LOC-OLDLOC)
1820 FOR XX=0 TO 8:NEXT XX
1830 ?(&FE60)=NUM
1840 FOR XX=0 TO 8:NEXT XX
1850 ?(&FE60)=NUM+1
1860 NEXT ZZ
1870 OLDLOC=LOC
1880 ENDPROC
```

PROGRAM NAME : SIMULATION
MACHINE : HP-WORKSTATION
SOFTWARE : ANSI C
FUNCTION : VISUAL VERIFICATION.

```
#include<stdio.h>
#include<stdlib.h>
#include<string.h>
#include<math.h>

#define V1      28.45
#define V2      33.43
#define V3      37.94
#define V4      41.26

#define FPATH   "./"
#define RPREFIX "dataev"
#define LOGNME  "smllog.txt"

#define DPREFIX "mat"
#define DCAL    "mat.cal"
#define RSLOPE  0.118630472
#define RINTER  5.91225117
#define RSIZE   512
#define NOITER  17
#define ERROR   0.00040
#define DINTER  1.4399
#define DSLOPE  0.0267
#define KEFF    536.29
#define EDG1    33.168
#define CEDG1   36488.65492
#define JUMP1   3.39
#define EDG2    37.414
#define CEDG2   52372.39391
#define JUMP2   2.5308
#define TP 2.506628275
#define PI 3.141592654

double atn(double);
double c(double,double*,double,double,double,
       double);
double ut(int,double,double,double,double);
double s(double);
double p(double);
int    r(int);
int    er(double);
double loadd(int,int,double);
void   loadr(int,double*);
void   logdat(char*);
double n(double);
double f(double,double);
double at(double,double,double,double);
void   save(int,int,double *);
void   spread(double *);
void   effic(double *);
void   filter(double,double,double,double *);
void   getab(double,double,double,double *,
       double *, double *,double *);
void   noise(double *);
void   norm(double,double *,double *);
void   comb(double *,double *);
double e(int);
double eff(int);
double ft(int,double*,double*);
void   model(long int,double,double,double,
       double *);
int    crunch(double *,double *,double *,double *
       ,double *);
void   exper(int,double *);
void   thick(double,double,double,double *,double
        *);
void   mean(int,double *,double *,double*);
void   dlog(int,char *,double *);

double DLAG=3;

void main(void)          /* Start of program */
{
  double a1,a2,a3,b,ftrans[4];
  double iodine,barium,water;
  int    x,y,z,its;
  char text[200];

   water=50; iodine=0.10; barium=0.10;

   model(500000,water,iodine,barium,ftrans);

   its=crunch(ftrans,&a1,&a2,&a3,&b);
   printf("Results: iterations:%2d  a1:%2.9lf
   a2:%2.9lf a3:%2.9lf b:%lf\n",its,a1,a2,a3,b);

   thick(a1,a2,a3,&iodine,&barium);
   printf("Iodine : %lf  Barium : %lf\n",
          iodine,barium);

}                          /* End of program */
```

```
/*************************************************/
/* Find the three experimental ft's              */
/* GIVEN  :id=experiment number                  */
/* DEFINES:V1,V2,V3,V4=Tube voltages kV.         */
/* RETURNS:Fractional transmittances F1,F2,F3,F4*/
/*************************************************/
void exper(int id,double ftrans[])
{
  ftrans[0]=loadd(id,1,V1);
  ftrans[1]=loadd(id,2,V2);
  ftrans[2]=loadd(id,3,V3);
  ftrans[3]=loadd(id,4,V4);

  printf("Experiment : FT1 %1.9lf FT2 %1.9lf FT3
  %1.9lf FT4 %1.9lf\n",ftrans[0],ftrans[1],ftran
  s[2],ftrans[3]);
}

/*************************************************/
/* Simulate the experimental procedure in full   */
/* Checks with the model                         */
/* GIVEN  : Water =equivalent thickness of H20   */
/*          iodine=equivalent thickness of I     */
/*          barium=equivalent thickness of Ba    */
/*           count=Count in incident spectrum    */
/* RETURNS: Three fractional transmittances      */
/*************************************************/
void model(long int count,double water,double iodi
ne,double barium,double ftrans[])
{
  int    x;
  double datai[1024],datat[1024],fcheck[4];
  double sa1,sa2,sa3,sb;
    printf("Modeling %3.1lf kg/m2 water, %3.1lf k
    g/m2 iodine,%3.1lf kg/m2 barium\n",water,iodi
    ne,barium);
    for(x=1;x<=4;x++)
    {
```

```
      loadr(x,datai);
      loadr(x,datat);
      filter(water,iodine,barium,datat);
      getab(water,iodine,barium,&sa1,&sa2,&sa3,&sb)
;
      effic(datai); spread(datai);
      effic(datat); spread(datat);
      norm(count,datai,datat);
      noise(datai); noise(datat);
      ftrans[x-1]=ft(x,datai,datat);
     }
     printf("Simulated  : FT1 %1.91f FT2 %1.91f F
     T3 %1.91f FT4 %1.91f\n",ftrans[0],ftrans[1],
     ftrans[2],ftrans[3]);
     printf("using        A1: %2.81f A2: %2.81f A
     3: %2.81f B: %2.81f\n",sa1,sa2,sa3,sb);
     loadr(1,datai);
     fcheck[0]=c(V1,datai,sa1,sa2,sa3,sb);
     loadr(2,datai);
     fcheck[1]=c(V2,datai,sa1,sa2,sa3,sb);
     loadr(3,datai);
     fcheck[2]=c(V3,datai,sa1,sa2,sa3,sb);
     loadr(4,datai);
     fcheck[3]=c(V4,datai,sa1,sa2,sa3,sb);
     printf("Model Check: FT1 %1.91f FT2 %1.91f F
     T3 %1.91f FT4 %1.91f\n",fcheck[0],fcheck[1],
     fcheck[2],fcheck[3]);
}

/*********************************************/
/* Caculates a1,a2,a3,b from ft's            */
/* GIVEN  : ftrans[]=3 fractional transmittances*/
/* DEFINES: NOITER  =No. of iters. Bi-Sec Methd */
/*          ERROR   =Convergence requirement    */
/* RETURNS: a1,a2,a3=Photoelectric constants    */
/*          b    =Scatter constant              */
/*********************************************/
int crunch(double ftrans[],double *a1,double *a2,d
ouble *a3,double *b)
{
  int    x,y,z;
  double datai[1024],datat[1024];
  double i,tot,res;
  int    ct,iter,l,its;
  double en,xb1,al,ah,xa1,le,r,xa2,xa3,sa1,sa2,sa
  3,sb;
  double xoa1,xoa2,xob,bh,bl,error;
  for(ct=0;ct<=3;ct++)
  {
   ftrans[ct]=1/ftrans[ct];
  }
  loadr(1,datai);
  loadr(2,datat);
  printf("Starting calculation !!!\n");
  /* Working on the A axis */
  xb1=0; al=0; ah=120;
  for(iter=0;iter<=NOITER;iter++)
  {
   xa1=(ah+al)/2.;
   le=(ftrans[0]*c(V1,datai,ah,ah,ah,xb1))-1;
   r =(ftrans[0]*c(V1,datai,xa1,xa1,xa1,xb1))-1;
   if ((le*r)<0) al=xa1; else ah=xa1;
  }
  printf("\nA1 = %1f\n",xa1);
  xb1=0; al=0; ah=120;
  for(iter=0;iter<=NOITER;iter++)
  {
   xa2=(ah+al)/2.;
   le=(ftrans[1]*c(V2,datat,ah,ah,ah,xb1))-1;
   r =(ftrans[1]*c(V2,datat,xa2,xa2,xa2,xb1))-1;
   if ((le*r)<0) al=xa2; else ah=xa2;
  }
 printf("\nA2 = %1f\n",xa2);
its=0;
if(xa1<xa2)
{
 xoa1=xa1;
 do
 {
  xob=xb1;
  bh=3; bl=0;
  for(iter=0;iter<=NOITER;iter++)
  {
   xb1=(bh+bl)/2.;
   le=(ftrans[1]*c(V2,datat,xa1,xa1,xa1,bh))-1;
   r =(ftrans[1]*c(V2,datat,xa1,xa1,xa1,xb1))-1;
   if ((le*r)<0) bl=xb1; else bh=xb1;
  }
  printf("%2d a1<a2 B1 = %1f ",its,xb1);

  xoa1=xa1;
  al=0; ah=120;
  for(iter=0;iter<=NOITER;iter++)
  {
   xa1=(ah+al)/2.;
   le=(ftrans[0]*c(V1,datai,ah,ah,ah,xb1))-1;
   r =(ftrans[0]*c(V1,datai,xa1,xa1,xa1,xb1))-1;
   if ((le*r)<0) al=xa1; else ah=xa1;
  }
  error=fabs((xa1-xoa1)/xa1)+fabs((xb1-xob)/xb1);
  printf(" A1 = %1f  Error = %1f\n",its,xa1,erro
  r);
  its++;
 }while((error>ERROR)&&(xa1<=xoa1));
}
else
{
 do{
    xob=xb1;
    bh=3; bl=0;
    for(iter=0;iter<=NOITER;iter++)
    {
     xb1=(bh+bl)/2.;
     le=(ftrans[0]*c(V1,datai,xa2,xa2,xa2,bh))-1;
     r=(ftrans[0]*c(V1,datai,xa2,xa2,xa2,xb1))-1;
     if ((le*r)<0) bl=xb1; else bh=xb1;
    }
    printf("%2d a1>a2 B1 = %1f ",its,xb1);
    xoa2=xa2;
    al=0; ah=120;
    for(iter=0;iter<=NOITER;iter++)
    {
     xa2=(ah+al)/2.;
     le=(ftrans[1]*c(V2,datat,ah,ah,ah,xb1))-1;
     r=(ftrans[1]*c(V2,datat,xa2,xa2,xa2,xb1))-1;
     if ((le*r)<0) al=xa2; else ah=xa2;
    }
    error=fabs((xa2-xoa2)/xa2)+fabs((xb1-xob)/xb
    1);
    printf(" A1 = %1f  Error = %1f\n",its,xa2,er
    ror);
    its++;
   }while((error>ERROR)&&(xa2>=xoa2));
   xa1=xa2;
 }
 printf("Found a1 and b  a1:= %1f  b=%1f\n",xa1,x
 b1);

 loadr(3,datai);
 al=0; ah=120;
 for(iter=0;iter<=NOITER;iter++)
 {
  xa2=(ah+al)/2.;
  le=(ftrans[2]*c(V3,datai,xa1,ah,ah,xb1))-1;
  r =(ftrans[2]*c(V3,datai,xa1,xa2,xa2,xb1))-1;
  if ((le*r)<0) al=xa2; else ah=xa2;
 }
 printf("\nA2 = %1f\n",xa2);

 loadr(4,datai);
 al=0; ah=120;
 for(iter=0;iter<=NOITER;iter++)
 {
  xa3=(ah+al)/2.;
  le=(ftrans[3]*c(V4,datai,xa1,xa2,ah,xb1))-1;
  r =(ftrans[3]*c(V4,datai,xa1,xa2,xa3,xb1))-1;
  if ((le*r)<0) al=xa3; else ah=xa3;
 }
 printf("\nA3 = %1f\n",xa3);
 *a1=xa1;
 *a2=xa2;
 *a3=xa3;
  *b=xb1;
 return(its);
}

/*********************************************/
/* Calculate equivalent thickness given a1,a2,b */
/* GIVEN  : a1 = Photoelectric constant <EDG1   */
```

```
/*          a2 = PE const.          >EDG1 <EDG2 */
/*          a3 = Photoelectric constant >EDG2   */
/* DEFINES : CEDG1 = EDG1^3 (1st Kedge cubed)   */
/*           CEDG2 = EDG2^3 (2nd Kedge cubed)   */
/*           JUMP1 = ΔU                         */
/*           JUMP2 = ΔU                         */
/* RETURNS : iodine, barium equivalent thick.   */
/************************************************/
void thick(double a1,double a2,double a3,double *
iodine,double *barium)
{
 double eqt;
 eqt=-(((a1*a1*a1)/CEDG1)-((a2*a2*a2)/CEDG1))/JUM
 P1;
 *iodine=eqt;
 eqt=-(((a2*a2*a2)/CEDG2)-((a3*a3*a3)/CEDG2))/JUM
 P2;
 *barium=eqt;
}

/************************************************/
/* Calcultate the fractional transmittance given*/
/* the arrays datai[] and datat[].              */
/* GIVEN  : datai[]=incident pulse height spect.*/
/*          datat[]=transmitted PHS             */
/*      y = Tube potential 1=V1,2=V2,3=V3,4=V4. */
/* DEFINES: DLAG   =Discriminator               */
/* RETURNS: Fractional transmittance            */
/************************************************/
double ft(int y,double datai[],double datat[])
{
 double toti,tott,ft,v;
 int x,start;
 if (y==1) v=V1;
 if (y==2) v=V2;
 if (y==3) v=V3;
 if (y==4) v=V4;
 start=(int)(((v-DLAG)-RINTER)/RSLOPE);
 if (start<0) start=0;
 toti=0;
 tott=0;
 for(x=start;x<=RSIZE;x++)
 {
   toti+=datai[x];
   tott+=datat[x];
 }
 ft=tott/toti;
 return(ft);
}

/************************************************/
/* Using a gausslan response the standard       */
/* deviation of which is defined by the function*/
/* r(x) to modify the array.  data[] in a manner*/
/* similar to limitted detector resolution.     */
/* Converts real spectra to pulse height        */
/*  distributions.                              */
/* GIVEN  : data[]=high res spectrum            */
/* RETURNS: Low resolution spectrum             */
/************************************************/
void spread(double data[])
{
  double result[1024];
  int x,y,st,en,s;
  double xx,yy,zz,uu,ss,d;
  for(x=0;x<=1023;x++) result[x]=0;
  for(x=0;x<=RSIZE;x++)
  {
   s=r(x);
   st=x-(3*s);
   if (st<0) st=0;
   en=x+(3*s);
   if (en>RSIZE) en=RSIZE;
   uu=(double)x;
   ss=(double)(s*s);
  ss*=-2;
    d=1/(TP*((double)s));
   for(y=st;y<=en;y++)
   {
    xx=(double)y;
    result[y]+=data[x]*d*exp(((xx-uu)*(xx-uu))/ss
    );
   }
  }
  for(x=0;x<=RSIZE;x++)
  {
    data[x]=result[x];
  }
}
/************************************************/
/* Adds the effect of the proportional detectors*/
/* efficiency to the spectrum contained in the  */
/* array data[].                                */
/* GIVEN  : data[]=spectrum incident on detector*/
/* RETURNS: Array data[] containing intensity   */
/* spectrum as the  detector sees it.           */
/************************************************/
void effic(double data[])
{
  int x;
  double energy;
  for(x=0;x<=1023;x++)
  {
   data[x]*=eff(x);
  }
}

/************************************************/
/* Combines the spectra  contained in the arrays*/
/* datai[] and datat[] into a single array      */
/*  returned as datai[].  This format is        */
/* consistent with data collected with the MCA  */
/* GIVEN  :datai[]=incident PH spectrum         */
/*         datat[]=transmited PH spectrum       */
/* RETURNS:A single spectrum in datai[]         */
/* 0-512 original datai[], 513-1023 datat[]     */
/************************************************/
void comb(double datai[], double datat[])
{
 int x;
 double temp[1024];
 for(x=0;x<=1023;x+=2)
 {
  temp[(x/2)]=datai[x]+datai[x+1];
 }
 for(x=0;x<=1023;x+=2)
 {
  temp[512+(x/2)]=datat[x]+datat[x+1];
 }
 for(x=0;x<=1023;x++)
 {
  datai[x]=temp[x];
 }
}

/************************************************/
/* Add noise to each element of the array data[]*/
/* GIVEN  : data[]=Pulse height spectrum array  */
/* RETURNS: Noisy pulse height spectrum         */
/************************************************/
void noise(double data[])
{
  int x;
  for(x=0;x<=1023;x++)
  {
   data[x]=n(data[x]);
  }
}

/************************************************/
/* Normalise the two spectra such that the count*/
/* in the array datai[] is fixed to 'count'.    */
/* This function does not change ft's           */
/* GIVEN  : count  =desired count in datai[].   */
/*          datai[]=incident spectrum.          */
/*          datat[]=transmitted spectrum.       */
/* RETURNS: Array datai[] with total count.     */
/*          datat[] scalled to the same extent. */
/************************************************/
void norm(double count,double datai[],double data
t[])
{
  double ratio,total;
  int x;
  total=0;
  for(x=0;x<=1023;x++)
```

```
  {
   total+=data1[x];
  }
  ratio=count/total;
  for(x=0;x<=1023;x++)
  {
   data1[x]*=ratio;
   datat[x]*=ratio;
  }
}

/************************************************/
/* Adds the effect of a water-matrix filter to  */
/* the spectrum in the array data[].            */
/* GIVEN  : water =equivalent thickness of H20  */
/*          iodine=equivalent thickness of I    */
/*          data[]=array containing spectrum    */
/* DEFINES: RSLOPE,RINTER=reference calibration */
/* RETURNS: array data[] modified by filter     */
/************************************************/
void filter(double water, double iodine,double bar
ium, double data[])
{
  int x;
  double energy;
  for(x=0;x<=1023;x++)
  {
    energy=(((double)x)*RSLOPE)+RINTER;
    data[x]=data[x]*exp(-at(energy,water,iodine,b
    arium));
  }
}

/************************************************/
/* Saves the simulation file in the same        */
/* format as the MCA software.                  */
/* GIVEN  : u=sample/experiment no.             */
/*          v=tube voltage 0=V1 1=V2 2=V3 3=V4  */
/*     data[]=array containg spectrum           */
/* DEFINES: FPATH = path to data files          */
/************************************************/
void save(int u,int v,double data[])
{
  int x;
  char fil[40],text[5];
  double en;
  FILE *fp,*fopen();
  strcpy(fil,"/users/cem/simulation/mdat");
  sprintf(text,"%d",v+(4*u));
  strcat(fil,text);
  strcat(fil,".dat");
  printf("Opening datafile %d %s\n",v+(3*u),fil);
  fp=fopen(fil,"w");
  fprintf(fp," %s\n","0");
  fprintf(fp," %s\n","0");
  fprintf(fp," %lf\n",0.0);
  fprintf(fp," %lf\n",0.0);
  for(x=0;x<=1023;x++)
  {
   fprintf(fp,"%5.0lf\n",data[x]);
  }
  fclose(fp);
 }

/************************************************/
/* Logs intermediate data ready for idl         */
/* GIVEN  : name = file name                    */
/*          data[]=array containg spectrum      */
/* DEFINES: FPATH = path to data files          */
/************************************************/
void dlog(int y,char name[],double data[])
{
  int x;
  double en;
  char fil[30],text[5];
  FILE *fp,*fopen();
  strcpy(fil,name);
  sprintf(text,"%d",y);
  strcat(fil,text);
  strcat(fil,".dat");
  printf("\nOpening datafile %s\n",fil);
  fp=fopen(fil,"w");
  for(x=0;x<=1023;x++)
  {
   fprintf(fp,"%5.3lf\n",data[x]);
  }
  fclose(fp);
 }

/************************************************/
/* Adds noise to the perfect count n.           */
/* GIVEN : n=count (double)                     */
/* RETURN: count with poisson noise             */
/************************************************/
double n(double n)
{
  double res,x,r,rn,i,d,t,tre;
  int flag,count;
  if(n>=1)
  {
   do
   {
    r=sqrt(n);
    rn=((double)rand()/(double)RAND_MAX);
    i=0.;
    t=0.;
    d=(6.*r)/1000.;
    tre=3.*r;
    flag=0;
    count=0;
    for(x=-tre ; (t<=rn)&&(x<=tre) ; x+=d)
    {
      i+=f(x,n);
      t=((i-(f(x-(3.*r),n)+f(x,n))/2.)*d)+0.00135;
      count++;
    }
    if (count<=1) flag=1;
    if (count>=1000) flag=1;
    if (rand()<((RAND_MAX)/2)) x-=d;
   }while(flag==1);
  }
  else
  {
   x=0;
  }
 return(n+x);
}

/*^^^^^^^^^^^^^^^^^^^^^^^^^^^^^^^^^^^^^^^^^^^^*/
/* Gaussian response function                   */
/* used only by noise function n()              */
/*^^^^^^^^^^^^^^^^^^^^^^^^^^^^^^^^^^^^^^^^^^^^*/
double f(double x, double n)
{
 return((1./sqrt(2.*PI*n))*exp(-0.5*((x*x)/n)));
}

/************************************************/
/* Function returns the number of mean free     */
/* paths at energy energy e associated with     */
/* a water matrix combination.                  */
/* GIVEN   : e=energy keV                       */
/*       water=equivalent thickness of water    */
/*      iodine=equivalent thickness of iodine   */
/* RETURNS :  MFP (i.e. I=Io EXP(-MFP))         */
/************************************************/
double at(double energy,double water,double iodine
,double barium)
{
  double res;
  if(energy<EDG1)
  {
   res=iodine*((15925.2*p(energy))+(0.2250*s(energ
   y)));
  res+=barium*((18955.3*p(energy))+(0.2405909*s(en
  ergy)));
  }
  if((energy<EDG2)&&(energy>=EDG1))
  {
   res=iodine*((125370*p(energy))+(0.2250*s(energ
   y)));
  res+=barium*((18955.3*p(energy))+(0.2405909*s(en
ergy)));
  }
  if(energy>=EDG2)
  {
   res=iodine*((125370*p(energy))+(0.2250*s(energ
   y)));
  res+=barium*((151477.6*p(energy))+(0.2405909*s(e
  nergy)));
```

```
  }
  res+=water*((491.26*p(energy))+(0.01602*s(energy
  )));
  return(res);
}

/*************************************************/
/* Function returns the photoelectric and        */
/* scatter constants given the equivalent        */
/* thickness of water and analytes.              */
/* GIVEN  : water=equivalent thickness of water  */
/*          iodine=equivalent thickness of iodine */
/* RETURNS: Constants a1,a2,a3,b                 */
/*************************************************/
void  getab(double water,double iodine,double bariu
m,double *a1,double *a2,double *a3, double *b)
{
 double third;
 third=1.0/3.0;
 *a1=pow(((18955.3*barium)+(15925.2*iodine)+(491.26
 *water)),third);
 *a2=pow(((18955.3*barium)+(125370*iodine)+(491.26
 *water)),third);
 *a3=pow(((151477.6*barium)+(125370*iodine)+(491.2
 6*water)),third);
  *b=(0.2250*iodine)+(0.01602*water)+(0.2405909*b
 arium);
}

/*************************************************/
/* Load the reference spectra into the array     */
/* Removes Si(Li) response.                      */
/* GIVEN    : id = Reference file number 1,2,3,4 */
/* DEFINES  : RSLOPE,RINTER calibration consts.  */
/*            FPATH   = Path to reference files. */
/*            RPREFIX = Non-numeric part of name */
/* RETURNS  : Array data[] containing r. spectrum*/
/*************************************************/
void loadr(int id,double data[])
{
  char fil[50],text[10],title[30],date[15];
  double rt,lt,en;
  int x;
  FILE *fp,*fopen();
  strcpy(fil,FPATH);
  strcat(fil,RPREFIX);
  sprintf(text,"%d",id);
  strcat(fil,text);
  strcat(fil,".dat");
  fp=fopen(fil,"r");
  fscanf(fp," %s",title);
  fscanf(fp," %s",date);
  fscanf(fp," %lf",&rt);
  fscanf(fp," %lf",&lt);
  for(x=0;x<=1023;x++)
  {
   fscanf(fp," %lf",&data[x]);
   en=(RSLOPE*(double)x)+RINTER;
   data[x]/=atn(en);
   if ((en>V1)&&(id==1)) data[x]=0;
   if ((en>V2)&&(id==2)) data[x]=0;
   if ((en>V3)&&(id==3)) data[x]=0;
   if ((en>V4)&&(id==4)) data[x]=0;
  }
  fclose(fp);
}

/*************************/
/* Write result to LOG.TXT */
/*************************/
void logdat(char text[])
{
 FILE   *fp,*fopen();
 char   fil[45];
 double eqt;
 strcpy(fil,FPATH);
 strcat(fil,LOGNME);
 printf("Opening logfile %s\n",fil);
 fp=fopen(fil,"a");
 fprintf(fp,"%s\n",text);
 fclose(fp);
}

/*************************************************/
```

```
/* Calculates the fractional transmittance for   */
/* experimental data collected using the MCA     */
/* with the sample caroussel.                    */
/* GIVEN  : sam = Sample number 0 to 7           */
/*          id  = Tube voltage 0=V1 1=V2 2=V3 3=V4 */
/*          v   = Tube voltage kV                */
/* DEFINES: FPATH   = path to data files         */
/*          PREFIX  = Non-numeric part of nme    */
/*          DLAG    = Discriminator lag kV       */
/*  RSLOPE + INTER  = Calibration                */
/* RETURNS: Fractional transmittance             */
/*************************************************/
double loadd(int sam,int id,double v)
{
  char fil[50],text[10],title[30],date[15];
  double rt,lt,en;
  int x,low,high;
  double data[1024],ft,tc1,tc2;
  double s[10],i[10],inter,slope;
  int f1[10],f2[10],f3[10],f4[10];
  FILE *fp,*fopen();
  strcpy(fil,FPATH);
  strcat(fil,DCAL);
  printf("Opening %s\n",fil);
  fp=fopen(fil,"r");
  for(x=0;x<=7;x++)
  {
   fscanf(fp," %lf",&s[x]);
   fscanf(fp," %lf",&i[x]);
   fscanf(fp," %d",&f1[x]);
   fscanf(fp," %d",&f2[x]);
   fscanf(fp," %d",&f3[x]);
   fscanf(fp," %d",&f4[x]);
  }
  fclose(fp);
  printf("i:%lf s:%lf a:%d b:%d c:%d d:%d\n",i[sam
  ],s[sam],f1[sam],
  f2[sam],f3[sam],f4[sam]);
  inter=i[sam];
  slope=s[sam];
  strcpy(fil,FPATH);
  strcat(fil,DPREFIX);
  sprintf(text,"%d",(4*sam)+id);
  strcat(fil,text);
  strcat(fil,".dat");
  printf("Opening data %s\n",fil);
  fp=fopen(fil,"r");
  fscanf(fp," %s",title);
  fscanf(fp," %s",date);
  fscanf(fp," %lf",&rt);
  fscanf(fp," %lf",&lt);
  for(x=0;x<=1023;x++) {fscanf(fp," %lf",&data[x]
  );}
  fclose(fp);
/*
  if (id==1) low=f1[sam]-((int)(DLAG/slope));
  if (id==2) low=f2[sam]-((int)(DLAG/slope));
  if (id==3) low=f3[sam]-((int)(DLAG/slope));
  if (id==4) low=f4[sam]-((int)(DLAG/slope));
*/
  low=(int)((((v-DLAG)-inter)/slope)+0.5);
  if (low<0) low=0;
  high=511;
  tc1=0; tc2=0;
  for(x=low;x<=high;x++)
  {
   tc1+=data[x+512];
   tc2+=data[x];
  }
  ft=tc1/tc2;
  return(ft);
}

/*************************************************/
/* Function calculates the ft's                  */
/* GIVEN : v    =Tube opperating potential kV    */
/*         ref[]= reference spectra              */
/*            a1=PE constant upto EDG1           */
/*            a2=PE constant EDG1 to EDG2        */
/*            a3=PE constant EDG2 to EDG3        */
/*            b =Scatter constant                */
/* DEFINES : RSIZE = No of active x[] in ref     */
/* RETURNS : fractional transmittance.           */
double c(double v,double ref[],double a1,double a
2,double a3,double b)
```

```
{
 int    x,y;
 double d,st,en,xx,ss,uu,s,res,tot;
 double at,low,high,temp,speed;
 double speci[1024],spect[1024];

 for(x=0;x<=1023;x++)
 {
  speci[x]=0;
  spect[x]=0;
 }

 for(x=0;x<=RSIZE;x++)
 {
  s=r(x);
  st=x-(3*s);
  if (st<0)     st=0;
  en=x+(3*s);
  if (en>RSIZE) en=RSIZE;
  uu=(double)x;
  ss=(double)(s*s);
  ss*=-2;
  d=1/(TP*((double)s));
  speed=eff(x)*d*ref[x];
  at=ut(x,a1,a2,a3,b);
  for(y=st;y<=en;y++)
  {
   xx=(double)y;
   temp=speed*exp(((xx-uu)*(xx-uu))/ss);
   speci[y]+=temp;
   spect[y]+=temp*at;
  }
 }
 res=0; tot=0;
 low=(int)(((v-DLAG)-RINTER)/RSLOPE);
 if (low<0) low=0;
 high=RSIZE;
 for(x=low;x<=high;x++)
 {
  tot+=speci[x];
  res+=spect[x];
 }
 res/=tot;
 return(res);
}

/*************************************************/
/* Calculates the absorption (I/Io) of an        */
/* absorber described by  photoelectric          */
/* constants a1,a2, and a3 and scatter constant  */
/* b  given the channel number x.                */
/* GIVEN    : x =channel number                  */
/*            a1=PE constant upto EDG1           */
/*            a2=PE constant EDG1 to EDG2        */
/*            a3=PE constant EDG2 to EDG3        */
/*            b =Scatter constant                */
/* DEFINES  : EDG1 = energy of 1st K-edge        */
/*            EDG2 = energy of 2nd K-edge        */
/* RETURNS  : absorption as I/Io (i.e. 0...1)    */
/*************************************************/
double ut(int x,double a1,double a2,double a3,doub
le b)
{
 double ek1,ek2,e,a;
 double u1,u2,u,res;
 ek1=EDG1;      /* Iodine */
 ek2=EDG2;      /* Barium */
 e=(RSLOPE*(double)x)+RINTER;
 if (e<ek1)              a=a1;
 if ((e>=ek1)&&(e<=ek2)) a=a2;
 if (e>ek2)              a=a3;
 u=(a*a*a*p(e))+(b*s(e));
 res=exp(-u);
 return(res);
}

/*************************************/
/* Calculate s(e) the Klein-Nishina  */
/* function for scatter absorption.  */
/* GIVEN  : e=energy                 */
/* RETURNS: value of s(E)=see lab book. */
/*************************************/
double s(double e)
{
 double fx,v,w,x,y,z,a;
 if (e<0.1) e=0.1;
 a=e/510.975;
 v=1/a;
 w=a*a;
 x=1+a;
 y=1+(2*a);
 z=1+(3*a);
 fx=((x/w)*(((2*x)/y)-(v*log(y))))+((v/2)*log(y))-
(z/(y*y));
 return(fx);
}

/*************************************/
/* Calculate p(e) the Bragg-Pierce   */
/* function for photoelectric absorption. */
/* GIVEN  : e=energy                 */
/* RETURNS: value of p(E)=1/(E^3)    */
/*************************************/
double p(double e)
{
 double res;
 if (e<0.1) e=0.1;
 res=1/(e*e*e);
 return(res);
}

/*************************************************/
/* Returns proportional detector resolution */
/* as the standard deviation of a gaussian. */
/* GIVEN  : x=channel                            */
/* RETURNS: standard deviation (channels)   */
/*************************************************/
int r(x)
int x;
{
  double e,chan,res;
  e=(((double)x)*RSLOPE)+RINTER;
  res=(DSLOPE*e)+DINTER;
  chan=res/RSLOPE;
  return((int)chan);
}

/*************************************************/
/* Returns proportional detector resolution */
/* as the standard deviation of a gaussian. */
/* GIVEN  : e=energy                             */
/* RETURNS: standard deviation (channels)   */
/*************************************************/
int er(e)
double e;
{
  double chan,res;
  res=(DSLOPE*e)+DINTER;
  chan=res/RSLOPE;
  return((int)chan);
}

/*************************************/
/* Relative efficiency function for  */
/* the gas flow proportional detector. */
/* GIVEN  : x=channel                */
/* RETURNS: relative efficiency      */
/*************************************/
double e(x)
int x;
{
  double e,chan,res;
  e=(((double)x)*RSLOPE)+RINTER;
  res=KEFF/(e*e*e);
  if (res>1) res=1;
  if (res<0) res=0;
  return(res);
}

/*************************************/
/* Absolute efficiency function for  */
/* the gas flow proportional detector. */
/* GIVEN  : y=channel                */
/* RETURNS: efficiency               */
/*************************************/
double eff(y)
int    y;
{
  static
```

```
double at[11]={1,6.34e-3,4.66e-3,3.70e-3,2.22e-3,
               8.05e-4,2.17e-4,1e-4};
   static double en[11]={0.1,8.20,13.60,17.75,
                         22.43,32.26,44.37,100};
   double e,a,b,res,e1,e2,x1,x2;
   int    x;
   e=(((double)y)*RSLOPE)+RINTER;
   for(x=0;((x<=7)&&(e>en[x]));x++);
   x2=at[x]; x1=at[x-1];
   e2=en[x]; e1=en[x-1];
   a=(((s(e1)*x2)-(s(e2)*x1)))/((p(e2)*s(e1))-(s(
   e2)*p(e1)));
   b=(((p(e1)*x2)-(p(e2)*x1)))/((p(e1)*s(e2))-(s(
   e1)*p(e2)));
   res=1-exp(-((a*p(e))+(b*s(e))));
   return(res);
 }

/*******************************/
/* Si(Li) detector efficiency */
/* as a function of energy.    */
/* GIVEN  : e=energy           */
/* RETURNS: efficiency         */
/*******************************/
 double atn(e)
 double e;
 {
  double at[11]={100,100,98,95,84,66,46,36,28,26,2
  6};
  double en[11]={0,10,15,20,25,30,35,40,45,50,100}
  double res,el,eh,al,ah;
  int    flg,x;
  for(x=0;((x<=10)&&(e>=en[x]));x++);
  ah=at[x]; al=at[x-1];
  eh=en[x]; el=en[x-1];
  res=(((ah-al)/(eh-el))*(e-el))+al;
  return(res/100);
 }


/*********************************************/
/* Routine to find mean and standard deviation */
/* GIVEN  :num   =no. of last data point      */
/*         data[]=data points                */
/* RETURNS:mean and standard deviation       */
/*********************************************/
void mean(int num,double data[],double *mn,double
 *sd)
{
  double tot,m,s;
  int x;
  tot=0;
  for(x=0;x<=num;x++)
  {
   tot+=data[x];
  }
  m=tot/((double)num);
  tot=0;
  for(x=0;x<=num;x++)
  {
   tot+=((data[x]-m)*(data[x]-m));
  }
  s=sqrt(tot/((double)num));
  *mn=m;
  *sd=s;
}
```

PROGRAM NAME : OVERLAP

MACHINE : HP WORKSATION

SOFTWARE : ANSI C

FUNCTION : CALCULATE OVERLAP AREAS

```
#include<stdio.h>
#include<math.h>
#include<string.h>

#define SIZE 30
#define PI 3.14159265358979323846

struct box
{
  int    x;
  int    y;
  double area;
};

struct ray_sum
{
  int         angle;
  int         projection;
  int         n_boxes;
  double      t_overlap;
 struct box b[150];
};


void   coords(int *, double *, double *, double,
double);
void   stfn(double *, double *, double * ,double *
,double ,double );
void   cross(int, double, double, double, double,
int, int, int *, struct box *);
double boxes(int *,struct box *,int,int);
void   verts(int,double,double,double,double,int *
,double *,double *);
double prpoly(int,double*,double*);
double area(double,double,double,double,double,
double);

void main(void)
{
 int    num,prj,ang;
 struct ray_sum ray;
 FILE *fp;

 fp=fopen("OVERLP30.CT","wb");
 for(prj=0;prj<SIZE;prj++)
 {
  for(ang=0;ang<SIZE;ang++)
  {
   ray.angle=ang;
   ray.projection=prj;
   ray.t_overlap=boxes(&ray.n_boxes,ray.b,prj,ang);
   fwrite(&ray,sizeof(ray),1,fp);
  }
 }
 fclose(fp);
}

void coords(int *flg,double *m,double *c,double
prj, double ang)
{
 double x1,y1,x2,y2,xt,yt,calc;
 calc=(double)(SIZE/2);

 yt=prj-calc;
 x1=(-calc*cos(ang))-(yt*sin(ang))+calc;
 y1=(-calc*sin(ang))+(yt*cos(ang))+calc;
 x2=(calc*cos(ang))-(yt*sin(ang))+calc;
 y2=(calc*sin(ang))+(yt*cos(ang))+calc;

 if(*flg==-1){*flg = (fabs(x1-x2)<fabs(y1-y2)) ?
 1 : 0 ;}

 if(*flg==1)
 {
  xt=x1;x1=y1;y1=xt;
  xt=x2;x2=y2;y2=xt;
 }
 *m=(y1-y2)/(x1-x2);
 *c=y1-(*m*x1);
}
void stfn(double *x1,double *y1,double *x2,double
*y2,double m,double c)
{
 *x1=0;
 *y1=c;
 if(*y1>SIZE)
 {
  *y1=SIZE;
  *x1=(SIZE-c)/m;
 }
 if(*y1<0)
 {
  *y1=0;
  *x1=-c/m;
```

```
 }
 *x2=SIZE;
 *y2=(m*SIZE)+c;
 if(*y2>SIZE)
 {
  *y2=SIZE;
  *x2=(SIZE-c)/m;
 }
 if(*y2<0)
 {
  *y2=0;
  *x2=-c/m;
 }
}

double boxes(int *num,struct box b[],int p,int a)
{
 double x,y,sx,ex,sy,ey,sm,sc,em,ec,t,tarea;
 double prj,ang,osy,oey;
 double sx1,sy1,sx2,sy2;
 double ex1,ey1,ex2,ey2;
 int c,flag,f1,f2;

 if (a==(SIZE/2)) p=SIZE-p-1;
 prj=(double)p;
 ang=(PI*((double)a))/SIZE;
 *num=0;
 if((a==0)||(a==(SIZE/2)))
 {
  sm=0;em=0;sc=prj;ec=prj+1;
  flag = (a==0) ? 0 : 1 ;
  sx1=0;sy1=p;sx2=SIZE;sy2=p;
  ex1=0;ey1=p+1;ex2=SIZE;ey2=p+1;
  for(c=0;c<SIZE;c++) cross(flag,sm,sc,em,ec,c,p,
  num,b);
 }
 else
 {
 flag=-1;
 coords(&flag,&sm,&sc,prj,ang);
 stfn(&sx1,&sy1,&sx2,&sy2,sm,sc);
 coords(&flag,&em,&ec,prj+1,ang);
 stfn(&ex1,&ey1,&ex2,&ey2,em,ec);
 sx = (sx1<ex1) ? sx1 : ex1;
 ex = (sx2>ex2) ? sx2 : ex2;
 osy=floor((sm*floor(sx))+sc);
 oey=floor((em*floor(sx))+ec);
  for(x=floor(sx);x<=floor(ex);x++)
  {
   sy=(sm*x)+sc;
   ey=(em*x)+ec;
   if(sy>ey) {t=sy;sy=ey;ey=t;}
   for(y=floor(sy);y<=floor(ey);y++)
   cross(flag,sm,sc,em,ec,(int)x,(int)y,num,b);
   if (osy!=floor(sy)) cross(flag,sm,sc,em,ec,(int
   )x-1,(int)floor(sy),num,b);
   if (oey!=floor(ey)) cross(flag,sm,sc,em,ec,(int
   )x-1,(int)floor(ey),num,b);
   osy=floor(sy);
   oey=floor(ey);
  }
 }
 tarea=0;
 for(c=0;c<(*num);c++) tarea+=b[c].area;
 return(tarea);
}

void cross(int flg,double sm,double sc,double
em,double ec,int x,int y,int *num,struct box
ox b[])
{
 int    s,t;
 double temp,cx1,cy1,dx1,dy1,dy2,cy2,a;
 int vnum;
 double vx[10],vy[10];
 vnum=0;
 cx1=(double)x;
 cy1=(sm*cx1)+sc;
 cy2=(em*cx1)+ec;
 dx1=(double)(x+1);
 dy1=(sm*dx1)+sc;
 dy2=(em*dx1)+ec;
 if(cy2>cy1)
 {
  temp=sc;sc=ec;ec=temp;
  temp=em;em=sm;em=temp;
  temp=cy1;cy1=cy2;cy2=temp;
  temp=dy1;dy1=dy2;dy2=temp;
 }
 verts(flg,cx1,cy1,(double)x,(double)y,&vnum,vx,vy
 );
 for(a=floor(cy1);a>=ceil(cy2);a--)
 verts(flg,cx1,a,(double)x,(double)y,&vnum,vx,vy);
 verts(flg,cx1,cy2,(double)x,(double)y,&vnum,vx,vy
 );

 if(floor(dy2)!=floor(cy2))
 {
  if(dy2>cy2)
  {
   if (em!=0) verts(flg,(ceil(cy2)-ec)/em,ceil(
   cy2),(double)x,(double)y,&vnum,vx,vy);
  }
  else
  {
   if (em!=0) verts(flg,(floor(cy2)-ec)/em,floor(
   cy2),(double)x,(double)y,&vnum,vx,vy);
  }
 }
 verts(flg,dx1,dy2,(double)x,(double)y,&vnum,vx,vy
 );
 for(a=ceil(dy2);a<=floor(dy1);a++)
 verts(flg,dx1,a,(double)x,(double)y,&vnum,vx,vy);
 verts(flg,dx1,dy1,(double)x,(double)y,&vnum,vx,vy
 );

 if(floor(cy1)!=floor(dy1))
 {
  if(cy1<dy1)
  {
   if (sm!=0) verts(flg,(floor(dy1)-sc)/sm,floor(
   dy1),(double)x,(double)y,&vnum,vx,vy);
  }
  else
  {
   if (sm!=0)  verts(flg,(ceil(dy1)-sc)/sm,ceil(
   dy1),(double)x,(double)y,&vnum,vx,vy);
  }
 }

 if(flg!=0)
 {
  t=x;x=y;y=t;
 }

 s=1;
 for(t=0;t<(*num);t++) if ((b[t].x==x)&&(b[t].y==y
 )) s=0;
 if(s)
 {
  if((x>=0)&&(x<SIZE)&&(y>=0)&&(y<SIZE))
  {
   b[*num].x=x;
   b[*num].y=y;
   b[*num].area=prpoly(vnum,vx,vy);
   *num=*num+1;
  }
 }

}


void verts(int flg,double x,double y,double lx,dou
ble ly,int *vnum,double vx[],double vy[])
{
 double t;
 int s;

if((x>=(lx-0.0000001))&&(x<=(lx+1.0000001))&&(y>=(
ly-0.0000001))&&(y<=(ly+1.0000001)))
 {
  if(flg!=0)
  {
   t=x;x=y;y=t;
  }
  if((x>=0)&&(x<=SIZE)&&(y>=0)&&(y<=SIZE))
  {
   vx[*vnum]=x;
   vy[*vnum]=y;
   *vnum=*vnum+1;
```

```
  }
 }
}

double prpoly(int num,double x[],double y[])
{
 int z,data[40];
 int    ox,s;
 double mx,my,overlap;
 overlap=0;

 if(num>=2)
 {
  x[num]=x[0]; y[num]=y[0];
  mx=0;my=0;
  for(z=0;z<num;z++)
  {
   mx+=x[z];
   my+=y[z];
  }
  mx/=(double)num; my/=(double)num;
  for(z=0;z<num;z++)
  {
   overlap+=area(x[z],y[z],x[z+1],y[z+1],mx,my);
  }
 }
 return(overlap);
}

double area(double x1,double y1,double x2,double
y2,double x3,double y3)
{
 double area,xa,xb,ya,yb;
 xa=x1-x3;
 ya=y1-y3;
 xb=x2-x3;
 yb=y2-y3;
 area=(fabs((xb*ya)-(xa*yb)))/2.0;
 return(area);
}
```

PROGRAM NAME : ART
MACHINE : HP WORKSTATION
SOFTWARE : ANSI C
FUNCTION : IMAGE RECONSTRUCTION

```
#include<stdio.h>
#include<math.h>
#include<string.h>

#define SIZE 30
#define OVER "OVERLP30.CT"
#define S    (SIZE*5)
#define W 0.004
#define RELAX 0.025
#define FINISH 0.0025

#define FILTER "*.*"

struct box
{
 int    x;
 int    y;
 double area;
};

struct ray_sum
{
 int        angle;
 int        projection;
 int        n_boxes;
 double     t_overlap;
 struct box b[S];
};


void main(void)
{
 int    iter,z,prj,ang,x,y;
 struct ray_sum ray;
 double sum,sd,oldsd,deltasd,error,imagesum,sqr
        temp,corection,max,min;
 double image[SIZE][SIZE];
 double expsum[SIZE][SIZE];
 unsigned plc[SIZE][SIZE];
 char name1[30],name2[30];
 FILE *fp;

 printf("Enter reconstruction data file name : ");
 scanf(" %s",name1);
 printf("Enter image data file name : ");
 scanf(" %s",name2);
 fp=fopen(name1,"rt");

 for(sum=0,ang=0;ang<SIZE;ang++)
 {
  for(prj=0;prj<SIZE;prj++)
  {
   fscanf(fp," %lf",&temp);
   expsum[prj][ang]=temp;
   sum+=temp/(W*SIZE);  /* Conc. per pixel */
  }
 }
 fclose(fp);
 sum/=(SIZE*SIZE);

 for(x=0;x<SIZE;x++)
 {
  for(y=0;y<SIZE;y++) image[x][y]=sum;
 }

  iter=0;
  deltasd=1;
  while(deltasd>FINISH)
  {
   oldsd=sd;

   fp=fopen(OVER,"rb");
   for(prj=0;prj<SIZE;prj++)
   {
    for(ang=0;ang<SIZE;ang++)
    {
     fread(&ray,sizeof(ray),1,fp);
/*
     printf("Angle     : %d Projection   : %d\n",r
     ay.angle,ray.projection);
     printf("Overlap   : %2.4lf\n",ray.t_overlap);
     printf("No. cells : %d\n\n",ray.n_boxes);
     printf("Last dSD  : %1.3lf\n\n",deltasd);
     printf("Iteration : %d\n\n",iter);
*/
     /*************************************/
     /* Evaluate ray_sum based on image data */
     /*************************************/
     imagesum=0;sqrs=0;
     for(z=0;z<ray.n_boxes;z++)
     {
      sqrs+=ray.b[z].area*ray.b[z].area;

      imagesum+=(image[ray.b[z].x][ray.b[z].y])*
      ray.b[z].area;
     }
     imagesum*=W;

     /*************************************/
     /* Compare exp. and calculated ray_sums    */
     /*************************************/
      error=expsum[ray.projection][ray.angle]-imag
      esum;
     corection=(RELAX*error)/(sqrs*W);

     /*************************************/
     /* Correct image data based on the error */
     /* Additive ART                      */
     /*************************************/
     for(z=0;z<ray.n_boxes;z++)
     {
      image[ray.b[z].x][ray.b[z].y]+=ray.b[z].area
      *corection;
      if (image[ray.b[z].x][ray.b[z].y]<0) image[r
      ay.b[z].x][ray.b[z].y]=0;
     }

    }
   }
   fclose(fp);
   iter++;
```

```
    /************************************/
    /* Evaluate image standard deviation */
    /************************************/
    for(sum=0,x=0;x<SIZE;x++)
    {
     for(y=0;y<SIZE;y++) sum+=image[x][y];
    }
    sum/=(SIZE*SIZE);
    for(sd=0,x=0;x<SIZE;x++)
    {
     for(y=0;y<SIZE;y++) sd+=(image[x][y]-sum)*(im
     age[x][y]-sum);
    }
    sd/=(SIZE*SIZE);
    deltasd=fabs((sd-oldsd)/sd);
    printf("%lf\n",deltasd);

  }

  fp=fopen(name2,"wt");
  for(x=0;x<SIZE;x++)
  {
   for(y=0;y<SIZE;y++)
   {
    fprintf(fp," %lf\n",image[x][y]);
   }
  }
  fclose(fp);
}
```

APPENDIX G : PROGRAM "HUBBLE"

Program "Hubble" can be used to simulate a source, absorber, detector experimental configuration. The program and associated data were too large to include in an appendix. This appendix shows how the filter installed in the x-ray was designed. The software contains three databases. These are used to describe the x-ray source, absorber and detector.

Source spectra were contained in separate files, each file contained a list of 1024 numbers representing the spectral shape of the source. These could be real spectra recorded using the multichannel analyser and Si(Li) detector or simulated spectra generated by software. A separate file contained the calibration information.

Absorption information obtained from Hubbles paper [1] was contained in a second database. The database contained the mass attenuation coefficients at a number of energies for each of the following elements and materials H, Li ,Be, B, C, N, O, F, Na, Mg, Al, Ar, K, Ca, Ti, Mn, Fe, Cu, Zn, Ga, Ge , As ,Br, Ag, Cd, Sn, Te, I, Cs, Ba, Ce, W, Au, Hg, Pb, U, Si, P, S, Cl and water. Where appropriate the K-edge energy for the element was also included in the database. The software was able to generate a value of the mass attenuation coefficient at any energy (5keV - 100keV) for any absorber contained in the database.

The detector database contained information describing the efficiency of the detector.

The software was menu driven. The absorber was described by selecting each element of interest in the database and typing in the equivalent thickness. The effect of a number of absorbers could be added together. The resulting absorption response was displayed graphically. Figure G.01 shows the attenuation curve for the filter used (20 kg/m^2 water, 0.6 kg/m^2 Bromine, 0.3 kg/m^2 copper). This information could also be displayed in the form I/I_0, see figure G.02.

At this stage a source file can be loaded. Figure

G.03 shows an experimentally recorded 60kV tube source spectra that was loaded into the database. The software extracts the region of interest from this spectrum, in this case 20kV to 60kV. The resulting spectrum is shown in figure G.04.

The detector response was then loaded into the database. The response is shown in G.05.

The effect of the detector and absorber can be added to or subtracted from the source spectra. In this case the response of the detector was removed and the effect of the absorber added. The resulting spectrum is shown in figure G.06. Changing the source spectra allowed the effect of the filter at different tube potentials to be investigated.

A cursor could be positioned on any graph and used to read values. The cursor could also be used to integrate counts over a range energies.

Reference

[1] Hubble, J.H.
Mass attenuation and Energy Absorption coefficients from 1keV to 20MeV."
Int. J. Appl. Radiat. Isot., Vol. 33, pp 126-1920, 1982

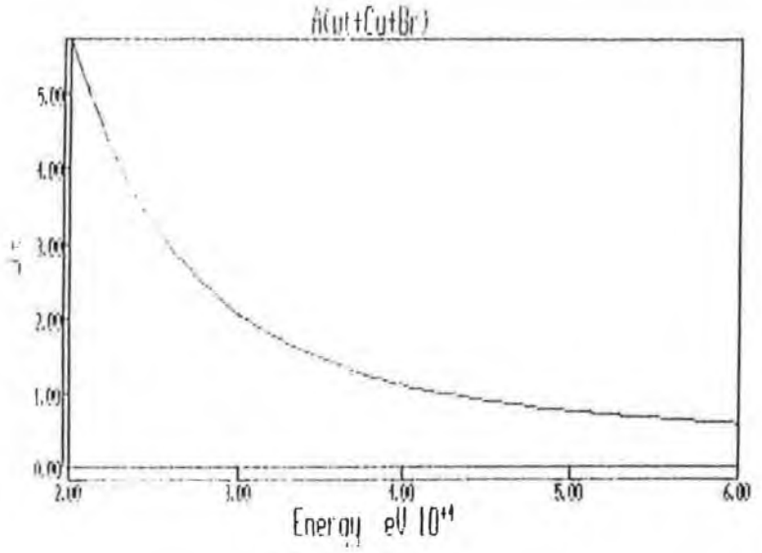

Figure G.01
Absorption Ut. (Water 20 kg/m^2, Copper 0.3 kg/m^2, Bromine 0.6 kg/m^2)

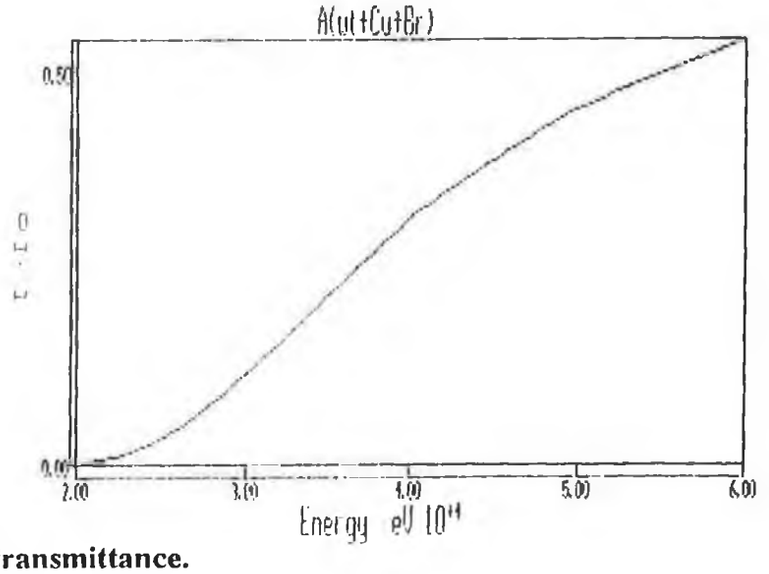

Figure G.02
Fractional transmittance.

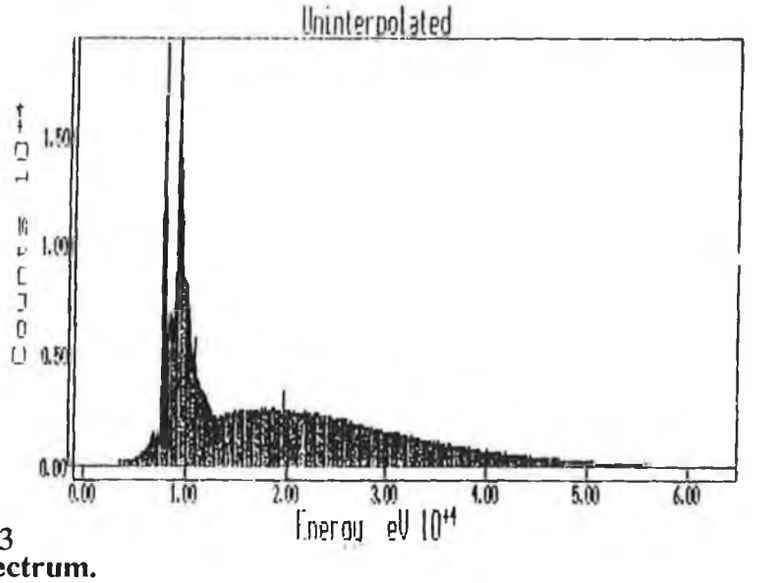

Figure G.03
Source spectrum.

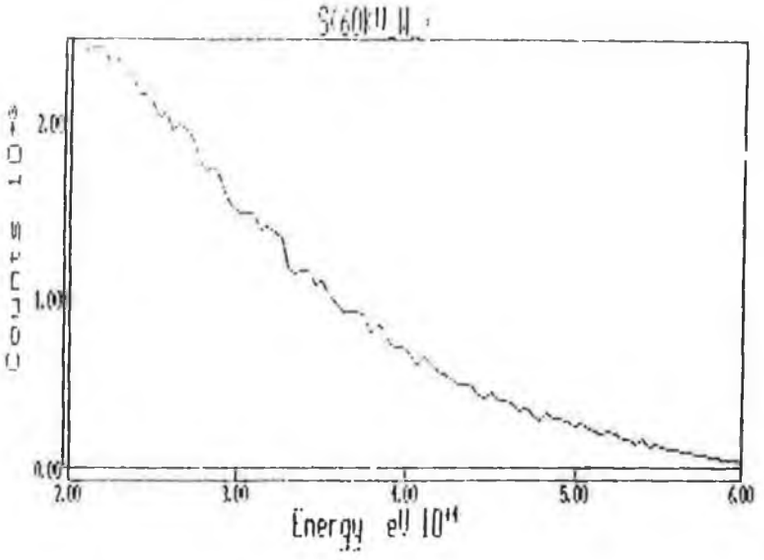

Figure G.04
Source spectrum in the region of interest.

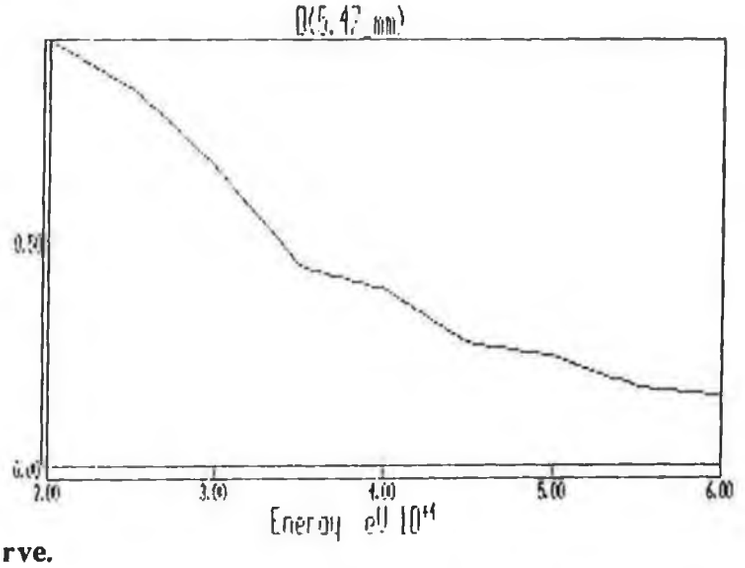

Figure G.05
Efficiency curve.

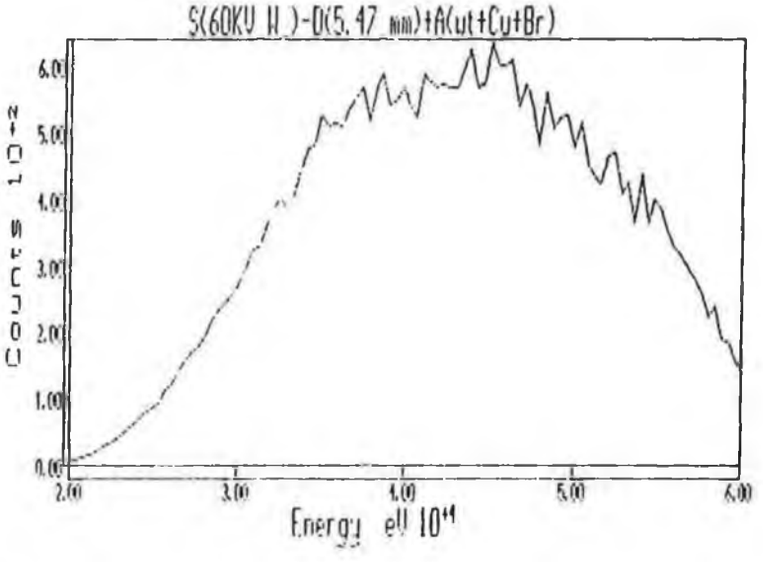

Figure G.06
Detector response removed from the source spectrum, and the absorber effect added.